

Doctoral Dissertation

Wang Tielin

Degradation of Aqueous
2-Amino-2-methyl-1-propanol
for Carbon Dioxide Capture



Telemark University College
Faculty of Technology

**Degradation of Aqueous 2-Amino-2-methyl-1-propanol
for Carbon Dioxide Capture**

Wang Tielin

Wang Tielin

**Degradation of Aqueous 2-Amino-2-methyl-1-propanol for
Carbon Dioxide Capture**

Thesis for the Degree of Doctor Philosophiae

Porsgrunn, Norway

October, 2012

Tel-Tek

Telemark University College

Tel-Tek

Telemark University College

Doctoral Dissertation at TUC, 2013

© Wang Tielin

ISBN 978-82-7206-365-7

ISSN 1893-3068

**Degradation of Aqueous 2-Amino-2-methyl-1-propanol
for Carbon Dioxide Capture**

Wang Tielin

Thesis submitted to the Telemark University College
for the degree of philosophiae doctor (PhD)

Acknowledgements

I would like to thank Professor Klaus J. Jens for his great support over the course of this project. His enthusiasm for his work is infectious, and has inspired me throughout the completion of my PhD study. Despite the growth in our research group during my tenure, he has always been accessible and responsive to any needs of mine. At the same time, he is a family man and always tells me how important family is. He is not afraid to encourage me to balance life outside of the lab with the demands of research. I have enjoyed my many personal interactions with Dr. Jens, and I feel I have learned a lot from him in all aspects of my life. I want to thank him for being my supervisor.

Without the financial support of the Research Council of Norway, this project would not have been possible. I would like to thank Ms. Marit Larsen (CEO of Tel-Tek) and Mr. Hans Aksel Haugen (head of Gass Tek) for taking me into Tel-Tek. I must extend a special thanks to Ms. Liv Axelsen as was of great assistance over the years, especially when I was new in Norway.

I would like to thank Professor Dag A. Eimer and Morten C. Melaaen who have always given me good suggestions when we met at each progress meeting. Dr. Eimer was always open and willing to share his more than thirty years of gas treating experience with us. I am thankful to Dr. Svein T. Hagen for his suggestion on experimental design for optimizing of operating parameters of ion chromatography. To Professor Tore Benneche in University of Oslo, I'd like to thank you for providing me the photochemical reactor. I would also like to thank the CO₂ laboratory managers and coordinators in TUC and Tel-Tek who have made my work much easier. They include Joachim Lundberg, Trond Risberg, Arve Lorentzen, Nora. C. I. Furuvik, Per M. Hansen and Chameera Jayarathna.

I have been fortunate to co-supervise three master students who worked on various parts of this project. Miguel Á. M. López and Chen Chen worked with me for developing cation IC method and FT-IR reaction system during the spring and summer of 2010, and Kristin S. Nomme who participated in a part of anion analysis work in 2011. I have enjoyed getting to know all of them, and I thank them for their hard work.

I would like to thank my colleagues and other graduate students. Ying Jiru, Han Jingyi and I have shared a lab and an office for entire PhD study experience. Our technical discussions have been stimulating and valuable, and I have enjoyed it. I must thank Li Bo and other friends for their supports, friendships, and everything else they have done for me.

Mostly, I would like to thank my wife Wang Fang. She was supportive and gave up a perfectly good job when I wanted to go to Norway for PhD study. I will never forget her sacrifice and dedication through these years. My son Wang Yizhe has given me great pleasure since he was born. He is always my energy to go further.

Wang Tielin

Oct., 2012

Abstract

Absorption-stripping with aqueous 2-amino-2-methyl-1-propanol (AMP), and especially AMP blends with other amines, such as monoethanolamine (MEA) and piperazine (PZ), presents an attractive option for carbon dioxide (CO₂) capture from flue gas in coal-fired power plants. Alkanolamine based solvents degrade in this service. The purpose of this work was to investigate AMP solvent degradation under thermal and oxidizing conditions, to measure rates of degradation for comparison with other solvents, to identify the degradation products and to identify possible degradation pathways. 5 mol/kg AMP without CO₂ loading was thermally stable up to 140°C under a blanket gas of N₂, exhibiting very low loss rates. However, with an initial CO₂ loading of 0.15 and 0.3 mol CO₂/mol AMP at 135°C, AMP lost 3.8(mol)% and 5.5 (mol)% after 5 weeks, respectively. The steric hindrance in AMP molecule slows down CO₂ induced degradation of AMP as compared to MEA, but it does not prevent oxazolidinone formation and oxazolidinone ring-opening into further degradation products.

The rate of oxidative degradation of AMP was investigated over a range of temperature, CO₂ loading, and AMP concentration. At 100 to 140 °C, degradation was found to be O₂ mass transfer limited in the employed batch reactors, however, the degradation rate increased with CO₂ loading. No significant effect of pH value was observed on the AMP degradation rate. Acetone, 2,4-lutidine, 4,4-dimethyl-2-oxazolidinone and formate were the main identified degradation products. Oxidative degradation of AMP likely proceeds through a H-abstraction step followed by production of a peroxy radical. The peroxy radical is proposed to decompose to primary products by intramolecular H-abstraction via a six-membered cyclic transition state. The reactions of AMP and the primary degradation products lead to the final degradation products. Acetone oxime and 4,4-dimethyl-1,3-oxazolidine were minor products at 100-140°C, but they were major products at 80°C. Temperature significantly affects the distribution of the ultimate degradation products.

UV radiation with a medium mercury lamp can dramatically accelerate the oxidation of AMP at 55°C. It seems that UV radiation does not change the primary degradation mechanism of AMP. The degradation products of UV accelerated oxidation are different from those of thermally accelerated oxidation of AMP, probably due to the impact of

temperature on the secondary reactions of the primary products. AMP oxidation is proposed to be initiated by a radical mechanism, but the reaction is not a chain reaction.

The degradation rate of 1.5 mol/kg PZ is 1.2 mmol/(kg·h) within 19 days, which is approximate half of that of 5 mol/kg AMP under 250 kPa O₂ and at 100°C. A possible degradation pathway of PZ is proposed based on the identified products. The degradation rate of AMP in AMP/PZ blends is close to that in a single AMP system, however, PZ degraded faster in the blends than it degraded individually at identical degradation conditions.

As compared to degradation of single MEA and AMP solvents, no new product was found in the degraded AMP/MEA mixture without CO₂ loading. Increasing the initial MEA concentration in the mixture, the amount of AMP loss decreased indicating that MEA protects AMP from oxidation. This inhibition effect of MEA on AMP degradation could be due to the fact that MEA degrades faster than AMP in the blends.

Contents

Acknowledgements	I
Abstract	III
Chapter 1 Introduction	1
1.1 CO ₂ emissions and environment.....	1
1.2 CO ₂ capture by amine-based absorption/stripping	3
1.3 Solvent degradation in absorption/stripping systems	5
1.4 Research objectives and scope.....	6
Chapter 2 Literature Review	8
2.1 AMP-based solvents	8
2.2 General degradation chemistry	12
2.2.1 Autoxidation	13
2.2.2 Electron abstraction and hydrogen abstraction mechanisms.....	14
2.2.3 Peroxide formation.....	17
2.2.4 Metal catalysts	20
2.2.5 Effect of CO ₂	22
2.4 Prior work on AMP degradation.....	24
2.4.1 Studies by the U.S. Army Edgewood Arsenal	24
2.4.2 Studies by IFP	25
2.4.3 Studies by the University of Texas at Austin.....	25
2.4.4 Studies by others	26
2.5 Conclusions.....	27
Chapter 3 Experimental Apparatus and Analytical Methods	28
3.1 Amine solution preparation and CO ₂ loading.....	28
3.2 Reaction systems.....	30
3.2.1 Autoclave reactors	30

3.2.2 Circulating closed-batch reaction system	32
3.2.3 Photochemical reactor.....	34
3.3 Cation chromatography	35
3.3.1 Apparatus description	36
3.3.2 Analysis procedure.....	36
3.3.3 Analysis error.....	37
3.3.4 Optimization for simultaneous determination of conventional amines	38
3.3.5 Analysis of amino acid.....	48
3.4 Anion chromatography	48
3.4.1 Apparatus description	48
3.4.2 Analysis procedure.....	50
3.4.3 Analysis error.....	51
3.4.4 Sodium hydroxide treatment for amide analysis.....	52
3.5 Gas chromatography-mass spectrometry.....	52
3.5.1 Apparatus description	52
3.5.2 Analysis procedure.....	53
3.5.3 Analysis error.....	55
3.6 Other analytical method used.....	56
3.6.1 Fourier transform infrared spectroscopy.....	56
3.6.2 Ultraviolet-Visible spectroscopy.....	59
Chapter 4 Thermal Degradation of AMP.....	60
4.1 Introduction.....	60
4.2 Thermal degradation without CO ₂	62
4.3 Thermal degradation in the presence of CO ₂	63
4.3.1 Degradation rate.....	63
4.3.2 Degradation product identification	66

4.3.3 Degradation pathways.....	71
4.3 Conclusions.....	72
Chapter 5 Oxidative Degradation Rate of AMP	73
5.1 Experiments in FT-IR based reaction system	73
5.2 Experiment in circulating closed-batch reaction system	76
5.3 Experiments at elevated temperatures	77
5.3.1 Experimental conditions	77
5.3.2 Comparison between AMP and conventional ethanolamines.....	79
5.3.3 Effect of initial concentration	81
5.3.4 Effect of temperature	82
5.3.5 Effect of oxygen partial pressure	83
5.3.6 Effect of agitation	84
5.3.7 Effect of metal ion	85
5.3.8 Effect of potassium persulfate.....	86
5.3.9 Effect of CO ₂ on AMP loss.....	87
5.3.10 Degradation of acid treated AMP	89
5.4 Conclusions.....	91
Chapter 6 Oxidative Degradation Products and Pathways of AMP	93
6.1 Oxidative degradation products of AMP	93
6.1.1 GC-MS identification.....	95
6.1.2 IC identification	99
6.1.3 Mass balance achieved in AMP oxidative degradation	100
6.2 Degradation pathways of AMP.....	101
6.2.1 Formation of acetone and ammonia.....	101
6.2.2 Formation of NO ₂ ⁻ and NO ₃ ⁻	104
6.2.3 Formation of carboxylic acid	105

6.2.4 Formation of DMOZD	106
6.2.5 Formation of 2, 4-lutidine	107
6.2.6 Large autoclave experiment at 80°C	109
6.3 Degradation of AMP accelerated by UV radiation	111
6.4 Oxidative degradation of 2-amino-1-propanol	119
6.5 Conclusions	123
Chapter 7 Degradation of AMP/PZ Blends	126
7.1 Thermal degradation of AMP-PZ blends	126
7.2 Oxidative degradation of PZ	129
7.2.1 PZ loss	129
7.2.2 Oxidative degradation products	130
7.2.3 Oxidative degradation pathways	133
7.2.4 Formation of nitrosopiperazine	140
7.3 Oxidative degradation of AMP-PZ blends	141
7.3.1 Overview of degradation products	141
7.3.2 Effect of temperature	142
7.3.3 Effect of composition	144
7.4 Conclusions	144
Chapter 8 Degradation of AMP/MEA Blends	146
8.1 Thermal degradation	146
8.2 Oxidative degradation	148
8.2.1 Overview of oxidative degradation products	148
8.2.2 Effects of operating parameters	150
8.3 Conclusions	154
Chapter 9 Conclusions and Recommendations	156
9.1 Conclusions	156

9.1.1 Degradation of AMP	156
9.1.2 Degradation of AMP/PZ blends.....	160
9.1.3 Degradation of AMP/MEA blends	161
9.2 Recommendations.....	162
9.2.1 Identification of degradation products	163
9.2.2 Further investigation of oxidation.....	164
9.2.3 Effect of metal ion	164
9.2.4 Environmental implications	165
References.....	166
Appendix A Publications and Presentations	175
Appendix B List of Chemicals	211
Appendix C Mass Spectra of Identified Products.....	217
Appendix D Details of IC Methods.....	235

Chapter 1 Introduction

This chapter gives an overview of CO₂ emission sources and environmental problems associated with these emissions. The targets for emission reductions are identified as well. Methods for CO₂ removal will be explored with focus on amine absorption/stripping system. Finally, the objectives and scope of the current project are described.

1.1 CO₂ emissions and environment

Towards the close of the 1980s, global warming has become generally recognized as the single most serious environmental problem facing the earth. The International Panel on Climate Change (IPCC, 2007) reported that the average global surface temperature has increased $0.74 \pm 0.18^{\circ}\text{C}$ over the past 100 years. Climate models from the same report predict a further increase of 1.1 to 6.4°C over the twenty-first century. These temperature increases have dramatic effects on the physical and biological environment, including polar ice cap recession, rising ocean levels, increasing insect and pest populations, increasing frequency and intensity of extreme weather events, species extinctions, human health and activities, etc.

Almost 100% of the observed temperature increase over the last 50 years has been due to the increase in the atmosphere of greenhouse gas (GHG) concentrations like carbon dioxide (CO₂), methane (CH₄), di-nitrogen oxide (N₂O) and halogenated hydrocarbons. Among these GHGs, CO₂ is the largest contributor with regard to its amount present in the atmosphere which contributes to 60 percent of global warming effects, although methane and chlorofluorocarbons have much higher green-house effect as per mass of gases (Yang et al., 2008).

There are increasing concerns for global warming caused by the effects of GHGs, particularly CO₂. Its annual emissions have grown by about 80% between 1970 and 2004, from 21 to 38 gigatonnes (Gt), and represented 77% of total anthropogenic GHG emissions in 2004, as shown in Figure 1.1. The CO₂ emission from human activities includes the combustion of fossil fuels in all major industries and other factors such as deforestation and desertification.

IPCC recently estimated that the global atmospheric concentration of CO₂ increased from a pre-industrial value of about 280 ppm to 379 ppm in 2005 (IPCC, 2007). As IPCC predicted, the atmosphere may contain up to 570 ppm CO₂ by the year 2100. The annual CO₂ concentration growth rate was 1.9 ppm per year during the year 1995-2005. It is generally accepted that an increasing atmospheric concentration of CO₂ will lead to an increase of the global temperature, and might lead to non-sustainable development of the earth climate with negative consequences for mankind.

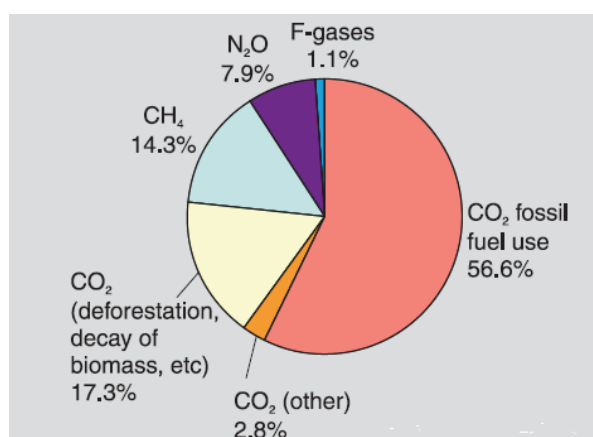


Figure 1.1 Share of different anthropogenic GHGs in total emissions in 2004 in terms of CO₂-eq (IPCC, 2007).

The long-term use of fossil fuels as a primary energy source is unavoidable. Global CO₂ emissions from fossil-fuel combustion reached a record high of 31.6 Gt in 2011, according to preliminary estimates from the International Energy Agency (IEA, 2012). As compared to emissions in 2010, this represents an increase of 1.0 Gt or 3.2%. Coal accounted for 45% of total energy-related CO₂ emissions in 2011, followed by oil (35%) and natural gas (20%). Control of carbon emissions to the atmosphere is the most important environmental issue of this decade, perhaps of this entire generation. The international response to mitigate global warming was to rectify the Kyoto Protocol, which was initially adopted on 11 December 1997 in Kyoto, Japan, and entered into force on 16 February 2005. As of April 2010, 191 states have signed and ratified the protocol. All developed countries across the world, except the United States, have entered the Kyoto Protocol to reduce world carbon emissions. Even in the US, approximately half of the states have embarked on carbon restriction laws. Therefore,

there is a demand for developing CO₂-reduction technologies around the world. CO₂ capture and sequestration (CCS) provides a mid-term solution to mitigate CO₂ environmental impacts and allows humans to continue to use fossil fuels until renewable fuel technologies mature.

1.2 CO₂ capture by amine-based absorption/stripping

The largest growth in GHG emissions came from energy supply, transport and industry because of burning of fossil fuels leading to CO₂ emission. Targeting the transportation sector for CO₂ removal is problematic since each automobile itself is only a small source of CO₂ emission, and it is too costly to install a removal system for each vehicle (Goff, 2005). For power generation, approximately one third of CO₂ emission is mainly from the extensive use of coal and natural gas (Davison, 2007). By 2004, CO₂ emissions from power generation represented over 27% of the total anthropogenic CO₂ emissions (IPCC, 2007). These fossil fuel fired power plants are large point source emitters that represent the best target for reducing CO₂ emissions.

There are three alternative methods to capture CO₂ from a power plant: post-combustion, pre-combustion and oxy-fuel capture systems (Pires et al., 2011). Pre-combustion capture involves combusting fuel with an O₂ stream to form syn-gas (carbon monoxide (CO) and hydrogen (H₂) mix). The CO can easily be converted to CO₂ by reacting it with water followed by separation of CO₂ from the H₂ before the combustion process. This type of process is most commonly associated with a coal gasified power plant, or an integrated gasification combined cycle (IGCC) power plant. For oxy-fuel combustion, the process involves burning fossil fuels in pure oxygen (>95%) mixed with recycled flue gas (RFG) instead of air (Mondal et al., 2012). The combustion products are almost pure CO₂ (typically 90%) and water vapour, which can be easily separated from the CO₂ by condensation. The CO₂ is now ready for transport and storage. The main problem with this method is separating oxygen from the air. This is usually done cryogenically which requires a lot of energy. Post-combustion capture refers to removing CO₂ from flue gas after the boilers and other environmental controls such as fly ash removal and flue gas desulphurization. The main drawback with this option is that the flue gas is at low pressure which means relatively low partial pressures of CO₂ and large volumes of gas to treat. However, this method can be typically built in to existing industrial plants and power stations without significant

modifications to the original plant. Therefore, post-combustion capture offers obvious advantage as retrofit option to existing plants as compared with the other approaches.

Technologies available or being considered for post-combustion CO₂ capture are cryogenic fractionation, membrane systems, adsorption and solvent absorption (Wang et al., 2011). Cryogenic separation of CO₂ is generally only used for gas streams with high concentration of CO₂ (typically > 90%). High energy requirement for refrigeration and dehydration of gas streams make the economics of cryogenic separation of CO₂ unsuitable for a flue gas application. Membrane permeation is also applicable to CO₂ removal from high-pressure gas streams, multiple stages and/or recycle of one of the streams are necessary which leads to increased complexity, energy consumption and costs. Physical adsorption is not yet considered attractive for large-scale separation of CO₂ from flue gas because the capacity and CO₂ selectivity of available adsorbents are low. Absorption in physical solvents is not economical when the CO₂ partial pressure is low. Consequently, the most economical and attractive method for separation of low pressure dilute CO₂ streams is chemical absorption.

Aqueous absorption/stripping using an amine is currently the only technology that is developed far enough for commercial application of CO₂ capture from flue gas. Alkanolamines such as monoethanolamine (MEA), diethanolamine (DEA), and N-methyl-diethanolamine (MDEA) have traditionally been investigated for this application. Other amines such as 2-amino-2-methyl-1-propanol (AMP) and piperazine (PZ) have been proposed as well. Among all amines, MEA is so far the benchmark solvent for post-combustion application.

Figure 1.2 shows a typical aqueous amine absorption/stripping process used for CO₂ capture. A flue gas stream containing approximately 10 vol. % CO₂ and 5 vol. % O₂ is counter-currently contacted with the aqueous amine solution in an absorber column, which is operating at 55°C and 1 atmosphere pressure (Rochelle et al., 2001). The CO₂ rich amine solution exits at the bottom of the absorber column and is then sent through a counter-current heat exchanger, where it is pre-heated by the lean amine solution before being sent to the stripper column. The CO₂ is liberated from the amine solution in the stripper, which operates at 120°C and 1 atmosphere pressure. In the stripper, heat is provided by the steam from the reboiler. The gas leaving the stripper is dehydrated and compressed before transport and

sequestration. The hot lean amine solvent is passed back through the cross-exchanger and back to the absorber for further CO₂ removal with a slip stream being sent to a reclaimer to remove solvent impurities.

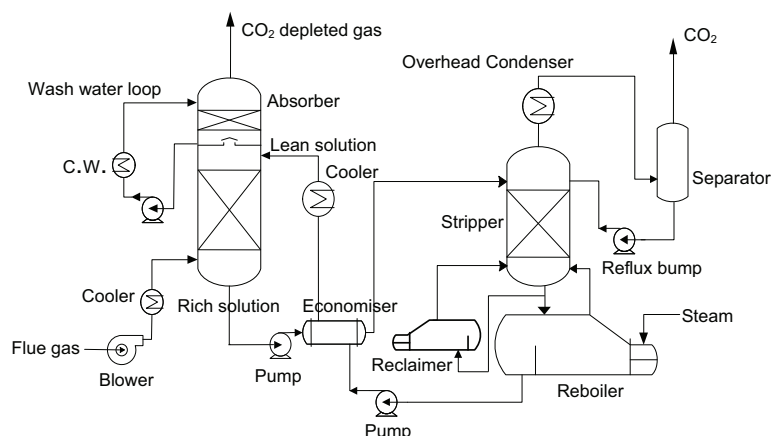


Figure 1.2 Schematic of typical amine-based absorption-stripping unit for CO₂ removal.

1.3 Solvent degradation in absorption/stripping systems

Solvent losses often occur in an amine-based absorption/stripping system due to solvent volatility and degradation. Volatility is the loss of volatile amine off the top of the absorber in the exiting, treated flue gas. A well designed water wash column can be used to recover the majority of amine losses through volatility.

Amine solvent degradation in the amine-based processes includes thermal-, carbamate polymerization- and oxidative degradation. Thermal degradation only occurs at high temperature and should not be a problem in flue gas applications (Rochelle et al., 2001). A major problem associated with these processes is solvent degradation through irreversible side reactions with CO₂ and flue gas impurities (e.g. O₂, SO_x and NO_x) (Strazisar et al., 2003), which results in numerous problems within the process. The effects of amine degradation include reduction of CO₂ absorption capacity, corrosion, foaming, fouling, increase in viscosity and release of pollutants from toxic degradation products. In the case of severe degradation, the solvent will need to be replaced and the degraded solvent must be disposed of in an environmentally acceptable manner.

Although amines have been used and studied for decades for removal of CO₂ from hydrocarbon streams, O₂ is usually not present in typical synthesis gas or natural gas streams. As such, there has been no practical incentive to study amine degradation caused by O₂. Therefore, although a number of studies have been carried out on degradation of different solvents due to CO₂, limited information concerning solvent degradation with O₂ is available in the literature. Since the desire to separate CO₂ from flue gas streams is gaining momentum, some studies concerning oxidative degradation of amine were performed in order to develop a better understanding of the oxidative degradation process. However, most of the studies were limited to conventional amines and degradation mechanism remains uncertain. This dissertation is mainly focused on investigating oxidative degradation of aqueous AMP and its blends used for CO₂ capture.

1.4 Research objectives and scope

Aqueous MEA solution is the baseline solvent used for CO₂ capture using aqueous amine solvents in an absorber-stripper system owing to MEA's high solubility in water, fast absorption rate, low viscosity, ease of handling, and low cost. However, the maximum CO₂ absorption capacity is limited by stoichiometry to 0.5mol CO₂/mol MEA. Furthermore, this solvent requires a high amount of heat for regeneration and generates a large amount of degradation products in service. AMP has been proposed as an attractive absorbent because of its advantages in absorption capacity, degradation resistance, and regeneration energy (Mandal and Bandyopadhyay, 2006).

The degradation behaviour and possible degradation pathways of AMP and AMP blends presented the motivation for the investigative work completed in fulfilment of this doctoral degree. The primary objective of the research was to develop a fundamental understanding of the degradation and degradation mechanisms that occur in aqueous AMP and AMP blends when used for CO₂ capture from flue gas feed streams. Degradation mechanisms have been postulated based on products present in thermal and oxidative degradation samples using identification of gas chromatography-mass spectrometry (GC-MS) and ion chromatography (IC) methods.

The scope of this work included modification of autoclave reactors and use of literature degradation methods to oxidize and thermally degrade AMP solutions and AMP blends.

Experiments were conducted in autoclaves to degrade AMP and AMP blends at accelerating conditions. The data from these experiments were used to construct a basic understanding of how AMP degrades.

The scope also included development and construction of a circulating closed-batch reaction system and a Fourier transform infrared spectrometry (FT-IR) based open-batch reaction system for degradation of AMP. The temperature was chosen to be close to absorber temperature in these two reaction systems. In the circulating closed-batch reaction system, the reaction gas was circulated and sparged into AMP solutions with a small pump. In the FT-IR based open-batch reaction system, air was bubbled through the AMP solutions combined with agitation by a turbo mixer. O₂ mass transfer is expected not to be limited within these two systems.

To reduce the length of degradation experiment, thermal acceleration is generally used in the laboratory studies of amine degradation. In this work, UV radiation was tested for acceleration of AMP oxidation. This new acceleration method was compared to thermal acceleration.

This work also focused on development of analytical methods for analysis of amines and degradation products in our laboratory. A method of simultaneous determination of degraded conventional amines and ammonium using a non-suppressed cation chromatography was developed. A statistics-based experimental design with response surface methodology was employed to optimise the IC operating parameters. Methods of anion chromatography and GC-MS were also developed.

Chapter 2 Literature Review

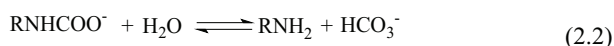
This chapter introduces AMP and AMP blends as viable solvents for post-combustion CO₂ capture from flue gas using an amine based absorption-stripping process and the current body of knowledge on the oxidative degradation of amines. Since there is little literature on AMP degradation, the degradation of traditional amines is included. Information of advantages of AMP-based solvents over traditional amines and general degradation chemistry is discussed.

2.1 AMP-based solvents

For the removal of CO₂ and H₂S from gas streams, aqueous alkanolamine solutions are industrially important solvents used in the natural gas, petroleum plants and ammonia industries. The process of using aqueous solutions of alkanolamines for CO₂ removal has been in commercial use since the early 1930s (Kohl and Nielsen, 1997) and is based on reaction of a weak base (alkanolamine) with a weak acid (CO₂) to produce a water soluble salt. This reaction is reversible and the equilibrium is temperature dependent. In the existing industrial processes, monoethanolamine (MEA), diethanolamine (DEA), di-2-propanolamine (DIPA), and N-methyldiethanolamine (MDEA) are commonly used alkanolamines. Aqueous MEA solution is the most frequently used absorbent due to its high reactivity with CO₂, low cost of the raw materials, high alkalinity, ease of reclamation, and low absorption of hydrocarbons (Isaacs et al, 1980).

Use of aqueous solutions of alkanolamines is currently the most developed technology for commercial application of post-combustion CO₂ capture from flue gas. Though alkanolamine absorption/stripping process has been used extensively for removal of acid gases since 1930s, conventional primary and secondary alkanolamines all show limited thermodynamic capacity to absorb CO₂. When a primary (or secondary) amine reacts with CO₂, stable carbamate is usually formed (Sartori and Savage, 1983) as shown in reaction 2.1, while carbamate hydrolysis (reaction 2.2) hardly takes place. Hence maximum CO₂ loading is limited by stoichiometry to 0.5 mol of CO₂/mol of amine when reaction 2.1 is the only reaction. In addition, there is a relatively high heat of absorption associated with the

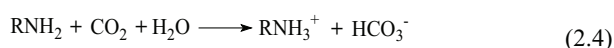
formation of carbamate ions, thus the cost of regenerating primary and secondary amines is high.



Aqueous tertiary amine (such as MDEA) solution reacts with CO_2 in a different way (reaction 2.3), here the amine simply acts as a base. Therefore, stoichiometry loading capacity can reach 1.0 mol CO_2 /mol of amine owing to formation of bicarbonate. In addition, the lower enthalpy of reaction leads to lower energy requirements for generation. However, the reaction rate constant of CO_2 with MDEA is only $3.5 \text{ m}^3 \cdot \text{kmol}^{-1} \cdot \text{s}^{-1}$ at 25°C (Crooks and Donnellan, 1990), this slow reaction rate make such solvent not feasible for CO_2 capture from flue gas stream.



Sartori and Savage (1983) presented a group of amines termed sterically hindered amines that have excellent absorption and desorption capacity. Sterically hindered amines were initially introduced to application in acid gas treating units by the EXXON Research and Engineering Company (Kohl and Nielsen, 1997). In contrast to primary alkanolamines, the rotation of bulky alkyl groups around the amino-carbamate group is restricted in sterically hindered amines (Veawab et al., 1998). This results in considerably lower stability of the carbamate compound. The carbamate thus readily reacts with water to form free amine and bicarbonate (reaction 2.2). Low carbamate stability making loading of CO_2 up to 1.0 mol of CO_2 /mol of amine. The possible overall reaction for the sterically-hindered amines can be written as shown in reaction 2.4 (Chakraborty et al., 1986):



One hindered amine of interest is 2-amino-2-methyl-1-propanol (AMP), in which the amino group is attached to a tertiary carbon atom (Figure 2.1).

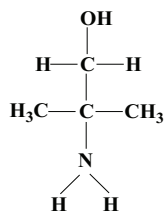


Figure 2.1 AMP structure.

Due to the bulkiness of the group attached to a tertiary carbon atom of AMP, the stability of carbamate is low when AMP reacts with CO_2 (Sartori and Savage, 1983). The low stability of the carbamate results in a theoretical CO_2 loading of 1.0 mol of CO_2 /mol of AMP. However, the mechanism of carbamate formation has been a controversial subject. Xu et al (1996) measured the kinetics of the reaction of CO_2 and AMP solutions and claimed that the results support a zwitterions mechanism to describe the reaction process. This conclusion is reinforced by the fact that CO_2 reacts directly with AMP in nonaqueous solvents. A recently DFT theoretical calculation shows a single-step, third order reaction as the most probable mechanism for the carbamates formation from CO_2 and AMP (Ismael et al., 2009). As this study shows, the apparently energy barrier is high for the reaction because of the solvent effect. The low stability of the carbamate demands further study on the possible role of AMP acting as a base. On the other hand, Chakraborty et al. (1986) presumed the hydration of CO_2 to be AMP catalysed as in the case of tertiary amines.

The kinetics of the reaction of CO_2 with AMP has been shown to be first order with respect to both CO_2 and AMP in a number of reports. However, the reported second-order reaction rate constants are found to show high discrepancy. Sharma (1965) reported a second order reaction rate constant of $1048 \text{ m}^3 \cdot \text{kmol}^{-1} \cdot \text{s}^{-1}$ at 25°C , while Chakraborty et al. (1986) identified a rate constant as low as $100 \text{ m}^3 \cdot \text{kmol}^{-1} \cdot \text{s}^{-1}$ at 42°C . Yih and Shen (1988) and Xu et al. (1996) reported that the rate constant has a value of $1245\text{-}1270 \text{ m}^3 \cdot \text{kmol}^{-1} \cdot \text{s}^{-1}$ at 40°C . The second order reaction rate constants at 20, 30 and 40°C were determined in a stirred cell to be 190, 369 and $740 \text{ m}^3 \cdot \text{kmol}^{-1} \cdot \text{s}^{-1}$ (Messaoudi and Sada, 1996), while the values of the constant were determined using a wetted wall column to be 439, 687 and 1179 at 21, 28.5 and 38.5°C (Saha and Bandyopadhyay, 1995), respectively. Although the reported reaction rate constants are not consistent with each other, they are apparently much higher than that of the reaction

between CO₂ and MDEA. In addition, the CO₂ solubility in AMP solutions is higher than that for MEA solutions at 40°C but lower at 80°C (Tontiwachwuthikul et al., 1991).

The largest problem concerning use of conventional alkanolamines as absorbents for CO₂ capture from flue gases is the amount of energy needed to regenerate the CO₂ rich solvent. In fact, to reduce the cost of CO₂ capture, AMP-based solutions have been investigated as attractive alternative solvents and proposed by a number of researchers. Zhang et al. (2008) compared CO₂ absorption capacity and regeneration behaviour of AMP with MEA, DEA, diethylenetriamine (DETA), and MDEA. The results have shown that AMP may be more suitable for application in industrial processes because it has less reboiler heat duty for regeneration, higher regeneration efficiency, and higher absorption capacity. The reported order of regeneration performance is AMP > MDEA > DETA > DEA > MEA. A study of CO₂ absorption and desorption using MEA as well as novel amines in a packed column was carried out by Yeh et al. (2001). Testing of AMP revealed that although absorption was somewhat less as compared to MEA, thermal regeneration was far easier. It can be speculated that if AMP is a substitute for MEA, an overall process benefit will be obtained if a structured packing is used. Gabrielsen et al. (2007) have reported experimental data for a CO₂ absorber with structured packing in a laboratory pilot plant using an aqueous AMP solution. The computational simulations using Aspen Plus program package demonstrate that 30 wt% AMP aqueous solution is a superior solvent to 30 wt% MDEA aqueous solution (Lee et al., 2009).

The use of mixed amine solvents in gas-treating processes is of increasing interest today. Mixed amines have been reported to maximize desirable qualities of the individual amines. The aforementioned experimental results indicate that AMP has the potential to be a superior absorbent for removal of CO₂, while the absorption rate of CO₂ into aqueous AMP is still slower than MEA. Encouragingly, it was found that addition of small amounts of MEA or DEA to an aqueous solution of AMP significantly enhances absorption rate (Xiao et al., 2000; Mandal et al., 2003 and 2006; Sakwattanapong et al., 2009). Addition of MDEA into AMP also increased their reaction rate constants as compared to AMP alone (Choi et al., 2007). Furthermore, blended MEA-AMP require lower heat energy consumption for solvent regeneration than that blended MEA-MDEA, and DEA-MDEA (Sakwattanapong et al., 2005). Choi et al. (2009) investigated removal characteristics of CO₂ using MEA-AMP blends. As compared to aqueous MEA and AMP solutions, aqueous blended MEA-AMP

solutions have a higher CO₂ loading than MEA and a higher reaction rate than AMP. Aroonwilas and Veawab (2004) have tested the performance of CO₂ absorption into aqueous solutions of blended amines including MEA-MDEA, DEA-MDEA, MEA-AMP and DEA-AMP. The results have shown that AMP-based solvents, especially MEA-AMP, are more effective in CO₂ absorption than MDEA-based solvents. The same group (Aroonwilas and Veawab, 2009) evaluated integration of a CO₂ capture unit using blended MEA-AMP solution into coal-fired power plants and claimed that a MEA-AMP blend exhibits great promise for CO₂ capture in supercritical coal-fired power plants.

In addition to conventional amines, other amines, such as piperazine (PZ), have also been mixed with AMP and proposed as novel absorbents for CO₂ capture. It has been shown that adding a small amount of PZ to AMP the rate of absorption of CO₂ can be enhanced to a large extent (Sun et al., 2005; Choi et al., 2007). As compared with 5M MEA, the AMP/PZ (3M/1.5M) system has about twice the specific capacity if operating between 40 and 80°C, and almost twice the CO₂ partial pressure at 120°C (Brüder., 2011). Other experimental results also show that PZ activated concentrated aqueous AMP solution appears to be a promising solvent system for efficient and cost-effective CO₂ capture from flue gas streams (Samanta, 2009; Dash, 2011). On the other hand, PZ has been proposed as new standard for CO₂ capture technology (Rochelle et al., 2011). The main disadvantage of using PZ as absorbent is the narrow operating loading range due to solubility limitation (Freeman et al., 2010a). However, the operating loading ranges were enlarged when AMP was added into PZ solutions (Han, 2012). This means that AMP-PZ blends could be good solvent candidates for CO₂ capture from flue gas.

2.2 General degradation chemistry

The reported thermodynamic and kinetic data indicate AMP-based solutions to be promising solvents for post-combustion CO₂ capture. Information based solely on solvent performance is, however, insufficient for evaluating practicability of the solvent. Other aspects such as degradation and corrosion need to be considered as well. Solvent degradation has been estimated to be around 10% of the overall CO₂ capture cost using aqueous MEA absorption technology (Rao and Rubin, 2002).

Under varying conditions, amine solvents in post-combustion CO₂ capture processes are subject to three types of degradation: thermal degradation, CO₂ induced degradation and oxidative degradation (Bedell, 2011). Thermal degradation (in the absence of O₂) takes place mainly at temperatures in excess of 200°C and is less studied. CO₂ induced degradation involves irreversible reactions between CO₂ and amines and is expected to take place in the stripper. Oxidative degradation requires oxygen, is based on radical reactions, is catalyzed by metal ions, results in oxidized fragments of the solvent, and is therefore expected to take place mainly in the absorber. Oxidation reactions account for about half the total amine degradation (Strazisar et al., 2003; Sexton and Rochelle, 2011). Screening and characterization of solvent oxidative degradation potential has emerged as a critical step in the early stages of solvent selection. It is probable that amine degradation will not be completely eliminated and therefore must be managed. A comprehensive understanding of degradation chemistry of amines is very important for proposition of degradation management strategies. The general chemistry related to amine degradation is discussed in this section.

2.2.1 Autoxidation

Under normal conditions in the presence of O₂, CO₂ is the only thermodynamically stable carbon compound. In other words, all organic compounds are only metastable intermediates on the way to CO₂ in the presence of free O₂ (Franz and Sheldon, 1991). Oxidation of organic materials can be roughly divided into homolytic- and heterolytic oxidation reactions. In heterolytic oxidation, the starting compounds are oxidized by an active oxygen species or a metal ion by a two-electron transfer reaction. Homolytic oxidations are free radical processes involving radicals formed by homolytic cleavage of covalent bonds. Explosions and combustion reactions, ageing of the polymers and oils, and many industrial oxidation reactions in homogeneous liquid or gas phases belong to homolytic oxidation reactions. Such reactions proceed spontaneously even at low temperatures, hence they are also called autoxidation.

Radical chain reactions can be divided into three stages: chain initiation, propagation, and termination. Figure 2.2 shows an autoxidation scheme of hydrocarbons. In the initiation process, some event like thermolysis and/or photolysis of weak covalent bonds may cause free radicals to be formed. Once free radicals are formed, they react with O₂ in a chain to

convert the starting material to peroxy radicals. Hydrogen abstraction from relatively weak C-H bonds by peroxy radicals, and addition to dioxygen of the resulting C-centered radicals, comprise the chain-propagating steps of autoxidation. In the chain-propagating steps, new radicals formed on the right-hand side when a radical consumed on the left-hand side. The propagation steps may then be repeated tens, hundreds or even thousands of times (Perkins, 1994). The repetitive character of these steps gives rise to the notion of a 'chain' or 'radical chain' reaction. The chain is ended by termination reactions in which free radicals collide and combine with each other to form non-radical products.

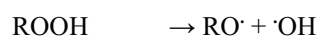
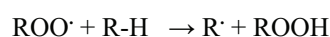
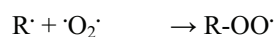
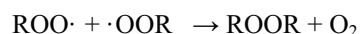
Initiation:**Propagation:****Termination:**

Figure 2.2 Scheme of hydrocarbon autoxidation.

2.2.2 Electron abstraction and hydrogen abstraction mechanisms

Radical chain reactions essentially occur through chain initiation, the attack at a covalent bond such that new radicals are formed. A radical chain reaction is easily initiated by photolysis. Homolytic fission of covalent bond may occur to form free radicals through irradiation of the reaction system with light of a wavelength which is absorbed by substrate molecule. Free radicals also can be produced on purpose by decomposition of a radical

initiator. For example, peroxides are usually used as radical initiators to induce polymerizations in industrial applications. The cleavage of the comparatively weak O-O bond in peroxides forms highly active $\cdot\text{OH}$ and $\text{RO}\cdot$ radicals as initiation radicals. Attack of an initiating radical at a covalent bond such that an existing bond is broken and a new one formed. The lower the energy of an existing bond and the greater the energy of an attacking radical, the attack of the radical at the bond takes place more easily. In some cases, however, initiation occurs by a process that is not well understood. For example, in the autoxidation of higher hydrocarbons, the initiation event is thought to be the spontaneous reaction with oxygen or by concentration of the thermal vibration energy into one bond (Franz and Sheldon, 1991).

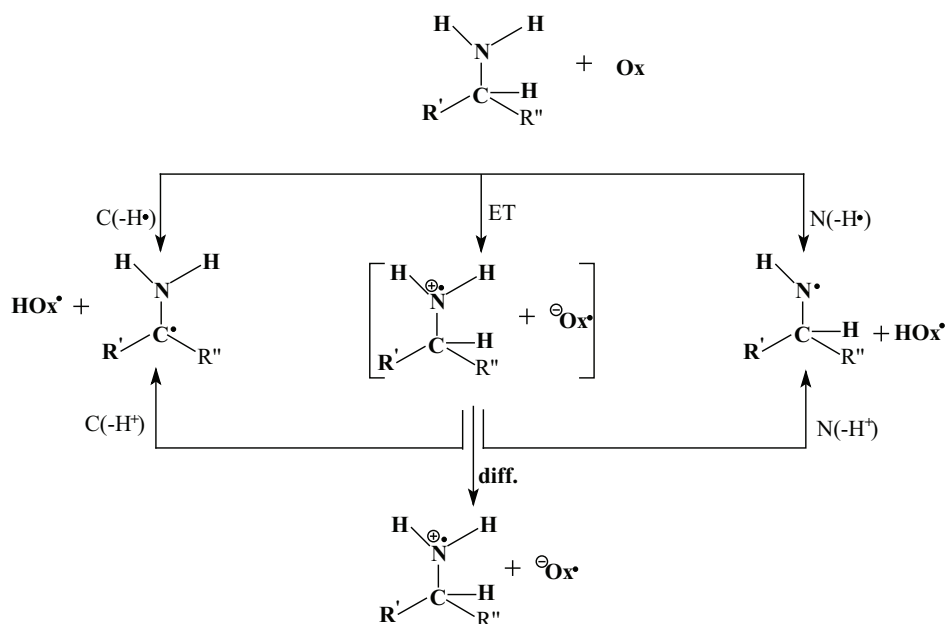


Figure 2.3 A general scheme for the oxidation of a primary or secondary amine by a one-electron oxidant (Armstrong et al., 2004).

Amines and hydrocarbons are oxidized by oxygen via a chain mechanism (Denisov and Afanas'ev, 2005). A general scheme for initiation of oxidation of a primary or secondary amine by a one-electron oxidant (Ox) is depicted in Figure 2.3. Oxidation of amine can be initiated by an oxidant via two mechanisms: electron abstraction (electron transfer, ET) and hydrogen abstraction. The oxidant may abstract an electron yielding an N-centered radical

cation, or abstract a hydrogen atom from the α -C atom (α position with regard to the amino functional group) or the N atom. Two H deficient products may be formed by proton transfer from the α -C or the N atom of the radical cation to $\text{Ox}^{\cdot-}$ if the time for outward diffusion from the initial encounter cage is long enough. The rates of the various processes in the scheme vary, depending on the structure of the amine and the oxidant (Armstrong et al., 2004). For tertiary amines, the reactions are similar except that the reactions N ($-\text{H}^{\cdot}$) and N ($-\text{H}^+$) are absent.

The electron abstraction and hydrogen abstraction mechanisms for amine were originally proposed by the US Army Chemical Research and Development Laboratories at Edgewood Arsenal in the 1960s. The proposition is based on series of studies that performed mainly on tertiary amines using chlorine dioxide (ClO_2) as a single electron oxidant (Dennis et al., 1967; Hull et al., 1967; Rosenblatt et al., 1967; Hull et al., 1969). The studies concluded that the two simultaneous mechanisms, either of which may predominate in a given circumstance, depends on the structure of the amine. The electron abstraction path would be expected to show only a small (secondary) kinetic isotope effect in reaction with α -deuterated amines. In contrast, the hydrogen abstraction path should provide a large (primary) kinetic isotope effect because carbon-deuterium bonds would be broken in the rate-limiting step. The experimental results showed that the rate-limiting step is the electron abstraction step, rather than the hydrogen abstraction step for the studied tertiary amines. The hydrogen abstraction mechanism dominated the reaction for benzylamine, the only primary amine investigated in the study (Hull et al., 1967).

The hydrogen abstraction mechanism was supported by experiments utilizing ionizing radiation. An investigation into the deamination of amino alcohols using ionizing radiation was carried out by Petryaev et al. (1984). The radiation was used to create initiating radicals like HO^{\cdot} , H^{\cdot} , and e^- (aq) as initiator for radical reactions in the absence of free oxygen. Eight α , β - and α , γ -amino alcohols were investigated, including MEA. Ammonia was identified among the final products in all cases. The deamination initiation of the investigated amino compounds was explained by the hydrogen abstraction mechanism. The H^{\cdot} and HO^{\cdot} radicals abstract a hydrogen atom from the hydroxyl-substituted carbon atom of the amino alcohols. In strongly alkaline solution, the deprotonation of the amino group increases the likelihood of the abstraction of a hydrogen atom from α -C atom and from the nitrogen atom. The authors

proposed that the deamination of the amino alcohols takes place by decomposition of the formed new radicals via a five-membered ring structure.

2.2.3 Peroxide formation

The presence of oxygen in the flue gas will cause oxidative degradation, particularly in the absorber column of a conventional thermal swing process. Chakma and Meisen (1997) reported that the degradation of MDEA was very slow under nitrogen at 200°C. However, 50 wt% MDEA aqueous solution degraded significantly under synthetic air (O_2 21%, N_2 79%, $CO + CO_2 < 0.5$ vpm, $C_nH_m < 0.1$ vpm, $H_2O < 2$ vpm, $NO_x < 0.1$ vpm) in a batch reactor at 140°C (Lepaumier et al., 2009a). The main degradation products were DEA, N,N-dimethyl-monoethanolamine, N-methyl-monoethanolamine (MAE) and bicine. Closmann (2011) investigated oxidation of 7m MDEA aqueous solution by bubbling 98% O_2 /2% CO_2 using a low-gas semi-batch reactor and cycling degradation apparatus at 55-120°C. DEA, MAE and bicine were identified as main products. Rooney et al. (1998) studied oxygen's role in alkanolamine degradation using compressed air containing 21.3% O_2 and also found DEA in degraded MDEA solutions in the presence of oxygen, but no DEA was detected when the experiments were conducted with a nitrogen blanket. Supap et al. (2001) have determined intrinsic kinetic data for the oxidative degradation of MEA. The study was conducted in a temperature range of 120-170 °C and a MEA concentration range of 2-11M at 241-345 kPa O_2 . The values obtained for the orders of reaction for MEA and O_2 were 1 and 1.5, respectively, which illustrated that the oxidative degradation of MEA is more sensitive to increases in O_2 concentration than in MEA concentration. All of these observations show that oxygen plays an important role in the processes of oxidative degradation of amines.

However, the way of how O_2 is getting into the oxidation mechanism is still not fully understood. The ground state of oxygen is a triplet with two unpaired electrons ($\cdot O_2$, a diradical) with parallel spins. Its direct reaction with organic substrate molecules in the singlet state is severely restricted. Although triplet oxygen is unreactive with singlet substrates and is unable to abstract hydrogen atoms from hydrocarbon substrates, it is a diradical and as such can undergo coupling with other radicals. Such radical-radical coupling reactions usually have zero activation energy (Sawyer, 1994). Once oxidation has been initiated by formation of the carbon-centered radical, subsequent reaction with O_2 should be extremely fast to form a peroxy radical (Sonntag and Schuchmann, 1997). Therefore, in the

presence of dissolved O_2 , peroxy radicals are to be expected as intermediates during oxidation of amines. Peroxy radicals would convert into peroxides via intermolecular hydrogen abstraction as well as intramolecular hydrogen transfer. Peroxy radicals participate as chain propagating species in the chain oxidation if the peroxy radicals are strong enough to break a hydrogen containing bond of the substrate. In the presence of a sufficient concentration of dissolved O_2 , the rate of initiated oxidation of amines does even not depend on the O_2 partial pressure (Denisov and Afanas'ev, 2005).

Chi and Rochelle (2002) adopted the electron abstraction mechanism as the initiation step and proposed that MEA oxidation was propagated by formation of peroxy radical (See reaction (II), Figure 2.4). This radical could react with another molecule of MEA to produce an amino-peroxide and another imine radical. Decomposition of the amino-peroxide would result in a hydrogen peroxide and an imine. The authors studied the degradation of MEA in the presence of metal ions but only monitored the evolution of ammonia, the proposed reaction pathways were not fully explained and confirmed. Sexton (2008) suggested that the amino-peroxide molecule from Figure 2.4 can lose an OH radical at highly basic conditions, leaving a free radical structure that decomposes to formamide and the formaldehyde radical. In basic amine solution, the formaldehyde radical will de-protonate, leaving a charged free radical that loses an electron and rearranges to form formaldehyde.

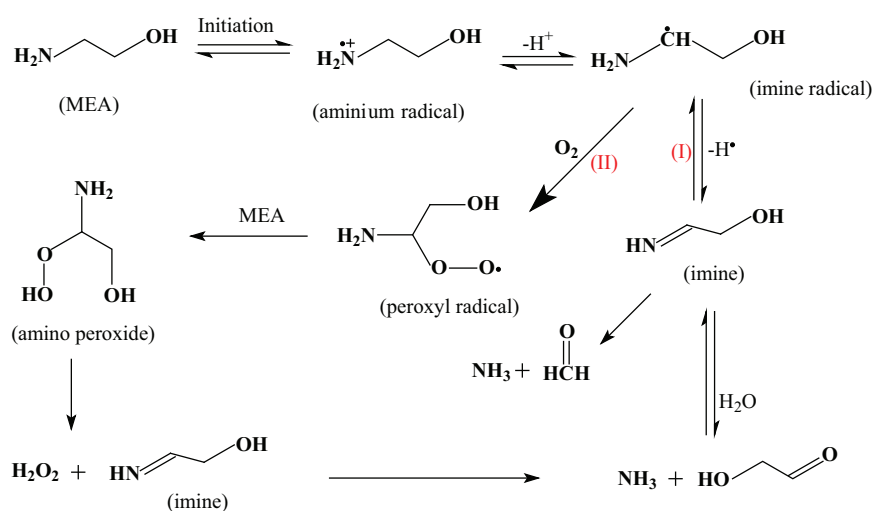


Figure 2.4 Proposed scheme of degradation of MEA by electron abstraction as initiation step (adapted from Chi and Rochelle 2002).

Delfort et al. (2011) and Bedell (2011) adopted hydrogen abstraction as initiation step for interpreting MEA oxidation and also proposed that propagation of the oxidation depend on formation of peroxy radical in the presence of oxygen. Figure 2.5 shows the proposed scheme for oxidation of MEA. The further reaction of the peroxy radical involves abstraction of a hydrogen atom from another MEA molecule similar to what is often proposed in hydrocarbon autoxidation.

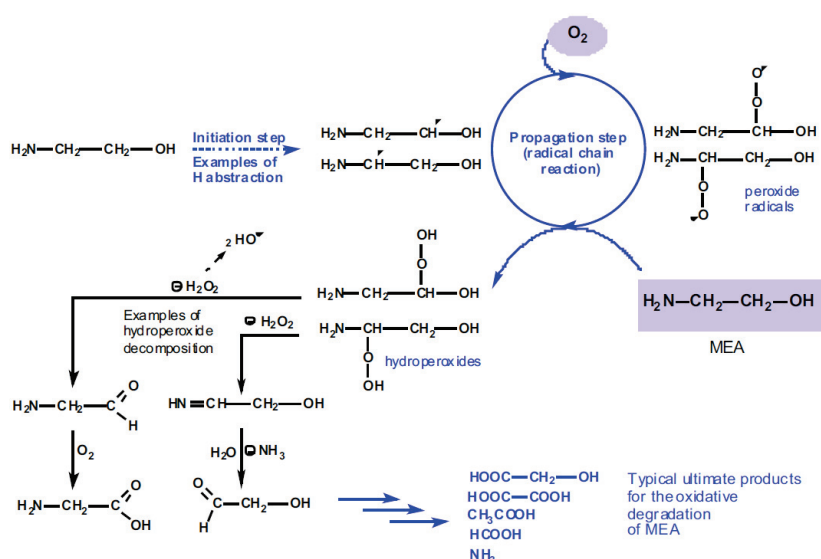


Figure 2.5 Proposed degradation mechanism of MEA oxidative degradation (Delfort, 2011).

Closmann (2011) proposed peroxy radicals as intermediates for interpreting the formation of DEA and MEA in degraded MDEA solutions. Several schemes were proposed to explain possible pathways for formation of degradation products. However, the formation of peroxides was not confirmed directly in the aforementioned investigations. Blachly and Ravner (1966) studied the stability of MEA and reported that peroxides were determined by the iodine-thiosulfate method in the degraded MEA aqueous solutions in the presence of dissolved metal ions at 55°C for 3-13 days. This result can be taken as direct evidence of the formation of peroxide during the degradation of MEA.

2.2.4 Metal catalysts

Due to fly ash leaching, the corrosive nature of alkanolamine solvents and their degradation products and due to addition of corrosion inhibitors to prevent equipment destruction, transition metal ions may be presented in amine solvents. Stainless steel is composed of iron, chromium and nickel. The corrosion inhibitors are usually heavy metal salts. Copper (II) is a relatively well known inhibitor in alkanolamine systems, especially in the presence of oxygen (Pearce, 1984; Wolcott et al., 1986; Cringle et al., 1987).

Transition metal ions react with other ions, radicals, and molecules in electron transfer reactions. A primary product of the oxidation of organic compounds is hydroperoxide, which is known as an effective electron acceptor. Hydroperoxides are decomposed catalytically by metal ions with the generation of free radicals via the following cycle of reactions (see Figure 2.6, Denisov and Afanas'ev, 2005).

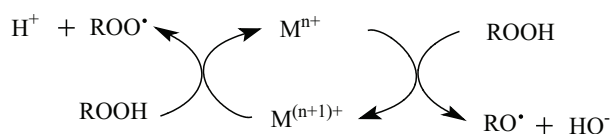


Figure 2.6 Peroxide decomposition catalyzed by metal ions.

Dissolved iron is the most probable metal catalyst because it is a corrosion product in alkanolamine-based absorption/stripping systems constructed of carbon steel. The direct reaction of ferrous ion may be an important source of free radicals and a way of getting oxygen into the oxidation mechanism. In aqueous solution, as shown in Figure 2.7, Fe^{2+} appears to react with O_2 , forming intermediates such as superoxide, peroxide and a hydroxyl radical (Bedell, 2011; Stumm and Lee, 1961).

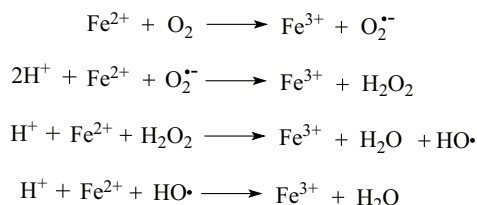


Figure 2.7 One electron reduction steps of dioxygen by Fe(II) (adapted from Bedell, 2011).

Although triplet oxygen is a radical itself, its non-radical chemistry dominates its reactivity (Sawyer, 1994). The hydroxyl radical ($\cdot\text{OH}$) is the most reactive member of the family of oxygen radicals. According to Figure 2.7, Fe^{2+} can activate triplet O_2 by converting it to $\cdot\text{OH}$ radical. $\cdot\text{OH}$ may initiate the oxidation of amines and produce new alkyl radicals. Newly formed alkyl radicals could react with O_2 to produce peroxy radicals and peroxides by hydrogen abstraction subsequently.

Catalysis of dissolved metals on amine oxidation has been observed in a number of studies. Blachly and Ravner (1966) examined the effects of dissolved iron, copper, nickel and chromium as oxidation catalysts in MEA systems. It was found that dissolved cupric ion (Cu^{2+}) at concentration as low as 1ppm was sufficient to cause perceptible degradation of MEA solution. The rates of copper catalyzed degradation were higher than iron catalyzed degradation at the same concentration. A concentration of 3.7 ppm nickelous ion (Ni^{2+}) was relative inert, but a tenfold increase in concentration caused noticeable degradation.

Chi and Rochelle (2002) studied oxidative degradation in the presence of iron at 55°C. The overall degradation rates were quantified by measuring ammonia (NH_3) evolution rates from the solutions with Fourier transfer infrared (FTIR) analysis. The results showed that iron is a catalyst for oxidation of MEA to NH_3 . As little as 1 mM iron can increase the rate by a factor of 5 with 0.4 mol CO_2 /mol MEA. Fe^{2+} from 0.0001 to 3.2 mM yielded degradation rates from 0.12 to 1.10 mM NH_3 evolved/h. Fe^{3+} did not appear to catalyze oxidation in unloaded MEA.

Goff and Rochelle (2004) investigated Cu^{2+} and Fe^{2+} catalyzed oxidation of MEA at 55°C and found the Cu^{2+} had a greater catalytic effect than Fe^{2+} . This confirms the result of Blachly and Ravner (1966), who also used NH_3 evolution rate as the indication of MEA oxidation. While at high concentrations of Cu^{2+} or Fe^{2+} (above 0.5 mM), the evolution rate of NH_3 appeared to be controlled by the rate of O_2 mass transfer.

A kinetic study of the oxidative degradation of CO_2 loaded MEA, with and without 0.1 mol% sodium metavanadate (NaVO_3 , a corrosion inhibitor), was performed in a stainless steel rotary-type autoclave with O_2 pressures of 250 and 350 kPa by Bello and Idem (2006). In this investigation, the MEA degradation rate was monitored by the reduction of MEA concentration in liquid phase using HPLC analysis instead of by measuring of NH_3 evolution

rate from the MEA solutions using FTIR. The study showed that presence of NaVO_3 led to an increased MEA degradation rate.

Sexton and Rochelle (2009) studied catalysts and inhibitors for oxidation of MEA by introducing 100 mL/min of 98% O_2 /2% CO_2 into a 350 mL of an agitated MEA solution and sparging 7.5 mL/min of 15% O_2 /2% CO_2 through 350 mL of MEA solution controlled at 55°C separately. Hydroxyethyl-formamide (HEF) production, Hydroxyethylimidazole (HEI) production and MEA losses increased by a factor of 3 when both Fe^{2+} and Cu^{2+} were present in solution as compared to Fe^{2+} alone. Chromium (Cr^{3+}) and nickel (Ni^{2+}) also catalyzed the oxidation of MEA. For oxidative degradation of MEA, the order of the catalytic potential of the tested metals is: $\text{Cu}^{2+} > \text{Cr}^{3+}/\text{Ni}^{2+} > \text{Fe}^{2+} > \text{V}^{5+}$.

2.2.5 Effect of CO_2

Removal of CO_2 from flue gas streams is the ultimate goal, thus it is essential to have a good understanding of the effect of CO_2 on amine degradation. There are two major effects of CO_2 on amine degradation in flue gas CO_2 capture: the impact on amine oxidation and CO_2 induced degradation involving irreversible reaction between CO_2 and amines at high temperature.

2.2.5.1 Effect on oxidative degradation

Previous reports on the effect of CO_2 loading on amines oxidation rate are contradictory. Bello and Idem (2006) studied kinetics of the oxidative degradation of CO_2 loaded MEA. The results showed that the rate of MEA degradation decreases with an increase in CO_2 loading for the MEA- H_2O - CO_2 - O_2 system. This result is consistent with other observations (Goff and Rochelle, 2004; Supap et al., 2006; Supap et al., 2009). The authors concluded that the presence of CO_2 lowers the O_2 solubility because of a salting-out effect and decreasing diffusion coefficient of O_2 . Supap et al. (2006) thought the presence of CO_2 to induce more stable products so that further degradation by reaction with MEA was reduced. Chi and Rochelle (2002) reported the opposite effect of CO_2 loading on MEA oxidation. A dramatic increase in NH_3 production rate was observed in CO_2 loaded solutions as compared to unloaded MEA solutions in the presence of iron as catalyst. It was suggested that the MEA carbamate species was more susceptible to oxidation than free MEA, and the low pH of the solution due to CO_2 loading allowed more iron to stay in solution and catalyze oxidation.

Some researchers quantified degradation rates using amine loss (Bello and Idem, 2006; Supap et al., 2006), while other researchers chose some degradation products as indicators of degradation of amines in their studies, such as measurement of NH_3 evolution rate from the amine solution (Chi and Rochelle, 2002; Goff and Rochelle, 2004) or the change of the concentration of anions produced during the degradation (Rooney et al., 1998). Quantification of the amine degradation rate using different criteria might lead to contrary conclusions. For example, H_2SO_3 , HNO_3 and CO_2 were found to cut down the route to NH_3 formation and instead induced the formation of formate and acetate heat stable salts in MEA solution (Chanchev et al., 2011). Therefore, quantification of degradation rate of amine using loss of amine directly is more reliable if the degradation mechanism is still not fully understood.

2.2.5.2 CO_2 induced condensation reactions

The mechanism of CO_2 induced degradation of traditional alkanolamines at high temperature has been studied by many researchers. DEA degradation in the presence of CO_2 was first studied by Kennard and Meisen (1980, 1985). DEA degradation reactions between aqueous solutions of DEA and CO_2 were carried out in a 600mL stainless steel autoclave at 90 to 205°C with total pressure of 1.5 to 6.9 MPa. MEA was detected in the DEA degraded samples. The principal degradation products were found to be 3-(hydroxyethyl)-2-oxazolidinone (HEOD), N,N,N-tri(hydroxyethyl)ethylenediamine (THEED), and N,N-bis(hydroxyethyl)-piperazine (BHEP). MDEA degradation in the presence of CO_2 was investigated by Chakman and Meisen (1997). It was found that MDEA degrades quite rapidly at elevated temperatures and CO_2 pressures. DEA was found as a product in the degraded samples of MEDA. A degradation scheme was proposed for explaining formation of the products which were identified by GC-MS.

Most of the studies were focused on MEA degradation in the presence of CO_2 since MEA is the benchmark solvent for postcombustion CO_2 capture application. Polderman et al. (1955) found that MEA can be converted to 2-oxazolidinone by heating the carbonate salt of MEA at temperatures encountered in gas treating plants. 2-oxazolidinone converted to N-(2-hydroxyethyl)imidazolidinone (HEIA) in the presence of MEA. The substituted imidazolidinone hydrolyzed to N-(2-hydroxyethyl)ethylenediamine (HEEDA) and CO_2 .

Davis (2009) studied thermal degradation of MEA and MEA blends by reaction with CO₂. The identified main degradation products of MEA are HEIA, HEEDA, MEA trimer, and MEA urea. The product, 2-oxazolidinone is very sensitive to nucleophilic reactions and easily reacts with another amine molecule to give other products, but imidazolidinone is stable and will accumulate.

Lepaumier et al. (2009b) performed a study on CO₂ induced degradation of seven amines degradation and tried to generalize potential pathways based on amine structure. They proposed a general pathway for ethanolamine degradation in the presence of CO₂ as shown in Figure 2.8. Primary amines lead mostly to N-(2-hydroxyethyl)imidazolidinone; secondary amines degrade into addition products and piperazines; tertiary amines mostly demethylate or dealkylate. Steric hindrance of the hindered amines prevents oxazolidinone ring-opening into an addition product, such as in the case of AMP. Therefore, tertiary and hindered amines are more stable than primary and secondary amines.

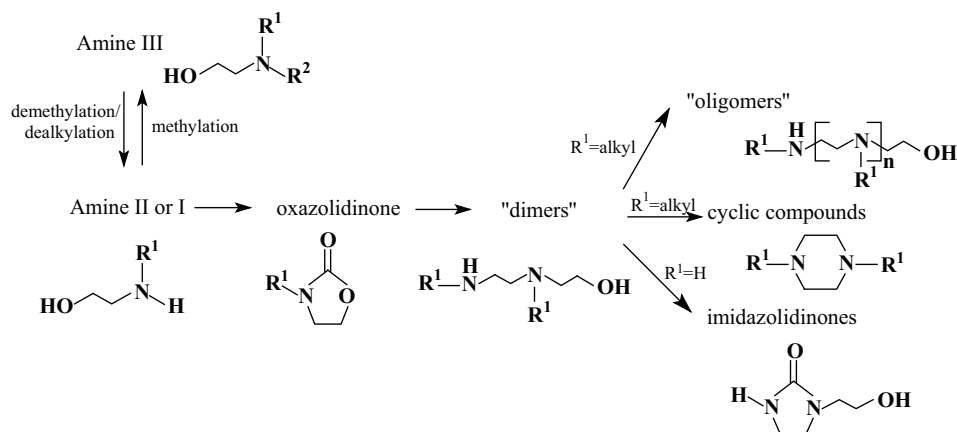


Figure 2.8 A general pathway for ethanolamine degradation with CO₂ (Lepaumier et al., 2009b).

2.4 Prior work on AMP degradation

2.4.1 Studies by the U.S. Army Edgewood Arsenal

An important specialized use of amine is in CO₂ scrubbers for atmosphere purification aboard nuclear-powered submarines. A series of studies concerning amine oxidation have been performed at Edgewood Arsenal by the U.S. Army Chemical Research and

Development Laboratory in 1960s. Dennis et al. (1967) reported oxidative fragmentation of AMP by chlorine dioxide (ClO_2) in phosphate buffer ($\text{pH}=8$) at room temperature to produce ammonia, acetone and formaldehyde. This degradation is unlike the oxidation of monofunctional amines which undergo only carbon-nitrogen scission. Formation of the products of AMP oxidation with ClO_2 seems due to fragmentation by N-C α as well as C α -C β bond scissions.

2.4.2 Studies by IFP

Lepaumier et al. (2009a) investigated oxidative degradation of 4mol/kg AMP aqueous solution at 140°C under 2MPa air in stainless steel reactors. After 14 days, N-methyl-AMP and 4,4-dimethyl-2-oxazolidinone were identified as main degradation products by GC-MS. These degradation products seem not accounted for in the general degradation schemes suggested by the authors. When AMP degraded at 140°C under 2MPa CO_2 , 3,4,4-trimethyl-2-oxazolidinone and 4,4-dimethyl-1-hydroxytertiobutyl-2-imidazolidinone were identified as well as the products produced under 2MPa air (Lepaumier et al., 2009b). In addition to the main products, various carboxylates (formate, acetate, oxalate and glycolate) were found in small amounts. Formate had the highest concentration (2410ppm) among the carboxylates. Nitrite and nitrate were also detected in small amounts (< 200ppm).

It could be speculated that formation of an oxazolidinone maybe due to the presence of CO_2 as well as the high temperature during the degradation experiments. This indicates that despite the steric hindrance, AMP is able to form the 5-membered oxazolidinone structure normally observed in carbamate polymerizations.

2.4.3 Studies by the University of Texas at Austin

To compare the thermal degradation behaviour of PZ with other amines, Freeman et al. (2010b) reported the apparent first order degradation rate constants of CO_2 loaded AMP at 135°C and 150°C. The thermal degradation rate of AMP was faster than PZ, but much slower than MEA. No degradation product was reported in this report.

Sexton (2008) studied oxidation of several amines including AMP. Aqueous amine solutions were batch loaded into 500mL glass jacketed reactors and degraded with 100 mL/min of 98% O_2 /2% CO_2 at 55°C in the presence of Fe^{2+} and Cu^{2+} separately. Mass

transfer was expected to be achieved by strong agitation at 1400 RPM. IC and HPLC analysis revealed that formate was the main degradation product but was still present in low concentration of 3 mM at 287h. This result indicates that AMP is resistant to oxidative degradation but is not 'non-degradable' under the experimental conditions.

Davis (2009) investigated the effect of steric hindrance of AMP on thermal degradation. AMP had the lowest set of rate constants with an activation energy of 31kcal/mol as compared to 2-amino-1-propanol and 1-amino-2-propanol. Due to the steric hindrance, AMP was expected to reduce the stability of the carbamate species which will reduce the likelihood of oxazolidinone formation. A 7m aqueous solution of AMP with a loading of 0.4 mol CO₂/mol AMP was degraded at 135°C. AMP only had slightly over 10% loss after 8 weeks. Imidazolidinone (m/z=187) and amine urea (m/z=205) were identified by IC-MS equipped with an electrospray ionization source. The results indicate that the steric hindrance in AMP does not prevent oxazolidinone formation. AMP does form a carbamate species that can continue to react to form oxazolidinone and the polymerization products in further.

2.4.4 Studies by others

Reza and Trejo (2006) performed an experimental study on the degradation of aqueous solutions of MDEA-DEA-AMP blends, under the presence of CO₂ and H₂S. The experiments were carried out in a stirred tank reactor at an elevated temperature of 200°C. Eight solutions were investigated with 10 wt% DEA, 35 wt% MDEA and varying concentrations of AMP, CO₂ and H₂S. It was found that all of the alkanolamines degraded and AMP was more resistant to degradation than DEA but less than MDEA. The DEA was 90% consumed only 20 hours into the 100 hours experiment and completely degraded by 40 hrs. The AMP was 80% decayed within the first 50 hours as well. The MDEA was 60% consumed by the end of the experiments. Additionally, the DEA and MDEA degradation rate was not a function of AMP concentration and the total AMP degradation was first order with respect to AMP in these experiments. This implies that AMP degradation was independent of the degradation pathway of the other two amines. Degradation products and mechanism were not specified and discussed in this study.

Eide-Haugmo et al. (2011) studied thermal degradation of AMP in the presence of CO₂. The AMP lost 12% after 4 weeks, when a 30wt% AMP solution with a loading of 0.5 mol CO₂/mol AMP was degraded under N₂ at 135°C. This result showed that AMP is less liable

to thermal degradation than MEA. The main degradation products included 4,4-dimethyl-2-oxazolidinone and 4,4-dimethyl-1-hydroxytertiobutyl-2-imidazolidinone which were identified by GC-MS.

2.5 Conclusions

The thermodynamic properties of concentrated AMP and some AMP blends have been examined by many researchers. AMP based solvents, especially PZ or MEA activated concentrated aqueous AMP solvents, appear to be viable solvents for efficient and cost effective CO₂ capture from flue gas streams.

Characterization of solvent degradation potential has emerged as a critical step in the early stages of solvent selection, while a very small amount of data is available in the area of AMP oxidation and thermal degradation. The available literature data have not made the chemical process of AMP degradation clear. On the other hand, although two primary mechanisms, electron abstraction mechanism and hydrogen abstraction mechanism, have been proposed for amine oxidation and widely cited in the literature, they are initiation steps of the radical reactions, neither of them can be used to interpret how oxygen acts during the amine oxidation processes. Understanding the degradation rates and the possible degradation pathways of AMP under oxidative and thermal degradation conditions is the focus of this dissertation. This study should focus on aqueous AMP solution and then extend to aqueous AMP analogs and AMP blends.

Chapter 3 Experimental Apparatus and Analytical Methods

This chapter details the experimental apparatus and methods used to degrade amine solutions at different conditions, as well as all the analytical methods employed to identify the major degradation products, measure the rate of amine loss and the rate of formation of degradation products. Information on apparatus descriptions, operating procedures and data interpretation are presented in detail. Information of the chemicals used including abbreviations, purity, and the commercial source can be found in Appendix B of this dissertation.

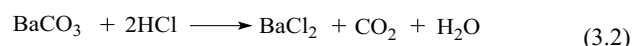
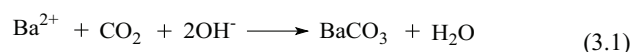
3.1 Amine solution preparation and CO₂ loading

All of the amine solutions in this work were prepared gravimetrically. The water used in this work was provided by a Millipore Milli-Q water purification system. The deionized water was produced at 18.2 MΩ·cm and was degassed at 23°C by a rotary evaporator (Büchi Rotavapor[®] R-210) before amine solution preparation. The concentration of amine, mol/kg, refers to mol amine per kg solution. The amines utilized for degradation studies in this dissertation were of 97-99.99% purity and used as received.

Amine solutions were loaded with CO₂ by sparging pure CO₂ through the solutions inside 500 mL gas washing bottles. The procedure is similar as described in the literature (Hilliard, 2008; Freeman, 2011). Pure CO₂ provided by AGA (Oslo, Norway) traveled through the inlet tube and the fritted disc above the bottom of the bottle. The fritted distributor dispersed the gas into the amine solution. The CO₂ gas flow rate was kept low in order to prevent amine solution from entrainment and heating the solution excessively since the reaction of amine with CO₂ is exothermic. CO₂ loadings are determined by placing the gas washing bottle on a scale while loading the CO₂ and recording the mass difference.

In order to verify the correct loading of CO₂ in solution, initial solutions were also verified with the standard precipitation-titration method (Ma'mun, et al., 2006) in every case. The liquid sample was added to a 250 mL Erlenmeyer flask containing 50 mL of 0.1 M sodium hydroxide (NaOH) and 50 mL of 0.3 M barium chloride (BaCl₂). The amount of the liquid sample was 0.5 to 1.0 gram which depended on the total CO₂ content of the sample.

The mixture was heated and kept at the boiling point for 5 minutes to enhance the barium carbonate (BaCO_3) formation, and then cooled to ambient temperature. The mixture was filtered with a $0.45 \mu\text{m}$ membrane in a filter funnel and washed with deionized water. The membrane, covered by BaCO_3 , was transferred to a 250 mL beaker. 50 mL deionized water was used to wash the filter funnel and transferred to the beaker to make sure that all precipitated BaCO_3 particles were collected into the beaker. 0.1 M hydrochloric acid (HCl) was added in excess (pH=2) to dissolve the BaCO_3 . The solution was heated and kept at the boiling point for at least 5 minutes to ensure that all the CO_2 released. The amount of excess HCl was titrated with 0.1 M NaOH in a titrator (Mettler Toledo T50) with the end of point of pH 7. Two to three parallels and one blind test were done for an identical sample. Equation 3.1 and 3.2 presents the chemistry of the analysis.



The volume of HCl and NaOH added by titration, and the weight of the sample analyzed are used in the calculation of the CO_2 loading (α , mol CO_2 per mol amine) with Equation 3.3 to 3.7.

$$n_{\text{CO}_2, \text{sample}} = \frac{C_{\text{HCl}} \cdot V_{\text{HCl}} - C_{\text{NaOH}} \cdot V_{\text{NaOH}}}{2} \quad (3.3)$$

$$n_{\text{CO}_2, \text{blank}} = \frac{C'_{\text{HCl}} \cdot V'_{\text{HCl}} - C'_{\text{NaOH}} \cdot V'_{\text{NaOH}}}{2} \quad (3.4)$$

$$n_{\text{CO}_2} = n_{\text{CO}_2, \text{sample}} - n_{\text{CO}_2, \text{blank}} \quad (3.5)$$

$$n_{\text{amine}} = C_{\text{amine}} \cdot m_{\text{sample}} \quad (3.6)$$

$$\alpha_{\text{CO}_2} = \frac{n_{\text{CO}_2}}{n_{\text{amine}}} \quad (3.7)$$

Where C_{HCl} is the concentration of HCl solution, mol/L; V_{HCl} is the volume of HCl solution added to dissolve BaCO_3 , mL. C_{NaOH} is the concentration of NaOH solution used for titration,

mol/L; V_{NaOH} is the volume of NaOH solution used for titration, mL; m_{sample} is the mass of the original sample, g; C_{amine} is the concentration of the amine, mol/kg. In this work, the concentration of amine was determined by cation chromatography, see section 3.3.

3.2 Reaction systems

3.2.1 Autoclave reactors

3.2.1.1 Apparatus description

Two kinds of autoclaves were used as batch reactors in this study. One was a 200 mL glass autoclave with stainless steel enclosure ('miniclave steel' type 1/200 mL 10 bar, Büchi Glas Ulster, Switzerland). The reactor was equipped with a magnetic bar and was put into an oil bath. Pressure and temperature were monitored and controlled respectively with a pressure gauge and a thermocouple (Pt1000). This reactor was modified for amine degradation experiments with fitting of tubing and valves for introducing gas and liquid sampling. To ensure that the desired O_2 pressure was maintained throughout the duration of the oxidation experiment, the reduction valve of O_2 source was kept open at a fixed setting. The gas inlet valve was also kept open and a check valve was preset in the gas inlet tubing to prevent the gas mixture flowing backwards. The schematic diagram of the miniclave after modification is shown in Figure 3.1.

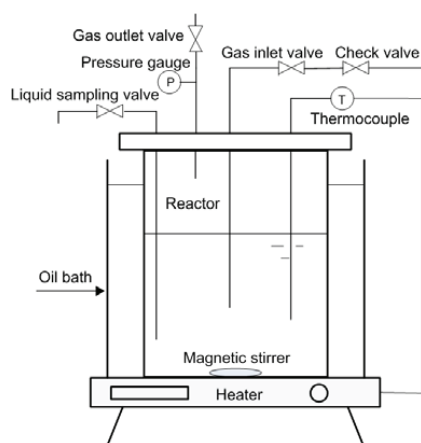


Figure 3.1 Schematic diagram of the 200 mL autoclave reactor.

The second kind of reactor was a 1000 mL glass jacketed autoclave (ecoclave, Büchi Glas Ulster) equipped with a turbo mixer (cyclone 075, Büchi Glas Ulster). The temperature of the solution in the reactor was controlled by a thermostat (Ministat 230, Huber, Germany) using a process control mode. The reactor is shown in Figure 3.2.

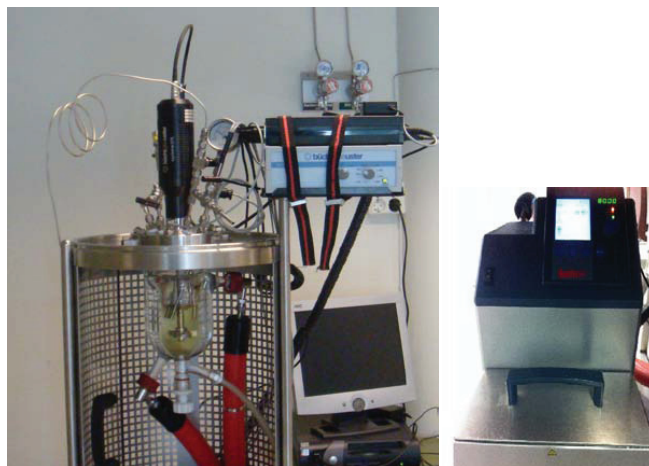


Figure 3.2 1000mL glass jacketed autoclave reactor and thermostat.

3.2.1.2 Experimental procedure

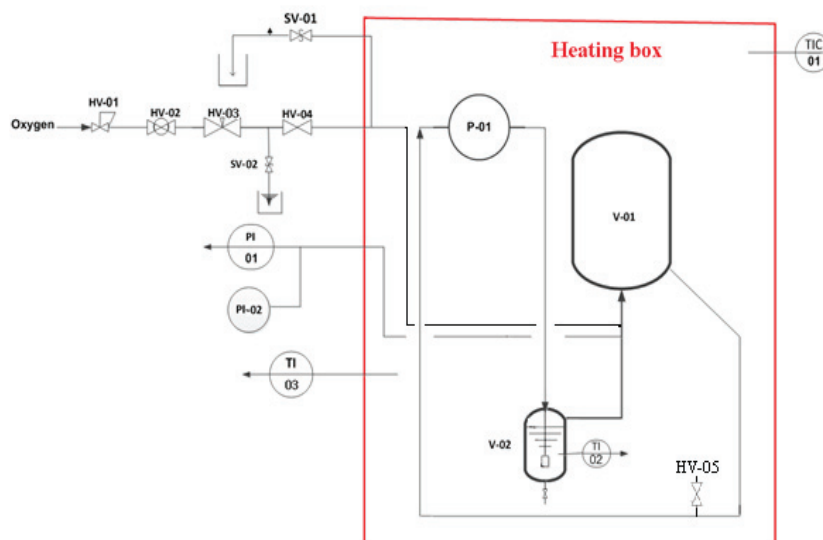
Most of the oxidation experiments in this project were performed in the 200 mL reactor. The experimental procedure of amine oxidation is similar to what is described in reported work (Supap et al., 2001). In a typical experimental run, 140 mL aqueous amine solution was degassed and loaded into the reactor. The solution was stirred at a speed of 200 rpm (a practical speed in the autoclave reactor) and heated to the desired temperature. O₂ was then introduced into the vessel up to the desired pressure through the gas inlet valve. To ensure that the desired O₂ pressure was maintained throughout the duration of the reaction, the inlet valve of O₂ was kept open at a fixed setting. A sample (~ 2 mL) of the reaction mixture was withdrawn from the reactor through the liquid sampling valve at appropriate predetermined intervals. Between sampling times, the tubing was thoroughly rinsed to prevent carryover contamination of the new sample. To avoid further degradation, each sample was quickly quenched by running cold water over the sampling bottle for several minutes, and then it was stored in a refrigerator. The samples were analyzed after each experimental run. Some runs

were conducted twice to check the reproducibility of the experiments. For the thermal degradation experiments, N_2 was introduced into the reactor instead of O_2 .

3.2.2 Circulating closed-batch reaction system

3.2.2.1 Apparatus description

A new closed-batch reaction system was designed and constructed for oxidation of AMP at the temperatures that close to the typical absorber temperatures. The new reaction system is comprised of a 500mL glass reactor, a small pump, a heating box, a data logger, fittings of Teflon and rubber tubing, and valves (see Figure 3.3). The glass reactor was fixed in the heating box. The reaction gas was circulated and bubbled through AMP solution with a fritted filter by the small pump (P-01). A 10L (V-01) glass tank was used as oxygen storage and a surge flask which was set after the reactor and before the inlet of the pump. PI-01, TI-02 and TI-03 were connected to a datalogger (Agilent BenchLink 34972A) to monitor the gas pressure in the system, the temperature of the solution and the temperature in the box, respectively. Compared with the experiments performed in the autoclave, oxygen mass transfer is expected to be improved within this closed system due to oxygen bubbling through the solution continuously.



HV-01: reducing valve; HV-02, 03,05: stop valves; HV-04: needle valve; SV-01, SV-02: one-way valve

Figure 3.3 Circulating closed-batch reaction system.

3.2.2.2 Experimental procedure

1. Purge the system to replace air by O₂

(1) Make sure that valves HV02, HV03, HV04, HV05 are closed. Open the control valve of O₂ resource (HV01) on the wall of the laboratory and adjust the reducing valve to the outlet pressure of 1.0 bar.

(2) Feed 100ml water into a 250ml beaker. Put the plastic tubing at the end of the safety valve (SV02) into the water.

(3) Open valve HV02, open valve HV03 slowly, and then open valve HV04 when the gas bubbles through the water in the beaker. Adjust the valve HV03 slowly till the pressure of 0.1bar is shown on PI02.

(4) Open the valve HV05, and then add a tubing to connect the outlet of HV05 to fume hood in the laboratory. The outlet gas of the tubing is to be collected by a gas bag after a while and the concentration of N₂ in the gas bag is to be analyzed by GC.

(5) When N₂ is replaced by O₂ completely, close the valve HV05, HV04, HV03 and HV02 in this order one by one.

2. Load amine solution

Open the plug cock of the reactor (V02) which connected to the V01. Feed 300ml prepared amine solution into V02 and then close the plug cock.

3. Start heating and bubbling.

(1) Switch on the power on the top of the heating box (Termaks). Set the temperature at 70°C.

(2) Start the data logger and computer. Double click 'Agilent Benchlinck Data Logger 3' on the desktop of the computer to start the data logger program. Click the icon 'Scan and Log Data', and then click the icon 'Start/stop' to start data logging.

(3) Switch on the pump.

4. Supplement oxygen

Check the pressure in the reaction system everyday to make sure that the pressure is around initial value. If the pressure is under the initial pressure, re-introduce O₂ into the reaction system. Feed 100ml water into a 250ml beaker. Put the plastic tubing at the end of the safety valve (SV03) into the water. Open valve HV02, open valve HV03, and then open the valve HV04 after the gas bubble through water in the beaker. Adjust the valve HV03

slowly till the pressure is up to initial value. Close the valve HV04, HV03 and HV02 in this order one by one.

5. Sampling

- (1) Switch off the pump.
- (2) Open the sampling tap carefully and withdraw 2ml solution using a small glass bottle with a plastic cover, and then close the tap.
- (3) Put the glass bottle into a refrigerator and switch on the pump again.

6. Stop experiment

- (1) Switch off the Termaks and the pump.
- (2) When the temperature is close to room temperature, turn off the data logger and shut down the computer.
- (3) Open the valve HV05 to equilibrate pressure.
- (4) Open the sampling tap to unload the amine solution and remove the reaction mixture to amine waste container.
- (5) Clean the reactor with water for several times.

3.2.3 Photochemical reactor

3.2.3.1 Apparatus description

Experiments of UV light initiated oxidation of amines were performed in a photochemical reactor (Applied Photophysics Ltd, UK) which was put into an oil bath. A 125W medium pressure mercury vapor lamp was suspended in a double-walled quartz immersion well. Cooling was provided by circulating tap-water through the double-walled jacket around the lamp. A thin cylindrical reaction vessel was fitted as a sleeve around the well allowing maximum 180 mL of amine solution to spread as annulus in the path of the UV beam. The lamp radiates predominantly 355-356 nm radiation with smaller amounts in the ultraviolet region. The reactor was modified for introducing gas by Teflon tubing and a fritted filter at the bottom of the reaction vessel. One thermocouple was used to control temperature of the oil bath, and another thermocouple combined with a data acquisition system (data logger, Agilent BenchLink 34972A) was used to monitor temperature of the amine solution in the reactor. Figure 3.4 shows setup of the reaction system.



Figure 3.4 UV reactor.

3.2.3.2 Experimental procedure

In a typical experimental run for the UV radiation accelerated oxidation, 130 mL aqueous amine solution was degassed and loaded into the photochemical reactor which was put in an oil bath. The amine solution was stirred by a small magnetic stir bar at a speed of 600 rpm and heated the oil bath to a desired temperature. O₂ was then introduced into the reactor at a flow rate of 50mL/min and was dispersed into the amine solution through the inlet tube and the fritted filter at the bottom of the reactor. The UV radiation was switched on after 10 minutes. The cooling water for protecting the lamp was regulated at an appropriate flow rate. Fine adjusted the temperature of the oil bath according to the temperature of the amine solution. A sample (~ 2 mL) of the reaction mixture was withdrawn from the reactor by a syringe with a long needle at appropriate predetermined intervals. The sample was analyzed immediately after each sampling.

3.3 Cation chromatography

Cation chromatography is the workhorse analytical method used in this work. It was used to quantify the concentrations of remaining amine and produced ammonium in the partially degraded amine solutions.

3.3.1 Apparatus description

The chromatographic system was a DX_500 ion chromatographic analyzer incorporating with a Dionex ICS-3000 isocratic pump. The system includes a LC20 chromatography enclosure, CD20 conductivity detector. A column heater and a thermal controller (Sidewinder temperature controller) used to control the column temperature. A Gilson 231XL sampling injector and a Gilson 402 syringe pump were used for sample auto-injection. The Dionex IonPac SCS1 cation-exchange column (4x250 mm) was used as the analytical column, and the Dionex IonPac SCG1 (4x50 mm) was used as guard column. The IonPac SCS1 column is a hydrophilic, low capacity weak cation exchanger designed for cation determinations using nonsuppressed conductivity detection. The substrate for the SCS1 is silica-based poly and the substrate is coated with carboxylic acid functionalized layer. The SCS1 column can be used with eluents of pH 2-7 and is compatible with typical organic solvents (such as acetonitrile and acetone) at concentrations up to 100% (Dionex, 2003). Chromeleon[®] software was used to control the entire system and analyze the conductivity output.

3.3.2 Analysis procedure

A sample was diluted gravimetrically 2000:1 with Milli-Q water (18.2 M Ω ·cm) and filtered with a 0.45 μ m filter. The filtered sample was inserted into a 2 mL glass sample vial and placed into the Gilson autosampler. The autosampler can hold up to 60 samples and was fully integrated with the Chromelon[®] software. The program was written to inject 800 μ L, in this way, the sample can be injected up to two times, depending on the sequence.

In Chromeleon[®], a sequence was made to direct the cation IC system to analyze the samples of interested. A sequence contained all the information needed for the cation IC to know which method to use, the position of the sample in the autosampler. The sequence also contained the identified name of each sample.

A dilute methanesulfonic acid (MSA) in water was used as the eluent and would elute the cations from the column. The column used in this work is designed for cation determination using non-suppressed conductivity detection and the new pump is an isocratic pump. The method used was titled 'DX_500 new pump.pgm' and is given in Appendix D1. In this method, there was three minutes before each sample, indicated as negative time, which

allows the system to equilibrate after completion of the previous sample in preparation for the current sample. For the analysis of partially degraded AMP sample, the concentration of MSA was 4mM, the flow rate of the eluent was $1.0 \text{ mL} \cdot \text{min}^{-1}$ and the total program lasted for 20 minutes. Piperazine is a cyclic-diamine and hard to elute by MSA. For the analysis of a partially degraded PZ sample, the eluent was 8mM MSA modified with 10% (v/v) acetonitrile.

A typical chromatogram for cation IC analysis of a partially oxidized AMP sample is shown in Figure 3.5. Sodium, ammonium and AMP peaks can be seen at 6.4, 6.9, and 8.8 minutes, respectively. Sodium ion, which might come from the glass reactor, was found in all the samples. Calibration curves were created in order to quantify the concentrations of ammonium and AMP in the original sample. At least six calibration standards were analyzed for AMP and ammonium ions. Standards of AMP and ammonium ion were created in the range of 0.01 to 10 mM. A quadratic regression was used to create the calibration curves. This mM concentration was adjusted using the dilution factor and then converted to mol/kg for reporting.

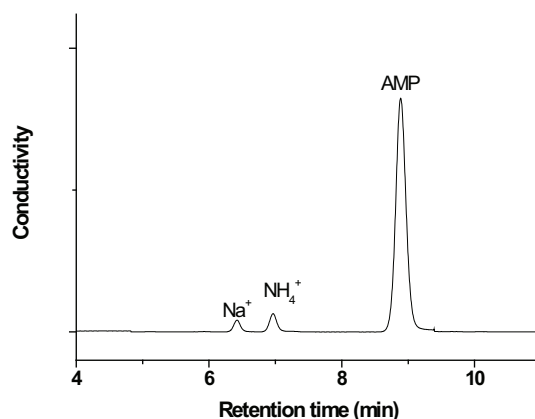


Figure 3.5 A typical cation IC chromatogram of partially oxidized AMP sample.

3.3.3 Analysis error

The primary limitation of the cation IC was the difficulty of accurately quantifying molecules that are very disparate in concentration. For example, most samples analyzed were 3-5mol per kg in AMP while the degradation products were generated in the range of relative

low concentration. The large dilution ratio (more than 1000) needed to quantify AMP lead to the area of the degradation products being minimized.

The error in the measurements will come from two sources, dilution errors and errors in the repeatability of the IC measurement due to changes in the column and injection size and detector conditions. The error introduced from the dilutions will be a function of the accuracy of the balance used, with accuracy to 0,0005g and the amount of sample used in each dilution. In this work, 0.05g of sample was added to 99.95g of water. The relative error in this measurement would be $\pm 1\%$ for the dilution and assuming the error in water addition would be negligible. The error in the cation IC will mainly come from repeatability. The average relative standard deviation in the repeatability of the measurements was less than 1.0% across all concentrations. All of the data points were then used to construct an overall calibration curve for AMP and ammonium on a molar basis which used a linear fit and had an $R^2=0.9996$, The other source of error in the reported data will come in the form of converting the concentration data by weight to molarity measurements. The density of solution was never verified after degradation and was assumed to be constant.

3.3.4 Optimization for simultaneous determination of conventional amines

Determination of ethanolamines is essential for the use of ethanolamine based solvents in post-combustion CO₂ capture from flue gas. A gas chromatographic (GC) technique has been developed and utilised (Kennard and Meisen, 1983; Chakma and Meisen, 1988; Dawodu and Meisen, 1993; Stratisar et al., 2003; Lawal et al., 2005) for analysis of partially degraded aqueous ethanolamine samples. However, water is a difficult solvent for use with the GC method (Poole, 2003) and analysis of high polarity analytes such as MEA is a demanding application (Supap, et al., 2006).

Amine analysis by liquid chromatography is well known (Tanaka et al., 1996; Weiss, 2004; Crea et al., 2005). Alkanolamine analysis by high performance liquid chromatography (HPLC) (Kaminski et al., 2002; Bello and Idem, 2006) or cation-exchange chromatography (IC) (Krol et al., 1992; Kadnar, 1999; Mrklas et al., 2003) has been reported. The reported IC methods in literature were not specifically developed for the analysis of the oxidative degradation alkanolamine samples, and were based on suppressed systems. Although the higher noise and drift generated with a non-suppressed detection results in an order of

magnitude lower sensitivity as compared to suppressed detection (Molnar et al, 1980), non-suppressed conductivity detection does produce linear calibration curves for alkanolamines and ammonium (Dionex, 2003), and does not need suppressor equipment. Furthermore, the degraded alkanolamine samples need to be diluted for IC analysis anyhow, which is different from trace analysis of alkanolamines in environmental water samples.

In this work, an IC method with non-suppressed conductivity detection for simultaneous determination of traditional ethanolamine mixture, MEA, DEA, and MDEA, was developed. A response surface methodology generated with a fractional factorial experimental design involving four factors was applied to optimize the chromatographic conditions. The developed method also can be used to detect volatile amines, such as monomethylamine (MMA) and dimethylamine (DMA).

3.3.4.1 Experimental design

A multivariate experimental design with response surface methodology was implemented and analyzed with the program MODDE 9.0 (Umetrics, Umeå, Sweden). The first step of a multivariate optimization process concerns the choice of the most influential factors. Four variables were varied at three levels in the experimental design: concentration of MSA (MSA, mM), concentration of ACN (ACN, v/v %), pump flow rate (FR, mL·min⁻¹) and column temperature (Temp, °C). Details are given in Table 3.1. The levels were chosen based on some pre-experiments or instrument limits. With this number of parameters and 3 replicates of the centre point, 27 experiments were needed.

One of the objectives was to obtain satisfactory peak shape and well-separated peaks. MEA, MDEA peak asymmetry and ammonium cation-MEA peak resolution were chosen as responses in the design. The reason is that previous experiments had shown MDEA peak shape to be the poorest due to tailing, and ammonium cation-MEA peak separation to be the most difficult.

All experiments were carried out in a randomized order. Multiple linear regression, MLR, was used for calculating the model. The variations in the model were represented by the 95% confidence interval for each model parameter. The fraction of variation of the responses is explained by the model, R^2 , and the fraction of variation of the responses that can be predicted by the model, Q^2 .

Table 3.1 Experimental design.

Experimental	Run Order	MSA Conc. (mM)	ACN Conc. (v/v %)	Temperature (°C)	Flow rate (ml·min ⁻¹)
1	8	2	0	34	0.6
2	12	8	0	34	0.6
3	17	2	8	34	0.6
4	19	8	8	34	0.6
5	27	2	0	44	0.6
6	16	8	0	44	0.6
7	18	2	8	44	0.6
8	6	8	8	44	0.6
9	14	2	0	34	1.4
10	1	8	0	34	1.4
11	9	2	8	34	1.4
12	11	8	8	34	1.4
13	10	2	0	44	1.4
14	3	8	0	44	1.4
15	24	2	8	44	1.4
16	22	8	8	44	1.4
17	21	2	4	39	1.0
18	7	8	4	39	1.0
19	4	5	0	39	1.0
20	20	5	8	39	1.0
21	15	5	4	34	1.0
22	5	5	4	44	1.0
23	23	5	4	39	0.6
24	25	5	4	39	1.4
25	2	5	4	39	1.0
26	13	5	4	39	1.0
27	26	5	4	39	1.0

3.3.4.2 Optimization of IC conditions

The IonPac SCS 1 column is a hydrophilic, low capacity weak cation exchange column designed for cation determination using non-suppressed conductivity detection. This investigation employed isocratic conditions using MSA as eluent. The four variables influencing the separation were investigated and optimized with the program MODDE 9.0. The sample size was fixed at 20 μ L and was not taken as a variable factor in order to increase the sensitivity of the degradation products by using comparatively low dilution ratios.

Performing the experiments according to the central composite face-centred (CCF) design, Table 3.1, produced the conclusion that all factors had a significant effect on one or more responses at a 95% confidence interval. However, three quadratic terms, MSA*MSA, FR*FR, Temp*Temp, and two two-factor interaction terms, MSA*FR, FR*Temp, were observed to have no significant effect on all the responses and therefore excluded in the model. Three-factor or higher interactions were disregarded. The quality of the model calculated was evaluated as shown in Figure 3.6. R^2 shows how well the data from the runs fit the model; Q^2 shows how well the model can predict a certain parameter. The resolution refers to the resolution between the peaks of the ammonium cation and MEA. Asymmetry 1 and Asymmetry 2 refer to the MDEA and MEA peak asymmetry, respectively. R^2 was found to be in our model between 0.916 and 0.973, and the values for Q^2 were found to be between 0.817 and 0.906. High values of both R^2 and Q^2 for all responses show that these responses can be well predicted by the model.

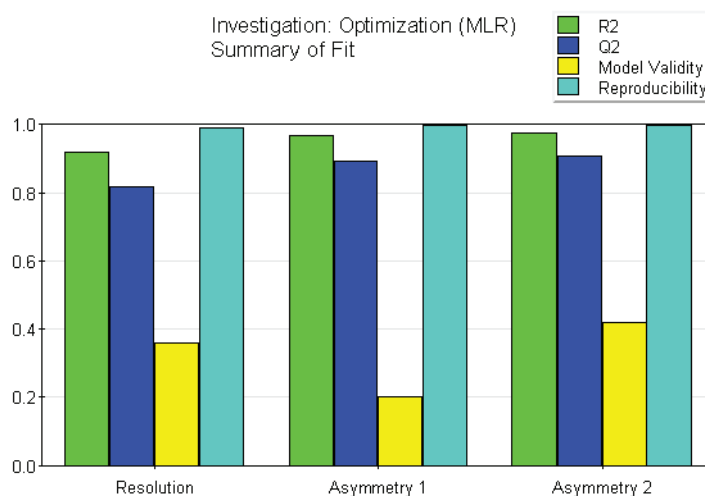


Figure 3.6 Summary of fit of the refined modelling.

Figure 3.7 shows the influence of each variable on the response and correlation coefficient values for statistics with 95% confidence. It can be observed that the concentration of ACN is the most important parameter and that it has a negative effect on Resolution and Asymmetry 1. This indicates that increasing the concentration of ACN will decrease Resolution and Asymmetry 1. Thus although adding ACN will improve the peak shape of MDEA, it will deteriorate the resolution between the peaks of ammonium and MEA.

The concentration of MSA has a slightly negative effect on Resolution and Asymmetry 1, while it has a positive effect on Asymmetry 2. The column temperature has no effect on Asymmetry 2. It only shows a slight negative effect on Resolution and Asymmetry 1. On the other hand, the SCS1 column manual recommends that it is better to operate at temperatures lower than 35°C (Dionex, 2003). However, for elimination of the effect of room temperature fluctuation, the column temperature was fixed at 34°C. The flow rate was found to have only a slight effect on Asymmetry 1.

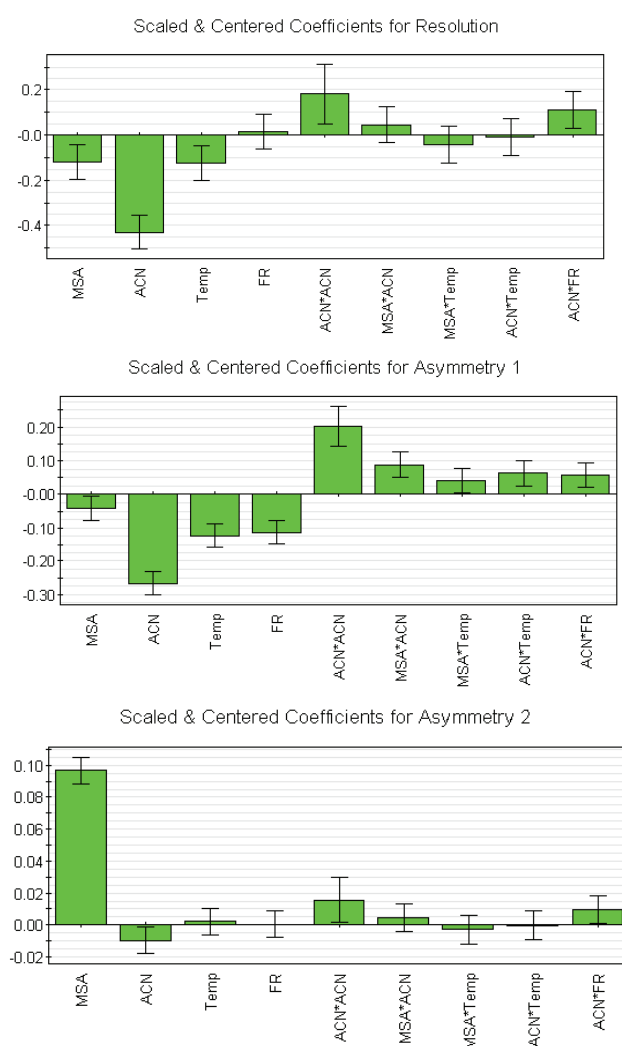


Figure 3.7 Regression coefficient plots obtained after model refinement for Resolution, Asymmetry 1 and Asymmetry 2.

Review of the responses with respect to effect of the parameters allowed prediction of optimal chromatographic conditions for case. Input values of $R_s > 1.5$, and Asymmetry=1 were set as targets for optimization of the parameters (the temperature fixed at 34°C). This optimization was conducted with interpolation because of the instrument limits. Three predictions were run and then compared to the experimental values. Details are given in Table 3.2. Very good agreement is observed between model predictions and experimental results. The resulting chromatogram from the best run is shown in Figure 3.8 (a). It is clear that the ethanolamines and ammonium cation show good peak shape and separation. Although there is no baseline resolution between the peaks of the ammonium cation and MEA, the peak resolution is high enough for quantitative analysis. Retention time of ammonium cation and each of the alkanolamines was less than 5 minutes; this is the reason why retention time was not taken as a response in the experimental design.

Volatile aliphatic amines, such as MMA and DMA, as presumable degradation products of alkanolamines have been put forward in the proposed schemes (Rooney et al, 1998; Lepaumier et al., 2009a), but no confirmation can be found in the literature. Released volatile amines may be harmful to both humans and the environment due to the produced toxic and carcinogenic compounds in sunlight by photo-oxidation in the atmosphere (Karl et al., 2011). The developed IC method also can be employed to monitor the formation of MMA and DMA. The typical chromatogram of standard chemicals is shown in Figure 3.8 (b).

Table 3.2 Calculated results from model prediction, compared to the experimental results for the same input values.

Input values for prediction				Predictions and experimental results					
MSA (mM)	ACN (v/v %)	Temp (°C)	Flow Rate (ml·min ⁻¹)	$R_{s,p} \pm SD$	$R_{s,exp}$	$Asy.1_p \pm SD$	$Asy1_{exp}$	$Asy.2_p \pm SD$	$Asy.2_{exp}$
3.0	1.5	34	1.0	2.36±0.15	2.25	1.77±0.07	1.83	0.74±0.02	0.75
5.0	3.0	40	1.4	1.91±0.13	1.79	1.19±0.06	1.24	0.80±0.02	0.81
8.0*	7.0	34	1.4	1.79±0.20	1.67	1.18±0.09	1.21	0.91±0.02	0.90

*the optimized conditions

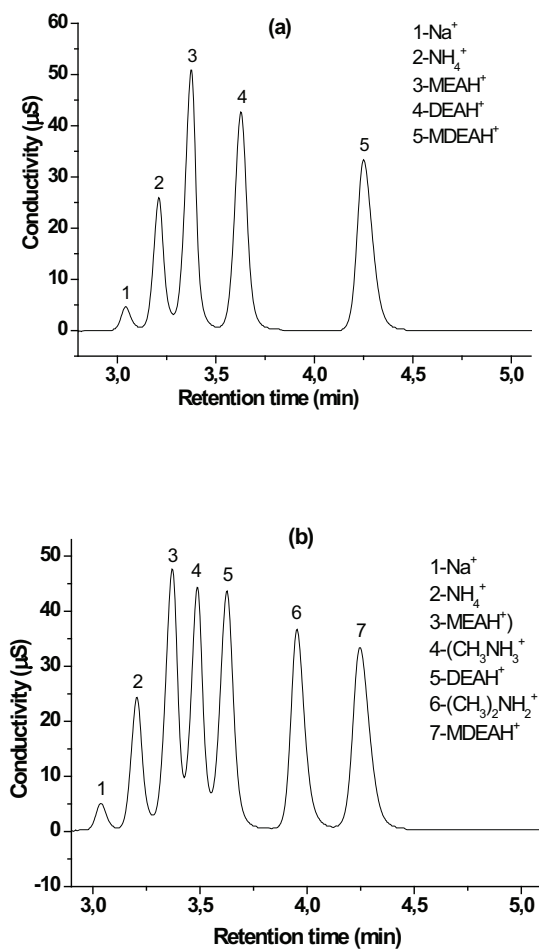


Figure 3.8 Examples of chromatogram for separation of ammonium, methylamine, dimethylamine and alkanol amines using the optimized method. Chromatographic conditions: MSA 8mM, ACN 7.0% (v/v), flow 1.4mL/min, column temperature 34°C.

3.3.4.3 Method validation

The SCS1 column allows simultaneous determination of MEA, DEA, MDEA, MMA, DMA and ammonium ions with non-suppressed conductivity detection. The lower limit of detection (LOD, corresponding to a signal-to-noise ratio of 3) of these ethanolamines and ammonium cation was estimated to be approximately 1.2-4.2 μM (Table 3.3).

Table 3.3 Parameters of cation method calibration.

n=4	LOD/ μ M	Slope	R ²	Range/mM
MEA	2.8	5.464	0.9991	0.01-10.0
DEA	4.2	5.694	0.9997	0.01-10.0
MDEA	3.0	5.684	0.9995	0.01-10.0
NH ₄ ⁺	1.2	4.945	0.9999	0.01-10.0
MMA	2.3	-	-	-
DMA	2.6	-	-	-

The reproducibility of the chromatographic assay was evaluated by injecting standard MEA solution as a representative compound at four different concentrations, in quadruplicate. In Table 3.4, the reproducibility of the IC analysis is represented by the relative standard deviation (RSD) of the peak area. The small RSD values obtained in the experiments are indicative of the overall reproducibility of the method.

Table 3.4 Reproducibility of MEA in a standard solution.

MEA (mM)	Peak Area (AU)	RSD (%)
0.5	2.7341	0.344
1.0	5.5663	0.259
2.5	13.691	0.108
5.0	27.502	0.102

Calibration graphs were obtained by plotting peak area against concentration of ethanolamines and ammonium cation in the range of 0.01-10mM. One of the advantages of using the SCS1 column with non-suppressed detection is that linear calibration curves can be produced for the ammonium cation and ethanolamines. Linear regression values with coefficients of determination larger than 0.999 are presented in Table 3.3. Examination of the results in Table 3.3 indicates that this optimized method can be used for determination of alkanolamines and ammonium ions at mM level for oxidative degradation investigations.

No appreciable change in retention time and separation efficiency was observed after one year of running under these optimized conditions. This demonstrates that the SCS1 column can be used at these conditions for analysis of degraded alkanolamine samples.

3.3.4.4 Method applications

Quantitative determination of the parent amine plays a key role in oxidative degradation studies of ethanolamine solvents for CO₂ capture. The primary aim of this investigation was to develop a rapid, reliable and cost-effective method for quantification of ethanolamines and some degradation products. This newly developed IC method was employed to determine ethanolamine, volatile amine and ammonium ions in the oxidative degradation studies of MEA, DEA and MDEA.

Figure 3.9 shows typical chromatograms of oxidative degraded samples of MEA, DEA and MDEA. The ethanolamines and the ammonium cation were well separated and no significant interference due to other species was observed. The results show that MEA and DEA were degradation products of DEA and MDEA, respectively, which are consistent with the previous reports (Kennard and Meisen, 1985; Chakma and Meisen, 1997). Some unknown peaks of the specific samples have so far not been identified, but it is clear that MMA and DMA were not detected in the liquid phase of the partially degraded ethanolamine solutions. MMA and DMA may escape from the basic ethanolamine solutions to the gas phase due to their alkalinity and volatility. Our experimental equipment did not permit us to quantify the volatile amines in the gas phase of the degraded ethanolamine system. Identification of MMA and DMA in the gas phase was tried to confirm the formation of the volatile amines. The gas mixture was slowly bubbled through dilute aqueous hydrochloric acid (HCl) solutions with high-speed stirring after the degradation experiment stopped. The solutions were subsequently analyzed by developed IC method after neutralization (pH=6.5). Neither MMA nor DMA was detected in the neutralized solutions. The concentrations of MMA and DMA were below detection limits even if they formed during the degradation processes. These results indicate that MMA and DMA may not be primary degradation products as proposed in the schemes for oxidative degradation of ethanolamines (Rooney et al., 1998; Lepaumier et al., 2009a).

The ammonium cation was quantified as a degradation product in both gas and liquid phase of the degradation samples. Figure 3.10 shows the ammonium cation concentration in the liquid phase of the degraded ethanolamine samples. The results show the ammonium cation concentration in the MDEA degradation samples is much lower than that in the degraded MEA and DEA degradation samples; this is due to ammonia being a primary

degradation product of MEA, and MEA being the major degradation product of DEA. However, ammonia was not a primary degradation product of MDEA and DEA. The increasing ammonium cation concentration with increasing reaction time can be explained in terms of increase of ammonia solubility in the MEA and DEA solutions as the gas phase ammonia partial pressure is increased due to its accumulation combined with the pH decrease of the respective solution.

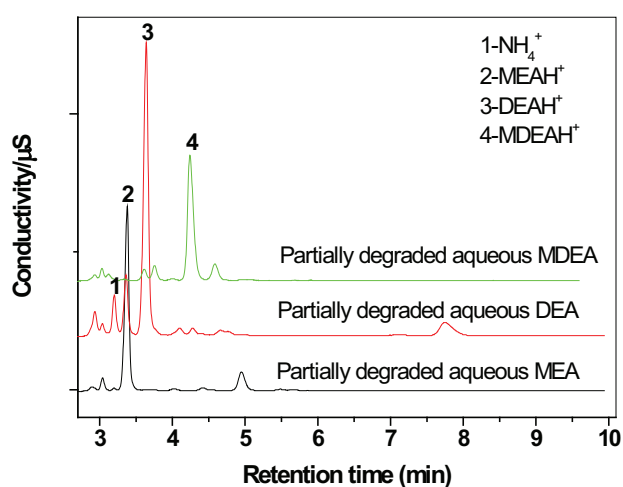


Figure 3.9 Typical chromatograms of partially degraded samples of MEA, DEA, and MDEA.

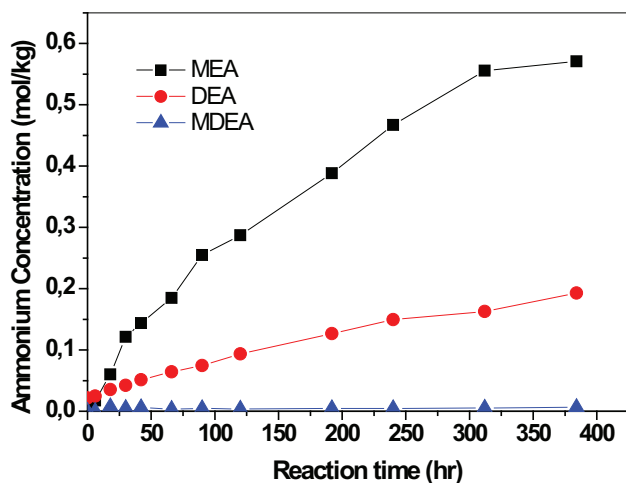


Figure 3.10 Ammonium concentration-time curves for the degradation samples of MEA, DEA and MDEA.

In conclusion, traditional ethanolamines and ammonium cations can be quickly determined at mM levels using non-suppressed detection on an IonPac SCS1 column utilising a mobile phase of methanesulfonic acid containing acetonitrile as organic modifier. The method has been developed and optimized using a fractional factorial design of experiments. Calibration plots for traditional ethanolamines and ammonium cations are linear even up to the concentrations of 10mM. Oxidatively degraded ethanolamine samples were analyzed under optimal system conditions and it was found that degradation products in the samples did not interfere with the quantitative and qualitative analysis of the samples. Monomethylamine and dimethylamine in the partially degraded ethanolamine systems were not detected by the developed method.

3.3.5 Analysis of amino acid

In order to directly detect several amino acids in the degraded amine solutions, such as formation of glycine in degraded PZ, a method based on cation IC was developed. Aqueous solution of 1.3 mM tartaric acid with 1.1 mM pyridine-2, 6-dicarboxylic acid was used as eluent. The operating procedure of the IC and the operating parameters were the same as that for amine analysis which has been described in Section 3.3.2. The target amino acids, glycine and [(2-aminoethyl)amino]acetic acid can be identified by this method.

3.4 Anion chromatography

Anion chromatography was used to quantify negatively charged products in the degraded amine solutions. The types of molecules quantified include carboxylate ions (formate, acetate, oxalate, glycolate, and pyruvate), nitrite and nitrate. Carbonate /bicarbonate were identified at the same time.

3.4.1 Apparatus description

The Dionex anion chromatography system includes a GP50 gradient pump module, EG40 eluent generation module (Serial No. 03120420), DC conductivity module, and LC25 chromatography oven. Attached to the system are a Gilson 231XL autosampler and a Gilson 402 syringe pump, which eliminates the need for manual user injection. The eluent contains varying concentrations of KOH in Milli-Q water (18.2 M Ω ·cm). The separation occurred

using an IonPac AG15 guard column (4×5mm) and an IonPac AS15 analytical column (4×250mm). The IonPac AS15 column substrate is composed of a macroporous resin bead consisting of ethylvinylbenzene crosslinked with 55% divinylbenzene. The anion-exchange layer is functionalized with alkanol quaternary ammonium groups. Dionex Chromeleon[®] software analyzed the conductivity output and controlled the entire system.

The IC system contained a 4-mm Anionic Self-Regenerating Suppressor (ASRS 300) to remove cationic species before anionic species were detected with the conductivity cell. The suppressor comprises of two regenerant chambers and one eluent chamber separated by ion-exchange membranes on opposites of the chamber, as shown in Figure 3.11 (Dionex Corporation, 2009). Electrodes are placed along the length of the regenerant chambers. When an electric potential is applied across the electrodes, the water regenerate chambers undergoes electrolysis to form hydrogen gas and hydroxide ions (OH⁻) in the cathode chamber while oxygen gas and hydronium ions (H₃O⁺) are formed in the anode chamber. Cation exchange membrane allows H₃O⁺ to move from the anode chamber into the eluent chamber to neutralize OH⁻. Sodium ions (Na⁺) attracted by the electric potential applied, move across the membrane into the cathode chamber to combine with the OH⁻ generated at the cathode. Thus the analyte is converted to a more conductive acid form. It should be noted that the eluent used was KOH, not NaOH in this study.

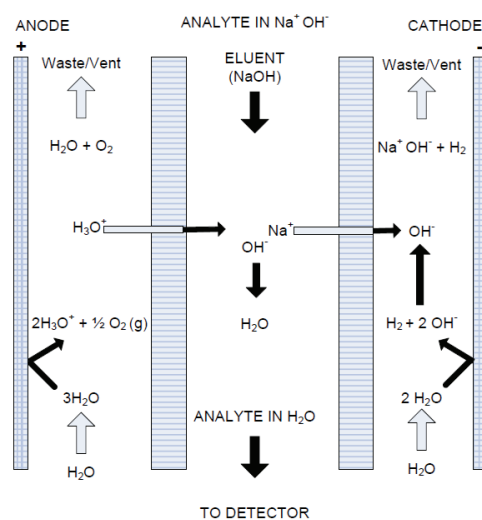


Figure 3.11 Schematic of ASRS 300 in autosuppression mode (Dionex Corporation, 2009).

3.4.2 Analysis procedure

The samples were diluted 50:1 to 200:1 with Milli-Q water and filtered with a 0.45 μ m filter. The filtered sample was inserted into a 2 mL glass sample vial and placed into the Gilson autosampler that holds 60 samples. In Chromeleon[®], a sequence was made to direct the anion IC and analyze the samples of interested. A sequence contained all the information needed for the anion IC to determine which method to use, which sample to inject and an identifying name of each sample.

The experimental sample was introduced from the sample vial via an injection needle in the autosampler. The majority of the sample was flushed through a 25 μ L injection loop to ensure that there is no cross-contamination from a previous sample. The remaining sample was passed through the injection loop and carried by the mobile phase to the inlet of the columns.

A method was used to control the various components of the system as well as adjusting the eluent gradient and setting the overall time for analysis. The method used was titled 'Anion Grad 60mM.pgm' and is given in Appendix D2. In this method, there were eight minutes before each sample, indicated as negative time, which allowed the system to equilibrate to a lower KOH concentration after completion of the previous sample in preparation for the current sample. The eluent KOH concentration over the course of 'Anion Grad 60mM.pgm' is shown in Figure 3.12. At the end of each run of the samples, there was a final sample with the 'Anion Stop.pgm' method. In this method, the suppressor and detector were turned off at time zero. Also, the pump was shut down at time 1min.

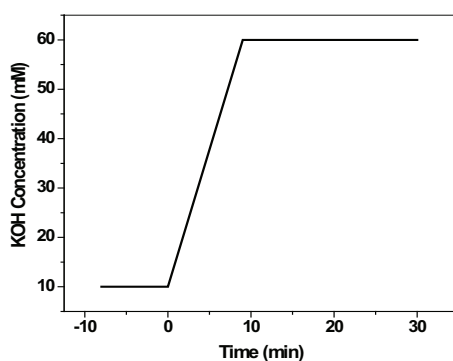


Figure 3.12 KOH gradient in anion IC method.

A typical chromatogram for anion IC analysis of a partially oxidized AMP sample is shown in Figure 3.13. A dominant formate peak can be seen at a retention time of 8.5 minutes. Smaller acetate-, carbonate-, nitrite-, oxalate- and nitrate peaks can be seen at 8.1, 12.2, 12.6, 13.8 and 20.9 minutes, respectively. The peak of glycolate at 7.8 minutes is very small in this “zoomed out” view. Calibration curves were created in order to quantify the concentration of species in the original sample. At least five or six calibration standards were analyzed for each anion of interest. Usually, standards were created in the range of 1 to 50 ppm for anions that are expected in low concentration such as formate, oxalate, nitrate, and so on. A quadratic regression was used to create the calibration curves. The output at the end of analysis was a ppm concentration of each analyte in the dilute sample. This ppm concentration was adjusted using the dilution factor for reporting.

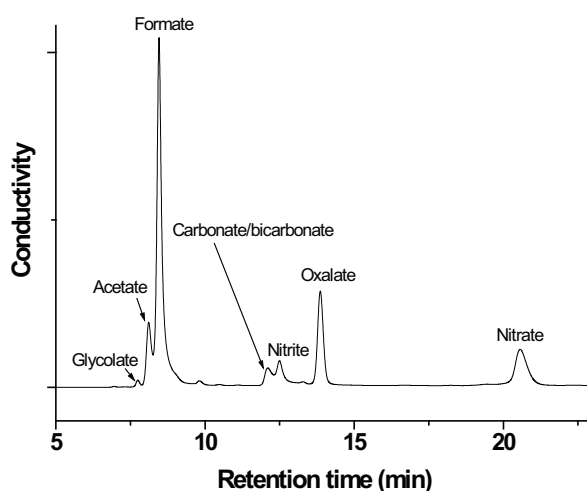


Figure 3.13 A typical anion IC chromatogram for partially oxidized AMP sample.

3.4.3 Analysis error

The error associated with the anion IC method is mainly due to peak area deviation and unsteady baseline. When the baseline was high or had a large bulge in it, all the peak areas calculated were suspect because their areas were decreased from what they would normally be with good separation and a low baseline. When a 6 point standard curve for formate was run in quadruplicate, the average standard deviation across all concentrations was $\pm 4.9\%$. This gives the overall error in the anion IC measurements of $\pm 4.9\%$ which is much larger

than the error associated with the cation IC measurements. The error in making the dilutions is much smaller than in cation IC since a much lower dilution ratio is used. In this case, the error associated with the dilutions will be less than 0.5%.

3.4.4 Sodium hydroxide treatment for amide analysis

Amides are molecules with a $R_1R_2N-R_3C=O$ functionality and are expected products in amine oxidation. Amides themselves are not readily detectable with the techniques employed for amine and carboxylic acid analysis. A base hydrolysis was used to hydrolyze the amide to its corresponding carboxylic acid and amine; the carboxylic acid can be detected by anion IC as described above. This method was employed to analyze the produced amides in degraded amine solvents by Sexton and Freeman (Sexton, 2008; Freeman, 2011).

The procedure for amide reversal was to treat a sample with an equal amount of 5M sodium hydroxide (NaOH). Generally, 0.5 g of each was used and the sample reacted for at least 24 hours before further dilution and analysis. The carboxylic acid released during the amide reversal was then quantified using anion IC. In the present work, some of the degraded AMP and PZ samples were treated by NaOH.

3.5 Gas chromatography-mass spectrometry

Gas chromatography-mass spectrometry (GC-MS) is one of the so-called hyphenated analytical techniques. Gas chromatography separates the components of a mixture and mass spectroscopy characterizes each of the components individually. GC-MS was mainly used to identify degradation products and quantify some major products in this work.

3.5.1 Apparatus description

The GC-MS instrument was an Agilent 7890A gas chromatograph coupling with a 5975C mass spectrometer. An Agilent 7683B automatic liquid sampler was used for sample injection. GC/MSD ChemStation software was used to control the entire system and acquire and process the data.

Two different chromatographic capillary columns were tried in the GC for analyte separation, one polar column, and one non-polar column. The polar column was expected to perform better for separation of polar degradation products in samples, while a non-polar

column was expected to perform better for non-polar products. The polar column was an Agilent Technologies J&W CAM (60 m × 0.32 mm × 1.0 μm) column, having a non-bonded base deactivated polyethylene glycol stationary phase. The non-polar capillary column was an Agilent Technologies J&W DB-5MS Ultra Inert (60 m × 0.32 mm × 1.0 μm) column having a Poly(dimethylsiloxyl)poly (1,4-bis(dimethylsiloxyl)phenyl)siloxane stationary phase. Both of the two columns provided analyte separation, but the non-polar column provided the better separation. Thus the DB-5MS UI column was used as the analytical column for GC separation in the subsequent experiments.

3.5.2 Analysis procedure

The samples were diluted 5:1 to 10:1 with Milli-Q water in terms of the initial amine concentration and degradation time and conditions. The diluted sample was transferred to a 2 mL glass sample vial and placed into the autosampler that holds 8 samples. Click the icon 'GCMS_online' on the desktop of the computer to start the GC/MSD ChemStation. In this ChemStation, a sequence can be made to direct the GC-MS and analyze the samples of interested. A sequence contained all the information needed for the GC-MS to determine which method to use, which sample to inject and an identifying name of each sample.

A method determines all the operating parameters of the GC-MS system. The method used was titled 'GCMS Amine.M' and main parameters are given in Table 3.5. The data were automatically saved in 'GCMS_off Data Analysis' when a method or a sequence was run. A typical chromatogram for partially degraded AMP sample is shown in Figure 3.14. A number of degradation products can be seen except for AMP and water.

Most compounds will fragment in a unique mass pattern with a certain ionization method. This unique mass pattern can be compared to the fragment pattern of standards available in an electronic library. Using a computer matching technique, the mass fragmentation patterns of the GC-separated analytes were compared with the standards available in the National Institute of Standards and Technology (NIST) library. The library match feature provides a list of probable compounds that match the mass of the parent analyte, based on the fragmentation pattern of the parent compound. Each compound on the list of matches is assigned a probability for an exact match. In some cases, the match with high match probability does not mean that this probable compound must be the parent

compound, since the NIST library returns many different compounds with the same mass. Therefore, in this work, computer fitting of the mass spectrum to the mass spectra database (MS Search 2.0) was used for initial product identification. Verification of the species was subsequently performed by comparing both the mass spectra and the GC retention time of commercially available pure standards with those of the initially identified compounds.

Table 3.5 Operating parameters of GC-MS.

1. Inlet	
type	split/splitless, in split mode
temperature	250 °C
pressure	12.8 PSI
split ratio	50:1
2. GC Oven	
initial temperature	110 °C
initial temperature hold time	1 min
ramp rate	5 °C/min
final temperature	220°C
final temperature hold time	10 min
Total run time	33min
3. Carrier gas	
type	UHP-grade helium
flow rate	1.5 mL/min
4. MSD parameters	
interface temperature	250 °C
EM voltage	1200 V
quad temperature	150 °C
source temperature	230 °C
5. Injector	
water washes before injection	3 times
sample washes	3 times
water washes after injection	3 times
injection volume	0.2 μ L
syringe size	10 μ L

For estimating relative concentration, some of identified degradation compounds were quantified in SIM mode, which means that the three main ions for each product were selectively chosen with the MS detector to enhance the sensitivity and confidence of the quantification. The calibration curves were obtained from commercial standards at different concentrations and performed before analysis of the degraded sample. Due to commercial unavailability of 4, 4-dimethyl-2-oxazolidinone, the estimation of its concentration was based on a standard with a similar chemical structure, 2-oxazolidinone.

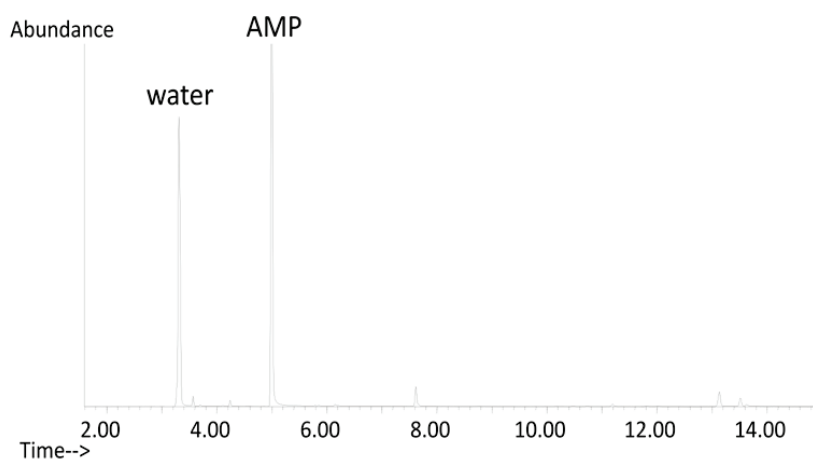


Figure 3.14 A typical GC-MS chromatogram for partially degraded AMP sample.

3.5.3 Analysis error

As mentioned in Section 3.3.4, the GC technique has been developed and utilised for analysis of partially degraded aqueous ethanolamine samples by a number of investigators. However, water is a difficult solvent for use with the GC method and analysis of high polarity analytes is a demanding application. The quantitative analysis of GC-MS was only employed to estimate some uncharged degradation products of AMP.

The error of GC-MS analysis was mainly due to peak area deviation and unsteady baseline. The uncertainty of quantification with GC-MS was $\pm 10\%$. The error of GC-MS analysis was estimated on standard deviation of peak areas across all concentrations.

3.6 Other analytical method used

3.6.1 Fourier transform infrared spectroscopy

Several other analytical methods were also used in this work. The first one is Fourier transform infrared spectroscopy (FT-IR), which was used to measure evolution rate of NH_3 from AMP aqueous solutions.

In Chapter 2, NH_3 has been shown to be the primary amino group degradation product for primary amines and therefore was used to quantify the relatively oxidative degradation rate of AMP in this study. The two sharp absorption peaks at 934 and 965 cm^{-1} are from the inversion transition of the ammonia hydrogen atoms and are the primary peaks used in the IR analysis of NH_3 (Goff, 2005). The absorption spectra from IR radiation can be used quantitatively to determine concentration of a compound using the Beer-Lambert law (Equation 3.8). Transmittance, T , is defined as the fraction of radiation that passes through the gas. Absorbance, A , is the logarithm of the inverse transmittance, and is proportional to a constant, the optical path length, and the concentration of the species in the gas sample. The molar absorptivity, ϵ , is unique for each molecule and each wavelength. In this work, the absorbance of the peak at 965 cm^{-1} was used to indicate the relative NH_3 concentration directly. Since no calibration was made due to the mirror in the gas cell being damaged during this project.

$$A = \log\left(\frac{I_0}{I}\right) = \log\left(\frac{1}{T}\right) = c l \epsilon \quad (3.8)$$

Where: A = absorbance

I_0 = incident radiation intensity

I = intensity of radiation after contacting sample

T = transmittance

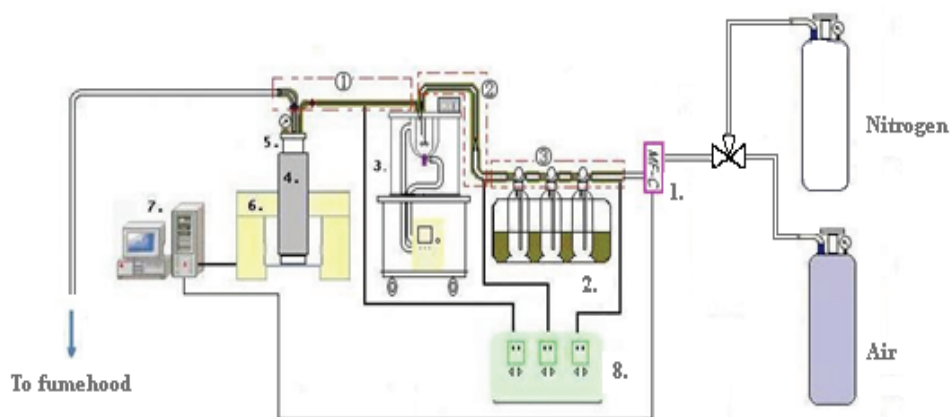
c = concentration of species in the sample

l = length of the light path through the sample in centimeters

ϵ = molar absorptivity, dependent on wavelength

Figure 3.15 shows the overall flow diagram and the experimental setup. The three flasks were used as pre-saturators to minimize the possibility of water loss of AMP solution in the reactor caused by the gas flow. The flow system was capable of sparging N_2 or air into a

1000mL jacketed glass reactor (Büchi Glas Ulster, Switzerland) equipped with a turbo mixer. The temperature of AMP solution in the reactor was controlled by a thermostat (Ministat 230, Huber, Germany). The system operated in a batch mode for the liquid phase. The flow rate of the inlet gas was controlled by a Bronkhorst High-Tech mass controller (model F-200CV). The inlet gas stream was pre-saturated and heated to desired temperature. The exit gas from the reactor was heated to eliminate water vapour condensation in the tubing leading to a PerkinElmer Spectrum One FT-IR spectrometer. PerkinElmer Spectrum and Timebase software were used to control the entire FT-IR system and acquire and process the data.



(1. Mass-flow controller; 2. Pre-saturator; 3. Autoclave; 4. Sirocco heating jacket with controller; 5. Gas cell; 6. FT-IR; 7. Computer; 8. Controller of heating belts. ①②③: Heating belts)

Figure 3.15 Experimental flow diagram for FT-IR based reaction system.

For a typical experimental run, 500mL AMP aqueous solution was fed into the autoclave with an agitation speed of 300 rpm. Temperatures of oil bath both for the pre-saturators and the autoclave were set at the same value. Gaseous sample left the autoclave and then went into the gas cell by passing a stainless steel tube that was heated up to 140°C, which is the upper limit of temperature tolerance of the heating belt. The set point of the heating jacket for the gas cell was 200°C to make sure that no vapour condensation occurs inside the gas cell. 0.1 L/min nitrogen was bubbled through the system after all the temperatures increased to the respective set point. Started to run PerkinElmer Spectrum and Timebase software and then scanned the background. When the IR background was stable,

0.1 L/min air was bubbled through the AMP solution and the gas cell was scanned by FT-IR every 2 minutes.

A typical IR spectrum of the gas phase is shown in Figure 3.16. The spectrum is consistent with the ammonia standard IR spectrum (Figure 3.17). The two sharp absorption peaks at 934 and 965 cm^{-1} can be used as the primary peaks in the IR analysis of NH_3 , which is taken as a degradation indicator of AMP. The peak at 965 cm^{-1} was used as the primary peak for semi-quantitative analysis of evolution of NH_3 from the AMP solutions in this work.

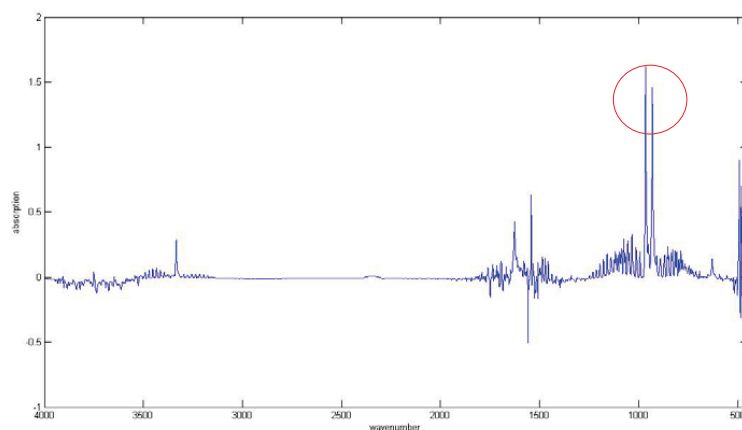


Figure 3.16 A typical FT-IR spectrum for the gas phase of AMP degradation system.

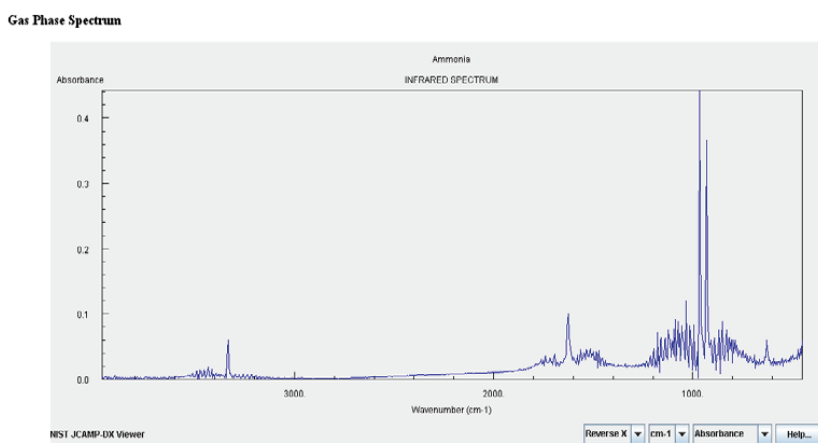


Figure 3.17 Standard spectrum for NH_3 (source: NIST/EPA Gas-Phase Infrared Database).

3.6.2 Ultraviolet-Visible spectroscopy

Ultraviolet Visible Spectroscopy (UV-VIS) was only used to check formation of 2, 4-lutidine in this work. The UV spectrophotometer was Shimadzu UV-1800 (Japan). UV-VIS spectra were recorded between 200-400 nm using a 1-cm path-length quartz cell, and pure water was used as the reference.

Chapter 4 Thermal Degradation of AMP

This chapter will be used to outline a possible pathway for AMP thermal degradation that based on the identified main degradation products and the relevant information in literature. Degradation rate measurements will also be given based on varying CO₂ loading.

4.1 Introduction

Solvents can spend over one-third of residence time of an industrial system above 100°C. Thermal degradation of an amine for post-combustion CO₂ capture is crucial in solvent selection. Thermal degradation in the stripping section of a CO₂ capture system will reduce solvent absorption capacity and increase the cost of amine replacement and disposal. Thermal degradation can also result in environmental issues relating to the unknown health effects and reactivity of many of the volatile products (Nguyen et al, 2010; Karl et al, 2011).

As reviewed in Chapter 2, CO₂ could lead to degradation of ethanolamine at elevated temperatures. Figure 4.1 shows the proposed reaction pathways for MEA thermal degradation in the presence of CO₂. MEA reacts with CO₂ to form MEA carbamate and that carbamate could form 2-oxazolidinone (OZD) through a dehydrolysis step. The OZD is very reactive and easily reacts with another MEA molecule to form an addition compound, N-(2-Hydroxyethyl)ethylenediamine (HEEDA). This ethylenediamine can be transformed into corresponding polyaddition compounds, MEA trimer and oligomer, or hydroxyethyl-imidazolidinone (HEIA) in further.

In order to assess the thermal degradation of aqueous AMP as it applies to CO₂ capture process, thermal degradation experiments were conducted on concentrated, aqueous AMP solutions. The thermal degradation includes the degradation caused by heat only and the degradation induced by CO₂ termed carbamate polymerization. Main degradation products are identified and compared to the MEA degradation pathways.

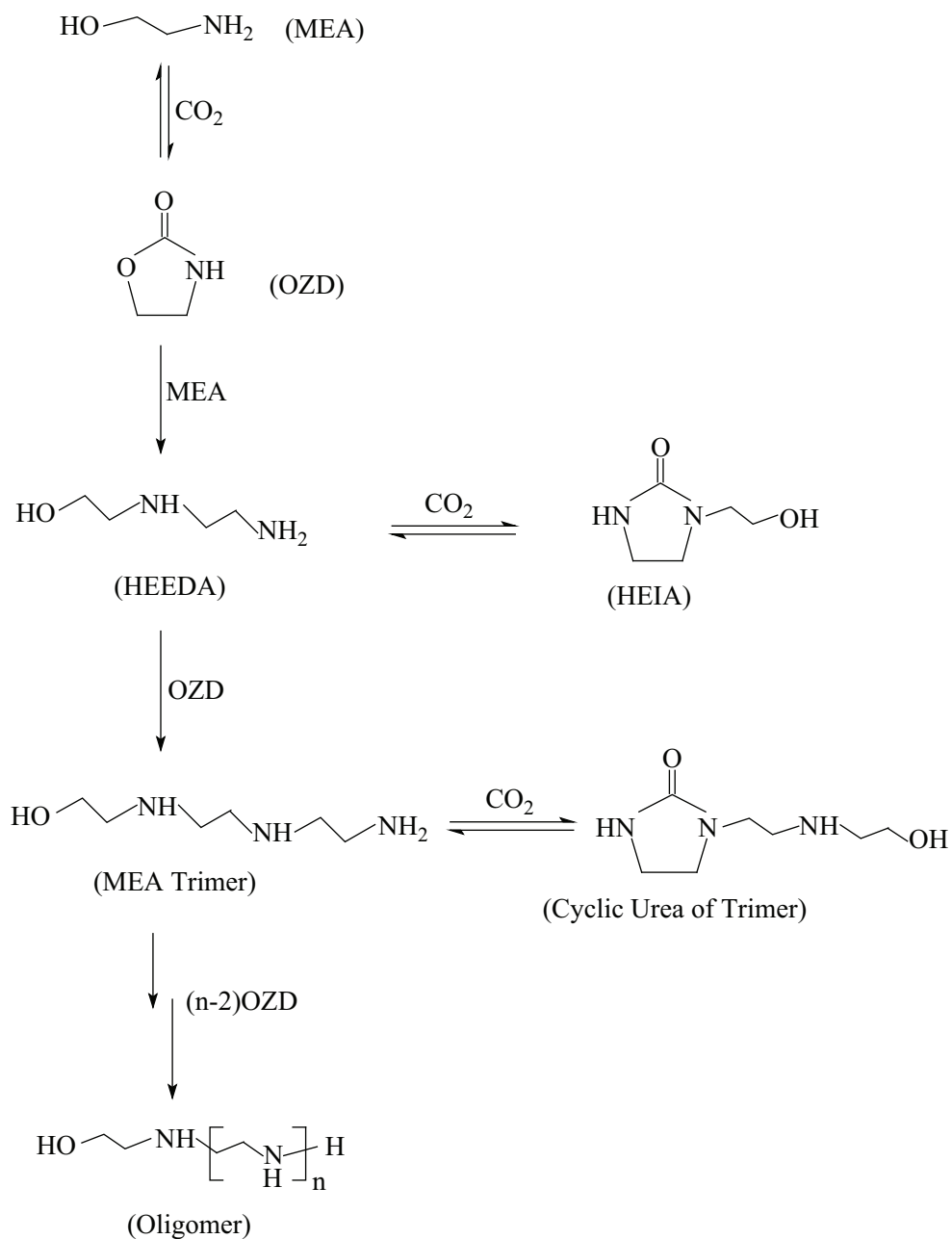


Figure 4.1 MEA thermal degradation pathways (adapted from Davis, 2009).

4.2 Thermal degradation without CO₂

Thermal degradation without loading of CO₂ was studied to know the contribution of degradation only due to temperature without any gas (CO₂ or O₂). The thermal degradation of unloaded AMP has been examined with experiment performed on 4 mol/kg AMP (mol/kg solution, the same hereinafter) at 140°C (Lepaumier et al., 2009b). No measurable AMP loss was detected within 15 days. The thermal degradation of aqueous AMP without CO₂ loading was examined again in the present work and the experimental duration was extended to 4 weeks. The experiments were carried out by heating 5 mol/kg AMP solutions under a blanket of nitrogen at 120°C and 140°C, respectively. Thermal degradation of AMP and generation of degradation products were tracked during the course of the experiments. The AMP loss was difficult to determine due to the very low overall degradation rate in this case. As can be seen in Figure 4.2, the observed AMP loss was very little at 120°C and 140°C. The formation of degradation products was minimal over 4 weeks. This result shows that the thermal degradation of AMP without CO₂ loading can be disregarded, at temperatures less than 140 °C. And therefore, thermal degradation of AMP only caused by heat was not taken into account in the later experiments.

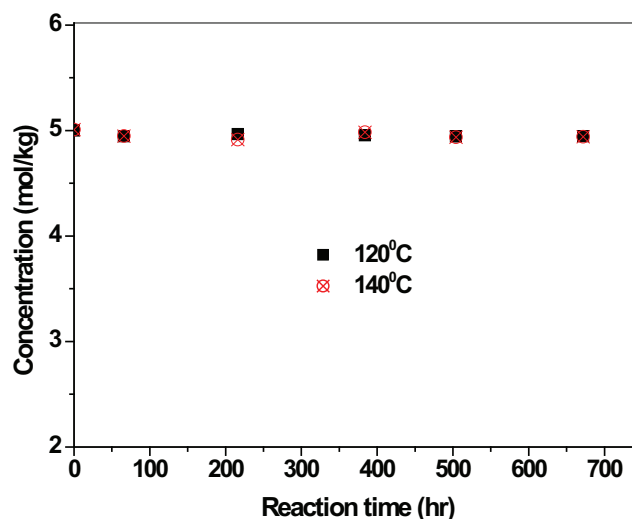


Figure 4.2 Changes in AMP concentration versus time (initial concentration of AMP = 5 mol/kg). Studies were conducted under nitrogen at 120 and 140 °C.

4.3 Thermal degradation in the presence of CO₂

Although aqueous AMP is stable at less than 140°C under the blanket gas of N₂, in previous work (Lepaumier et al, 2009b), it has been found that CO₂ is a strong catalyst for thermal degradation of AMP. In that investigation, the degradation experiments were conducted using a 4 mol/kg AMP aqueous solution at 140°C. AMP loss was up to approximately 21% after 15 days, when a 2MPa CO₂ pressure was added to the initial vapour pressure. The thermal degradation rate of CO₂ loaded AMP was faster than piperazine (PZ), but much slower than MEA (Freeman et al, 2010). Davis (2009) screened various structure analogs of MEA including AMP to test the effects of chain length and steric hindrance on thermal degradation. All of the tested amines were loaded with CO₂ to a loading of 0.4 mol of CO₂/mol of amine in that work. The ability of increased temperature to accelerate AMP degradation has been observed. The previous studies of thermal degradation of AMP have not significantly varied CO₂ loading to investigate the effect of CO₂ loading. To further explore the thermal degradation of AMP, the effect of CO₂ loading on AMP thermal degradation was examined with experiments performed on 4.75 mol/kg AMP at 135 °C (slightly above normal stripper temperatures). AMP loss was measured and the degradation products were identified by GC-MS and IC. The possible degradation pathway is discussed in terms of the identified products and compared to that for MEA.

4.3.1 Degradation rate

Davis (2009) determined that degradation of MEA was approximately first order in CO₂ concentration as a doubling of MEA loss with an increase of CO₂ loading from 0.2 to 0.4 mol CO₂/mol amine with 7 m MEA (m: mol amine/kg H₂O, the same hereinafter) at 135 °C was observed. The effect of CO₂ on AMP thermal degradation has not been studied previously, but it was hypothesized to follow the similar trends found with MEA.

In this work, 4.75 mol/kg AMP solutions with two initial CO₂ loadings were degraded for 5 weeks under nitrogen at 135 °C, respectively. The plot of AMP loss percent against reaction time is shown in Figure 4.3. As can be seen in Figure 4.3, AMP loss was 3.8% at a loading of 0.15 mol CO₂/mol AMP at 135 °C over 5 weeks. The AMP loss increased to 5.5% when the initial CO₂ loading increased to 0.3 mol CO₂/mol AMP. The amount of AMP loss

increased with increased CO₂ loading as expected. However, AMP loss was not doubled with an increase of CO₂ loading from 0.15 to 0.3 mol CO₂/mol AMP.

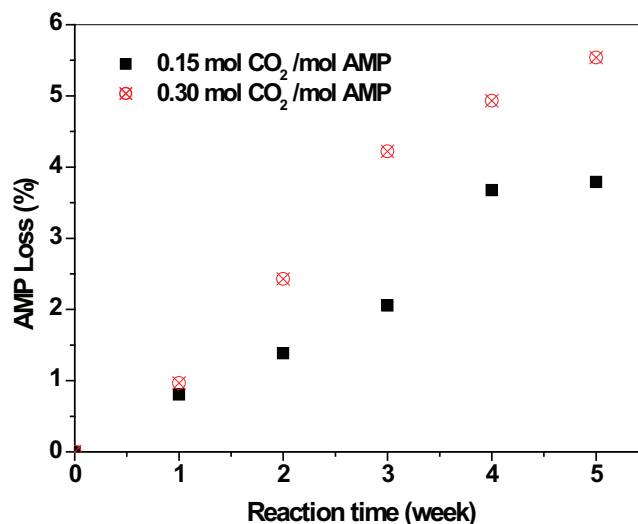


Figure 4.3 AMP loss percent versus time (initial concentration of AMP = 4.75 mol/kg). Studies were conducted under nitrogen at 135 °C.

Data for the thermal degradation of CO₂ loaded AMP solutions suggested that AMP loss could be represented with a first order rate law. Thus, the degradation behaviour would follow Equation 4.1:

$$-\frac{dc_{AMP}}{dt} = k_1 c_{AMP} \quad (4.1)$$

Where c_{AMP} is the concentration of AMP solution, k_1 is the pseudo first order reaction rate constant. Solving this equation yields the following for c_{AMP} in terms of time (t) with a constant (k_1) of integration equal to the initial AMP concentration, $c_{AMP,0}$ (Equation 4.2).

$$\ln\left(\frac{c_{AMP}}{c_{AMP,0}}\right) = -k_1 t \quad (4.2)$$

Equation 4.2 provides a relationship for the concentration of AMP with time and allows the determination of an apparent first order rate constant. Using the raw data, the calculated first

order rate constant of k_1 was 13.1×10^{-9} and $18.6 \times 10^{-9} \text{ s}^{-1}$ for the initial CO_2 loading of 0.15 and 0.3 mol $\text{CO}_2/\text{mol AMP}$, respectively.

Freeman et al. (2010) have reported that the apparent first order rate constant for solution of 7m AMP ($\sim 4.3 \text{ mol/kg}$) with an initial loading of 0.4 mol $\text{CO}_2/\text{mol AMP}$ was $21 \times 10^{-9} \text{ s}^{-1}$ at $135 \text{ }^\circ\text{C}$. The apparent first order rate constants with three different CO_2 loadings at $135 \text{ }^\circ\text{C}$ are plotted in Figure 4.3. It was found that the first order rate constants of AMP with three CO_2 loadings increased linearly as the CO_2 loading increased (ignored the slight difference between the initial AMP concentrations). The thermal degradation of AMP with high CO_2 loading was not investigated in this work due to the pressurization restriction of our glass autoclave reactors.

For comparison, the apparent first order reaction rate constant of thermal degradation of 5 mol/kg of MEA with an initial CO_2 loading of 0.4 mol $\text{CO}_2/\text{mol AMP}$ is also shown in Figure 4.4. It is clearly that although CO_2 under high temperature can lead to AMP degradation, the AMP solution is up to almost 7 times more resistant to thermal degradation than 5 mol/kg MEA solution (30 wt%) at $135 \text{ }^\circ\text{C}$.

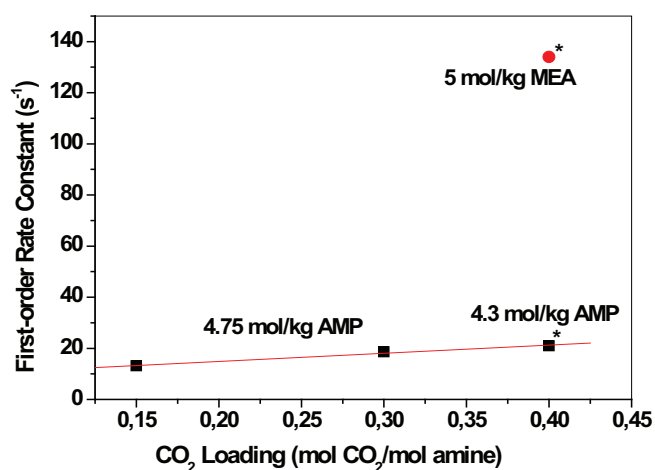


Figure 4.4 Apparent first order rate constants for AMP and MEA at $135 \text{ }^\circ\text{C}$. (*Freeman et al., 2010)

4.3.2 Degradation product identification

GC-MS was employed to identify the non-ionic degradation products that were formed during the AMP thermal degradation process. Three of the main degradation products were identified by GC-MS method. A typical GC-MS chromatogram for the thermally degraded AMP sample is shown in Figure 4.5.

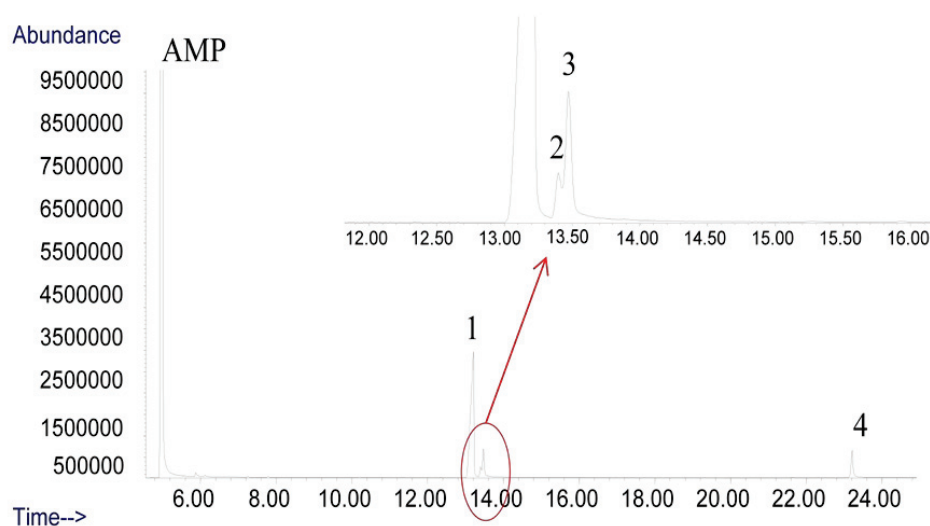


Figure 4.5 Chromatogram of a 4.75 mol/kg AMP aqueous solution with a loading of 0.3 mol of CO₂ per mol AMP held at 135 °C for 5 weeks. In addition to AMP, the products were identified as DMOZD (peak 1), AMPAMP (peak 2), unknown (peak 3), DMHTBI (peak 4).

Computer fitting of the mass spectrum to the mass spectra database (NIST MS search 2.0) was tried to identify the main products in the thermally degraded AMP samples. The identification was followed by the use of standards (if commercially available) to confirm the identification of the components in the samples.

One of the major products observed in the thermally degraded AMP aqueous solutions was 4, 4-dimethyl-2-oxazolidinone (DMOZD, peak 1). The confidence of the mass fragmentation pattern of DMOZD in the degradation samples matched that documented in the mass spectrometer database was by 78%. The spectrum of the identified DMOZD in the

degraded sample and the spectrum of DMOZD in the database are shown in Figure 4.6. As can be seen in Figure 4.6, the mass fragmentation pattern of DMOZD in our samples matched that documented in the mass spectrometer database. However, this identification was not confirmed by an authentic standard since DMOZD is not commercially available.

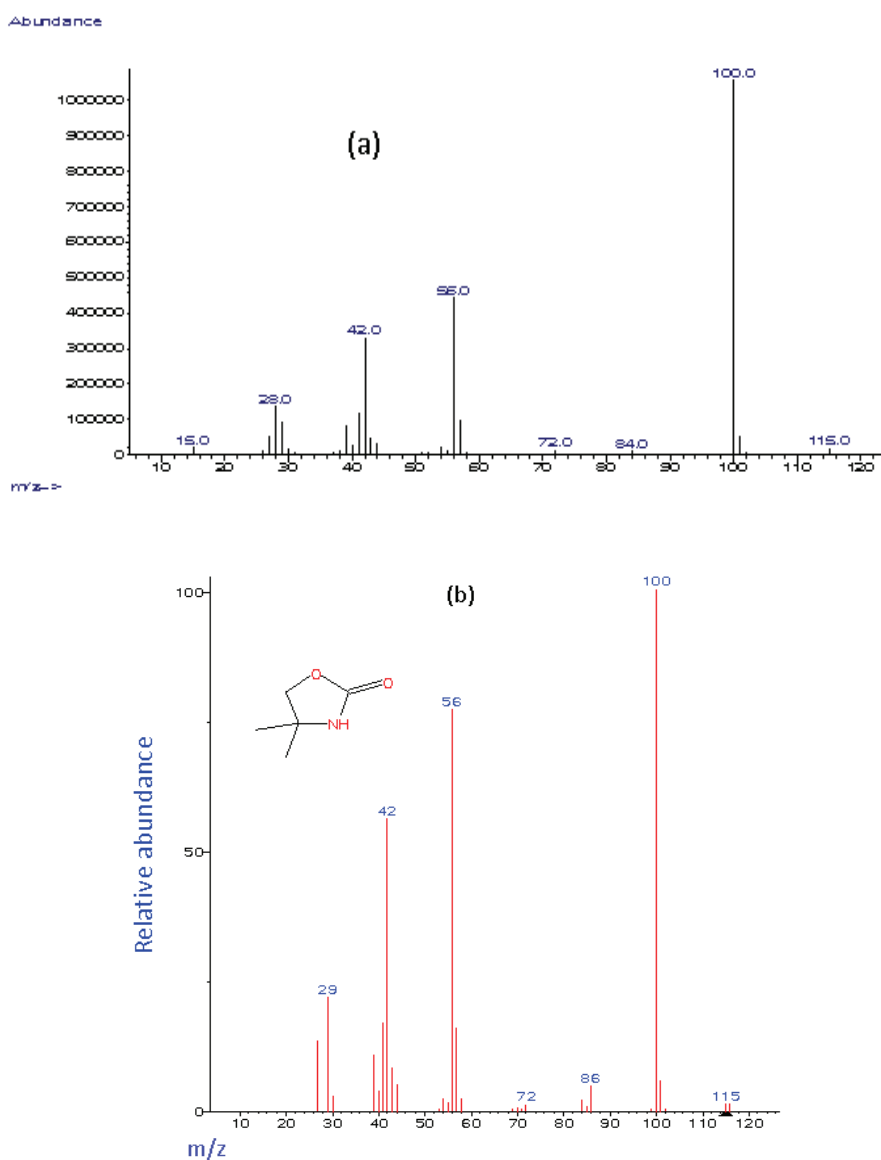


Figure 4.6 (a) Mass spectrum of the compound identified as DMOZD in a 4.75 mol/kg AMP aqueous solution with a loading of 0.3 mol of CO_2 per mol AMP held at 135 °C for 5 weeks; (b) Mass spectrum of DMOZD in NIST database.

The confidence of computer fitting of the mass spectra of peak 2, 3 and 4 (Figure 4.4) to the mass spectra in the database was very low (less than 20%). It is probably due to exclusive of the mass spectra of these three compounds in the database. Thus the mass spectra of these formed products of the current amine thermal degradation with CO₂ cannot be matched.

The ionization source in mass spectrometer used in this work was an electron impact ionization source (EI). This ionization process often follows cleavage reactions that give rise to fragment ions which, following detection and signal processing, convey structural information about the analyte. But EIMS does not exhibit a molecular ion peak of the analyte, if the analyte is a relatively heavy molecule, a high polar molecule, or a molecule with low thermal stability.

Since the degradation products are amine derivatives, they could be polar molecules and have relatively big molecule mass. We therefore may not find the molecular ions from the mass spectra. However, we can analyze the fragment ions in the spectra to identify the possible products. Figure 4.7 (a) shows the mass spectrum for the peak 2 at 13.4 min in the Figure 4.5. According to the analysis of the fragment ions of the spectrum, the peak at 13.4 min might be 2-[(2-amino-2-methylpropyl) amino]-2-methyl-1-propanol (AMPAMP). This identification was confirmed by authentic standard 2-[(2-amino-2-methylpropyl) amino]-2-methyl-1-propanol. The standard was supplied by Aldrich[®] (Milwaukee, USA), and the product number was S347027. This standard was diluted with Milli-Q water and run on GC-MS at the identical conditions as that for the AMP degradation samples. Figure 4.7 (c) shows the gas chromatogram of the standard aqueous AMPAMP. As can be seen from Figure 4.7 (c), there were some impurities in the standard solution or the standard was not very stable in the GC conditions that resulted in some small peaks except for the main peak, however it does not affect the confirmation. The predominant peak at 13.4 min should be AMPAMP, and the corresponding mass spectrum is shown in Figure 4.7 (b). The retention time of the standard was 13.4 min, which is the same as that of the identified peak. On the other hand, the main ion peaks in the mass spectrum of the identified peak are consistent with those of the authentic standard. Therefore, the identification of AMPAMP in the degradation samples of AMP is reliable.

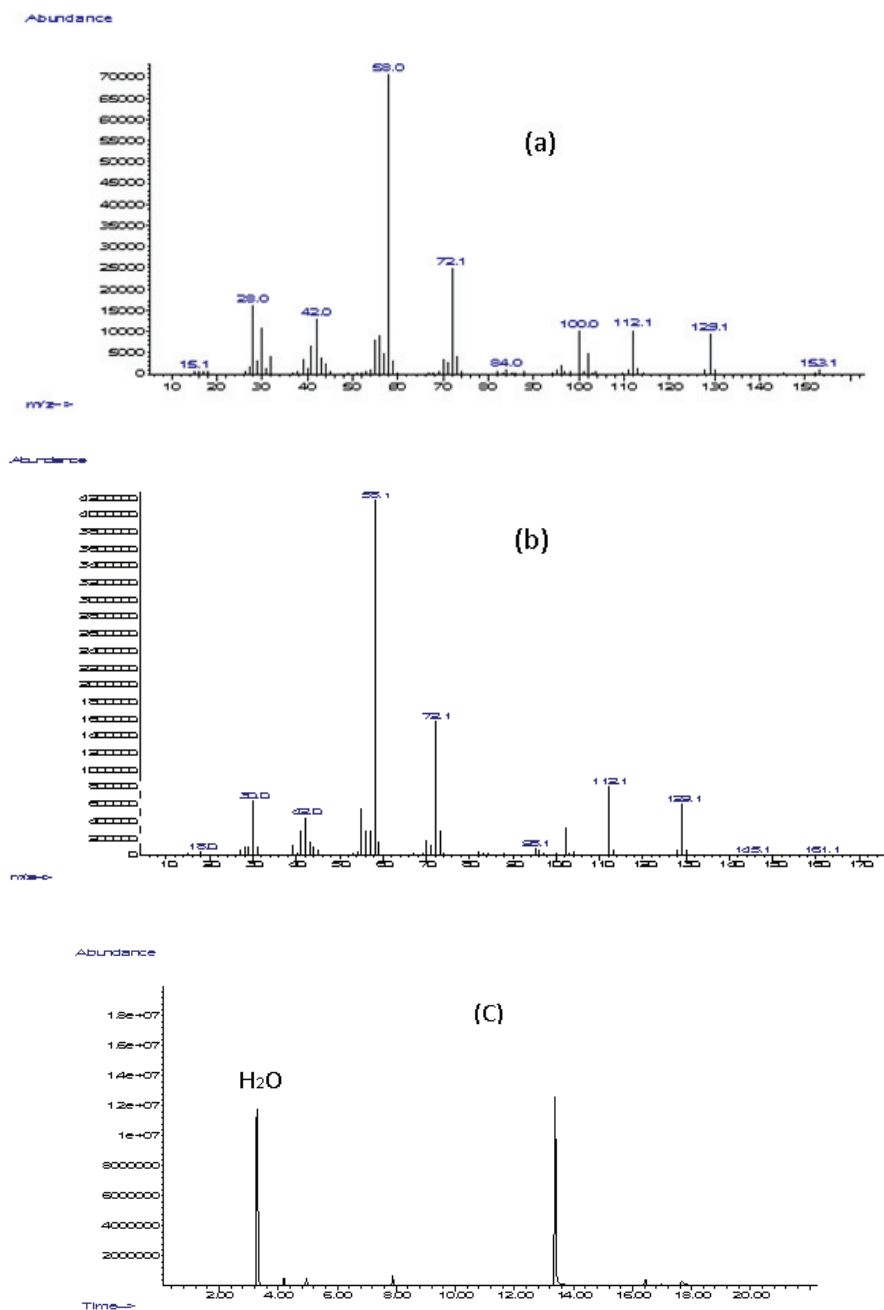


Figure 4.7 (a) Spectrum of the compound identified as AMPAMP in a 4.75 mol/kg AMP aqueous solution with a loading of 0.3 mol of CO₂ per mol AMP held at 135 °C for 5 weeks. (b) Spectrum of standard AMPAMP. (c) Gas chromatogram of standard AMPAMP aqueous solution.

Figure 4.8 shows the mass spectrum of peak 4 at 23.2 min in Figure 4.5. According to the analysis of the fragment ions of the spectrum, the peak at 23.2 min may be 4, 4-dimethyl-1-hydroxytertiobutyl-2-imidazolidinone (DMHTBI, peak 4). Unfortunately, the standard of DMHTBI is not commercially available for confirmation. However, Davis (2009) has found and identified DMHTBI by IC-MS in a thermal degraded AMP solution in the presence of CO₂. The protonated imidazolidinone, $m/z=187$ (see Figure 4.9). This is a strong support for the identification of DMHTBI. And DMHTBI was reported as a major degradation product of AMP in the presence of CO₂ (Lepaumier et al., 2009b; Eide-Haugmo et al., 2011). The chemical structures of the identified products are summarized in Figure 4.10. All of these identified products fall within the degradation pathway for carbamate polymerization. Peak 3 in Figure 4.5 remains unknown.

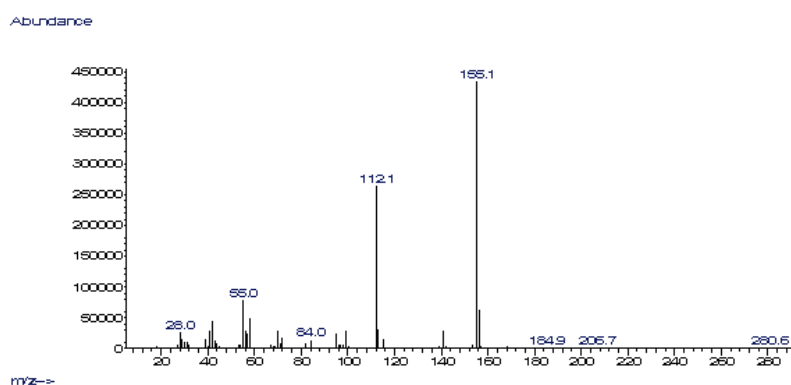


Figure 4.8 Spectrum of the peak 4 (Figure 4.5) in a 4.75 mol/kg AMP aqueous solution with a loading of 0.3 mol of CO₂ per mol AMP held at 135 °C for 5 weeks.

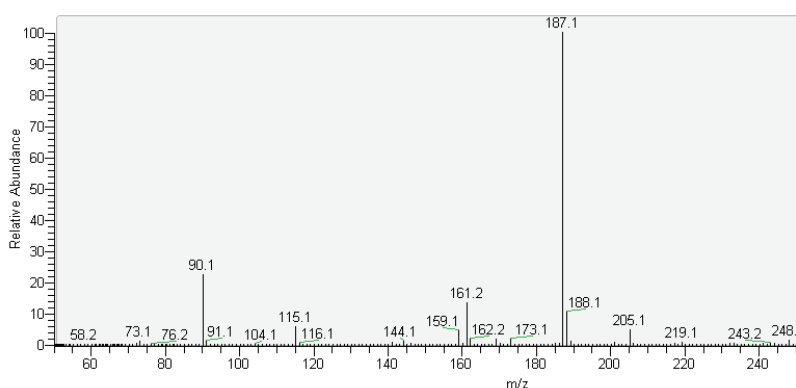


Figure 4.9 MS spectrum for a solution of 7 m AMP with a loading of 0.4 moles of CO₂ per mole of amine held at 135 °C for 8 weeks and injected by syringe pump (Davis, 2009).

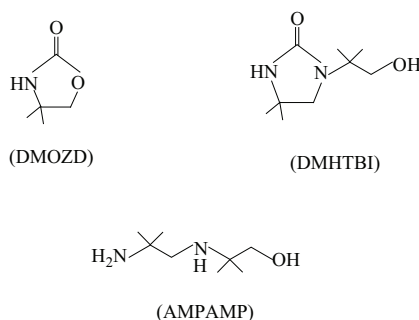


Figure 4.10 Structure of the identified products.

4.3.3 Degradation pathways

Thermal degradation of MEA in the presence of CO₂ occurs in a process termed carbamate polymerization, as presented in Figure 4.1. For AMP thermal degradation, it was postulated that the reactivity of DMOZD is very low due to the steric hindrance. The steric hindrance of the two methyl groups adjacent to the nitrogen atom prevents oxazolidinone ring-opening into an addition product (Lepaumier, 2009b). However, the identification of the products in this work and the reported results (Davis, 2009; Lepaumier et al., 2009b; Eide-Haugmo et al., 2011) demonstrate that AMP also can undergo the similar reactions as MEA does in the presence of CO₂.

A possible degradation pathway of AMP with CO₂ is proposed in Figure 4.11, which is based on the identified products and the literature results (Davis, 2009; Lepaumier et al., 2009b). The difference as compared to MEA is that DMOZD is slightly more stable due to the mild hindrance and will hence accumulate in the solution contrary to 2-oxazolidinone (OZD). AMP trimer and further polymeric products were not observed in AMP degradation samples that could be due to the steric hindrance either. These results indicate that the steric hindrance in AMP molecule can slow down CO₂ induced degradation of AMP as compared to MEA, but it does not prevent oxazolidinone formation and oxazolidinone ring-opening into further degradation products.

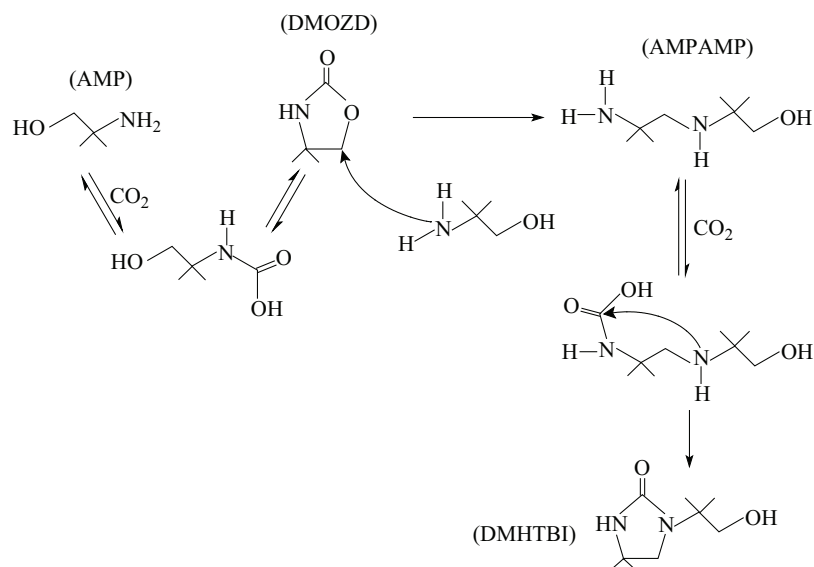


Figure 4.11 Scheme for degradation of AMP with CO₂.

4.3 Conclusions

Aqueous AMP solutions were thermally degraded using closed-batch reactor. AMP is stable at temperatures less than 140°C under nitrogen. However, as with traditional alkanolamines, AMP can be degraded thermally in the presence of CO₂. For 4.75 mol/kg AMP solution, the calculated first order rate constant of k_1 was 13.1×10^{-9} and $18.6 \times 10^{-9} \text{ s}^{-1}$ at 135°C with an initial CO₂ loading of 0.15 and 0.3 mol CO₂/mol AMP, respectively.

A Possible pathway for AMP thermal degradation was proposed and validated via GC-MS analysis. At 135°C, the major products included 4, 4-dimethyl-2-oxazolidinone, 2-[(2-amino-2-methylpropyl) amino]-2-methyl-1-propanol, and 4,4-dimethyl-1-hydroxytertiobutyl-2-imidazolidinone. The presence of the products were identified but not quantified. All of these products fall within the degradation pathway for carbamate polymerization. AMP does form a carbamate and continue to form 4, 4-dimethyl-2-oxazolidinone. The steric hindrance in AMP does not prevent oxazolidinone species formation but make it less favourable than in the case of MEA.

Chapter 5 Oxidative Degradation Rate of AMP

This chapter presents a discussion of the oxidation rate of aqueous AMP solutions, utilizing all relevant data collected with the batch methods described in Chapter 2 including two kinds of autoclave reactors, circulating closed-batch reaction system and FT-IR based reaction system. The effects of important process parameters, AMP concentrations, O₂ partial pressure, CO₂ loading, potential catalysts, pH value, and agitation on the oxidation rate of AMP are presented.

5.1 Experiments in FT-IR based reaction system

NH₃ has been shown to be the amino group oxidation product for primary amines and was used as an indicator of the relatively oxidative degradation rate of MEA. The Rochelle group in the University of Texas at Austin (Chi and Rochelle, 2002; Goff and Rochelle, 2004) has reported a FT-IR based method to measure the production of NH₃ in the studies of MEA degradation. In the present work, a FT-IR based experimental rig (see Figure 3.15) was set up for measuring the rate of NH₃ evolution from AMP solution, which was expected to indicate the relative oxidation rate of AMP. Unfortunately, we had to give up this project midway since a mirror in the gas cell was damaged. However, results of preliminary experiments still provided some useful information on AMP oxidation.

The initial experiment was carried out with 500 mL of 3 mol/kg aqueous AMP solution at 50°C. The AMP solution was placed inside an autoclave reactor and reaction air was sparged through the solution after passed through three pre-saturators at a rate of 0.5 L/min. Nitrogen was purged through the flow system at a rate of 1L/min in order to remove residual gas in the gas cell before the oxidation of AMP getting started. Each compound in the gas sample absorbs infrared radiation independently, resulting in a cumulative absorption spectrum. A typical spectrum has been shown in Figure 3.16, which is the sum of the absorbance spectra for each compound in the gas sample. The two sharp absorption peaks at 934 and 965 cm⁻¹ are from the inversion transition of the ammonia hydrogen atoms and can be used as the primary peaks in the IR analysis of NH₃. In this thesis, the raw data of integrated area underneath the peak centered at 965 cm⁻¹ was used to indicate the relative

amount of NH_3 stripped from AMP aqueous solution directly since calibration was not made due to the damage of the gas cell.

The raw data generated with the FT-IR at the experimental conditions is shown in Figure 5.1. This figure plots the integrated area underneath the peak from 955 to 975 cm^{-1} against degradation time in minutes. This result demonstrates that NH_3 formed when air passed through the AMP aqueous solution at 50°C . AMP, a sterically hindered primary amine, is postulated to be more resistant to oxidative degradation than conventional ethanolamines. However, formation of NH_3 indicates that the steric hindrance in AMP does not prevent its oxidative degradation, even under a typical absorber temperature.

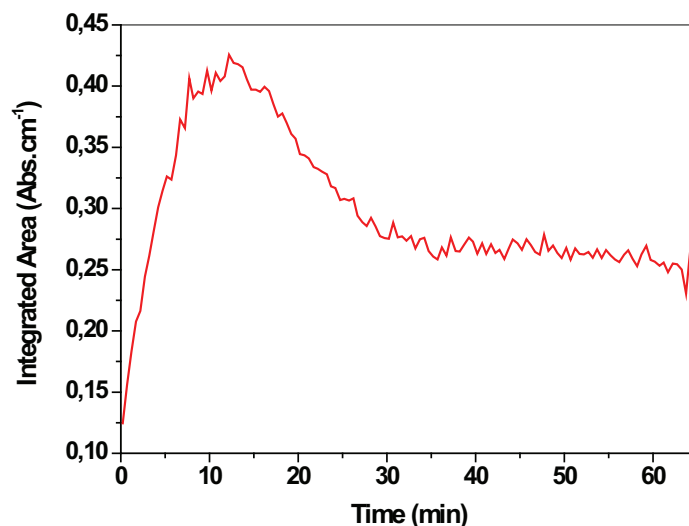


Figure 5.1 FT-IR raw data for oxidation of 3 mol/kg AMP with air at 50°C .

Figure 5.1 illustrates a phenomenon that air strips out the dissolved NH_3 in the AMP solution until the rate becomes constant in the first hour. It is similar as observed in MEA oxidation (Chi, 2000; Goff, 2005). Chi (2000) developed an unstable state model to predict this phenomenon based on material balance. The change in concentration of NH_3 in the liquid phase over time is equal to the rate at which NH_3 is produced minus the rate at which NH_3 is stripped. The developed unstable state model predicted the observed behaviour of NH_3 evolution from the MEA solutions quite well. The time it takes to reach the stable state was

indicated by a time constant, which depends on gas-liquid ratio, gas-liquid equilibrium characteristics of NH_3 at reactor temperature and condenser temperature. In this work, no condenser was set after the reactor, but the gas exiting from the reactor was heated to 140°C . The experimental result still shows that it needs time to reach a stable state for stripping out the dissolved NH_3 .

Figure 5.2 shows the integrated area underneath the peak from 955 to 975 cm^{-1} when 0.5 L/min air passed through 5 mol/kg AMP solutions at different temperatures. The raw data in Figure 5.2 indicate that relative evolution rate of NH_3 from AMP solutions increased with increased temperature as expected. Higher temperature could lead to faster oxidative degradation rate of AMP. On the other hand, solubility of NH_3 in the AMP solution decreased when the temperature was raised. No measurable AMP loss was observed using cation IC analysis within 2 day experiments. And the formation of anionic products, such as formate, was very little. These results show that the degradation of AMP was slow at the experimental conditions.

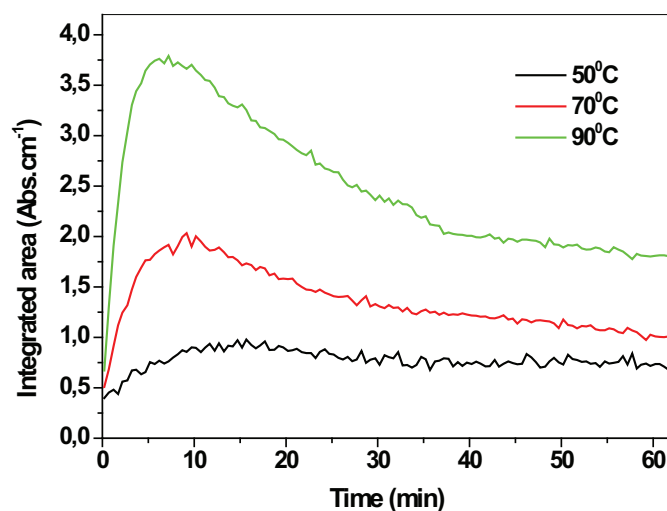


Figure 5.2 FT-IR raw data for oxidation of 5 mol/kg AMP with air at different temperature.

5.2 Experiment in circulating closed-batch reaction system

The initial design of the circulating closed-batch reaction system included the oxidative reactor and a 10L gas bottle which were placed in a heating box. A small pump was used to circulate the reaction gas. 5 mol/kg AMP was degraded in this system at 70°C in the presence of 0.5 mM ferric oxalate [Fe(C₂O₄)], 0.1 mM chromium sulfate [Cr₂(SO₄)₃] and 0.05 mM nickel sulfate (NiSO₄). These metals were chosen to simulate the metals that may be found in stainless steel systems. The reaction gas was oxygen with a total pressure of 1.1 bar.

Several methods were utilized to analyze the samples including GC-MS and anion IC. The corresponding AMP loss was not performed because of the difficulty in detecting small changes on the cation IC. The AMP solution was found to degrade under the experimental conditions. This chapter as a whole highlights the effect of solution characteristics on the loss of AMP as the primary dependent variable. The production of degradation products will not be described in detail in this chapter. The identification of AMP degradation products and possible degradation mechanisms will be discussed in Chapter 6.

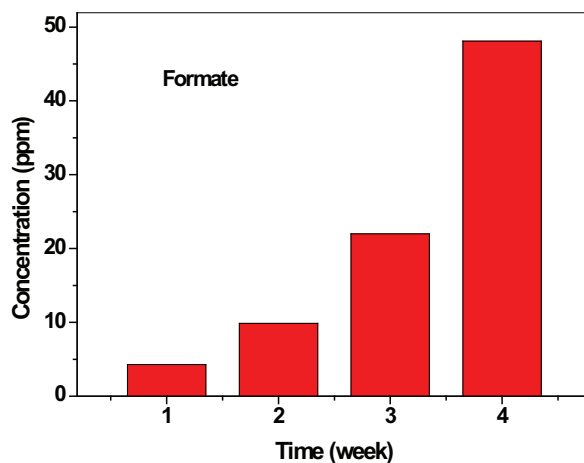


Figure 5.3 Formation of formate during oxidation of 5 mol/kg AMP in the presence of 0.6 mM Fe (C₂O₄), 0.1 mM Cr₂(SO₄)₃ and 0.05 mM NiSO₄ at 70°C in the circulating closed-batch reactor (total pressure = 1.1 bar).

After four weeks, acetone and 4, 4-dimethyl-2-oxazolidinone were identified as major non-ionic products with concentration of 17mM and 10mM, respectively. Analysis of anion IC revealed that formate is the main anionic product that is universally found during AMP

oxidative degradation. Figure 5.3 shows generation of formate within four weeks. This result shows that AMP was degraded but the degradation rate was still slow under these experimental conditions.

5.3 Experiments at elevated temperatures

In CO₂ capture plants, the most probable location of oxidation is anticipated in absorber due to the high O₂ concentration in there. Typical operation temperatures for absorber are in the range of 40-60°C (Wang et al., 2011). Oxidative degradation experiments at industrially relevant absorber temperatures occur on the order of months, and with this experimental design, a large number of reactors needed to be used. The results of gas analysis of FT-IR based experiments and liquid phase analysis of degraded AMP aqueous solution in the circulating closed-batch reactor have shown that AMP is not 'non-degradable' under a temperature closed to typical absorber temperatures. However, the degradation rate of AMP at the relatively low temperature was low and required long experimental time to accumulate enough degradation products for accurate detection. In order to speed up the degradation reactions, elevated temperatures (100-140°C) were used in the most of later experiments for AMP degradation study so that experiments could be carried out in a relatively short time rather than months.

On the other hand, in an absorption/stripping system the dissolved or entrained O₂ can be carried over to cross-exchanger that will result in oxidation in higher temperatures, even if the O₂ is not depleted in the absorber. The possibility of that dissolved or entrained oxygen is carried over to the desorber resulting in an oxidative environment at higher temperatures has generally been assumed to be low (Closmann, 2011). However, due to a lack of pilot or full-scale data from flue gas CO₂ capture systems, the extent of entrainment or dissolution of O₂ in these applications is generally unknown.

5.3.1 Experimental conditions

Oxidative degradation experiments with AMP aqueous solution were run in batch reactors using 250-350 kPa O₂ at 100-140°C. A summary of the experiments performed investigating the oxidation of concentrated AMP solutions at accelerating conditions is shown in Table 5.1. All experiments were performed with 5 mol/kg of AMP, except for the

first one, 3mol/kg of AMP. Two metal ions (Fe^{2+} and Cu^{2+}), one radical initiator (potassium persulfate, $\text{K}_2\text{S}_2\text{O}_8$) and sulphuric acid (H_2SO_4) were tested for their effects on oxidative degradation of AMP.

Table 5.1 Summary of experiments performed at elevated temperatures and pressures.

Expt. No.	AMP mol/kg	Reactor*	T °C	P _{O₂} kPa	CO ₂ Ldg mol /mol AMP	Other conditions
E1	3	small	120	250	-	-
E2	5	small	120	250	-	-
E3	5	small	100	250	-	-
E4	5	small	140	250	-	-
E5	5	small	120	350	-	-
E6	5	small	120	300	-	-
E7	5	small	120	250	0.15	-
E8	5	small	120	250	0.30	-
E9	5	small	120	250	-	0.1 mM FeC_2O_4
E10	5	small	120	250	-	0.1 mM CuSO_4
E11	5	small	120	250	-	7.5 g/L $\text{K}_2\text{S}_2\text{O}_8$
E12	5	small	120	250	-	H_2SO_4 , pH=12
E13	5	small	120	250	-	H_2SO_4 , pH=10
E14	5	small	120	250	-	-
E15	5	large	120	250	-	-

* small reactor-200 mL minicalve, large reactor-1L autoclave equipped with a turbo mixer.

Liquid samples of the reaction mixtures were withdrawn from the reactors at predetermined intervals and analyzed after each experimental run. AMP loss was determined by cation IC and used for calculation of the degradation rates. The overall rates of the amine degradation were calculated as $\delta C/\delta t$, where δC is the change in amine concentration, while

δt is the change in reaction time from 0 to time t . Instantaneous degradation rate was measured as the slope at any reaction time of the AMP concentration-reaction time curves. The instantaneous degradation rates were calculated as follows. Initially, a concentration-time curve was plotted for all the experiments performed. This was followed by curve fitting of the data by using an exponential function available on Origin 8.0 (OriginLab, USA). The fitting equation was differentiated to obtain the rate of each instant time.

The repeatability of the entire experimental procedures and the impact of the reactor itself were assessed with two experiments (Expt. 2 and Expt. 14) performed in miniclave reactors. The two experiments of AMP oxidation were conducted at 120 °C with stirring speed of 200 rpm and with 250 kPa O₂ in the absence of adding any catalyst or inhibitor. The raw data for AMP loss is compared in Figure 5.4. The results of AMP loss in these two oxidation experiments are good agreement with each other. The relative deviations of AMP concentration of duplicate runs are less than 2%.

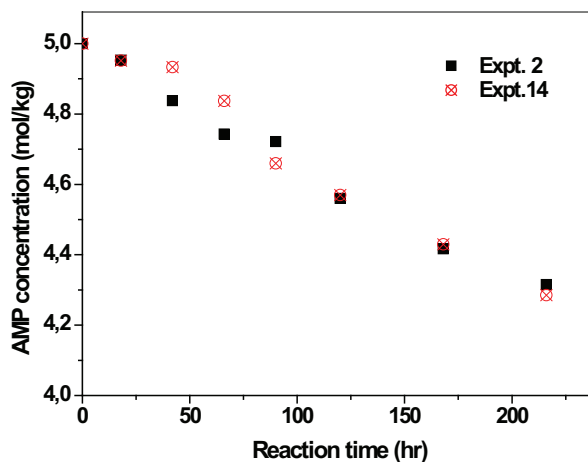


Figure 5.4 Comparison of AMP loss in two baseline experiments (initial concentration of AMP = 5 mol/kg, temperature = 120°C, O₂ pressure = 250 kPa). The two experimental runs were conducted in May 2010 and June 2011, respectively.

5.3.2 Comparison between AMP and conventional ethanolamines

According to the electron abstraction mechanism that has been reviewed in Chapter 2, AMP could be more resistant to oxidative degradation as it has no α -hydrogen atom (α position with regard to amino functional group), hence is not able to form an imine which is

assumed to be the first step in the proposed electron abstraction mechanism (Chi and Rochelle, 2002; Goff and Rochelle, 2004). In order to investigate the relative stability of AMP in the presence of O₂ at elevated temperatures, the overall degradation rate of AMP was compared with those of the traditional ethanolamines MEA, DEA, and MDEA under 350kPa O₂ and 120°C.

During the experiments, it was noticed that the colour of all the investigated amine solutions gradually turned to brown as degradation progressed. The odour of the solutions also became more pungent with reaction time. The loss rates of the different amine are shown in Figure 5.5. The relative overall loss rate is defined as

$$\frac{c_0 - c_i}{c_0} \times 100 \quad (5.1)$$

Where c_0 is the initial concentration of starting amine, mol/kg; c_i is the remaining concentration of the starting amine, mol/kg.

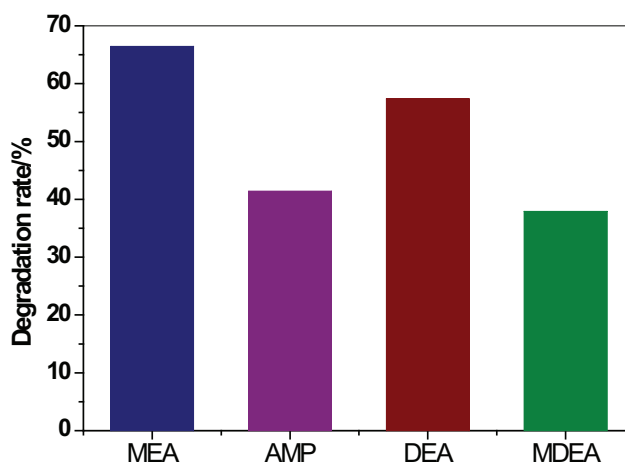


Figure 5.5 Degradation rates of different amines at 384 hours under 350 kPa O₂ and 120°C (initial concentration = 5 mol/kg).

As can be seen in Figure 5.5, the relative overall loss rate of MEA, AMP, DEA and MDEA after 384 hours was 66.4%, 41.4%, 57.3% and 37.9%, respectively. The degradation rate of AMP was much less than that of MEA, but was slightly higher than that of MDEA under the identical conditions. The experimental result indicates that the stability of AMP is

similar as MDEA at the experimental conditions, is not as stable as anticipated by electron abstraction mechanism which has been proposed as a possible initiation step for the oxidative degradation of amines.

5.3.3 Effect of initial concentration

The effect of AMP initial concentration was evaluated by comparing the oxidation rate of 3 mol/kg AMP with that of 5 mol/kg AMP under 250 kPa O₂ at 120°C. Figure 5.6 illustrates the changes in the AMP concentration and instantaneous degradation rates versus reaction time at two different concentrations. With 3 mol/kg AMP, the initial degradation was 3.1 mmol/(kg·h), while with 5 mol/kg AMP, the overall rate of AMP degradation was 4.7 mmol/(kg·h). This result illustrates the detrimental effect of higher AMP concentration on the overall degradation rate. However, the instantaneous rates declined over time, and were more rapid at higher initial concentration. The instantaneous rates were very close at 384h. And therefore the difference between the overall rates ($\delta C/\delta t$) after 384 hours was much smaller than that of the initial rates. With 3 mol/kg AMP, the overall degradation rate of AMP was 2.2 mmol/(kg·h), while with 5 mol/kg AMP, the overall degradation rate of AMP was 2.6 mmol/(kg·h). In most of the later experiments the initial concentrations of AMP were fixed at 5 mol/kg, which is comparable to 30 wt% MEA (~ 5 mol/kg) aqueous solution.

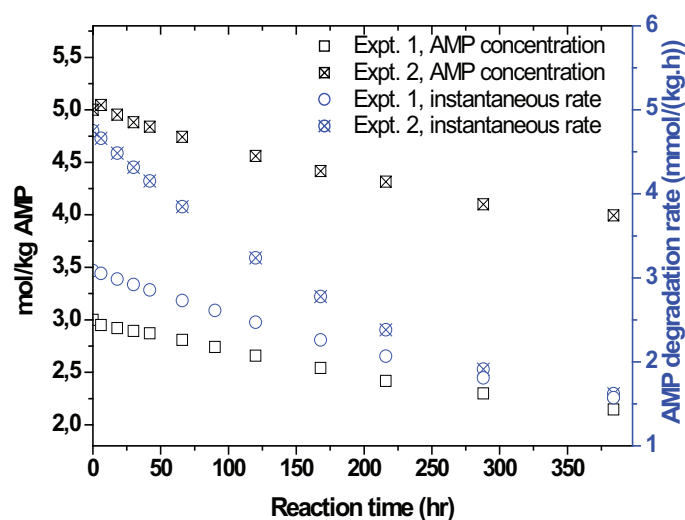


Figure 5.6 Changes in AMP concentration and instantaneous rate versus time. Experiments were conducted at 120 °C and 250 kPa O₂.

5.3.4 Effect of temperature

The effect of temperature on AMP oxidative degradation was examined by degrading solutions at constant AMP concentration and O₂ partial pressure. Figure 5.7 is a plot of remaining AMP concentration versus degradation time at 100-140°C for an initial AMP concentration of 5 mol/kg and under an O₂ partial pressure of 250 kPa. These experiments were carried out in the small miniclave reactors. As can be seen in Figure 5.7, the decrease in AMP concentration with reaction time was more rapid at higher temperature (140°C) than at the lower temperature (100°C). The overall degradation rates ($\delta C/\delta t$) at 100, 120 and 140°C were calculated as 2.2, 2.6, 3.4 mmol/(kg·h) after 384 hours, respectively. As expected, the overall rates of the oxidative degradation of AMP increased with raising temperature.

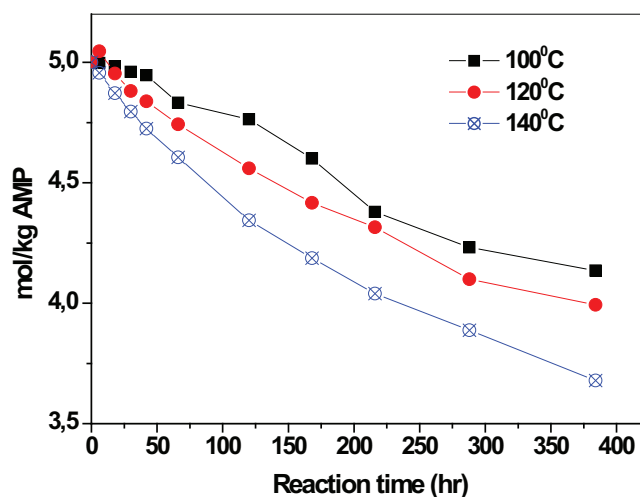


Figure 5.7 Changes in AMP concentration versus time (initial concentration of AMP = 5 mol/kg). Experiments were conducted at temperatures ranging from 100-140 °C and at oxygen pressures of 250 kPa.

The data shown in Figure 5.7 is clearly a first order process with respect to the concentration of AMP. This observation is supported by the fact that the concentration profiles for AMP can be well characterized by an exponential regression. Under a fixed oxygen partial pressure of 250 kPa, the first order reaction rate constants, k_1 , at 100, 120 and 140°C are 1.5×10^{-7} , 1.8×10^{-7} , and $2.6 \times 10^{-7} \text{ s}^{-1}$, respectively.

The rate constant, k_1 , was predicted to have an Arrhenius temperature dependence with the form in Equation 5.2 where k_1 and the pre-exponential factor, A , have units of inverse time, the activation energy, E_a , is in Joule per mole, R is the universal gas constant, and the temperature, T , is in Kelvin. A linearized form of Equation 5.2 is shown in Equation 5.3.

$$k_1 = A \cdot e^{\left(-\frac{E_a}{RT}\right)} \quad (5.2)$$

$$\ln k_1 = \ln A - \frac{E_a}{R} \cdot \frac{1}{T} \quad (5.3)$$

The structure of Equation 5.3 suggests a linear relationship between $\ln k_1$ and $1/T$. A plot comparing the calculated $\ln k_1$ value and $1/T$ for experiments with 5 mol/kg of AMP under 250 kPa O_2 can be used to estimate the activation energy. The activation energy for 5mol/kg AMP oxidation at the fixed 250 kPa O_2 was estimated at a value of 17 kJ/mol. This value is much smaller than expected. As is well known, provided that the activation energy is smaller than 40 kJ/mol, the reaction is too fast to determine its rate. The oxidation of AMP, however, is obviously a slow reaction. The low value of calculated activation energy may be resulted from the influence of oxygen mass transfer. If the influence of mass transfer process of O_2 was not eliminated in the gas-liquid phase reaction, the apparent reaction rate constant is the overall reaction rate constant including the impact of O_2 mass transfer process. The low calculated activation energy indicates possibly complete consumption of oxygen in the reactor at high temperature. The effect of O_2 mass transfer will be discussed further in the next sections.

5.3.5 Effect of oxygen partial pressure

The effect of the O_2 partial pressure was evaluated with 5 mol/kg AMP at 120°C by comparing the results obtained at 250 kPa O_2 pressure versus those at 300 and 350 kPa O_2 pressure (see Figure 5.8). The AMP concentration declined over time, and was more rapid with higher O_2 pressure. After 120 h, the overall rate of AMP degradation with 250 kPa O_2 was 3.7 mmol/(kg·h), while at the same temperature, the rates with 300 kPa and 350 kPa O_2 pressure were 5.9 and 13 mmol/(kg·h), respectively. After 216 h, the overall rate of AMP degradation with 250 kPa O_2 was 3.2 mmol/(kg·h), while with 350 kPa O_2 , it was 9.2

mmol/(kg·h). This result confirms that oxygen concentration, or oxygen pressure, is a crucial parameter in the degradation rate of AMP.

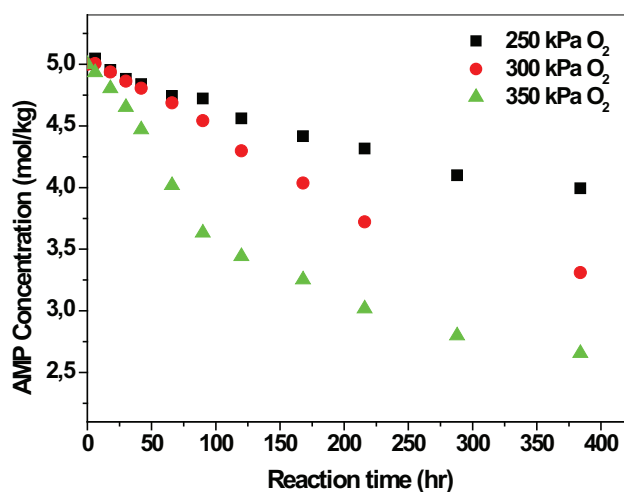


Figure 5.8 Changes in AMP concentration versus time (initial concentration of AMP = 5 mol/kg). Experiments were conducted at 120°C and oxygen pressures ranging from 250 kPa to 350 kPa.

5.3.6 Effect of agitation

AMP degraded with oxygen in the reaction vessel is a two-phase system. Oxygen should be dissolved in AMP solution first. The rate of oxygen diffusion into AMP solution depends, first, on the mode and rate of mixing the gas and liquid, and second, on the partial pressure of oxygen.

The strong dependence of degradation rate on O₂ partial pressure and the low estimated activation energy imply that the oxidative degradation of AMP may be controlled by O₂ mass transfer at elevated temperatures. If the degradation rates of AMP are controlled by the rate of O₂ mass transfer, it can be expected that the degradation rate will be increased when agitation rate increases under a certain oxygen pressure. In order to investigate the possibility that the data being measured is actually the O₂ mass transfer limited, one experiment was performed in the autoclave with a turbo mixer. The data generated in the turbo mixed reactor were consistent with this assumption, and the observed results were shown in Figure 5.9. It

shows clearly that increase of agitation rate increased the degradation rate of AMP dramatically, similar as observed for MEA (Goff and Rochelle, 2004).

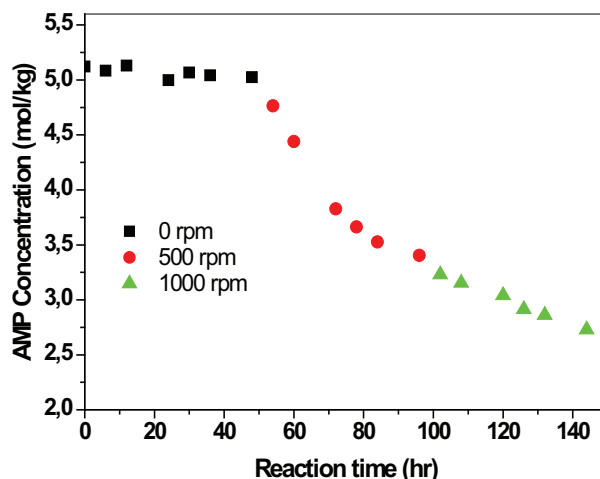


Figure 5.9 Changes in AMP concentration versus time and stirring speed (initial concentration of AMP = 5 mol/kg). Experiments were conducted under 250 kPa O₂ at 120°C.

5.3.7 Effect of metal ion

Recall from Chapter 2 that both of Fe²⁺ and Cu²⁺ have been shown to catalyze the oxidation of MEA. Fe²⁺ and Cu²⁺ are potential catalysts for AMP oxidation and thus the effects of dissolved iron and copper on the degradation rate of AMP were examined. 0.1mM ferrous oxalate (FeC₂O₄) and 0.1mM copper sulfate (CuSO₄) were added into the AMP solutions, respectively. But no significant catalytic effect on AMP oxidation was observed with addition of these two metal ions (see Figure 5.10). A number of factors could probably explain the fact that the degradation rate of AMP shows a very weak dependence upon addition of Fe²⁺ and Cu²⁺. It is most likely that AMP oxidation at the elevated temperatures was limited by oxygen mass transfer. In this case, the catalytic effects cannot be observed since the degradation was not controlled by reaction kinetics. The second possibility is that the catalytic effects of Fe²⁺ and Cu²⁺ on the oxidation of AMP might be much weaker than what was observed on the oxidation of MEA in the previous studies (Blachly and Ravner, 1966; Chi and Rochelle, 2002; Goff and Rochelle, 2004). Therefore, the catalytic effect is too weak to observe with adding of the catalysts in low concentration using the experimental method.

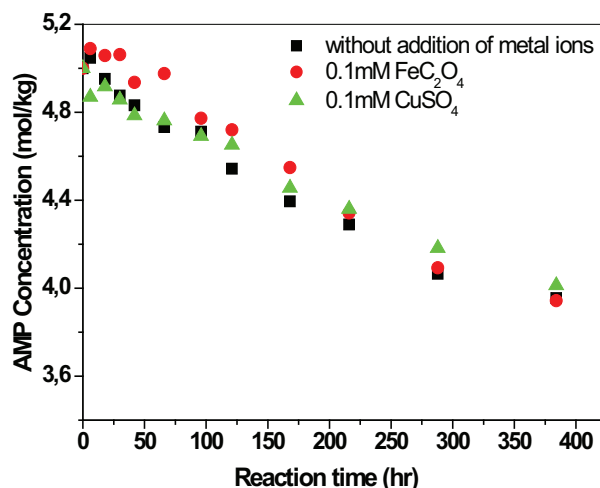


Figure 5.10 Changes in AMP concentration versus time and metal ions (initial concentration of AMP = 5 mol/kg). Experiments were conducted under 250 kPa O₂ at 120°C.

5.3.8 Effect of potassium persulfate

Amine is believed to be oxidized by oxygen via a radical mechanism (Denisov and Afanas'ev, 2005). We will propose a possible degradation pathway of AMP based on the identified products and the context of the current amine degradation schemes in Chapter 6. Oxygen is supposed to play an important role in this mechanism of AMP degradation. The initiating radicals in solution abstract a hydrogen atom at the carbon atom adjacent to the OH group to form a new radical ($\text{HO}\dot{\text{C}}\text{HC}(\text{CH}_3)_2\text{NH}_2$), because the C-H bond adjacent to hydroxyl group is the weakest hydrogen-containing bond in AMP molecule. The newly formed alkyl radical can transform to the corresponding peroxy radical by a fast reaction with O₂. Thereafter, the peroxy radical propagate the oxidative degradation of AMP. In the presence of sufficient concentration of dissolved oxygen, the rate of the initiated oxidation does not depend on the oxygen pressure, but the initiation step limits the oxidation rate.

In order to further verify the possible mass transfer phenomenon, experiment was performed to look at the effect of an initiator on the oxidation rate of AMP. Potassium persulfate was used as a radical initiator to accelerate the initiation step of the oxidation of AMP in this work. Having a weak O-O bond, peroxides split easily into free radicals, which are usually used to initiate a free radical reaction. K₂S₂O₈ decomposes by O-O bond

homolysis to produce sulfate radicals. In alkali aqueous solutions, generation of hydroxyl radical and superoxide anion except for sulfate radical was proved experimentally by Furman et al. (2010). The formed radicals were expected to accelerate the initiation step of AMP oxidation. Thus, the degradation rate of AMP would be increased dramatically in the presence of sufficient dissolved oxygen. The experimental result (see Figure 5.11) shows that the degradation rate only increased approximately 2.5% after 66 hours when the initial concentration of $K_2S_2O_8$ up to 7.5g/L. In other words, the increasing of the degradation rate of AMP was not high as expected. We speculate that the formation of peroxy radicals was limited by O_2 mass transfer.

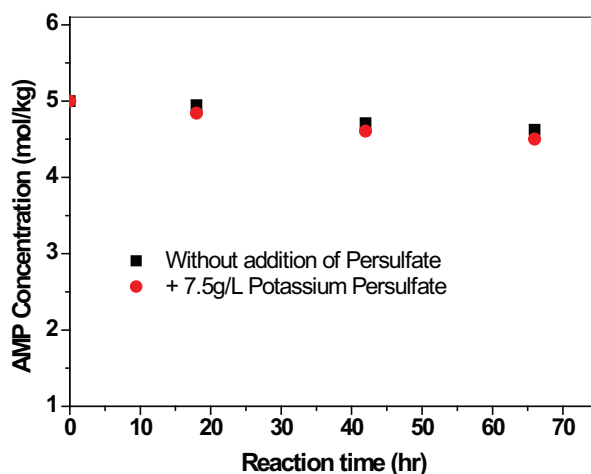


Figure 5.11 Changes in AMP concentration versus time with and without potassium persulfate addition (initial concentration of AMP = 5 mol/kg). Experiments were conducted under 250 kPa O_2 at 120°C.

5.3.9 Effect of CO_2 on AMP loss

Although MEA oxidation was studied extensively, previous reports on the effect of CO_2 loading on MEA oxidation rate are contradictory as described in Chapter 2. An important observation from the obtained data in this work is that the AMP solutions with CO_2 loading appear to degrade faster than the solutions without CO_2 loading. The data shown in Figure 5.12 demonstrate that a significant increase in the degradation rate of CO_2 loaded solution compare to the unloaded AMP solutions in the experimental conditions. After 120 hours, the degradation rate of AMP was 8.8%, 11.6%, and 13.2% for the solutions with loading of 0,

0.15 and 0.30 mol CO₂ /mol AMP, respectively. GC-MS analysis and anion IC analysis revealed that CO₂ had no significant effect on the concentrations of produced anions and acetone, but the concentration of DMOZD increased dramatically in loaded solutions (Figure 5.13). These results indicate that the oxidation mechanism of AMP did not change in CO₂ loaded solutions. The formation rate of DMOZD increased might mainly due to the much higher concentration of CO₂ in loaded solutions.

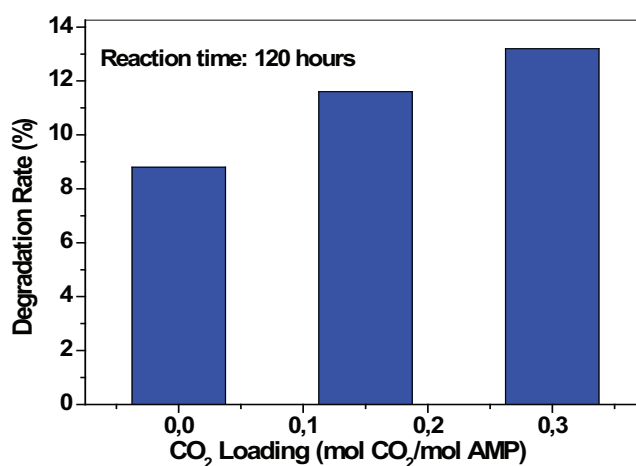


Figure 5.12 Effect of CO₂ loading on AMP degradation rate (initial concentration of AMP = 5 mol/kg). Experiments were conducted under 250 kPa O₂ at 120°C.

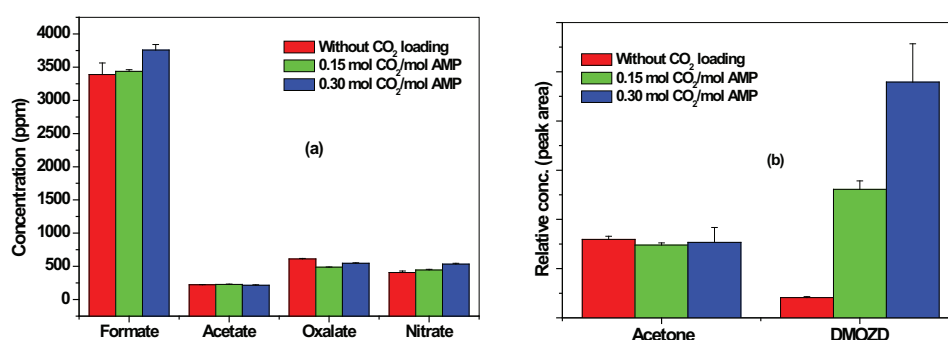


Figure 5.13 Formation of the products in the partially degraded AMP after 120 hour (initial concentration of AMP = 5 mol/kg). Experiments were conducted under 250 kPa O₂ at 120°C.

5.3.10 Degradation of acid treated AMP

When acid gas, CO_2 , was loaded into AMP solution, the pH value of the solution is decreased. The changes in the pH value of CO_2 loaded AMP solutions were measured by a HI 8314 Portable Analog pH meter (Hanna Instruments) at room temperature. Figure 5.14 shows the changes in the pH values of 5 mol/kg AMP solutions after loading of CO_2 . Zero CO_2 loading which corresponds to a solution pH of 12.9 and 0.3 mol CO_2 /mol AMP loading which corresponds to a pH of 10. The pH of AMP solution decreased approximately 3 pH units when it was loaded with CO_2 to a loading of 0.3 mol of CO_2 /mol of AMP.

The degradation of AMP discussed in previous section was written in terms of free AMP as the actively degrading species. In the presence of CO_2 , there are three possible species of AMP that could undergo oxidative degradation: free AMP, protonated AMP (AMPH^+) and the AMP carbamate (AMPCOO^-). The AMP carbamate is readily to react with water and forms free amine and bicarbonate finally due to its low stability. Therefore, in loaded solutions, the main species of AMP that could undergo oxidative degradation are free AMP and AMPH^+ .

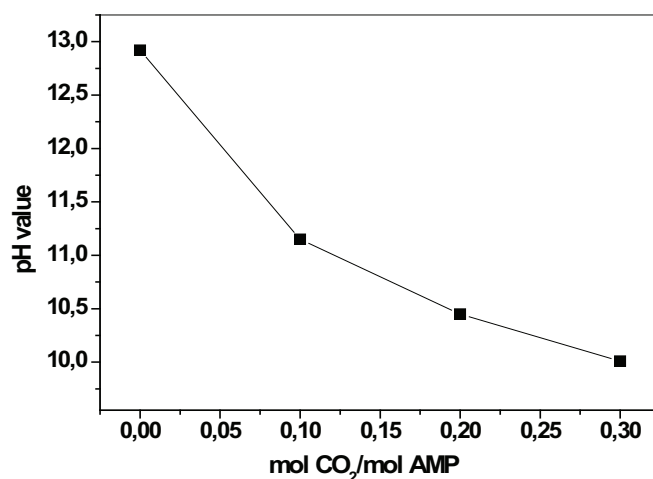
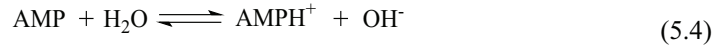


Figure 5.14 The pH value of CO_2 loaded AMP solutions at room temperature (concentration of AMP = 5 mol/kg).

The concentration ratio of protonated AMP and free AMP is related with the pH of the solution. The basic reaction for conversion of free AMP to protonated AMP in aqueous solution was considered to occur as reaction 5.4:



The dissociation equilibrium constant K_a and pK_a are defined as:

$$K_a = \frac{[\text{AMPH}^+][\text{OH}^-]}{[\text{AMP}]} \quad (5.5)$$

$$pK_a = -\lg K_a = -\lg \frac{[\text{AMPH}^+]}{[\text{AMP}]} - \lg [\text{OH}^-] \quad (5.6)$$

Now defining ion product constant $K_w = [\text{H}^+][\text{OH}^-]$, and $pK_w = -\lg K_w$, we get the following equation:

$$\lg \frac{[\text{AMPH}^+]}{[\text{AMP}]} = pK_w - (pK_a + \text{pH}) \quad (5.7)$$

At a certain temperature, pK_w and pK_a are constants. According to Equation 5.7, the relative concentration of protonated AMP would be increased as the pH value is decreased.

If O_2 solubility alone were accounting for the change in degradation rates, the solutions without CO_2 loading should degrade fastest. Due to the salting out effect, O_2 solubility should decline as CO_2 is loaded. However, the degradation result presented in Figure 5.12 above clearly shows that the rate of AMP oxidation is an increasing function of CO_2 loading. This observation may result either from the change of the ratio of $[\text{AMPH}^+]/[\text{AMP}]$ due to pH change, or result from CO_2 induced reactions. In order to verify the possibilities, the solution pH of 5 mol/kg AMP in the absence of CO_2 was manipulated with addition of sulfuric acid (H_2SO_4). The solution pH value was measured before the degradation experiments.

Two experiments (Expt. 12 and Expt. 13) were performed to verify the impact of the pH value on AMP oxidation. The initial pH values at room temperature were 12 and 10, respectively. The AMP solutions were degraded at 120°C and 250 kPa O_2 . The ratio of $[\text{AMPH}^+]/[\text{AMP}]$ should be increased as the solution becomes more acidic. Figure 5.15 shows the overall AMP losses after 14 days. For comparison, the AMP loss of 5mol/kg AMP without H_2SO_4 treatment which was degraded under identical conditions after 16 days also is shown in Figure 5.15. No significant change of the overall degradation rate of AMP was observed when the initial AMP solutions were treated with addition of different amounts of

H₂SO₄. This result combined with the observation in Section 5.3.9 suggests that the dependence of AMP oxidation on CO₂ loading is mainly due to CO₂ induced reactions.

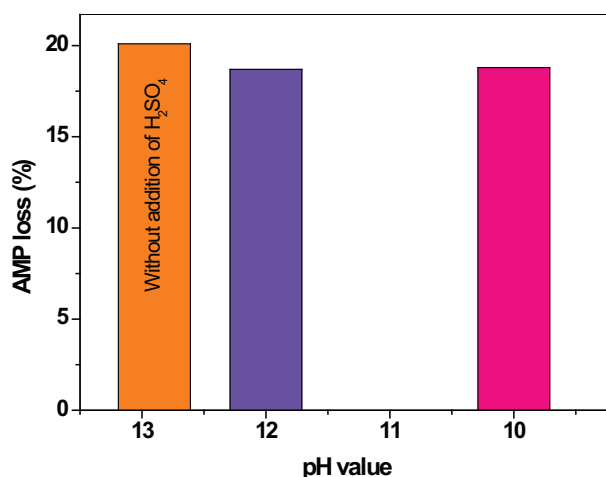


Figure 5.15 Effect of pH value on AMP degradation rate (initial concentration of AMP = 5 mol/kg). Experiments were conducted under 250 kPa O₂ at 120°C.

5.4 Conclusions

AMP solutions were degraded using a FT-IR based reaction system, a circulating closed-batch reaction system and autoclave reactors. The results from the experiments performed in the FT-IR based reaction system and the circulating closed-batch reaction system indicate that AMP is not ‘non-degradable’ in the presence of O₂ even at typical absorber temperatures. But the degradation rate is low at temperatures close to typical absorber temperatures. In order to shorten the length of the experiment, most of the oxidation experiments were performed in autoclave reactors at temperatures of 100-140 °C, and O₂ pressures of 250-350 kPa. The oxidative degradation rate of AMP was much lower than that of MEA, but was close to that of MDEA at identical conditions.

Under accelerated conditions, the oxidative degradation rate of AMP increased slightly as the temperature was increased, but increased significantly with increasing O₂ concentration. No significant catalytic effect on AMP oxidation was observed with addition of 0.1 mM FeC₂O₄ and 0.1 mM CuSO₄, respectively. As a radical initiator, 7.5 g/L potassium

persulfate was added into the AMP solution, the oxidation rate of AMP was not increased as originally expected. However, AMP oxidation rate increased dramatically as the agitation rate was increased. Results from these experiments show that the oxidative degradation of AMP can be partially controlled by O₂ absorption under elevated temperatures.

The effect of CO₂ loading on MEA oxidation rate is contradictory. An important observation from AMP oxidation is that the AMP solutions with CO₂ loading appear to degrade faster than the solutions without CO₂ loading. The impact of pH change on AMP oxidation can be disregarded. GC-MS analysis and anion IC analysis suggested that the dependence of AMP oxidation on CO₂ loading mainly resulted from CO₂ induced reactions.

Chapter 6

Oxidative Degradation Products and Pathways of AMP

The research objectives of this project were outlined in Section 1.4. Significant time and energy were committed towards the main objective which was to develop an understanding of AMP oxidation behaviour and mechanisms. A summary of the oxidative degradation products of AMP aqueous solution is provided in this chapter. A separate set of degradation pathways of thermal degradation of AMP in the presence of CO₂ has been presented in Chapter 4. This chapter presents proposed oxidative degradation pathways for AMP aqueous solution based on the data collected from oxidative degradation of this solvent. The pathways explain the production of the major identified or quantified products in this work. The presence of certain degradation products in degraded AMP samples led to preliminary formulation of possible pathways, but not necessarily mechanisms. In this chapter, the pathways are described along with supporting data from the oxidative degradation experiments, and the context of the current amine degradation schemes. In addition, Experiments of AMP oxidation in the presence of UV radiation were performed in a photochemical reactor.

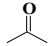
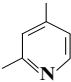
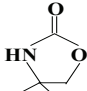
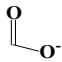
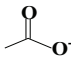
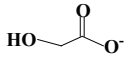
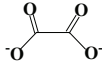
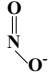
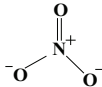
6.1 Oxidative degradation products of AMP

Gas chromatography-mass spectrometry (GC-MS), cation IC and anion IC were employed to identify the oxidative degradation products in an attempt to understand the degradation mechanisms of AMP. A summary of the identified degradation products of AMP solutions degraded at accelerating conditions (100-140°C, 250-350 kPa O₂) is provided in Table 6.1. The major products of AMP included NH₃, acetone, 2, 4-lutidine, DMOZD, and formate. NH₃ was detected as its cation form (NH₄⁺) in the liquid phase. Additionally, acetone oxime, trimethyl-pyridines, acetate, oxalate, glycolate, nitrite and nitrate were detected at low concentrations throughout the experiments performed at elevated temperatures, although they do not represent major products.

Higher oxygen pressure and oxidation temperature than in industrial application were used in order to reduce the length of experiments. The use of high O₂ pressure increased

degradation rates as shown in Figure 5.8. The use of high O₂ pressure does not change the principal reaction pathways because we noticed the formation of the same degradation products at different O₂ pressures except that the relative amounts of the products varied. The experimental design of using high oxidation temperature is based on the assumption that the elevated temperature does not affect the mixture of degradation products or introduce new reaction mechanisms. Although we detected the same products in all experiments performed at accelerating conditions that were listed in Table 5.1, an additional experiment was performed at a relatively low temperature (80°C) to test the effect of temperature on the degradation pathways and to verify the assumption.

Table 6.1 Identified degradation products of aqueous AMP solution.

Compound	CAS#	Analytical method	MS fitting probability	Standard Verification	Structure
Acetone	67-64-1	GC-MS	83%	Yes	
2, 4-Lutidine	108-47-4	GC-MS	49%	Yes	
DMOZD	26654-39-7	GC-MS	78%	No	
Formate		Anion IC	-	Yes	
Acetate		Anion IC	-	Yes	
Glycolate		Anion IC	-	Yes	
Oxalate		Anion IC	-	Yes	
Nitrite		Anion IC	-	Yes	
Nitrate		Anion IC	-	Yes	
Ammonium		Cation IC	-	Yes	NH ₄ ⁺

6.1.1 GC-MS identification

Since the same products were identified in different experimental conditions as those listed in Table 5.1, the oxidative degradation sample of 5 mol/kg AMP at 120°C and 250 kPa O₂ is taken as an example to demonstrate identification of the products using GC-MS. At the outset of the study, a single sharp peak corresponding to AMP appeared in the gas chromatogram (Figure 6.1 (a)). After 384 hours, a number of degradation products were observed (Figure 6.1 (b)). The major products were acetone, 2, 4-lutidine, and DMOZD, which were identified by MS library match (NIST MS Search 2.0). Computer fitting of the mass spectrum to the mass spectra database to identify the main products was followed up by use of standards to confirm identification of the components in the degraded AMP samples.

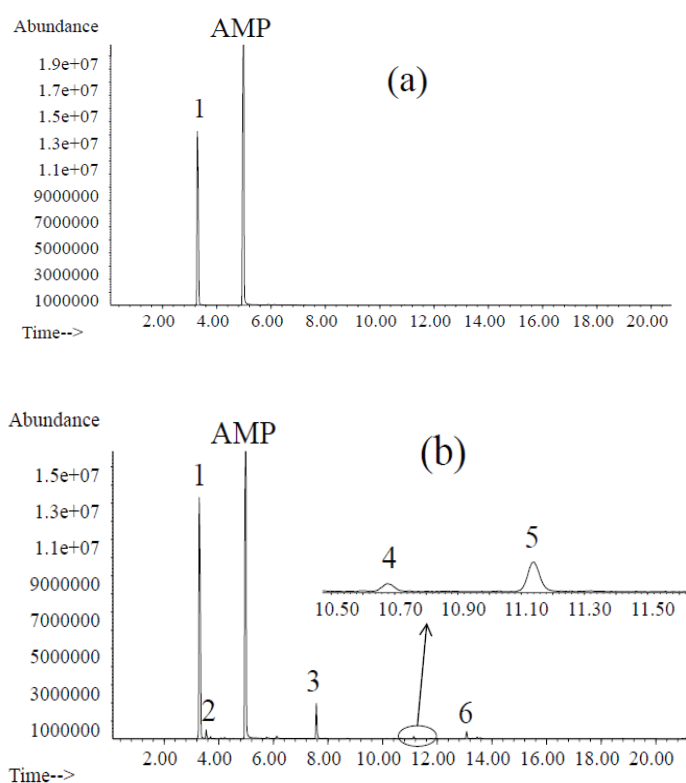


Figure 6.1 (a) Gas chromatogram of AMP aqueous solution at the beginning of the experiment (0 h) using 5 mol/kg AMP at 120 °C with 250 kPa O₂; (b) Chromatogram of a partially degraded AMP aqueous solution at 384h using 5 mol/kg AMP at 120 °C with 250 kPa O₂. In addition to water (peak 1) and AMP, the products were identified as acetone (peak 2), 2, 4-lutidine (peak 3), trimethyl pyridines (peak 4 and 5), and DMOZD (peak 6).

The retention time of the identified acetone in the partially degraded AMP solution was the same as that of the authentic standard. The identified peak was spiked with acetone. The known spike enhanced the identified peak and no new peak was created. Typical mass spectra obtained for acetone in degraded AMP samples and acetone standard as shown in Figure 6.2 indicate that the mass fragmentation pattern of acetone in partially degraded AMP samples matched that of the acetone standard as well as that documented in the mass spectrometer database.

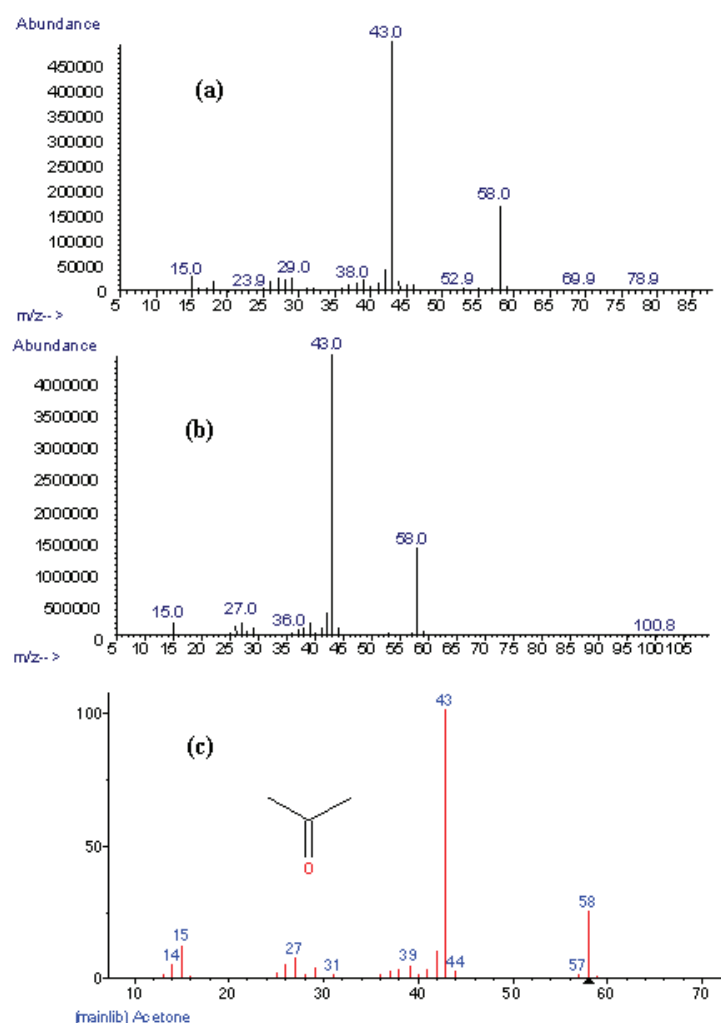


Figure 6.2 (a) Spectrum of acetone in degraded sample of AMP-H₂O-O₂ system at 120°C using 5 mol/kg AMP with 250 kPa O₂; (b) Spectrum of standard sample of acetone; (c) Spectrum of acetone in the database.

The retention time of the identified 2, 4-lutidine in the partially degraded AMP solution was the same as that of the 2, 4-lutidine standard. The identified peak was spiked with 2, 4-lutidine. The known spike enhanced the identified peak and no new peak was created. The mass spectra are shown in Figure 6.3. The confidence of the mass fragmentation pattern of 2, 4-lutidine in the degradation samples matched that documented in the mass spectrometer database by 49%. But it should be noted that the confidence of the mass spectrum of authentic 2, 4-lutidine standard matched that documented in the database by only 51%.

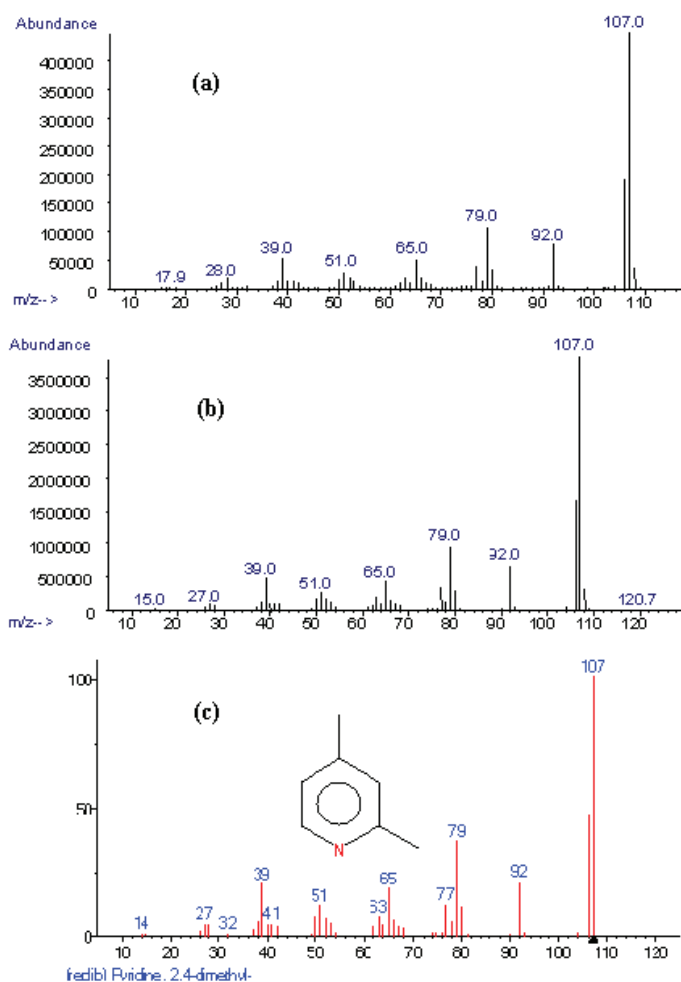


Figure 6.3 (a) Mass spectrum of 2, 4-lutidine in degraded sample of AMP-H₂O-O₂ system at 120°C using 5 mol/kg AMP with 250 kPa O₂; (b) Mass spectrum of standard sample of 2, 4-lutidine; (c) Mass spectrum of 2, 4-lutidine in the database.

The identified products may have been formed during the GC analytical process due to the rigorous operating conditions of the GC-MS. To check this suspicion, UV-VIS spectroscopy was used to determine if 2, 4-lutidine was a degradation compound formed in the reactor. The operating conditions of UV-VIS spectroscopy are much milder. As can be seen in Figure 6.4, lutidine standard and the AMP degradation sample have the same absorption peaks at 258 nm, which is the characteristic absorption of the pyridine ring. These results demonstrate that 2, 4-lutidine was produced in the reactor and indicate that the secondary product was not formed in the GC.

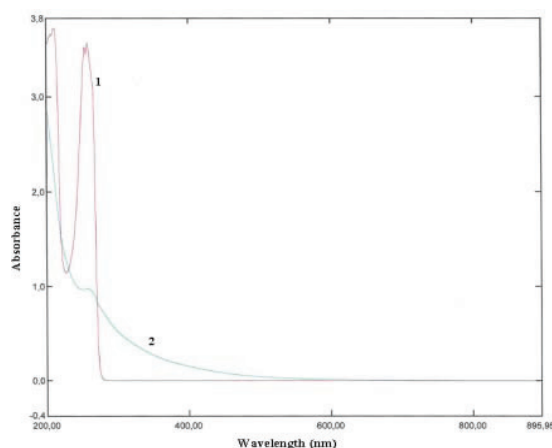


Figure 6.4 UV-VIS spectra of (1) 2, 4-lutidine standard and (2) aqueous solution of partially degraded AMP.

After identification, the three main degradation products were quantified by GC-MS. The uncertainty of quantification by GC-MS was $\pm 6\%$. The error of GC-MS analysis was estimated by standard deviation of peak areas across all concentrations. It should be noted that the uncertainty of estimation of DMOZD may be higher. This estimation was based on 2-oxazolidinone as the standard since DMOZD is not commercially available. Figure 6.5 shows the results at 120°C and 250 kPa O₂. As can be seen in Figure 6.5, acetone was formed in advance of 2, 4-lutidine and DMOZD. In addition, the concentration ratio of acetone to 2, 4-lutidine decreased with reaction time. We detected the same degradation products under other conditions of temperature and oxygen pressure, except that the relative amounts of the products varied (see Table 6.2). Since the distribution of the three products was similar also

at somewhat lower oxygen pressure, such products could also be formed at the lower pressure of the actual process.

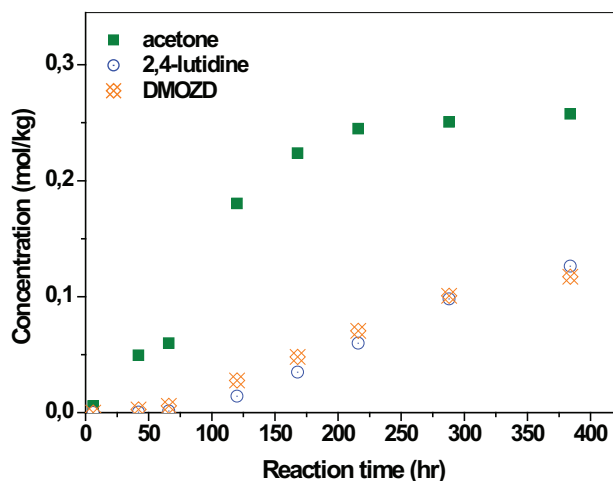


Figure 6.5 Formation of acetone, 2, 4-lutidine and OMOZD in the AMP degradation experiment (120 °C, 250 kPa O₂, initial concentration of AMP = 5 mol/kg).

Table 6.2 The main degradation products in degraded AMP aqueous solutions at 216 h under different experimental conditions (initial AMP concentration = 5 mol/kg).

Product	Concentration (mol/kg)			
	100°C/ 250kPa O ₂	120°C/ 250kPa O ₂	140°C/ 250kPa O ₂	120°C/ 350kPa O ₂
acetone	0.21	0.23	0.33	0.67
2,4-lutidine	0.057	0.060	0.087	0.17
DMOZD	0.065	0.071	0.099	0.19

6.1.2 IC identification

Cation IC and anion IC were used in this study to analyze positively and negatively charged species in the aqueous solutions of degraded AMP. Ammonium, several carboxylic acids, nitrite, and nitrate were identified and quantified as oxidative degradation products of AMP, although they were present in only small amounts except for NH₄⁺ and formic acid. The typical cation and anion chromatograms of a partially degraded AMP solution have been shown in Figure 3.5 and Figure 3.13, respectively. Sodium ions were found in all the samples. The sodium might come from the glass reactor because the reactor was contacted with alkaline solution at high temperatures.

6.1.3 Mass balance achieved in AMP oxidative degradation

The oxidative degradation experiments performed on AMP solutions all suffer from a common failure to close the overall mass balance. The AMP loss measured by cation IC is not balanced with the formation of the identified products. This was true of both the carbon (C) and nitrogen (N) balance.

The N and C Mass balance achieved in the experiment (E14) is provided in Table 6.3 as an example of the mass balance closure usually achieved in this project. During the experiment E14, 1007 mmol AMP per kg solution was lost or 1007 mmol N from AMP per kg solution and 4028 mmol C from AMP per kg solution. Very low levels of glycolate, acetone oxime and other minor degradation products were disregarded. If all of the lost AMP was recovered in degradation products, as in the ideal scenario, the recovery percentage would be 100%. However, only 56.8% of the lost N and 62.6% of the lost C were recovered in the main detectable degradation products. The data indicate that there are still unidentified degradation products that contain both N and C in the liquid reaction mixture. Since only liquid samples were analyzed in this work, volatile products, such as NH₃ in the gas phase could also reduce the mass balance closure.

Table 6.3 Nitrogen and carbon mass balance in degraded AMP solution (5 mol/kg PZ, 120°C, 250 kPa O₂, 16 days).

	Conc. mmol/kg	Nitrogen balance		Carbon balance	
		N conc. mmol/kg	N identified %	C conc. mmol/kg	C identified %
AMP lost	1007	1007	-	4028	-
Degradation products:					
Acetone	257.7	NA	-	773.1	19.2
2,4-lutidine	126.3	126.3	12.5	884.1	21.9
DMOZD	117.2	117.2	11.6	586	14.5
Ammonium	294.8	294.8	29.3	NA	-
Nitrate and nitrite	33.9	33.9	3.4	NA	-
Formate	233.8	NA	-	233.8	5.8
Oxalate	12.7	NA	-	25.4	0.6
Acetate	12.1	NA	-	24.2	0.6
Total Mass recovered in products		572.2	56.8	2526.6	62.6

6.2 Degradation pathways of AMP

Once the major degradation products were identified and quantified and the effects of the main operating parameters were established, we turned our efforts toward the identification of possible reaction pathways for oxidative degradation of AMP. Although the lost AMP was not completely recovered in the generation of degradation products, the major identified products accounted for the most of the N and C loss from AMP.

6.2.1 Formation of acetone and ammonia

Amine can be oxidized via radical mechanisms. As presented in Chapter 2, two mechanisms as possible initiation steps for oxidation of amines have been proposed: electron abstraction and hydrogen abstraction, i.e. the oxidant could abstract an electron from the nitrogen atom giving an N-centered radical cation or the oxidant could abstract a hydrogen atom from the nitrogen, α -carbon or β -carbon atom (α , β -position with regard to the amino functional group). In the case of the N-centered radical cation the molecule could subsequently split off a proton from the α C-H group. Further abstraction of an electron by the oxidant will lead to an imine which can be readily hydrolyzed by water. The formation of a radical on the tertiary carbon in the α -position of the nitrogen atom in AMP is basically impossible as it has no α -hydrogen, and hence is not able to form an imine which is assumed to be a first step in the electron abstraction mechanism. Therefore, the oxidative degradation of AMP observed in this work cannot be explained with the proposed electron abstraction mechanism. It is more likely that AMP is degraded via a hydrogen abstraction mechanism as an initial step.

How initiating H-abstraction occurs, i.e. the initiating step is not clear. Similar to liquid phase autoxidation of higher hydrocarbons we expect initiating radicals to be formed continuously, but seldom. Concentration of thermal vibration energy onto one bond or reaction with oxygen could be the initiating event (Franz and Sheldon, 1991). Hence, formation of initiating radicals is enhanced as temperature and/or oxygen partial pressure is increased. The weakest hydrogen-containing bond is expected to be readily attacked. The exact bond dissociation enthalpies (BDEs) for the hydrogen-containing bonds of AMP are not available. The BDEs of the hydrogen containing bonds in the $-\text{NH}_2$, $-\text{OH}$ and $-\text{CH}_2/-\text{CH}_3$ groups, which are also present in the AMP molecule, were used for comparison. Tert-butylamine, methanol and ethane were used as reference compounds. According to literature

(Anslyn and Dougherty, 2006; Lalevée et al., 2002), the C-H bond adjacent to the OH group is the weakest hydrogen-containing bond in the AMP molecule (see Table 6.4), and thus HO \dot{C} HC(CH₃)₂NH₂ could be predominantly formed.

Table 6.4 Reference bond dissociation energies.

Compound	Bond	BDE (kcal/mol)	References
methanol	CH ₃ O-H	104.4	Anslyn and Dougherty, 2006
methanol	HOCH ₂ -H	94	Anslyn and Dougherty, 2006
ethane	CH ₃ CH ₂ -H	98.2	Anslyn and Dougherty, 2006
Tert-butylamine	(CH ₃) ₃ CNH-H	95 ^a (101 ^b)	Lalevée et al., 2002

^a Experimental error ~ 2 kcal/mol. ^b predicted from computational method.

Once a radical is created, it will react rapidly with oxygen at a rate close to the rate of a diffusion controlled process (Sonntag and Schuchmann, 1997). Thus peroxy radicals are expected to be the primary oxidation products in the presence of O₂. Formation of peroxide has been observed during air oxidation of MEA (Blachly and Ravner, 1966). We propose that the newly formed carbon-centered radical from AMP is converted into the corresponding peroxy radical (**1**) by a fast reaction with O₂ as shown in Figure 6.6. Then the peroxy radical decays into further products. This pathway may explain the dramatic effect of O₂ partial pressure on the AMP oxidation rate, as shown in Figure 5.8.

Hydrogen-abstraction reactions by peroxy radicals are common. These transformations involve intramolecular as well as intermolecular H-transfer (Sonntag and Schuchmann, 1997). The decay of the peroxy radical (**1**) is speculated to occur by intramolecular hydrogen abstraction through a six-membered cyclic transition state, together with formation of a \cdot OH radical. This step is proposed in analogy to intramolecular decomposition of the 2, 4-dimethyl pentane peroxy radical in aqueous solution (Sonntag and Schuchmann, 1997). Figure 6.6 describes the proposed degradation pathway for AMP. The peroxy radical (**1**) abstracts a hydrogen atom from the N-H bond intramolecularly via a six-membered cyclic transition state. After ejection of a \cdot OH radical from this transition state, it decomposes to formic acid and an imine (**2**). The imine is not expected to remain stable in aqueous solution, and should readily hydrolyze to ammonia and acetone. At the same time, the peroxy radical (**1**) could

also decompose to formic acid and an enamine (3) via a similar intramolecular hydrogen abstraction from a C-H bond combined with $\cdot\text{OH}$ radical formation. The enamine is in equilibrium with an imine and may thus also degrade to acetone and ammonia.

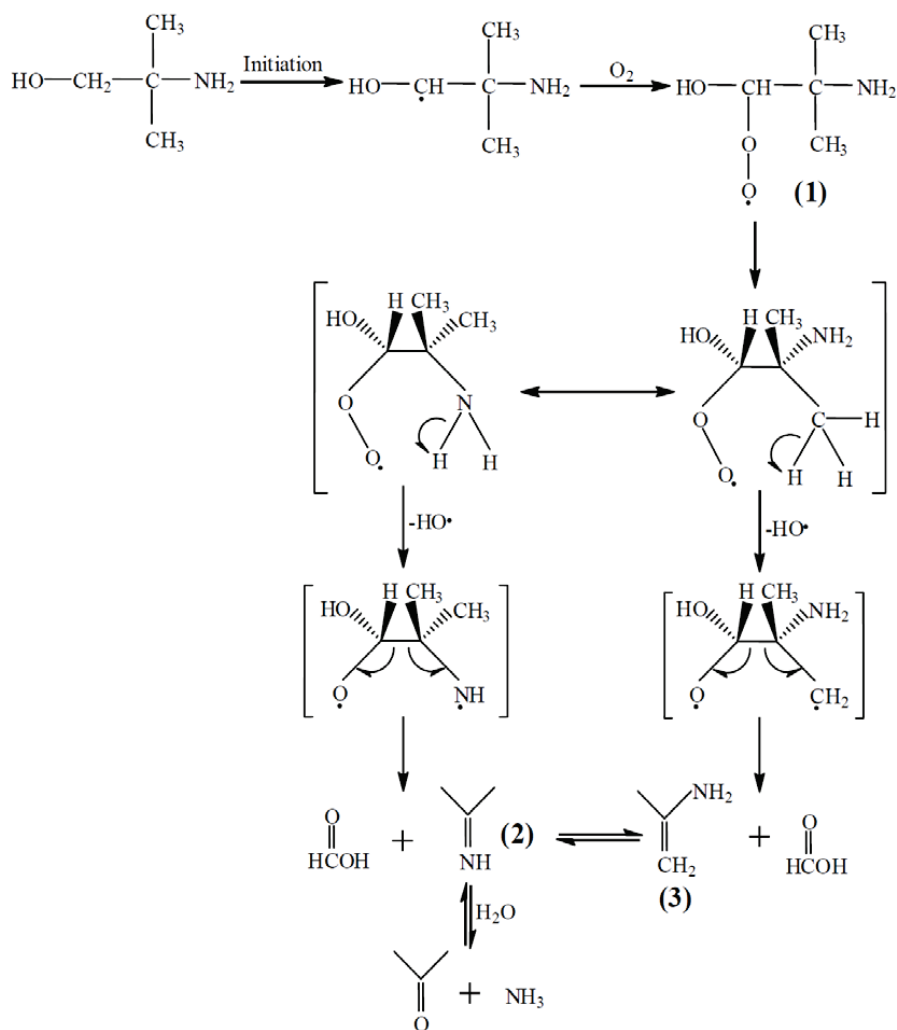


Figure 6.6 Scheme for the decay of AMP to primary products. Degradation pathways following the formation of a peroxy radical (1) to yield an imine (2) or an enamine (3) are illustrated.

our case, parallel with $\text{NO}_2^-/\text{NO}_3^-$ formation, the ammonium ion concentration increased with reaction time. This is probably due to the decreasing pH value of the liquid phase. Moreover, ammonia from the gas phase may re-dissolve into the liquid phase as the ammonia in the liquid phase is consumed through $\text{NO}_2^-/\text{NO}_3^-$ formation.

6.2.3 Formation of carboxylic acids

The carboxylic acid ions, such as formate, acetate, oxalate and glycolate have been determined as AMP degradation products. Figure 6.8 shows the anionic degradation product formation rates for a 5mol/kg AMP solution subjected to oxidative degradation. The major ionic degradation product is formate; in fact, formate is present at much higher concentration than any other carboxylate ion at the end of the experiment. This result agrees with the proposed scheme as shown in Figure 6.6, formic acid is a primary product of AMP oxidation.

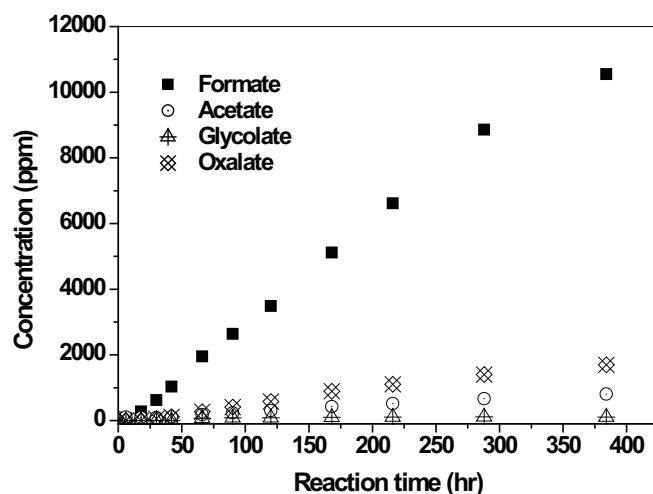


Figure 6.8 Formation of carboxylic acids in the AMP degradation experiment (120 °C, 250 kPa O_2 , initial concentration of AMP = 5 mol/kg).

In fact, carboxylates have been detected from oxidative degradation of many ethanolamines, but no general mechanism has been proposed to account for their formation. Rooney et al. (1998) proposed an explanation for carboxylic acid formation from MEA oxidation. According to the proposed schemes, monomethylamine (MMA) should be a product along with formation of formic acid. However, no proof of formation of MMA can be found in the report. Furthermore, MMA was not detected in a degraded MEA system

using our developed cation IC method in the present work, as described in Chapter 3. Ye and Zhang (2001) proposed another route to carboxylic acid formation from MDEA. In aqueous solution, equilibrium exists between MDEA and ethylene glycol. Ethylene glycol can be oxidized into oxalic acid and then formic acid. The authors also proposed that MDEA can be directly oxidized to acetic acid. The mechanism was not detailed in the report. Lepaumier et al. (2009a) suggested formation of ethylene oxide which is hydrolyzed into ethylene glycol leading to carboxylic acids in MEA oxidation. However, none of the proposed schemes can explain the formation of carboxylic acids during AMP oxidation.

In the presence of $\cdot\text{OH}/\text{O}_2$, Stefan et al. (1996; 1999) observed carboxylic acid formation (formic-, acetic-, oxalic- and glycolic acid) from acetone degradation in aqueous solutions and their proposed mechanism of acetone decomposition in the presence of $\cdot\text{OH}/\text{O}_2$ can be applied to explain the formation of small amounts of oxalic-, acetic- and glycolic acid in the case of AMP oxidative degradation process. Formaldehyde, pyruvic acid and pyruvaldehyde were detected in acetone degradation (Stefan and Bolton, 1999), but these by-products were not detected in AMP degradation samples. It may be that these intermediates cannot accumulate to any significant degree in the slow oxidation process of AMP.

6.2.4 Formation of DMOZD

As depicted in Chapter 4, CO_2 reacted with AMP to form DMOZD. The steric hindrance in the AMP molecule does not prevent oxazolidinone formation. It is interesting to note that DMOZD was identified as a major degradation product of AMP at all the AMP oxidation experiments despite the fact that no CO_2 was introduced into the reaction system. DMOZD has also been identified and quantified by Lepaumier et al (2009a). In that investigation, 4 mol/kg aqueous AMP solution was degassed to strip CO_2 and then loaded into a stainless steel reactor. Analytical synthetic air ($\text{CO}+\text{CO}_2<0.5\text{vpm}$) was fed into the batch reactor to 2 MPa at 140 °C. It was estimated that the amount of CO_2 introduced into the reactor was less than 0.02 μmolar . In terms of the percentage of formation of the identified product defined by the authors, the percentage of formation of DMOZD was estimated at 1.3×10^{-5} even although all the CO_2 introduced into the system was converted to DMOZD. Surprisingly, the percentage of formation of DMOZD in Lepaumier's investigation was 0.5. These earlier observations suggest that CO_2 could be a degradation product of AMP in the AMP- O_2 - H_2O system under these experimental conditions. The complete mineralization of the carboxylic

acids from the decay of acetone may be the most probable source of CO₂. The Eschweiler-Clarke reaction which was proposed by Lepaumier et al. (2009a) as a less possible pathway for N-methylated AMP formation is another possible source of CO₂. However, in our case this pathway seems unlikely since the accompanying product, *N*-methylated AMP, was not found.

6.2.5 Formation of 2, 4-lutidine

2, 4-Lutidine formation has never been reported as an oxidative degradation product of AMP, but it was actually the principal product of aqueous AMP degradation at the elevated temperatures used in this work. Figure 6.9 illustrates the proposed pathway for the formation of 2, 4-lutidine (6). Formaldehyde, which could be generated through decomposition of acetone, can be converted by various pathways, such as oxidation to formic acid as was suggested by Stefan et al. (1999) or through condensation with acetone to form a α , β -unsaturated ketone (4). Analogous to keto-enol tautomerism, the enamine (3) is in equilibrium with the imine (2) because a hydrogen atom can switch its location between the heteroatom (nitrogen) and the second carbon atom. In the proposed mechanistic pathway, the polarized enamine (5) reacts with the α , β -unsaturated ketone (4) to form 2, 4-lutidine in the presence of O₂. Although the equilibrium of imine-enamine tautomerism is usually poised toward the imine, reaction between the polarized enamine (5) and the α , β -unsaturated ketone (4) may shift the equilibrium in favor of the enamine.

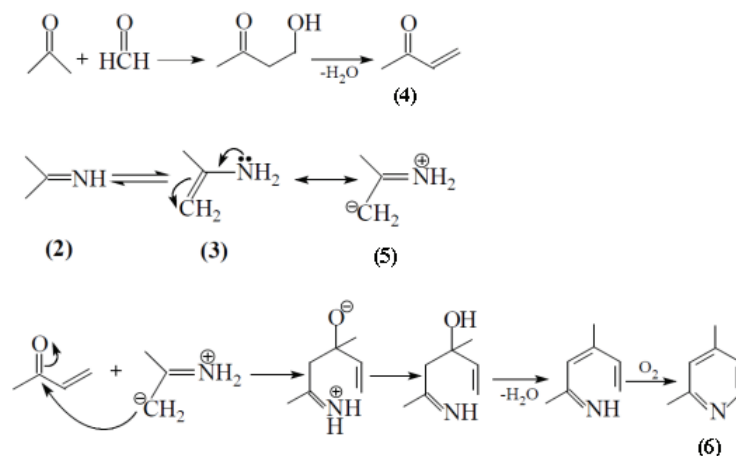


Figure 6.9 Scheme for formation of 2, 4-lutidine.

The synthesis of alkyipyridines is readily achieved by a liquid-phase reaction of aldehyde or ketone mixtures with NH_3 (Grayson and Dinkel, 1984), however, in this synthesis 2, 4-lutidine is a minor product. To confirm the possibility of 2, 4-lutidine generated via the proposed mechanism as shown in Figure 6.9, the fate of a mixture of acetone, formaldehyde and NH_3 (molar ratio 2:1:1) in alkali condition ($\text{pH}=12$) in the presence of 250 kPa O_2 at 120 °C was investigated. 1.03 g ammonium hydroxide (based on ammonia), 7.18 g acetone and 1.87 g formaldehyde in 80 mL of water was treated with 5 M potassium hydroxide to $\text{pH}=12$. The mixture was loaded into a glass reactor with stainless steel lock and heated to 120 °C. After the temperature increased to the desired value, O_2 was introduced into the reactor up to the total pressure of 370 kPa. After 1 hour, 2, 4-lutidine was detected as a major product by GC-MS. The chromatogram at 24 h (Figure 6.10) shows that small amount of trimethyl pyridines were produced in addition to 2, 4-lutidine. Small amounts of trimethyl pyridines were also detected in the partially degraded AMP samples. These results provide additional support that 2, 4-lutidine can be produced through the proposed pathways. 2, 4-Lutidine was also identified as a product of the reaction of acetone, formaldehyde and ammonia in the presence of O_2 at 60 °C, but in less concentration. It seems that higher temperature is favourable for lutidine formation.

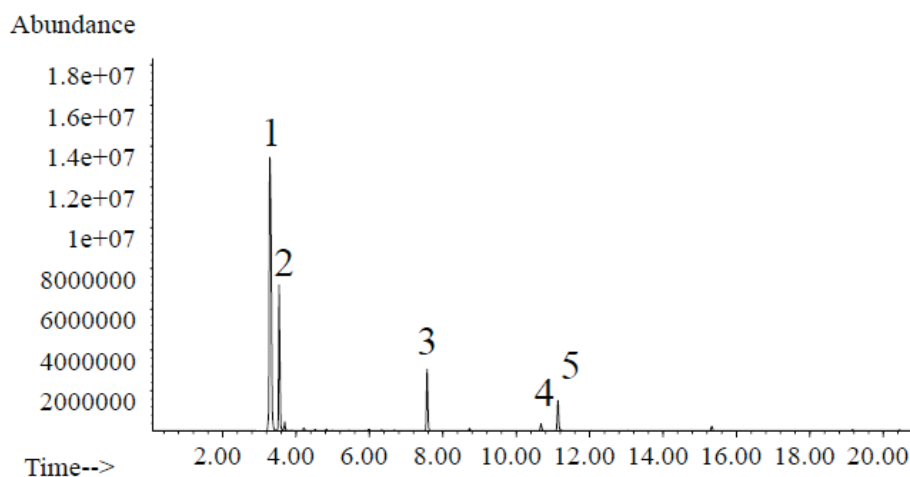


Figure 6.10 Gas chromatogram of a model reaction mixture of acetone, formaldehyde and ammonia in KOH solution at 120°C with 250 kPa O_2 (24 h). Peak 1 is water, peak 2 is acetone, peak 3 is 2, 4-lutidine, peak 4 and peak 5 were identified as trimethyl pyridines.

6.2.2 Formation of NO_2^- and NO_3^-

Nitrite (NO_2^-) and nitrate (NO_3^-) ions were observed during the AMP oxidation process, and NO_2^- was formed in advance of NO_3^- . In addition, NO_2^- and NO_3^- demonstrated different time profiles in the oxidative degradation of AMP in the presence of O_2 (see Figure 6.7). The concentration of NO_3^- ascended linearly with reaction time while NO_2^- concentration at first increased and then decayed with reaction time, indicating that NO_2^- and NO_3^- could be produced through consecutive oxidation of NH_3 by $\cdot\text{OH}$.

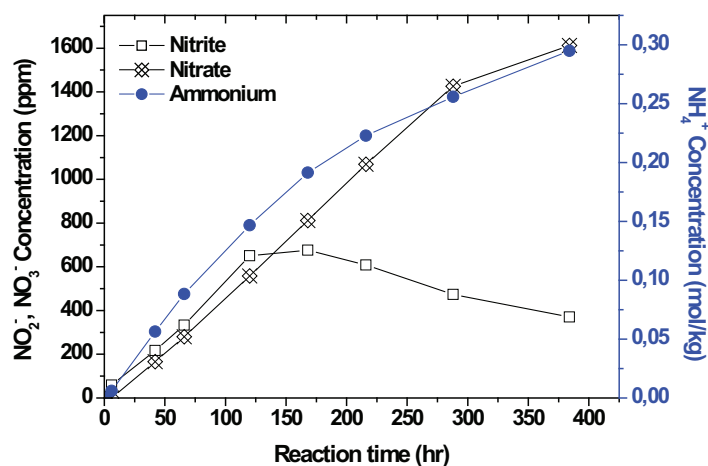
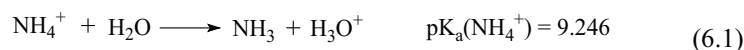


Figure 6.7 Formation of nitrite, nitrate and ammonium in the AMP degradation experiment (120 °C, 250 kPa O_2 , initial concentration of AMP = 5 mol/kg).

The formation of NH_3 is due to hydrolysis of the imine (2). According to the dissociative equilibrium of ammonia in water, the concentration of NH_3 (in molecular form) and that of the cation form (NH_4^+) are approximately equal at pH 9.25 (see Equation 6.1).



Therefore, once formed, NH_3 is the predominant component of ammonia in the basic AMP solution. NH_3 would be oxidized to $\cdot\text{NH}_2$ by the attack of $\cdot\text{OH}$, then $\cdot\text{NH}_2$ would be oxidized to $\cdot\text{NHOH}$. The unstable $\cdot\text{NHOH}$ would rapidly convert to NH_2O_2^- and consequently to NO_2^- . Gradually, NO_2^- would be oxidized to NO_3^- . An example of NO_2^- and NO_3^- formation similar to this case has appeared previously (Huang et al., 2008). In that case, $\cdot\text{OH}$ radical generated by H_2O_2 photolysis could oxidize NH_3 to NO_2^- and ultimately to NO_3^- in aqueous solution. In

6.2.6 Large autoclave experiment at 80°C

The degradation pathways discussed above are based on data collected at temperatures of 100-140°C. In order to investigate the effect of temperature on the degradation pathway, an experiment was performed in the large autoclave reactor with 5mol/kg AMP under 250 kPa O₂ at a relatively low temperature, 80°C. The temperature of the miniclave reactors fluctuated around the setting value with 5-6°C. The temperature control in large autoclave reactor was much better. When the temperature was set at 80°C, the deviation was ± 0.2°C.

6.2.6.1 Formation of 2, 4-lutidine

Figure 6.11 shows a typical gas chromatogram of an AMP solution that was degraded 13 weeks at 80°C. 2, 4-Lutidine has been identified as one of major products of AMP oxidation at 100-140°C. It was still found as a degradation product at 80°C, but compared with production of acetone, it was present in much less concentration than that found at 100-140°C. This observation is consistent with the result of the synthesis experiments, the reaction of acetone, formaldehyde and ammonia in the presence of O₂. The lower the temperature is, the less 2, 4-lutidine is formed.

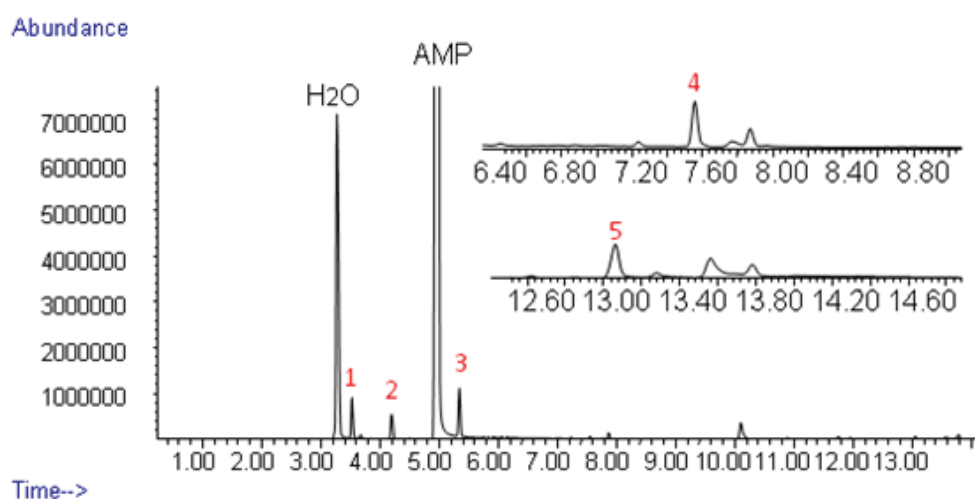
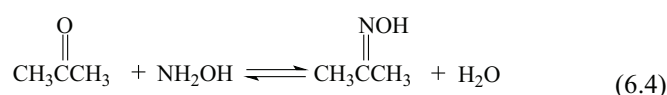
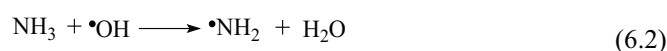


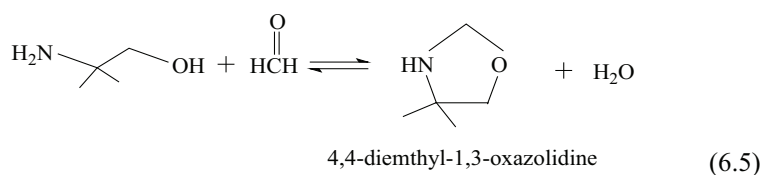
Figure 6.11 Gas chromatogram of a partially degraded AMP aqueous solution after 13 weeks using 5 mol/kg AMP at 80°C with 250 kPa O₂. Based on comparison to a library of MS spectra, in addition to water and AMP, the identified products were acetone (peak 1), acetone oxime (peak 2), 4, 4-dimethyl-1, 3-oxazolidine (peak 3), 2, 4-lutidine (peak 4), and DMOZD (peak 5).

6.2.6.2 Formation of acetone oxime and 4, 4-dimethyl-1, 3-oxazolidine

Figure 6.11 shows that acetone oxime (peak 2) and 4, 4-dimethyl-1, 3-oxazolidine (peak 3) were the major products of AMP oxidation at 80°C except for acetone. Acetone oxime could be produced via a hydroxylamine route, as shown with Equations 6.2-6.4. The primary degradation product of AMP, NH₃ was oxidized to NH₂OH by •OH radical, and then NH₂OH reacted with acetone to form acetone oxime.



Formaldehyde, which could be generated through decomposition of acetone in the presence of •OH radical, can be reacted with AMP to produce 4, 4-dimethyl-1, 3-oxazolidine at relatively low temperature, as is shown by Equation 6.5. These two new major products, acetone oxime and 4, 4-dimethyl-1, 3-oxazolidine, can be produced from AMP and the primary degradation products which were identified or proposed in the AMP solutions degraded at 100-140°C. This result indicates the oxidation of AMP might undergo the same primary degradation pathway at different temperatures, but different temperature may result in a different product distribution due to the impact of temperature on the secondary reactions between the primary products.



6.2.6.3 Effect of temperature on final product distribution

To obtain a clearer understanding of the effect of temperature on the distribution of the final degradation products, the AMP solution degraded for 13 weeks at 80°C was removed into a miniclave reactor and the degradation was continued at 120°C in the presence of 250

kPa O₂. The gas chromatogram in Figure 6.12 compares the AMP solution degraded for 13 weeks at 80°C with that of the reaction mixture after a continued heating for 24 hours at 120°C. The chromatograms show that concentration of acetone oxime and 4, 4-dimethyl-1, 3-oxazolidine decreased significantly when the reaction mixture was heated for 24 hours at 120°C, and that concentration of acetone and 2, 4-lutidine increased dramatically. This result clearly shows the effect of temperature on the distribution of the final degradation products and explains why 4, 4-dimethyl-1, 3-oxazolidine and acetone oxime were not observed as major degradation products of AMP at 100-140°C.

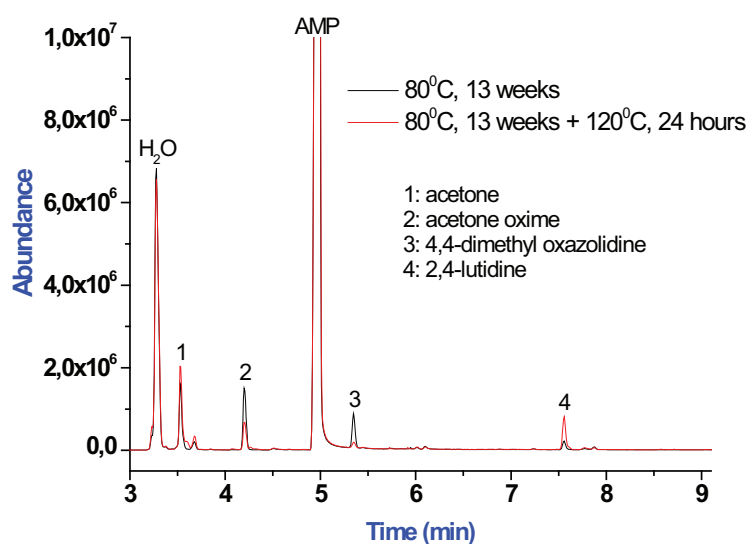


Figure 6.12 Comparison of the gas chromatogram of the degraded AMP solution at 80°C after 13 weeks and that of the reaction mixture after heated 24 hours at 120°C (initial AMP concentration = 5 mol/kg).

6.3 Degradation of AMP accelerated by UV radiation

Amine oxidation is believed to occur via a radical mechanism. Radical reactions must first be initiated. If sufficient oxygen is dissolved in solution, the initiation is the limiting step of amine oxidation (Denisov and Afanas'ev, 2005). At low temperature, the degradation rate of amine is slow. Therefore, in order to shorten the length of the experiments from months to days, most of the degradation experiments are conducted at elevated temperatures. However, as described previously, high temperature might affect secondary reactions, which will lead

to different distributions of the final products. Since a quantum of ultraviolet (UV) radiation, or even of visible light, carries sufficient energy to break different covalent bonds in organic compounds, the amine oxidation is expected to be accelerated by high-energy radiation even at low temperature.

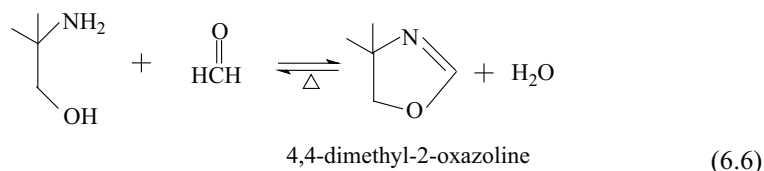
This section is used to test the effect of UV radiation on oxidative degradation of AMP at typical absorber temperature in order to develop a new method to reduce the length of experiments of oxidation of alkanolamines from months to days (or even hours) without inducing new degradation mechanisms. On the other hand, this experiment was also conducted to verify the radical degradation pathway of AMP proposed previously. In this work, UV radiation from a medium pressure mercury lamp was used to accelerate oxidative degradation of AMP. The lamp radiates predominantly 355-356 nm radiation. The radiation of wavelength 355-356 nm is equivalent to approximately 78 kcal/mol¹, which is lower than the BDE of the weakest H-containing bond in AMP molecule. The experiments were conducted using 1 mol/kg AMP with sparging of O₂ through the AMP solution at 55°C. Large amounts of products were identified and compared with those found in thermally accelerated oxidations of AMP.

The nonionic products identified with GC-MS included acetone, acetone oxime, formamide, 4, 4-dimethyl-2-oxazoline, acetamide, 4, 4-dimethyl-1, 3-oxazolidine, N-formyl-AMP (suspected), DMOZD and methenamine. N-formyl-AMP was speculated based on analysis of the mass spectrum, but was not confirmed by an authentic standard. Compared with thermally accelerated oxidation of AMP, 4, 4-dimethyl-2-oxazoline, N-formyl-AMP and methenamine are 'new' products, and formamide appeared in much higher concentration.

2-Oxazolines are versatile heterocycles, which are used as a protecting group, coordinating ligand, and activating moiety in synthetic organic chemistry (Gant and Meyers, 1994), and hence are studied extensively. Many methods exist for preparation of oxazolines, one of the synthetic routes involves reaction of aliphatic aldehydes with 2-aminoethanol to the corresponding 2-alkyl-2-oxazoline in good yield (Takahashi and Togo, 2009). Since AMP belongs to 2-aminoethanol family and formaldehyde is an expected degradation product of

¹ The energy generated by a single photon is given by $E = h\nu = hc/\lambda$. Using $E_{mol} = 6.02 \times 10^{23} E$ gives the energy value per mole.

AMP, 4, 4-dimethyl-2-oxazoline could be formed in the UV experiment via a similar route as shown in Equation 6.6.



Equations 6.5 and 6.6 describe two parallel reactions for AMP and formaldehyde with each other. An experiment was performed to verify these two reactions. 1mol/kg AMP was reacted with 0.5 mol/kg formaldehyde at 55°C. The two expected products, 4, 4-dimethyl-1, 3-oxazolidine and 4, 4-dimethyl-2-oxazoline were detected after 1 hour (see Figure 6.13). 4, 4-Dimethyl-1, 3-oxazolidine was predominant over 4, 4-dimethyl-2-oxazoline. This result is in accordance with the result of the UV experiment, in which concentration of 4, 4-dimethyl-1, 3-oxazolidine was much higher compared with 4, 4-dimethyl-2-oxazoline. Formaldehyde was not detected in all the previous AMP oxidation experiments since formaldehyde is expected to be readily oxidized to formic acid in the presence of O₂.

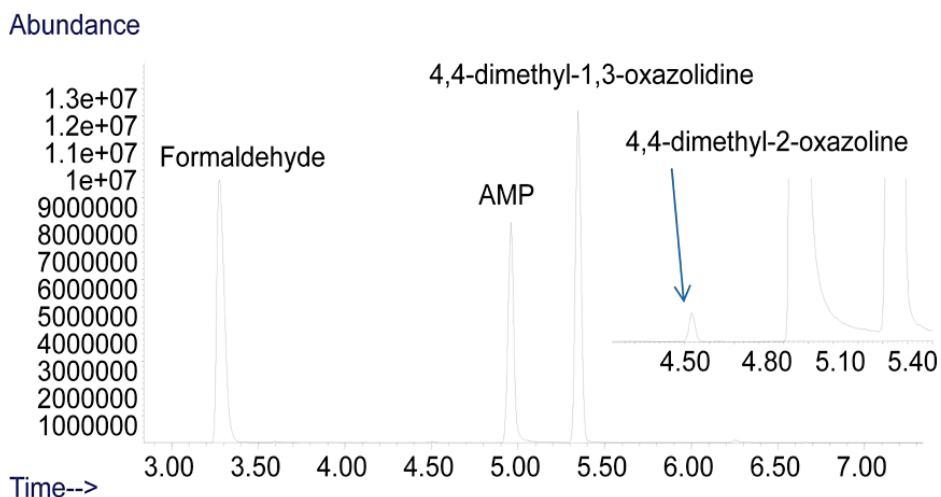
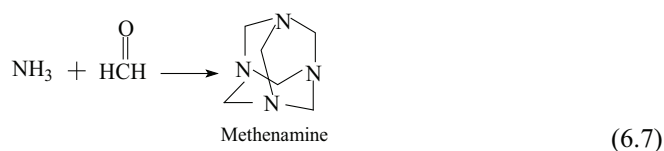
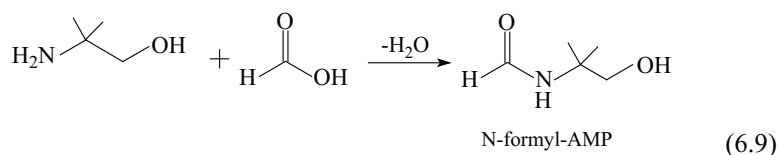
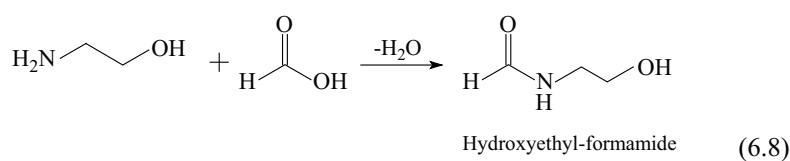


Figure 6.13 AMP and formaldehyde at 55°C (initial AMP concentration = 1 mol/kg, Formaldehyde concentration = 0.5 mol/kg).

Methenamine is a heterocyclic organic compound, which has a cage-like structure, similar to adamantane. It is useful in the synthesis of other chemical compounds and is easily prepared by reaction of formaldehyde and ammonia (Eller et al., 2005). This reaction as shown in Equation 6.7, can be conducted in the gas-phase or in solution. Both of NH_3 and formaldehyde belong to the expected products of AMP oxidation according to the proposed schemes, thus it is not surprising to detect methenamine in the reaction mixture. However, the concentration of methenamine declined dramatically when heating the sample to $100\text{ }^\circ\text{C}$ for hours. This could be the reason why methanamine is not detected in the oxidations of AMP at elevated temperatures.



Sexton (2008) observed hydroxyethyl-formamide (HEF) as an important product of MEA oxidation in the presence of Fe^{2+} at $55\text{ }^\circ\text{C}$. The author suggested that HEF is produced by reaction of MEA and formaldehyde, followed by oxidation to the amide. Lepaumier et al. (2011) also found HEF in MEA oxidation at $55\text{ }^\circ\text{C}$, and proposed that HEF is formed by reaction of MEA and formic acid (Equation 6.8). Since MEA has been found to react with formic acid to give HEF, we also suspected that there could be similar reaction between AMP and formic acid to produce N-formyl-AMP at $55\text{ }^\circ\text{C}$ as described by Equation 6.9.



In order to verify the identification of the suspected N-formyl-AMP peak, and identify its possible formation route, a mixture of 1 mol/kg AMP and 0.15 mol/kg formic acid was reacted at $55\text{ }^\circ\text{C}$. A new peak was observed by GC-MS analysis after 2 hours, with the same

retention time as that of the suspected degradation product of AMP in the UV experiment. The gas chromatogram of the reaction mixture of AMP and formic acid as well as the gas chromatogram of partially degraded AMP from the UV experiment are compared in Figure 6.14. This result gives positive proof that the suspected product in the UV experiment is N-formyl-AMP and can be produced by reaction of AMP with formic acid. In the thermally accelerated experiments, no measurable N-formyl-AMP was found. We speculate that N-formyl-AMP is readily hydrolyzed to AMP and formic acid at higher experimental temperatures. This speculation will be verified in a later experiment.

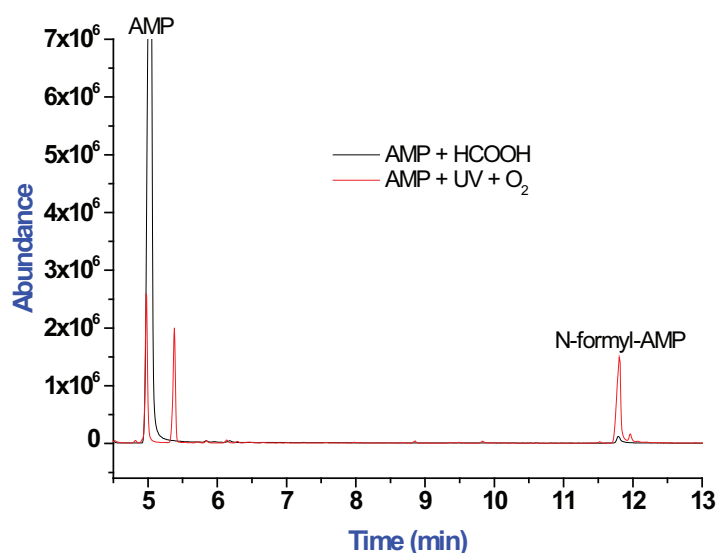


Figure 6.14 Comparison of the gas chromatogram of the mixture of AMP and formic acid after 2 hour reaction and the gas chromatogram of a degraded AMP solution in the presence of UV radiation and O₂ after 48hours. Both experiments were performed at 55°C (initial AMP concentration = 1 mol/kg).

As discussed above, all the ‘new’ products were formed by reactions of AMP with its primary degradation products, ammonia, formic acid, and formaldehyde. That means the proposed primary pathway for thermally accelerated oxidation of AMP can still be used to account for the result of AMP oxidation in the presence of UV radiation. To verify the thermal stability of these ‘new’ products, the UV reaction mixture was removed into a miniclave reactor and the degradation was continued in the presence of O₂ at 120°C. As shown in Figure 6.15, after 24 hours, the ‘new’ found products in the UV experiment,

formamide (peak 2), 4, 4-dimethyl-2-oxazoline (peak 3), N-formyl-AMP (peak 6), and methenamine (peak 7) disappeared almost completely. The amount of acetone oxime (peak 1) and 4, 4-dimethyl-1, 3-oxazolidine decreased also. This result suggests that these ‘new’ products were not detected as major products at elevated temperatures due to their instability at elevated temperatures. It should, however, be noted that one unknown compound (peak 5) noticeably increased.

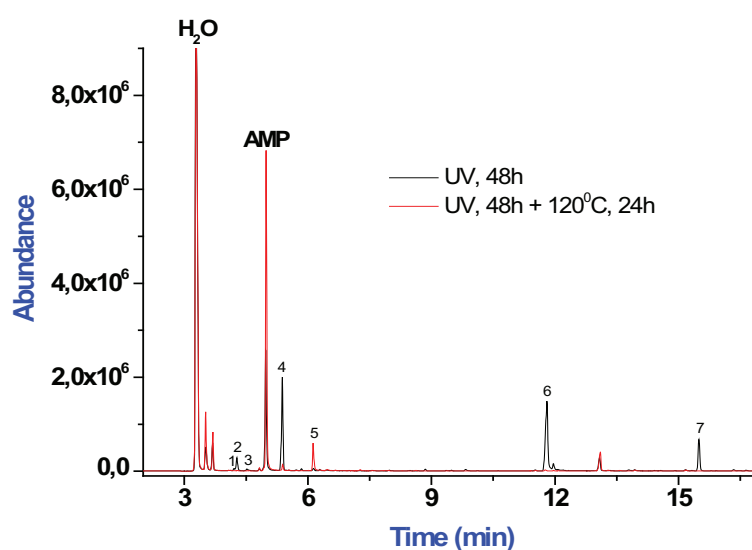


Figure 6.15 Comparison of the gas chromatogram of the degraded AMP solution in the presence of UV radiation at 55°C after 48 hours reaction time and that of the reaction mixture after heating for 24 hours without UV radiation at 120°C (initial AMP concentration = 1 mol/kg). The labeled products: acetone oxime (peak 1), formamide (peak 2), 4, 4-dimethyl-2-oxazoline (peak 3), 4,4-dimethyl-1,3-oxazolidine (peak 4), unknown (peak 5), N-formyl-AMP (peak 6), methenamine (peak 7).

Another speculation is that the final products may be affected by degradation rate. In the UV experiment, the degradation rate of AMP is much faster than that in thermally accelerated experiments. Consequently, the formation rates of the primary products and intermediates are much higher accordingly. For example, if the formation rate of formaldehyde is increased substantially, there is a higher probability that formaldehyde is able to react with other primary products and/or intermediates before it is oxidized to formic acid.

It was also of interest to check what is going on at dark condition after the oxidation of AMP is initiated by UV radiation. An experiment was performed on 1 mol/kg aqueous AMP solution with UV radiation in the presence of O₂ at 55°C. The UV light was switched off after 30 hours, but O₂ was continued sparged through the solution. AMP loss and formation of degradation products was monitored. The results are shown in Figure 6.16-6.18. It is interesting to note that AMP loss stopped and the concentration of all the identified products did not increase after the UV light was switched off. This result shows that oxidative degradation of AMP becomes negligible when the UV radiation is turned off. Since a radical chain reaction is cyclic process which can start over again once initiated (Perkins, 1994). It seems that AMP is oxidized through a radical mechanism but the oxidation is not a chain reaction. The proposed degradation pathway of AMP in Figure 6.6 supports this speculation, since the produced ·OH radicals are consumed by the secondary reactions according to the proposed schemes, such as NH₃ oxidation and acetone decomposition. Thus the ·OH radicals cannot serve as chain carriers during AMP oxidation.

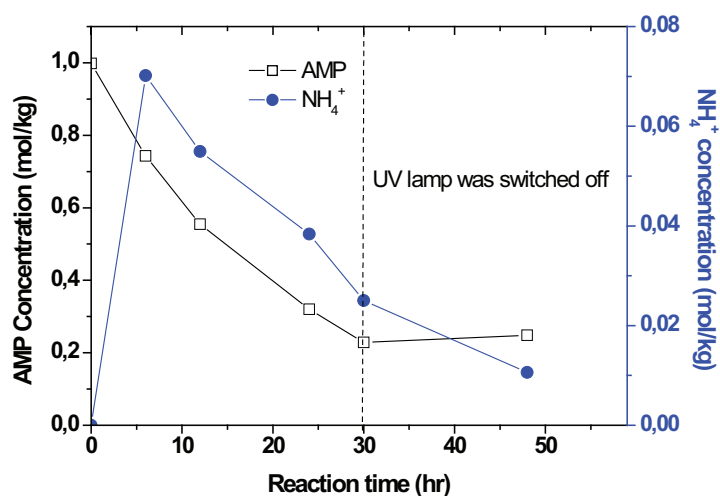


Figure 6.16 AMP loss and formation of NH₄⁺ in the UV experiment. The experiment was performed using 1 mol/kg AMP in the presence of UV radiation and oxygen at 55°C.

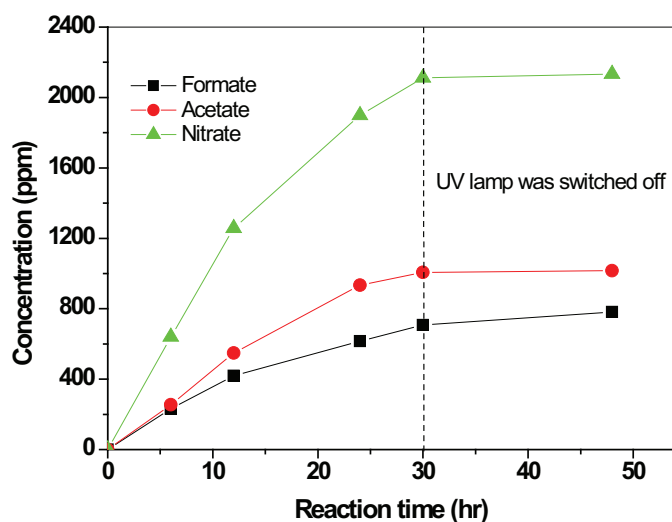


Figure 6.17 Formation of anionic products in the UV experiment. The experiment was performed using 1 mol/kg AMP in the presence of UV radiation and oxygen at 55°C.

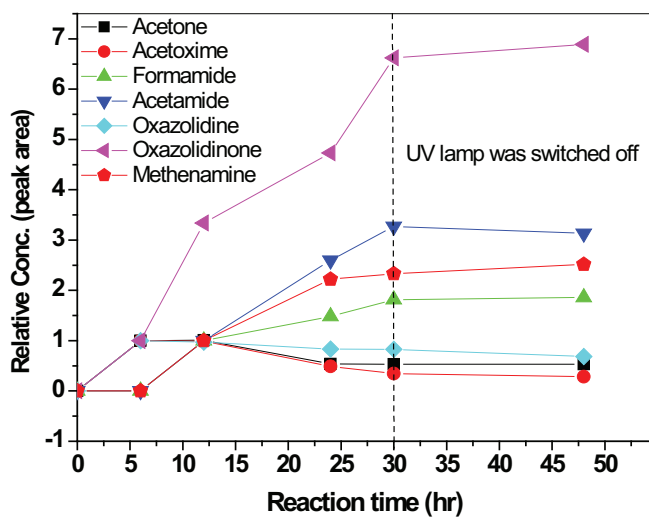
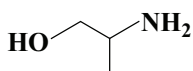


Figure 6.18 Generation of the products identified by GC-MS. The experiment was performed using 1 mol/kg AMP in the presence of UV radiation and oxygen at 55°C.

6.4 Oxidative degradation of 2-amino-1-propanol

Oxidative degradation of a structural analog of AMP, 2-amino-1-propanol (APN) is presented in this section. Anionic products of APN will be identified and compared to those of AMP oxidation. Figure 6.19 shows the structure of APN.



2-amino-1-propanol

Figure 6.19 Chemical structure of 2-amino-1-propanol.

As compared to AMP, one of the two methyl group on the α -carbon is replaced by a hydrogen atom in APN molecule. This means that APN is only slightly sterically hindered and the effect of the single additional methyl group should be “milder” than two additional methyl groups in AMP. 3 mol/kg aqueous solution of APN was degraded under 250 kPa O_2 at 120 °C. APN loss and formation of ammonium in the liquid phase were determined as shown in Figure 6.20. As expected, the overall degradation rate of APN (4.2 mmol/(kg·h) after 384 hours) is almost 2 times of that of 3mol/kg AMP degraded at the same conditions.

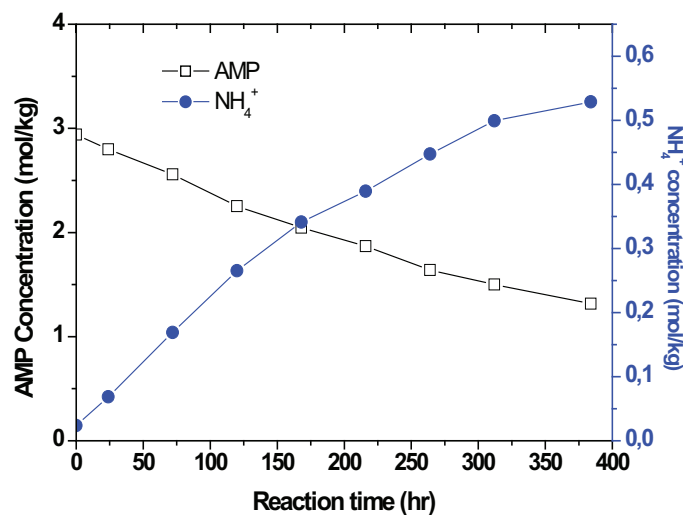


Figure 6.20 Amine loss and formation of ammonium in the APN degradation experiment (120 °C, 250 kPa O_2 , initial concentration = 3 mol/kg).

The effect of replacing a C-H bond by a C-C bond at the α -carbon on the rate of amine degradation rate is beyond the scope of this investigation. The focus in this case was to test if the proposed AMP oxidation schemes could also be used to explain formation of oxidative degradation products of structural analogs of AMP. Oxidative degradation products must be identified and quantified in order to speculate possible degradation pathways for APN. Unfortunately, inside the frame of this work we have not been able to find a suitable column for separation of the non-ionic degradation products of APN by GC-MS analysis. However, some speculation on the primary degradation pathways of APN can still be made by examining the oxidation products identified using anion IC.

If APN is degraded by a similar pathway as proposed for the oxidation of AMP, acetic- and formic acid could be predominate over other anionic products. The pathway for initial hydrogen abstraction and ultimate formation of acetic- and formic acid is presented in Figure 6.21. The initial hydrogen abstraction from the C-H bond adjacent to the OH group is considered to be more likely as compared to C-H abstraction from other C-H bonds since it is the weakest C-H bond in the APN molecule according to the BDEs of C-H bonds in the corresponding reference compounds. The approximate C-H bond strength for $(\text{CH}_3)_2\text{CH-H}$ is 95.1 kcal/mol versus 94 kcal/mol for a $\text{HOCH}_2\text{-H}$ bond (Anslyn and Dougherty, 2006), making it slightly more difficult to abstract a proton from the α -carbon. The C-H bond in the methyl group is the strongest C-H bond, additionally, primary carbon radical is less stable than a secondary carbon radical, and thus hydrogen abstraction from the methyl group is not likely to occur.

After initiation, the degradation pathway could be speculated to be similar as what described for AMP degradation in Figure 6.6. Forming of a carbon-centered radical is followed by the production of a peroxy radical in the presence of dissolved O_2 in solution. The peroxy radical could decay by intramolecular hydrogen abstraction from the $-\text{NH}_2$ or $-\text{CH}_3$ group through a six-membered cyclic transition state. After ejection of a $\cdot\text{OH}$ from this transition state, it could decompose to formic acid and an imine. The imine is not stable in aqueous solution, and would hydrolyze to ammonia and acetic acid. Thus formic acid and acetic acid are the two primary anionic products. In the presence of $\cdot\text{OH}/\text{O}_2$, acetic acid can be further oxidized to glycolic- and subsequently oxalic acid (Stefan and Bolton, 1999), and NH_3 can be oxidized to nitrite and nitrate.

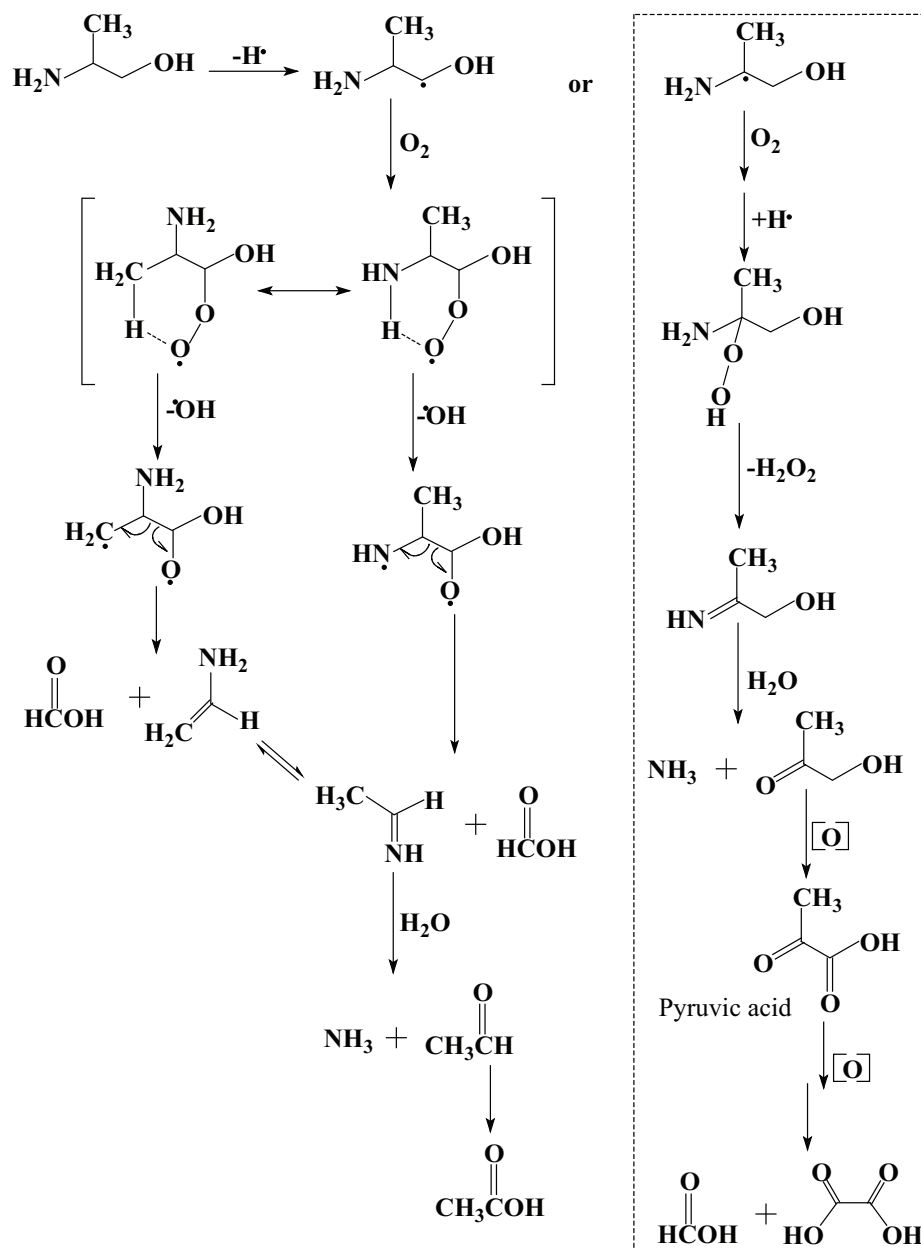


Figure 6.21 Pathway for formation of anionic products from 2-amino-1-propanol.

Since APN molecule contains an α -hydrogen atom and the α C-H bond is just slightly stronger than the C-H bond in the $-\text{CH}_2$ group adjacent to OH group, the initial hydrogen-abstraction may also occur at this α C-H bond except for the $-\text{CH}_2$ group adjacent to OH group. A pathway and mechanism for the initial hydrogen abstraction from the α -H, and ultimate formation of pyruvic acid is proposed in the dashed box in Figure 6.21. In this pathway, the peroxy radical cannot decay by intramolecular hydrogen abstraction from the $-\text{NH}_2$ or $-\text{CH}_3$ group through a six-membered cyclic transition state as proposed for hydrogen abstraction from the carbinol carbon. But it could be expected to form a peroxide through intermolecular hydrogen abstraction. The peroxide can decompose to NH_3 and hydroxyacetone, ultimately resulting in formation of pyruvic acid. Pyruvic acid is reported to be instable in the presence of $\cdot\text{OH}$ radical (Stefan and Bolton, 1999). It can ultimately decay to oxalic- and formic acid. As mentioned previously, the α C-H bond is slightly stronger than the C-H bond in the $-\text{CH}_2$ group adjacent to OH group, thus the proposed degradation pathway in the dashed box could be slightly less favourable.

The partially degraded APN samples were analyzed by anion IC. All the expected anionic products were identified as shown in Figure 6.22. It is interesting to note that pyruvic acid (detected in the form of pyruvate ion) was identified as one of major anionic products of APN, while it was not detected in AMP oxidation. The retention times of the anions in Figure 6.23 are different to those in Figure 3.13 due to replacement of the anion IC injection system and connecting tubing.

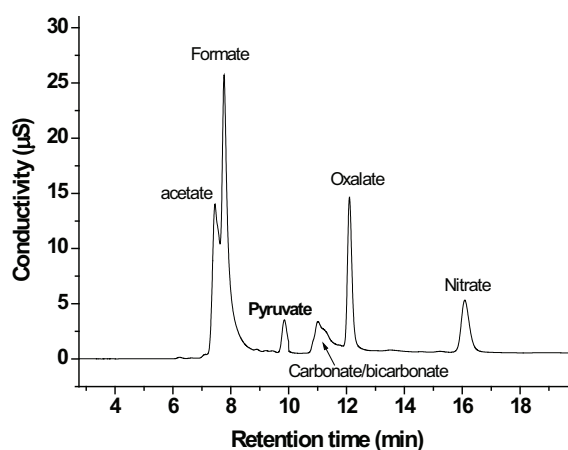


Figure 6.22 Anionic chromatogram of partially degraded APN.

Quantification of carboxylates in degraded APN is shown in Figure 6.23. As can be seen, acetate is the predominant anionic product. Acetic acid is a primary product and acetate can hence accumulate in much higher concentration in APN solution as compared to AMP. According to the proposed pathway in Figure 6.21, the molar ratio of acetate to formate should be smaller than 1:1. However, the experimental result shows that the ratio was higher than 1 and increased with reaction time. This is probably due to mineralization of the carboxylic acids, since formic acid is oxidizable at a much higher rate constant by $\cdot\text{OH}$ radicals than acetic acid (Chin and Wine, 1994). During the oxidation of APN, $\cdot\text{OH}$ radical concentration is not sufficient for complete mineralization of the carboxylic acids, and hence more formic acid is consumed than acetic acid, which leads to a higher end of concentration of acetic acid as compared to formic acid.

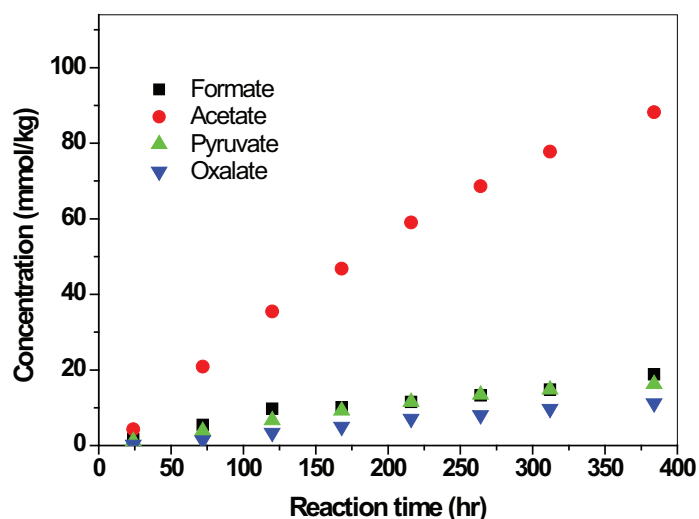


Figure 6.23 Formation of carboxylates in the APN degradation experiment (120 °C, 250 kPa O_2 , initial concentration = 3 mol/kg).

6.5 Conclusions

This chapter presents identified oxidation products of aqueous AMP solution. At elevated temperatures (100-140°C) the identified products include acetone, 2, 4-lutidine, 4, 4-dimethyl-2-oxazolidinone, carboxylate ions (formate, acetate, oxalate, glycolate), nitrite, nitrate, ammonium and some minor products. 2, 4-lutidine is still a product at 80°C, but it is

not anymore a major product. Acetone oxime and 4, 4-dimethyl-1, 3-oxazolidine are minor products at 100-140°C, but they are major products at 80°C. The differences associated with the final product composition are significant enough to show the temperature influence on the product distribution.

Based on the identified products of AMP and the context of the current amine degradation schemes, a possible degradation pathway for the production of the identified products is proposed. The likelihood of an initial hydrogen-abstraction on the methylene group adjacent to the OH group is greater than that on the amino- or methyl group. In the presence of dioxygen, $\cdot\text{OH}$ radical can be generated through a peroxy radical formation step followed by intramolecular hydrogen-abstraction giving formic acid and an imine (or enamine). This is the main oxygen containing pathway towards the primary AMP degradation. As a subsequent process, the formed imine is not stable and the $\cdot\text{OH}$ radicals will lead to a series of secondary reactions in the presence of O_2 , such as oxidation of acetone, formaldehyde, and ammonia. The reactions of AMP and the primary degradation products lead to formation of amides, formation of lutidine, oxazolidinone and oxazolidine. The temperature has a significant effect on the secondary reactions and thus affects the distribution of the ultimate product mixture.

In the case of oxidation by UV acceleration at 55°C, the identified AMP degradation products are different from those of the thermally accelerated oxidation at elevated temperatures. However, these new products can still be explained by the proposed pathway for AMP oxidation at thermal accelerated conditions. It appears that UV radiation does not change the primary degradation mechanism of AMP, but that the low temperature leads to different final products from those detected at the elevated temperatures.

Oxidation of a structural analog of AMP, 2-amino-1-propanol, was investigated at 120°C. The result of anion IC analysis supports that 2-amino-1-propanol degrades through a similar pathway as proposed for AMP oxidation. However, since the 2-amino-1-propanol molecule contains an α -hydrogen, the initial H-abstraction can also occur on the α C-H bond.

The primary oxidation steps of the investigated aminoethanols are the abstraction of a hydrogen atom followed by reaction with O_2 to form peroxy radicals. The peroxy radicals decompose to further products by intra- or intermolecular hydrogen abstractions. A summary

of the possibly primary oxidation pathways of aminoethanol compounds is presented in Figure 6.24. The initial H-abstraction is more likely to take place at the carbinol carbon. If there is α -H present in the molecule, the H-abstraction can also occur in the α -position. The formed aldehydes are readily oxidized to the corresponding acids. α -hydroxy ketone can be partially degraded to further products. If R is an alkyl group, it is not possible to exclude a pathway for peroxy radical decomposition through an intramolecular H-abstraction step as shown in the dashed box in Figure 6.24.

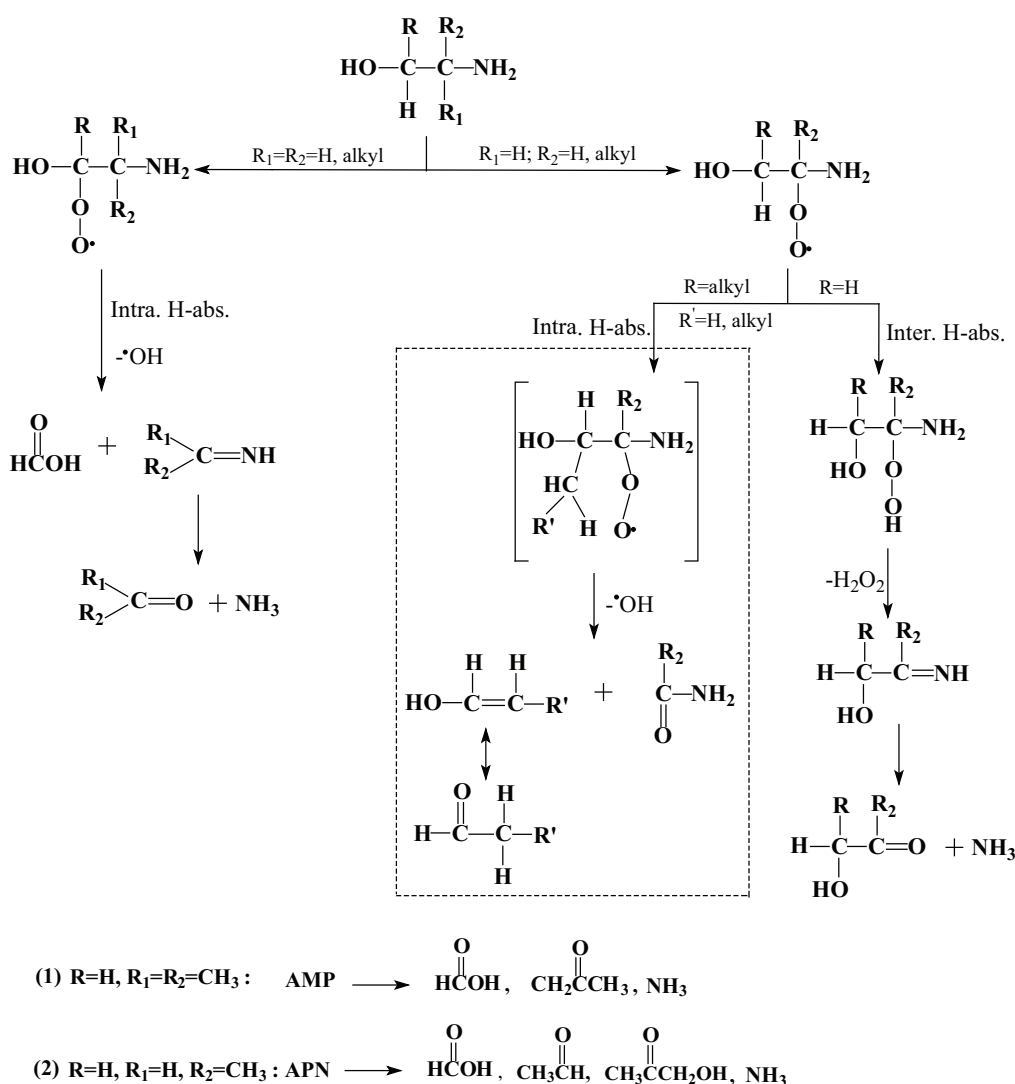


Figure 6.24 Summary of the schemes for the primary oxidative degradation of aminoethanols.

Chapter 7 Degradation of AMP/PZ Blends

This chapter describes thermal and oxidative degradation of AMP/PZ blends which appear to be a promising solvent system for efficient and cost effective CO₂ capture from flue gas streams. Two thermal- and a number of oxidative degradation experiments were conducted on the aqueous PZ solutions and AMP/PZ blends. The degradation products are identified with available methods and possible pathways for formation of main products are proposed.

7.1 Thermal degradation of AMP-PZ blends

Thermal stability of AMP has been presented in Chapter 4. Thermal stability of PZ has been identified as a significant advantage of aqueous PZ solvent to be used for CO₂ capture applications (Freeman, 2011). In order to assess thermal stability of AMP and PZ in AMP/PZ blends, two experiments were performed on AMP/PZ blends, one with and one without CO₂ loading, respectively. The composition of the AMP/PZ mix of interest for this dissertation is 3.5 mol/kg AMP combined with 1.5 mol/kg PZ (which termed standard blend hereinafter) and was the focus of the thermal- and the oxidative degradation experiments. The temperature chosen for thermal degradation was 135 °C which is slightly higher than a typical desorber temperature.

When a standard aqueous AMP/PZ blend was degraded under N₂ atmosphere at 135 °C, no measurable AMP and PZ loss was observed after 5 weeks. However, AMP and PZ were degraded significantly in the presence of CO₂. As can be seen in Figure 7.1, when the standard AMP/PZ blend with an initial loading of 0.3 mol of CO₂/ mol total amine was degraded at 135 °C, AMP and PZ lost 6.4% and 8.5% after 5 weeks, respectively. The overall degradation rate of AMP was 0.27m mol/(kg·h), the overall degradation rate for PZ was 0.15 m mol/(kg·h) after 5 weeks.

It has been shown in Chapter 4 that AMP loss during thermal degradation is approximately first order in amine concentration. The experiments performed by Freeman (2011) for aqueous PZ at 135-175 °C showed the PZ loss during thermal degradation also to be approximately first order in PZ concentration. In AMP/PZ blend, the losses of AMP and

PZ are still first order in their respective concentration during thermal degradation. This observation is supported by the fact that the thermal degradation concentration profiles for AMP and PZ of the standard blend can be well characterized by exponential regression. The calculated first order reaction constants for AMP and PZ degradation are 1.9×10^{-8} and $2.7 \times 10^{-8} \text{ s}^{-1}$, respectively. This first order reaction rate constant of AMP is close to that of 4.75 mol/kg AMP which was degraded separately at similar conditions. However, the estimated reaction rate constant for PZ is approximate 23 times greater than the reported rate for 8m PZ which was separately degraded with the same loading and temperature (Freeman, 2010). Although the estimated rate constant for PZ could contain a large error due to insufficient data points, the result clearly shows that the thermal degradation of PZ in the blend is faster than that in a single PZ system.

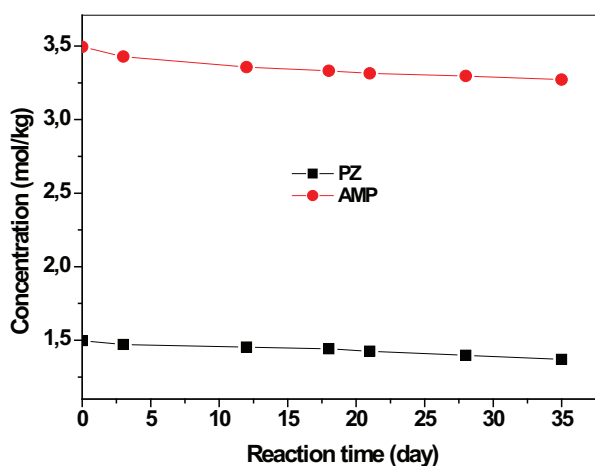


Figure 7.1 Changes in AMP and PZ concentration versus time. Experiment was performed on the standard blend with a loading of 0.3 mol CO₂/mol total amine at 135 °C.

The degradation samples of the thermal experiment in the standard AMP/PZ blend with CO₂ loading were analyzed by GC-MS. A typical gas chromatogram is shown in Figure 7.2. The major identified products included DMOZD (peak 1) and N-methylpiperazine (MPZ, peak 2). AMPAMP (peak 3), 1-(2-aminoethyl)piperazine (AEP, peak 5), DMHTBI (peak 6) and a suspected product, 1,4-di(2-aminoethyl)piperazine (DAEP, peak 7). N,N'-dimethylpiperazine (DMP) was also identified in small amounts. DMOZD, AMPAMP and DMHTBI are expected products as they were found in separately degraded AMP in presence of CO₂. MPZ, AEP, DMP and DAEP have been found as thermal degradation products of PZ

degraded with CO₂ individually (Freeman, 2011). The unknown peak 4 was consistently found in thermally degraded AMP solutions in the presence of CO₂. The predominant degradation product for PZ was MPZ. The determined concentration of MPZ was 43 mmol/kg after 5 weeks, which accounted for a 34% loss of PZ. The predominant product for AMP was DMOZD, at a concentration of 93 mmol/kg after 5 weeks. The formation of DMOZD explains 42% of the loss of AMP.

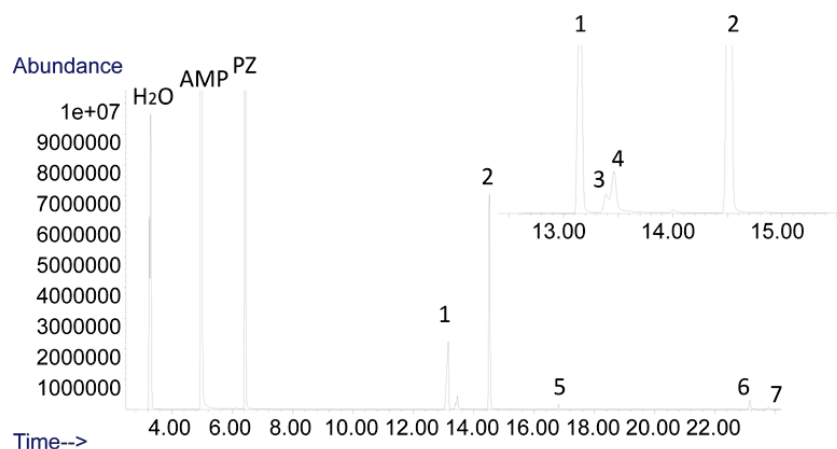
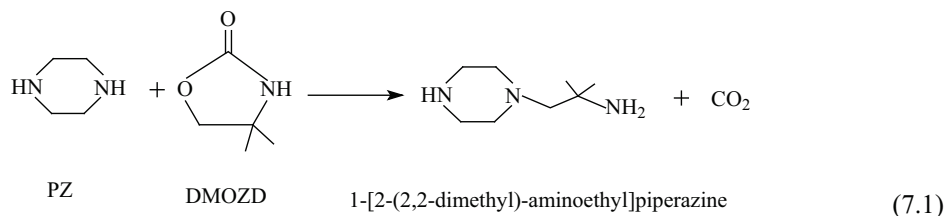


Figure 7.2 Chromatogram of a thermally degraded AMP/PZ aqueous blend (3.5 mol/kg AMP + 1.5 mol/kg PZ) with a loading of 0.3 mol of CO₂ per mol total amine held at 135 °C for 5 weeks. In addition to water, AMP and PZ, the identified products were DMOZD (peak 1), MPZ (peak 2), AMPAMP (peak 3), Unknown (peak 4), AEP (peak 5), DMHTBI (peak 6), and DAEP (peak 7).

Since PZ is a strong nucleophile, Davis (2009) proposed that PZ would attack the oxazolidinone intermediate to form a MEA/PZ species during thermal degradation of MEA/PZ blend. We suspected that PZ could participate a similar reaction to form 1-[2-(2,2-dimethyl)-aminoethyl]piperazine in the AMP/PZ blend, as shown in reaction 7.1. However, the expected product was not detected with the available methods.



7.2 Oxidative degradation of PZ

7.2.1 PZ loss

PZ is more expensive than MEA, so it is imperative that PZ has a lower degradation rate than MEA if it is to be an economically viable solvent component. However, only few investigators have studied PZ degradation alone since PZ is generally used as a promoter to increase CO₂ absorption kinetics. Dannis et al. (1967) studied oxidation of PZ by sodium hypochlorite at room temperature, which resulted in carbon-carbon cleavage to give formaldehyde along with ethylenediamine (EDA). Oxidation of PZ in the presence of metal catalysts at 55 °C was investigated by Sexton (2008). The results showed that aqueous PZ solutions were degraded but at much lower rates than MEA solutions. Closmann (2011) investigated 8m PZ oxidation in an integrated solvent degradation system apparatus (ISDA). The oxidative reactor was set at 55 °C, and the thermal reactor was set at 90-120 °C. 8m PZ in ISDA was generally resistant to oxidation as compared to other solvents such as 7 m MEA and 7 m MDEA. Freeman (2011) reported that concentrated PZ was degraded from 55 to 70 °C with a mechanism that is first order in O₂ partial pressure. CO₂ concentration was found to have a weak effect on PZ oxidation as compared to O₂ and temperature. Several suspected and identified products were reported, but the quantified products in all experiments only accounted for a very small portion of the overall loss of carbon and nitrogen in the solvent. No degradation mechanism of PZ oxidation was disclosed in the reports.

The purpose of separately studying PZ oxidation in the present work was to understand the oxidation pathways of individual PZ before attempting to understand the oxidation pathways of AMP/PZ blends. Two aqueous solutions of 1.5 mol/kg PZ were degraded with 250 kPa O₂ at 80 and 100 °C, respectively. The generation of the degradation products was monitored with the available techniques in our laboratory. Cation IC and anion IC were performed on all the samples, while GC-MS was only performed on selected samples, since the concentrations of most of the non-ionic products in the initial stage of the oxidations were too low to be quantified using GC-MS.

Figure 7.3 illustrates PZ losses versus degradation time for the two experiments. The overall degradation rate of PZ within 38 days at 80 °C was estimated to be 0.47 mmol/(kg·h).

At 100°C within 19 days, the overall degradation rate was determined to be 1.2 mmol/(kg·h), which is approximate 1/2× the rate observed for 5 mol/kg AMP degraded separately at identical conditions. The data for oxidation of unloaded PZ solutions suggest that PZ loss could be represented with a first order rate law. The apparent first order reaction constants were calculated using the raw data shown in Figure 7.3. The value of first order reaction constant was estimated to be $1.0 \times 10^{-7} \text{ s}^{-1}$ and $3.3 \times 10^{-7} \text{ s}^{-1}$ for 80 and 100 °C, respectively. Given the two experimental temperatures, an activation energy for PZ oxidation can be calculated for the oxidation performed in the batch reactors. According to the Arrhenius relationship, the activation energy for PZ oxidation at the experimental conditions was estimated at 66 kJ/mol.

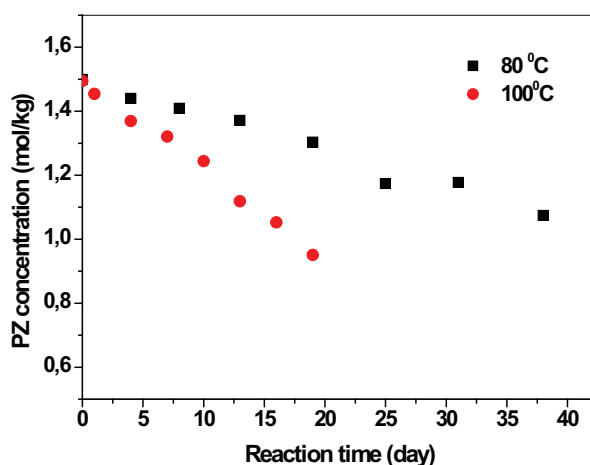


Figure 7.3 Profiles of PZ loss versus degradation time (Initial concentration of PZ=1.5 mol/kg). Experiments were conducted under 250 kPa O₂ at 80 and 100 °C, respectively.

7.2.2 Oxidative degradation products

The most prominent degradation products of PZ were identified by GC-MS as EDA, 1-formylpiperazine (FPZ) and 2-oxopiperazine (OPZ) (see Figure 7.4). In addition, 1-nitrosopiperazine (1-mononitrosopiperazine, MNPZ), 2-(1H-imidazol-1-yl)ethanamine (suspected, without confirmation) and 2, 5-piperazinedione (2, 5-dione) were identified in relatively low concentration in the degraded 1.5 mol/kg PZ samples. Formation of EDA, FPZ, OPZ and MNPZ was quantified by GC-MS.

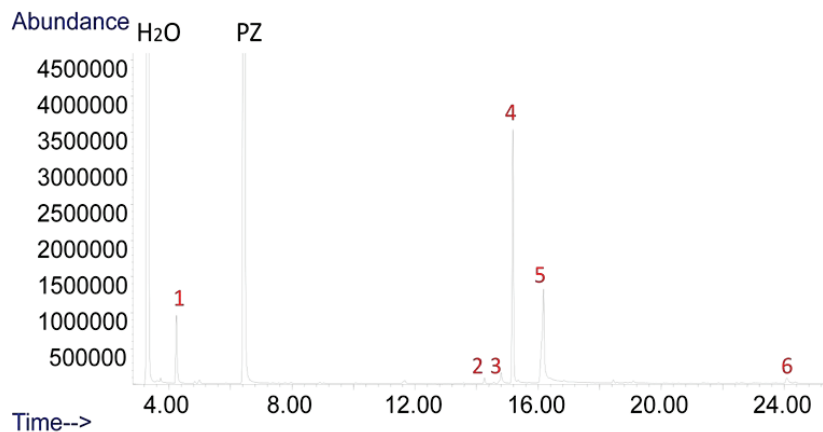


Figure 7.4 Chromatogram of a partially oxidized PZ aqueous solution (Initial concentration of PZ = 1.5 mol/kg). Experiment was held under 250 kPa O₂ at 100 °C for 19 days. In addition to water and PZ, the products were identified as EDA (peak 1), MNPZ (peak 2), 2-(1H-imidazol-1-yl)ethanamine (peak 3), FPZ (peak 4), OPZ (peak 5), and 2, 5-dione (peak 6).

The heat stable salts were identified by anion IC, including formate and oxalate. Acetate, glycolate, nitrate and nitrite were also found in small quantities. The generation of carboxylates and their corresponding amides is shown in Figure 7.5. Formation of formyl amides and oxalyl amides in degraded 1.5 mol/kg PZ solutions was determined by NaOH hydrolysis technique as described in Chapter 3. Concentrations of formyl amide and oxalyl amide were calculated by subtracting the amount of free formate and oxalate ions from the total concentrations of formate and oxalate after alkaline treatment, respectively. The agreement between the formyl amides quantified on the anion IC through NaOH hydrolysis method and FPZ quantified directly on GC-MS indicates that FPZ is likely to be the only formyl amide in degraded PZ solution. This result is consistent with what has been observed in the oxidation of 8m PZ (Freeman, 2011). Therefore, only the data of FPZ formation obtained from GC-MS analysis is included in later mass balance calculation. The molar concentration of oxalyl amides was very rough in the mass balance calculation (see Table 7.1). Since PZ has two amino groups and oxalic acid has two carbonyl functional groups both can form a double amide. The same is true for EDA, a major amine product for PZ oxidation. The possible amide structures of the reaction of PZ or EDA with oxalic acid have been proposed by Freeman (2011). For simplicity, N-oxalyl PZ was taken as the only generated oxalyl amide in the following calculation of nitrogen mass balance.

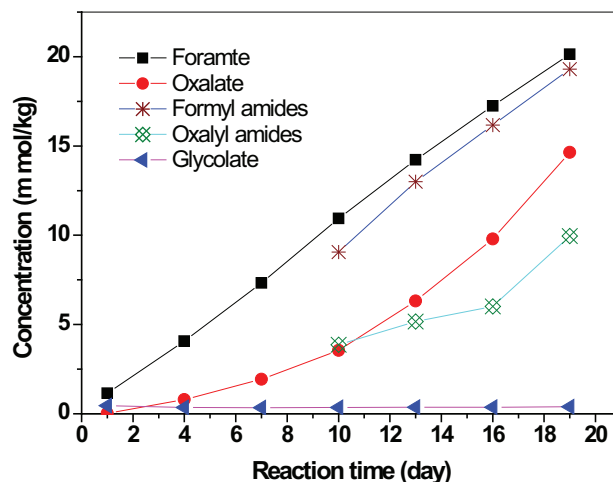


Figure 7.5 Generation of carboxylates and their corresponding amides in degraded PZ solution under 250 kPa O₂ at 100 °C (initial concentration of PZ=1.5 mol/kg).

Both two oxidative degradation experiments of aqueous PZ solutions conducted in this work suffer from a common failure to close the overall mass balance. The PZ loss observed by cation IC analysis is not balanced with the identified degradation products. Table 7.1 provides an example of the N and C mass balance achieved in the experiment of oxidation of 1.5 mol/kg PZ at 100 °C. Cation IC was used to quantify the amine loss percentage and formation of the total NH₄⁺ in the liquid phase while GC-MS and anion IC enabled determination of the amount of each identified degradation product. The formation percentages of all degradation compounds are presented together in order to show the percentage of nitrogen and carbon mass balance closure. This represents the percentage of PZ loss that was recovered in each of the products in terms of either N or C.

During the experiment conducted at 100 °C, 544.1 mmol of PZ per kg solution was lost, or 1088.2 mmol N from PZ per kg solution and 2176.4 mmol C from PZ per kg solution were lost after 19 days. Only 46.1% of the N loss from PZ and 21.1% of the C loss from PZ were recovered in the detectable degradation products. NH₄⁺ was the most dominant product with 264.7 mmol per kg solution at the end of the experiment and accounted for 24.3% of the total N loss from PZ. This percentage is much higher than that observed in 8m PZ degraded in an open reaction system (Freeman, 2011). This is not surprising since NH₃ can be stripped by the reaction gas from the PZ solution in the open system, which was used by Freeman (2011).

Except for NH_4^+ , EDA, OPZ and FPZ were the most major products with 59.9, 31.4 and 20.3 mmol per kg solution at the end of the experiment, respectively.

Table 7.1 Nitrogen and carbon mass balance in degraded PZ solution (1.5 mol/kg PZ, 100°C, 250 kPa O_2 , 19 days)

	Conc. mmol/kg	Nitrogen balance		Carbon balance	
		N conc. mmol/kg	N identified %	C conc. mmol/kg	C identified %
PZ lost	544.1	1088.2	-	2176.4	-
Degradation products:					
EDA	59.9	119.7	11.0	119.7	5.5
FPZ	20.3	40.6	3.7	101.5	4.7
OPZ	31.4	62.7	5.8	125.4	5.8
MNPZ	1.4	2.8	0.3	2.8	0.1
Ammonium	264.7	264.7	24.3	NA	-
Oxalyl amides*	10.0	10.0	0.9	59.7	2.7
Nitrate and nitrite	0.5	0.5	0.05	NA	-
Oxalate	14.6	NA	-	29.3	1.3
Formate	20.1	NA	-	20.1	0.9
Acetate	1.9	NA	-	1.9	0.1
Glycolate	0.25	NA	-	0.25	0.01
Total Mass recovered in products		501.0	46.1	460.7	21.1

* Nitrogen concentration was estimated as only N-oxalyl PZ generated.

7.2.3 Oxidative degradation pathways

Mass balance for PZ oxidative degradation has been discussed above. However, only 46.1 % of the N loss and 21.1 % of the C loss can be explained by the identified products. This result indicates that there are still unidentified degradation products containing both N and C. Despite an unsatisfactory mass balance, the products that were consistently identified can be discussed.

7.2.3.1 Oxidative degradation of EDA

For the amine-based products, EDA was quantified with the highest concentration in the oxidative degradation products of aqueous PZ solutions. On the other hand, EDA is a

diamine itself. EDA may be degraded at conditions that caused degradation of PZ. Generation of EDA in the PZ oxidation experiments is shown in Figure 7.6. The profiles for EDA generation show that the concentration at first increased and then decayed with reaction time, indicating that EDA could be an intermediate in PZ oxidation as expected.

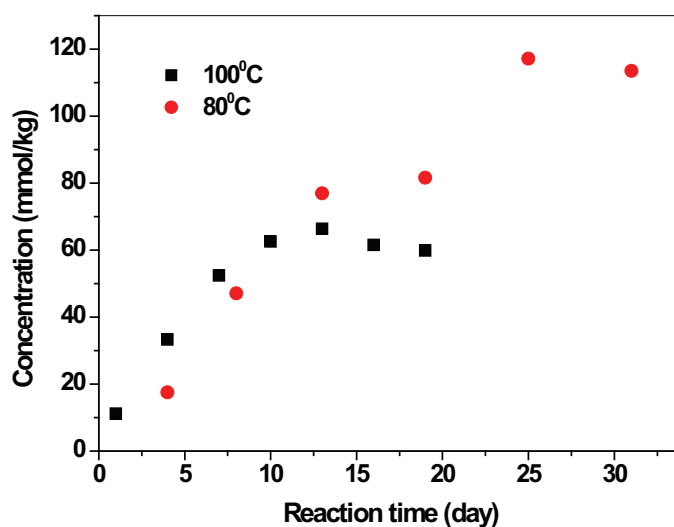


Figure 7.6 Generation of EDA in degraded PZ solution under 250 kPa O₂ at 80 and 120°C (initial concentration of PZ = 1.5 mol/kg). The estimation is based on GC-MS analysis.

Since EDA is an intermediate during PZ oxidation, investigation of the principal products of EDA oxidation is helpful to understand the degradation pathway of PZ. An aqueous solution of 1 mol/kg EDA was oxidized at 120°C with agitation at 200rpm under 250 kPa O₂ before attempting to explain formation of the identified products in PZ oxidation. The loss of EDA is severe in this experiment, with 39% of the initial EDA lost after 11 days of oxidation. The most prominent products identified by GC-MS included OPZ (mass spectrum is provided in Appendix C10) and 2-(1H-imidazol-1-yl)ethanamine (suspected). Ionic product generation was also observed, as shown in Figure 7.7. Carboxylate products were primarily formate, oxalate and acetate. Glycolate was only found in a very small quantity. When 1.3 mM tartaric acid and 1.1 mM piperidinedicarboxylic acid was used as eluent in the cation chromatograph, glycine was also identified in the degraded EDA samples (see Figure 7.8).

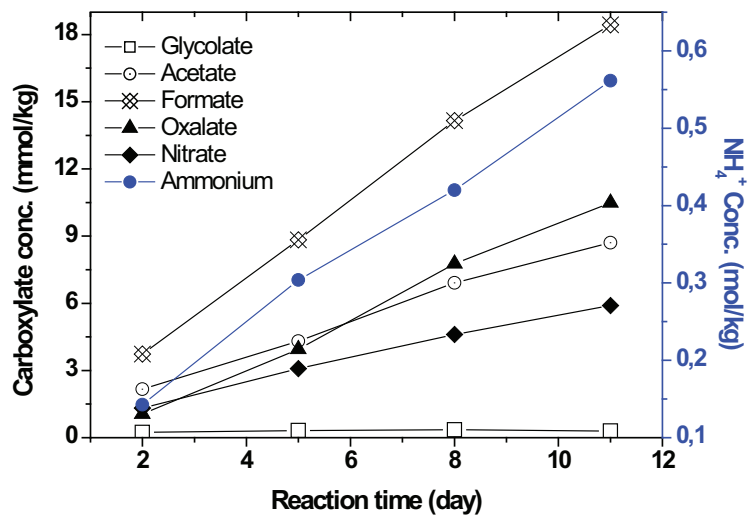


Figure 7.7 Profiles for ionic products in degraded EDA solution under 250 kPa O_2 at 120°C (initial concentration of EDA=1.0 mol/kg).

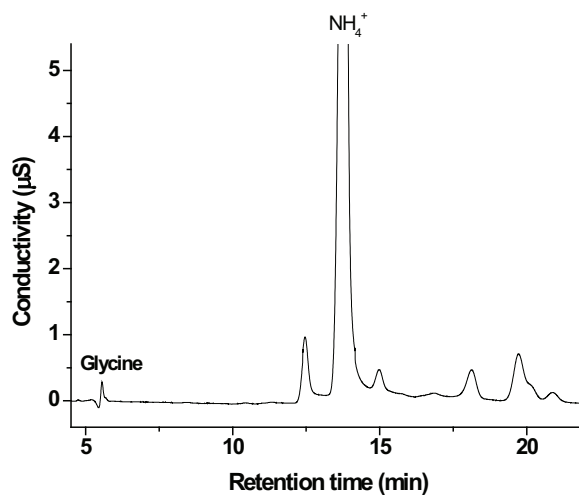


Figure 7.8 Cation chromatogram of degraded EDA solution (eluent: 1.3 mM tartaric acid +1.1 mM 2, 6-pyridinedicarboxylic acid).

OPZ as a main product of EDA oxidation was unambiguously determined by GC-MS analysis. The possible mechanisms of piperazinone formation in oxidation of ethylenediamines have been proposed by Lepaumier et al. (2009a). The authors studied oxidation of four aliphatic ethylenediamines with 2 MPa air at 140 °C, including N,N-dimethylethylenediamine, N,N'-dimethylethylenediamine, N,N,N'-trimethylethylenediamine and N,N,N',N'-tetramethylethylenediamine (TMEDA). Except for TMEDA, the main identified degradation products were piperazinones. Although piperazinone was not the main product, it was still found as a product in degraded TMEDA solution. Similar as the mechanisms proposed by Lepaumier and her colleagues (2009a), OPZ may be formed during oxidation of EDA via the pathways as shown in Figure 7.9. Ring closure of two different intermediates (**1** and **2**) can lead to the same product, OPZ. The intermediate **1** is obtained by addition of EDA with glycolic acid, and the compound **2** is produced by addition of EDA with glycine. Both glycolic acid and glycine are identified products of the oxidation of EDA. The two mechanisms seem possible, but the two intermediates have not been identified with the available methods in our laboratory.

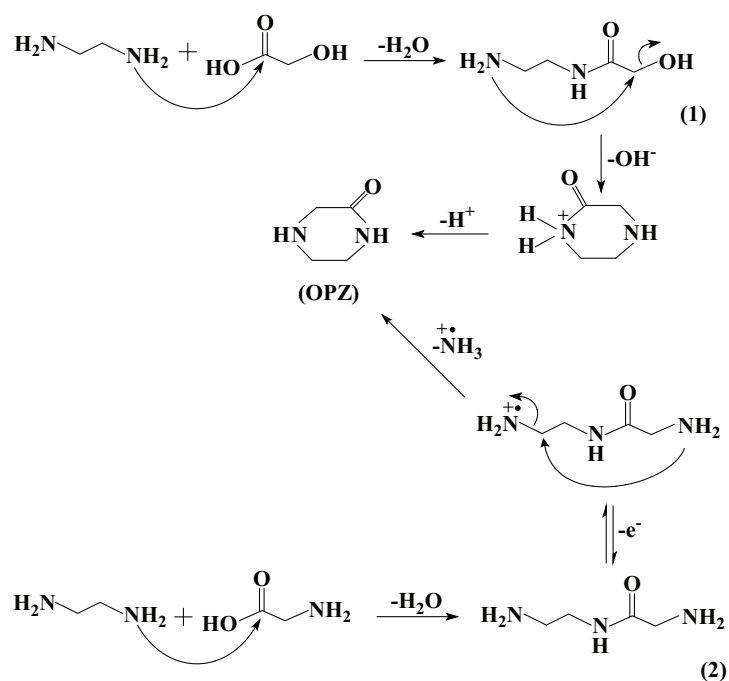


Figure 7.9 Pathways for OPZ formation from EDA.

In order to verify the two proposed pathways for formation of OPZ from EDA, two experiments were conducted with EDA. 1mol/kg EDA reacted with 0.1 mol/kg glycolic acid and 0.1 mol/kg glycine under N₂ at 120°C, respectively. The reaction mixtures were analyzed by GC-MS. After 24 hours, OPZ was detected in the reaction mixture of EDA and glycine. The chromatogram after 96 hours is shown in Figure 7.10. But OPZ was not found in the mixture of EDA and glycolic acid. This result indicates that reaction of EDA and glycine at the experimental conditions does lead to formation of OPZ. The experiments did not confirm the mechanisms proposed in Figure 7.9. However, the result is a strong support that OPZ can be formed due to the reaction of EDA and glycine.

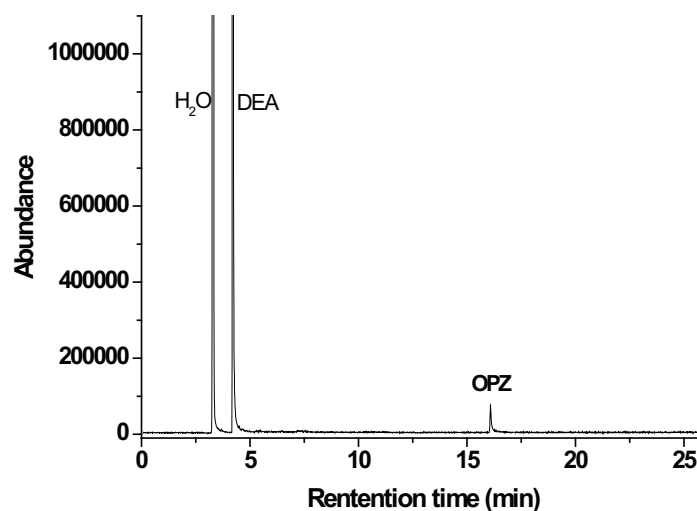


Figure 7.10 Gas chromatogram of aqueous mixture of 1 mol/kg EDA and 0.1 mol/kg glycine. The mixture had been heated to 120°C under N₂ for 96 hours.

7.2.3.2 Possible degradation pathway of PZ

The major oxidative degradation products of 1.5 mol/kg PZ are listed in Table 7.1 including experimental degradation details. The major products indicate that pathways for the production of EDA exist when oxidation of aqueous PZ occurs. Despite the seeming lack of data, some speculations on the degradation pathways of PZ can still be made by examining formation of the identified products.

A possibly primary degradation pathway for PZ is presented in Figure 7.11. This pathway accounts for formation of the identified products, including EDA, FPZ, OPZ and carboxylic acids. Formaldehyde is expected to be detected in solution as formate ion. The amino acids, glycine and AEAAC have been identified in small quantity by cation IC. The following section provides an explanation of the whole pathway.

In analogy to the proposal for the alkanolamines, PZ oxidation is also assumed to be initiated through a radical forming step. The initiation step of PZ oxidation involves a hydrogen-abstraction from one of the four methylene carbons in the PZ molecule, resulting in a free radical centered on a methylene carbon. In the presence of dissolved O₂, the formed carbon centered radical converts to a peroxy radical through a fast reaction with O₂. After that, the formed peroxy radical may be expected to decay through another hydrogen-abstraction step by two different possible pathways. The difference between the two pathways for decomposition of the peroxy radical is how the hydrogen-abstraction takes place, i.e. intermolecular or intramolecular.

In the aqueous alkaline environment of the degraded solvent, the peroxy radical could convert to a peroxide by intermolecular hydrogen-abstraction. The peroxide could decompose by homolysis of the O-O bond to produce an oxygen-centered radical and a •OH radical. The formation of the oxygen-centered radical in Figure 7.11 is then followed by the formation of 2-hydroxyl-PZ. The 2-hydroxyl-PZ will be oxidized to [(2-aminoethyl)amino]acetaldehyde (AEAAD) via ring-opening, in analogy to imine hydrolysis (Layer, 1963). The aldehyde function is expected oxidized into an acid, which leads to formation of [(2-aminoethyl)amino]acetic acid (AEAAC), followed by ring closure giving OPZ. In analogy to the proposal for oxalic acid formation from oxidative degradation of MEA (Rooney et al., 1998), another possible pathway for degradation of AEAAD is formation of oxalic acid and EDA due to cleavage of N-C bond. According to the proposed degradation pathway for PZ, EDA is an intermediate, which is in accordance to the profiles for generation of EDA presented in Figure 7.6. EDA is expected to degrade to glycine and glycolic acid. The formed glycine reacts with EDA, which may lead to OPZ, as presented in Figure 7.9. The presence of AEAAD has not been proven in this study, but evidence of its existence comes in the formation of AEAAC identified in the degraded aqueous PZ solutions.

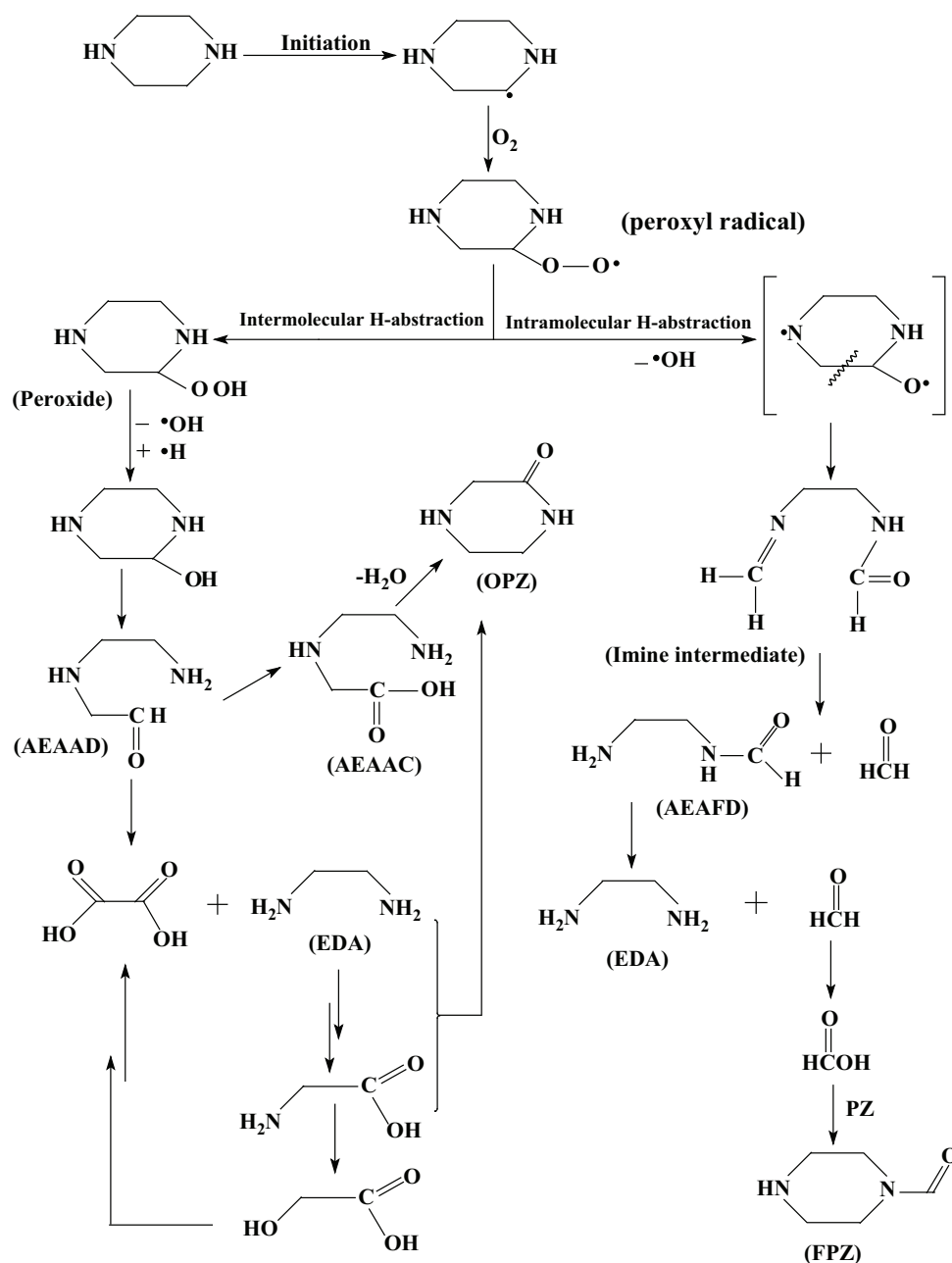


Figure 7.11 Possible pathways for oxidative degradation of PZ. Degradation pathways following the formation of a peroxy radical to yield observed products are illustrated.

It is also possible that the PZ peroxy radical abstracts a hydrogen atom intramolecularly from the amino group similar as proposed for AMP degradation in Figure 6.7. After ejection of a $\cdot\text{OH}$ radical, a reactive imine intermediate is formed through homolytic cleavage of the C-C bond. The imine intermediate is not stable in aqueous solution, and is hydrolyzed to form formaldehyde and [(2-aminoethyl)amino]formaldehyde (AEAFD). The AEAFD is also unstable and could decompose to formaldehyde and EDA. The formaldehyde may then be readily oxidized into formic acid. Finally, the strong nucleophile PZ can attack the carbonyl group to produce FPZ.

7.2.4 Formation of nitrosopiperazine

MNPZ was consistently identified in all the degraded PZ solutions and AMP/PZ blends. MNPZ has been shown to pose a carcinogenic risk in animal models of human diseases (Lijinsky and Kovatck, 1993). Considering that MNPZ is toxic, attention must to be paid to identify the formation of MNPZ although it was found only in small quantities.

Flue gas contains NO_x which may be a source of nitrosamine formation in the amine based absorption/desorption process for CO₂ capture. The reaction gas used for PZ oxidation experiments in this work was high purity O₂ (99.999+%). It means that no NO_x was introduced into the reaction system. However, nitrite was detected in the PZ solutions. It seems that nitrite could be the source of the nitrosating species in this case.

The nitrosation of amines may be achieved in acidic or alkaline conditions. In the present text focus is put on formation of MNPZ in alkaline PZ solution, formation of MNPZ in acidic conditions is omitted on purpose. In aqueous solution, the rate of nitrosation drops rapidly at $\text{pH} > \text{pK}_a$ of HNO₂ because of decreasing concentration of the active nitrosating species. No nitrosation caused by aqueous nitrite has been observed at higher pH than 7.5 (Douglass et al., 1978). However, formaldehyde can catalyze conversion of various secondary amines to nitrosamines by the nitrite ion in neutral and basic medium (Keefer and Roller, 1973). The proposed mechanism involves nucleophilic attack of the nitrite anion on an iminium ion formed by reaction of amine and aldehyde. The final step is nitrosamine formation and release of the carbonyl catalyst through collapse of the adduct at the same time. Chloral and benzaldehydes are also catalysts, but less active than formaldehyde, while acetone and acetaldehyde are reported to show no catalytic activity.

Formaldehyde is supposed as a primary product of oxidation of PZ, nitrite was detected in the oxidized PZ solutions. Similar as the proposed mechanism of catalysis involving initial interaction of aldehyde with the secondary amine (Keffer and Roller, 1973), MNPZ is probably formed through the scheme as shown in Figure 7.12.

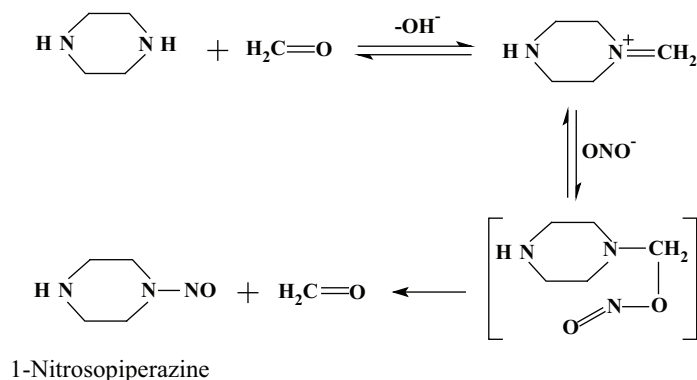


Figure 7.12 Scheme for MNPZ formation from PZ.

Nielsen (2012) and Voice (2012) have reported formation of MNPZ in PZ solution and PZ/AMP blends. MNPZ is stable once formed. In order to verify the possibility of decomposition of MNPZ using thermal degradation, one experiment was conducted in the present work. A degraded PZ solution with an initial concentration of 1.5mol/kg PZ, which has been oxidized using 250 kPa O₂ at 80°C for 38 days, was heated to 150°C in the absence of O₂. GC-MS analysis shows that MNPZ in the solution decreased by 60.2% after 24 hours. This result demonstrates that thermal degradation of MNPZ looks promising, however, MNPZ may not be completely destroyed under the stripper conditions, and the reaction mechanism of this degradation reaction needs to be more investigation.

7.3 Oxidative degradation of AMP-PZ blends

7.3.1 Overview of degradation products

Aqueous AMP/PZ blends were degraded with 250 kPa O₂ in the autoclave reactors at 80-120°C. The major degradation products of the experiments with aqueous AMP/PZ blends included acetone, EDA, DMOZD, 2, 4-lutidine, FPZ, OPZ, and the heat stable salts formate, acetate and oxalate. The presence of ammonia in degraded amine was measured as NH₄⁺ using cation IC. Glycolate, nitrate, 1, 4-diformylpiperazine, MNPZ and 2-(1H-imidazol-1-

yl)ethanamine (suspected) were detected in small quantities. In the degraded AMP/PZ blends with an initial CO₂ loading, MPZ, DMPZ, and AMPAMP were also found in small quantities. The major identified products in the blend are consistent with that in individually degraded AMP and PZ solutions.

7.3.2 Effect of temperature

Oxidation of AMP and PZ are expected to be accelerated with increased temperature. The effect of temperature on oxidation of AMP/PZ blends was investigated with 250 kPa O₂ at temperatures of 80-120°C. The losses of AMP and PZ in all the experiments are compared in Figure 7.13. As expected, the higher temperature increased both of the losses of AMP and PZ. The overall degradation rates of AMP at 80, 100 and 120°C within 13 days were calculated to be 0.16, 0.62, 2.5 mmol/(kg·h), respectively. At the same time, the overall degradation rates of PZ at 80, 100 and 120°C within 13 days were calculated to be 0.45, 1.9, 3.2 mmol/(kg·h), respectively. This result shows that the degradation rate of AMP in the blends was close to that in the single AMP system, but PZ degraded faster in the blends than it degraded individually at the same degradation conditions.

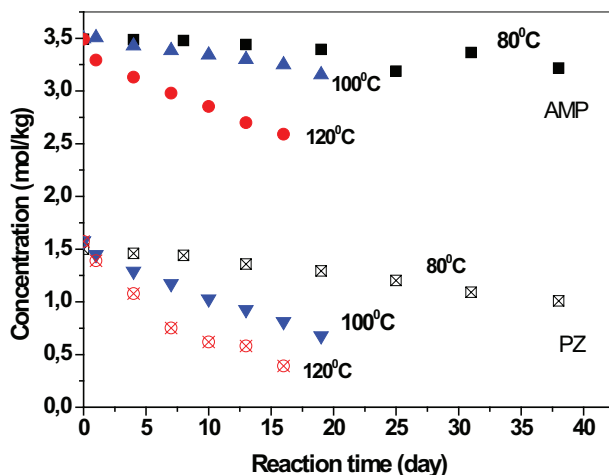


Figure 7.13 AMP and PZ concentration against degradation time (Initial concentration of PZ= 1.5 mol/kg). The experiments were conducted under 250 kPa O₂ at 80 - 120°C.

Linear rates of loss of AMP and PZ have been regressed from the data which are shown in Figure 7.13. Using the regressed rates, activation energies for AMP or PZ can be extracted

based on Arrhenius behaviour of rates with temperature. As discussed in section 5.3, the estimated activation energy for 5mol/kg AMP was much less than the expected value due to oxygen mass transfer limitation when AMP was oxidized separately at accelerating conditions. In the experiments for oxidation of AMP/PZ blends, oxygen mass transfer was slightly improved by replacement of the magnetic stirrers. The calculated activation energy for AMP and PZ in the standard blend over the experimental temperature range is 84 kJ/mol and 56 kJ/mol, respectively. The estimated activation energy for PZ in the blend is smaller than that for the single PZ system.

As shown in Figure 7.11, the oxidative degradation of PZ requires that the PZ ring opens. It is likely to be a more energy intensive degradation mechanism than the production of an amide through reaction of PZ and formate to form FPZ as Closmann (2011) speculated. Since more carboxylic acids and aldehydes were produced by addition of AMP, more PZ derived amides are expected to be formed in the blends. Comparison of the generation of FPZ in the AMP/PZ blend and the single PZ system is shown in Figure 7.14. Much higher concentration of FPZ was observed in the blend than in the single PZ system. This could be one of the main factors that lead to a higher degradation rate of PZ in the blends.

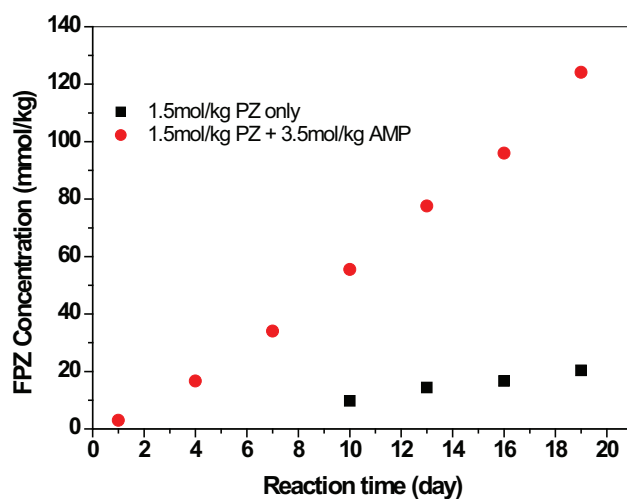


Figure 7.14 Comparison of the generation of FPZ in the AMP/PZ blend and the single PZ system. The experiments were conducted under 250 kPa O₂ at 100°C.

7.3.3 Effect of composition

The effect of blend composition on the oxidation of AMP was investigated with 250 kPa O₂ at 100°C. As can be seen in Figure 7.15, the degradation rate of AMP decreased slightly when the initial concentration of AMP was fixed at 3.5 mol/kg but the initial concentration of PZ was increased from 0 to 1.5 mol/kg. O₂ mass transfer limitation is the likely reason leading to this result. Since single PZ degrades slower than AMP and the concentration of PZ is lower than that of AMP in the blend, the addition of PZ has a slight effect on the oxidation rate of AMP.

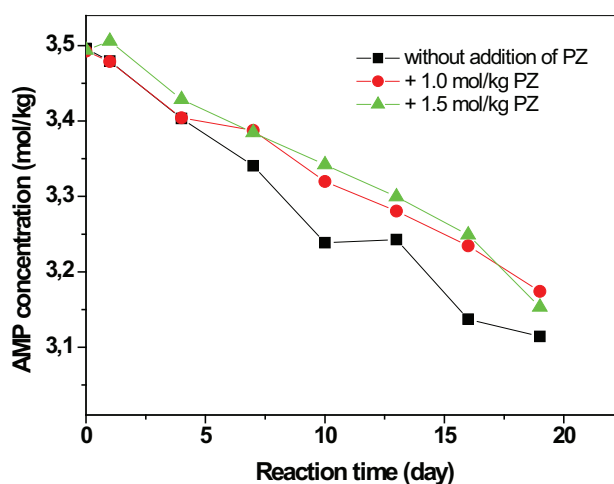


Figure 7.15 Effect of addition of PZ on AMP degradation rate. The experiments were conducted under 250 kPa O₂ at 100°C (Initial concentration of AMP=3.5mol/kg).

7.4 Conclusions

AMP/PZ blend (3.5 mol/kg AMP + 1.5 mol/kg PZ) without CO₂ loading was stable at least at a temperature less than 135 °C under a blanket gas of N₂. However, significant degradation of the AMP/PZ blend occurred in the presence of CO₂ at 135 °C. At an initial loading of 0.3 mol of CO₂/ mol total amine, the standard blend exhibited 8.5% PZ loss and 6.4% AMP loss during 5 weeks. The most abundant degradation products of thermally degraded AMP/PZ blend are N-methyl-PZ (MPZ) and 4,4-dimethyl-2-oxazolidinone (DMOZD). MPZ accounts for 34% of the PZ loss and DMOZD accounts for 42% of the AMP loss during thermal degradation.

The rate of PZ loss was measured in 1.5 mol/kg PZ which was degraded with 250 kPa O₂. The overall rate of PZ loss at 80 °C within 38 days was 0.47 mmol/(kg·h). At 100°C, the overall degradation rate within 19 days was 1.2 mmol/(kg·h), which is approximate half of the rate observed for separately degraded 5 mol/kg AMP. These rates indicate that aqueous PZ solution is slightly more resistant to oxidation when tested in a batch reactor as compared to aqueous AMP solution. Except for the anionic products, the PZ oxidation products which were quantified at greatest concentration were NH₄⁺, EDA, OPZ and FPZ. MNPZ, 2-(1H-imidazol-1-yl)ethanamine and 2, 5-dione were identified as minor products. A mass balance was performed on the end samples of the PZ oxidation experiments at 100°C, ~46% of the lost nitrogen and ~21% of the lost carbon of PZ were recovered in the major quantified degradation products.

Despite an unsatisfactory mass balance, a PZ degradation pathway has been proposed based on identified products which were consistently detected in all the degradation samples. PZ oxidation is proposed to be initiated through H-abstraction followed by peroxy radical formation in the presence of O₂. In comparison with AMP oxidation, the key difference in PZ oxidation is the manner of peroxy radical decomposition.

When the AMP/PZ blend was oxidized in the batch reactor at 80-120°C, the degradation products included the heat stable salts formate, acetate and oxalate, the AMP derived products acetone, 2,4-lutidine, DMOZD, and the PZ derived products EDA, OPZ and FPZ, etc. No new product was detected as compared with individually degraded AMP or PZ. The degradation rates of AMP and PZ were estimated. The results show that the degradation rate of AMP is close to that in the single AMP system, but PZ loss rate is higher than that in the single PZ system. The reactions between PZ and the AMP degradation products are likely to lead to increased PZ loss rate in the AMP/PZ blends. When the initial concentration of PZ was increased from 0 to 1.5 mol/kg, the overall degradation rate of AMP decreased but not dramatically.

MNPZ was consistently identified in all the degraded samples of PZ and AMP/PZ blends. Most of the formed MNPZ can be destroyed when the reaction mixture was heated to 150°C in the absence of O₂.

Chapter 8 Degradation of AMP/MEA Blends

This chapter presents an investigation of the degradation behaviour of AMP/MEA blends based on data obtained at accelerated degradation conditions. Except for one thermal degradation experiment, a total of eight oxidation experiments were performed on AMP/MEA mixtures in autoclaves with 250-350 kPa O₂ and at 100-140°C. The blend derived degradation products are compared with those of individually degraded AMP and MEA. The effects of process parameters, such as temperature, oxygen partial pressure and blend composition are discussed.

8.1 Thermal degradation

Thermal degradation of MEA/AMP blend was studied by Davis (2009). 7m MEA-2m AMP aqueous solutions containing a loading of 0.4 mol CO₂/mole of alkalinity were thermally degraded over a range of 100 to 150 °C. The loss rate for AMP in these experiments was less than the loss rate for a non-blended aqueous AMP system in the presence of CO₂. Only three degradation products 2-ethylenediamine-2-methyl-1-propanol, N-(2-hydroxyethyl)-ethylenediamine (HEEDA), N-(2-hydroxyethyl)imidazolidinone (HEIA) were identified by IC-MS and HPLC. 2-Ethylenediamine-2-methyl-1-propanol is a cross product, formed from the reaction of AMP with OZD.

In the present project, an aqueous AMP/MEA blend (3mol/kg AMP +2mol/kg MEA) with a CO₂ loading of 0.3 mol CO₂/mol amine was degraded at 135°C. The rate constant for reaction of MEA and AMP with CO₂ was $1.4 \times 10^{-7} \text{ s}^{-1}$ and $1.9 \times 10^{-8} \text{ s}^{-1}$, respectively. This result shows that the rate constant for the reaction of AMP with CO₂ is about one order of magnitude smaller than MEA. In this case the amount of degraded AMP would be smaller than MEA in the blend. Contrary to an earlier report (Davis, 2009), the rate constant of AMP in the blend is close to what was found for the reaction of 4.75 mol/kg AMP with CO₂ (initial loading of 0.3 mol CO₂/mol AMP) in the absence of MEA at 135 °C, i.e., no protective effect of MEA on AMP from thermal degradation was observed. Much lower concentration of MEA used in the present work could be one reason for the disparate result.

Recall from Chapter 4 that MEA reacts with CO₂ to form OZD, and OZD being very reactive and easily reacting with another MEA molecule to form HEEDA. Subsequently HEEDA reacts with CO₂ to form HEIA. The steric hindrance in AMP slows down its thermal degradation but does not prevent oxazolidinone formation and oxazolidinone ring-opening into further degradation products. The degradation of AMP and MEA in the blend could follow the same degradation pathways as in the thermally degraded single solutions. We can expect that some cross products may be formed since AMP and MEA can react with the two oxazolidinones, OZD and DMOZD, respectively.

Table 8.1 Thermal degradation products identified in an AMP/MEA blend.

Compound	Abbr.	CAS #	Structure	Status
N-(2-hydroxyethyl)ethylenediamine	HEEDA	111-41-1		P.I.
N-(2-hydroxyethyl)-2-imidazolidinone	HEIA	3699-54-5		P.I.
2-[(2-Amino-2-methylpropyl)amino] ethanol	AMPAE	68750-16-3		P.I.
2-[(2-Amino-2-methylpropyl)amino]-2-methyl-1-propanol	AMPAMP	72622-74-3		P.I.
4, 4-Dimethyl-2-oxazolidinone	DMOZD	26654-39-7		P.I.
2-Ethylenediamine-2-methyl-1-propanol	EDAMP			S.P.
4,4-dimethyl-1-hydroxytertbutyl-2-imidazolidinone	DMHTBI			S.P.
2-Oxazolidinone	OZD	497-25-6		P.I.
1-hydroxytertbutyl-2-imidazolidinone	HTBI			S.P.

P.I.: Positively identified; S.P.: Suspected product, which has not been confirmed by an authentic standard chemical due to its commercial unavailability.

A summary of the major non-ionic products identified by GC-MS is provided in Table 8.1. The expectation of cross product formation was supported by examining the products. The cross degradation product AMPAE can be formed due to reaction of MEA with DMOZD. At the same time AMP reacted with OZD to form EDAMP, subsequently EDAMP reacted with CO₂ to form HTBI. As mentioned above, the rate constant of the reaction of AMP with CO₂ in the blend is slightly higher than that of individually degraded AMP. This result might be due to the cross reactions, i.e. formation of EDAMP and HTBI.

8.2 Oxidative degradation

8.2.1 Overview of oxidative degradation products

Oxidative degradation of individual AMP has been studied in Chapter 5 and 6, and oxidative degradation of MEA has been widely studied since it is the benchmark molecule. The degradation products of MEA and the proposed pathways for generation of degradation products were recently summarized by Gouedarda et al. (2012). In order to verify our analysis methods, one experiment was performed on a single MEA solution. An aqueous solution of 5 mol/kg MEA was degraded under 250 kPa O₂ at 120°C. Cation IC and anion IC were performed on all the samples, while GC-MS was only performed on selected samples, since the concentration of most of the non-ionic products was too low for quantification by GC-MS in the initial stage of the oxidations.

The key degradation compounds of MEA which have previously been reported and summarized (Gouedarda et al., 2012) were also detected in this study. The major observed degradation products included ammonia, N-(2-hydroxyethyl)formamide (HEF), N-(2-hydroxyethyl)acetamide (HEA), N-(2-hydroxyethyl)imidazole (HEI) and carboxylic acids (formic-, acetic-, oxalic- and glycolic acid). Additionally, nitrite, nitrate were detected at low concentrations. The formation of HEF and HEA can be explained by reactions of MEA with formic- and acetic acid, while the mechanism of HEI formation still needs further work. Formation of HEF and HEA in the case of MEA suggests that carboxylic acids play one more role in further degradation of the solvent in addition to the well known formation of heat stable salts.

For the oxidative degradation experiments of AMP/MEA blends, a total of eight degradation experiments were conducted with the blends of AMP/MEA. The operating temperatures ranged from 100 to 140°C, the O₂ partial pressure ranged from 250 to 350 kPa, and the AMP-MEA ratio was varied as shown in Table 8.2.

Table 8.2 Summary of experimental degradation conditions for AMP/MEA blends and calculated first order reaction rate constants.

Expt. No.	Initial AMP conc. (mol·kg ⁻¹)	Initial MEA conc. (mol·kg ⁻¹)	Temp. (°C)	O ₂ press. (kPa)	Apparent first order reaction rate constant/ ×10 ⁻⁷ s ⁻¹	
					MEA	AMP
AM1	4	1	120	250	13.6 ± 0.97	4.54 ± 0.53
AM2	3	2	120	250	12.7 ± 1.17	3.96 ± 0.45
AM3	2	3	120	250	7.55 ± 0.23	3.56 ± 0.09
AM4	2	3	120	350	12.2 ± 0.53	5.31 ± 0.25
AM5	3	2	140	250	19.5 ± 1.14	6.37 ± 0.68
AM6	3	2	100	250	5.37 ± 0.57	1.72 ± 0.16
AM7	4	2	120	250	10.6 ± 0.76	3.10 ± 0.32
AM8	4	4	120	250	7.07 ± 0.26	2.37 ± 0.11

We detected the same degradation products under different composition, temperature and oxygen pressure, except that the relative amounts of the products varied. The oxidative degradation products in the AMP/MEA blends are similar to those observed in separately degraded AMP and MEA. The major MEA derived products included HEF, HEA and HEI. In comparison with degradation of single AMP and MEA solutions, no new oxidative degradation product was detected in the AMP/MEA mixtures. This result indicates that AMP and MEA are oxidized in parallel in AMP/MEA blends.

It should be noted that DMOZD was detected in the degraded AMP/MEA mixtures, but no 2-oxazolidinone (OZD) was found. OZD is very reactive and hence it cannot accumulate in the degraded blends. Although DMOZD is much more stable than OZD due to steric hindrance, MEA can still react with DMOZD to form 2-ethylenediamine-2-methyl-1-propanol (Davis, 2009). AMP can also react with OZD in a similar way. Thus cross products

as described in Section 8.1 can be expected to be formed in the presence of CO₂. However, further degradation products of OZD and DMOZD were not detected in this work as these degradation products are expected at low concentration only because the blends were not loaded with CO₂.

8.2.2 Effects of operating parameters

8.2.2.1 Effect of temperature and O₂ pressure

The concentration profiles for AMP and MEA decreased linearly with degradation time when plotted in a semi-logarithmic scale. This suggests an overall first order reaction with respect to the amines. Equation 4.2 provides a relationship for the concentration of AMP (or MEA) with time and allows the determination of an apparent first order rate constant. Figure 8.1 shows an example of $\ln(c/c_0)$ against reaction time in a mixture of 3mol/kg AMP and 2 mol/kg MEA that was degraded at 120°C and 250 kPa O₂. The slopes of the plots represent the apparent first order reaction rate constants for AMP and MEA, respectively.

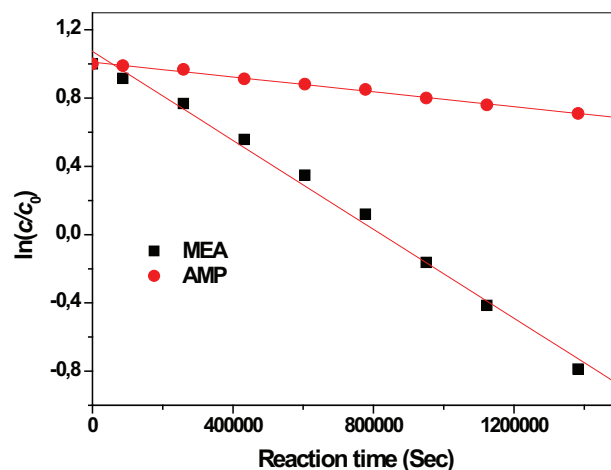


Figure 8.1 Plot of $\ln(c/c_0)$ against reaction time (3mol/kg AMP + 2 mol/kg MEA degraded at 120°C and 250 kPa O₂).

All the calculated first order reaction constants for AMP and MEA under other reaction conditions are presented in Table 8.2. Although MEA and AMP oxidation could be oxygen mass transfer limited at the experimental conditions, it does not affect comparison of the

relative degradation rates of AMP and MEA in the blends. The results show that the rate of MEA degradation was higher than that of AMP in all the different blend compositions at all experimental conditions. As can be seen in Table 8.2, both of the overall rates of AMP degradation and MEA degradation increased with rising temperature as expected. It should be noted that the duration of each experiment was only 1 week, the degradation of AMP was low, and thus the measured reaction rate constants could have a large error.

Generation of carboxylate ions was measured in all samples. The comparison of formate and oxalate concentration for the case of 3mol/kg AMP-2mol/kg MEA at 120°C and 140°C is shown in Figure 8.2. Generation of both formate and oxalate was enhanced at higher temperature, as expected with increased oxidation rates of AMP and MEA. This result indicates that the earlier analyzed enhanced degradation rates of AMP and MEA at higher temperatures are potentially true which is also reflected in increased concentration of degradation products.

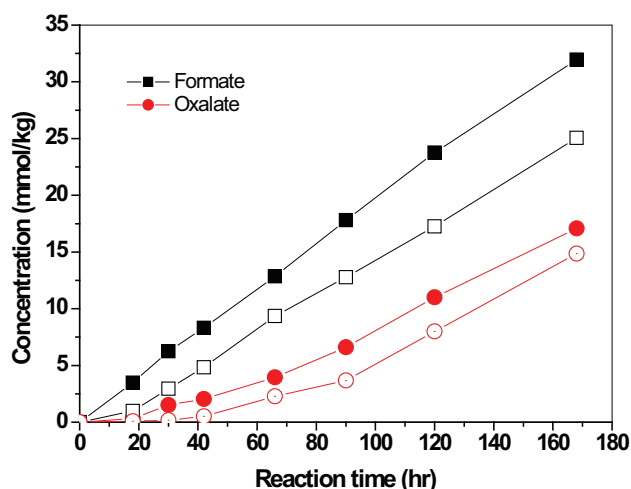


Figure 8.2 Effect of temperature on generation of formate (■) and oxalate (●) at 120°C (open points) or 140°C (solid points). The experiments were conducted with 3 mol/kg AMP + 2 mol/kg MEA under 250 kPa O₂.

Based on previous assumption that AMP and MEA may be oxidized in parallel in the AMP/MEA blends, and the fact that acetone, 2, 4-lutidine and DMOZD are universally found during AMP oxidative degradation, we therefore take these three main degradation products

of AMP as its degradation indicators. Figure 8.3 shows the amount of formation of acetone, 2,4-lutidine and DMOZD after 168 hours reaction time using a mixture of 3 mol/kg AMP and 2 mol/kg MEA under 250 kPa O₂. As can be seen in Figure 8.3, the amount of acetone, 2, 4-lutidine and DMOZD increased with rising temperature. As proposed in Chapter 6, it is believed that acetone is an intermediate of AMP oxidation which decomposes to acetic acid and formaldehyde in the presence of ·OH radicals. Therefore, the end result of the formation rate of acetone increased less than those of 2, 4-lutidine and DMOZD.

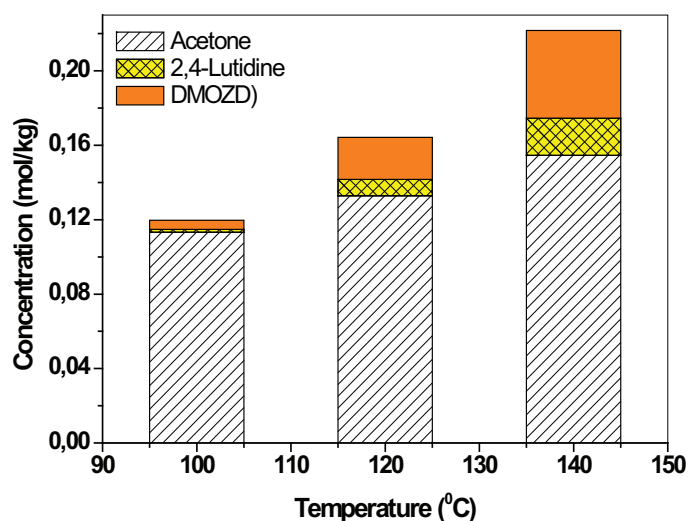


Figure 8.3 Comparison of the amount of formation of acetone, 2, 4-lutidine and DMOZD with 3mol/kg AMP + 2 mol/kg MEA from 100 to 140°C under 250 kPa O₂ after 168 hours.

As discussed in Chapter 5, the oxidation of concentrated AMP could be O₂ mass transfer limited under accelerated conditions. Since AMP degradation by oxygen in the reaction vessel is a two-phase system. O₂ should be dissolved into the aqueous solution first. The dissolved O₂ reacts with amine followed by degradation. For the same reason, the overall degradation rates of AMP and MEA were also affected by O₂ partial pressure as they were oxidized individually. The degradation rates were expected to increase with increasing O₂ partial pressure due to the increased dissolved O₂ in the aqueous solutions.

Most of the oxidation experiments in this project were performed with an oxygen partial pressure of 250 kPa. In order to investigate the effect of O₂ partial pressure on the degradation of AMP in the AMP/MEA blends, two of the eight experiments were conducted at different O₂ pressures. For a 2 mol/kg AMP and 3 mol/kg MEA blend at 120°C, the first order reaction constant for AMP increased by 49% when O₂ pressure was increased from 250 kPa to 350 kPa, and the first order reaction constant for MEA increased by 61%. This result demonstrates that O₂ partial pressure has a significant effect on both oxidation rates of AMP and MEA in the blends. The type of identified products is exactly same at the two different O₂ partially pressures. However, oxidation of concentrated AMP and MEA could be O₂ mass transfer limited under accelerated conditions, and thus higher O₂ pressure could cause higher degradation rates of AMP and MEA. The amount of formation of the major three products of AMP at two different O₂ pressures is shown in Figure 8.4.

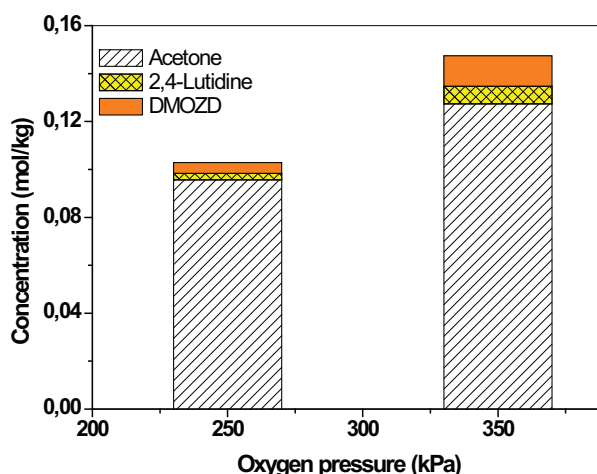


Figure 8.4 Comparison of the amount of formation of acetone, 2, 4-lutidine and DMOZD with 2mol/kg AMP + 3 mol/kg MEA at 120°C under 250 kPa and 350 kPa O₂ after 168 hours.

8.2.2.2 Effect of blend composition

Another factor explored in this work is the effect of blend composition on the oxidation of AMP in the blends. As can be seen in Table 8.2, the degradation rate of AMP decreased when the initial concentration of AMP was fixed at 4 mol/kg while the initial concentration of MEA was increased. Figure 8.5 shows the amount of formation of acetone, 2, 4-lutidine

and DMOZD after 168 hours degradation of the AMP/MEA blends. The data clearly show that the amount of acetone, 2, 4-lutidine and DMOZD decreased with raised MEA concentration. The degradation rate of AMP and the formation rates of the indicators decreased indicating MEA protects AMP from oxidation in the mixture when initial MEA concentration is increased. As mentioned above, AMP and MEA could be degraded separately in the blends, but MEA degrades faster than AMP. On the other hand, the oxidation of concentrated MEA and AMP could be O₂ mass transfer limited under the experimental conditions. In this case, MEA competed with AMP for O₂ and thus be the reason for a decreased degradation rate of AMP.

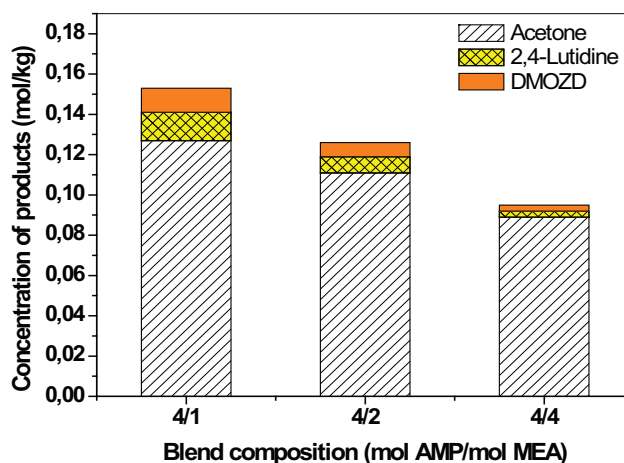


Figure 8.5 Comparison of the amount of formation of acetone, 2, 4-lutidine and DMOZD with AMP/MEA blends at 120°C and 250 kPa O₂ after 168 hours.

8.3 Conclusions

An aqueous AMP/MEA blend (3mol/kg AMP +2mol/kg MEA) with a CO₂ loading of 0.3 mol CO₂/mol total amine was degraded at 135°C. The rate constants for the reaction of CO₂ with AMP and MEA were $1.9 \times 10^{-8} \text{ s}^{-1}$ and $1.4 \times 10^{-7} \text{ s}^{-1}$, respectively. The rate of the reaction of MEA with CO₂ is approximate one order of magnitude higher than that of AMP. Since both MEA and AMP can attack oxazolidinones derived from MEA and AMP, cross products, AMPAE, EDAMP and HTBI were formed during thermal degradation in the

presence of CO₂. However formation of cross products would not be confirmed yet by use of authentic standards.

For AMP/MEA blends, the major oxidative degradation products include ammonia, acetone, 2, 4-lutidine, 4, 4-dimethyl-2-oxazolidinone, N-(2-hydroxyethyl)formamide, N-(2-hydroxyethyl)acetamide, N-(2-hydroxyethyl)imidazole, and formate. As compared with oxidative degradation of single MEA and AMP, no cross product was found in the degraded mixtures. This result indicates that AMP and MEA are degraded in parallel in the blends.

The pseudo first order reaction rate constants for AMP and MEA in AMP/MEA blends were measured. Both the overall degradation rates of MEA and AMP increased with raising temperature and oxygen partial pressure, respectively. Acetone, 2, 4-lutidine and DMOZD were three typical degradation products of AMP. It was found that acetone formation rate increased less than those of 2, 4-lutidine and DMOZD. These results indicate that acetone was an intermediate as proposed in earlier the AMP degradation pathway. MEA degraded faster than AMP in AMP/MEA blends under different experimental conditions. When increased initial MEA concentration, the amount of AMP loss decreased indicating that MEA protects AMP from oxidation. The inhibition effect of MEA on AMP degradation could be due to the fact that MEA degraded faster than AMP in the blends, however, this “protecting” effect of MEA is not expected to operate in a situation with high O₂ partial pressure.

Chapter 9 Conclusions and Recommendations

This chapter provides a summary of conclusions of this research into the degradation of aqueous AMP and AMP blends for post-combustion CO₂ capture from coal-fired flue gas. The conclusions developed in this thesis are largely based on data obtained in closed and batch-operated autoclave reactors at elevated temperatures. Recommendations are made for further study in order to enhance understanding of degradation of aqueous AMP solution for CO₂ capture.

9.1 Conclusions

9.1.1 Degradation of AMP

9.1.1.1 Thermal degradation of AMP

AMP is stable at temperatures less than 140°C under nitrogen atmosphere. However, significantly thermal degradation of AMP occurred in the presence of CO₂. At 135°C, 4.75 mol/kg AMP solution with 0.3 mole CO₂ per mole AMP thermally degrades with a first order rate constant of $18.6 \times 10^{-9} \text{ s}^{-1}$, or approximately 260 mmole per kg entire solution after 5 weeks. The increasing concentration of CO₂ increases the thermal degradation of concentrated AMP. At 135 °C, AMP degradation increased as a linear function of CO₂ loading up to 0.4 mole CO₂ per mole AMP (higher CO₂ loading was not investigated).

The major degradation products of thermally degraded 4.75 mol/kg AMP are 4, 4-dimethyl-2-oxazolidinone (DMOZD), 2-[(2-amino-2-methylpropyl) amino]-2-methyl-1-propanol (AMPAMP), and 4,4-dimethyl-1-hydroxytertiobutyl-2-imidazolidinone (DMHTBI). AMP does form a carbamate and continue to form DMOZD. The steric hindrance in AMP does not prevent oxazolidinone species formation. AMPAMP is believed to be formed from a S_N2 type ring opening reaction of DMOZD with AMP. DMHTBI could be formed from the reaction of AMPAMP with CO₂ followed by an intramolecular nucleophilic reaction. All of these reactions follow a carbamate polymerization type degradation pathway. Due to the steric hindrance in the AMP molecule, DMOZD is stable and will hence accumulate in degraded AMP solution contrary to 2-oxazolidinone (OZD) in degraded MEA solution.

However AMP trimers and further polymeric products were not observed in AMP degradation.

9.1.1.2 Oxidative degradation of AMP

The expected degradation product NH_3 was detected by FT-IR immediately when air was bubbled through AMP solution at 55°C . No measurable AMP loss was observed and formation of carboxylic acids was very little in the solution within 2 days of experiment. A 5 mol/kg AMP solution with addition of 0.5 mM Fe^{2+} , 0.1 mM Cr^{3+} and 0.05mM Ni^{2+} was degraded in the circulating reaction system with 1.1 bar O_2 at 70°C . After 4 weeks of degradation, 48 ppm formate was detected as main product in the AMP solution. Aqueous AMP solutions do degrade in the presence of O_2 , albeit at much lower rates than MEA solutions.

In order to shorten the length of the experiment, most of the experiments were conducted in autoclave reactors at temperatures of $100\text{-}140^\circ\text{C}$, and O_2 pressures of 250-350 kPa. Under accelerated conditions, the oxidation rate of AMP increased slightly with raised temperature, but increased significantly with increased O_2 partial pressure. 5 mol/kg AMP was degraded at 120°C , the overall degradation rate with 350 kPa O_2 was approximate 3 times of that with 250 kPa O_2 after 16 days. The addition of 0.1 mM FeC_2O_4 and 0.1 mM CuSO_4 did not affect the rate of AMP oxidative degradation. However, AMP oxidation rate increased dramatically with increased agitation rate. The rate dependence on agitation rate as well as O_2 partial pressure indicates that the oxidative degradation of AMP could be partially controlled by O_2 mass transfer under elevated temperatures. The implication of these results is that dissolved oxygen in AMP solvent increases the rate of AMP oxidation as the solvent is heated in the cross-exchanger and piping to the stripper in industrial application of AMP-based solvents.

At $100\text{-}140^\circ\text{C}$, the identified products of AMP included acetone, 2, 4-lutidine, 4, 4-dimethyl-2-oxazolidinone, carboxylate ions (formate, acetate, oxalate, glycolate), nitrite, nitrate, ammonium and some other minor products. Although 2, 4-lutidine was still found as a product, it was not a major product any more at 80°C . Acetone oxime and 4, 4-dimethyl-1, 3-oxazolidine were minor products at $100\text{-}140^\circ\text{C}$, but they were major products at 80°C . A reaction mixture of AMP solution, which was degraded for 13 weeks at 80°C , was removed into a miniclave reactor and continued to degrade in the presence of 250 kPa O_2 at 120°C .

The concentration of acetone oxime and 4, 4-dimethyl-1, 3-oxazolidine dramatically decreased after 24 hours reaction time.

Based on the identified AMP degradation products, possible degradation pathways for the formation of these products were proposed as shown in Figure 9.1. The likelihood of an initial hydrogen-abstraction step to occur on the methylene group adjacent to the OH group is greater than that on the amino group or methyl group, since this C-H bond is the weakest hydrogen-containing bond in AMP molecule. In the presence of oxygen, a peroxy radical (**2**) is formed by a fast reaction of the initial C-centered radical (**1**) with O₂ (see Figure 9.1). After ejection of a ·OH radical, the peroxy radical (**2**) is decomposed to form formic acid and an imine (or enamine) by intramolecular hydrogen-abstraction. The imine is expected to be readily hydrolyzed to acetone and ammonia. The formed primary products are not stable and ·OH radicals are very active, thus this situation will lead to a series of secondary reactions in the presence of O₂, such as oxidation of acetone and formaldehyde, and oxidation of ammonia. The reactions of the primary products result in formation of lutidine, oxazolidinone and oxazolidine. For the unloaded AMP solution, mineralization of the carboxylic acids is the source of CO₂ in the presence of ·OH radicals. The temperature has a significant effect on these secondary reactions, and thus various distributions of the final products were observed at different temperatures.

In the proposed degradation pathway for AMP, the oxidation rate is supposed to be limited by the occurrence of an initiation step in the presence of sufficient concentration of dissolved oxygen. The rate of initiating radical formation can be increased by high-energy radiation or by heat. The effect of UV radiation on AMP oxidation was investigated by experiments conducted at 55°C. A medium pressure mercury vapour lamp was used to accelerate oxidation of AMP. Four of the identified products in the UV experiments, formamide, 4,4-dimethyl-1,3-oxazolidine, methenamine and N-formyl-AMP were not major products in the thermal accelerated experiments. However, all of these new products can be formed through secondary reactions of the primary degradation products included in the proposed pathway for thermal accelerated oxidation of AMP. Furthermore, the amount of these new products almost disappeared as the reaction mixture was heated to 120°C for 24 hours. It seems that UV radiation does not change the primary degradation mechanism of AMP. Temperature could be the main factor that affects the secondary reactions of the primary products.

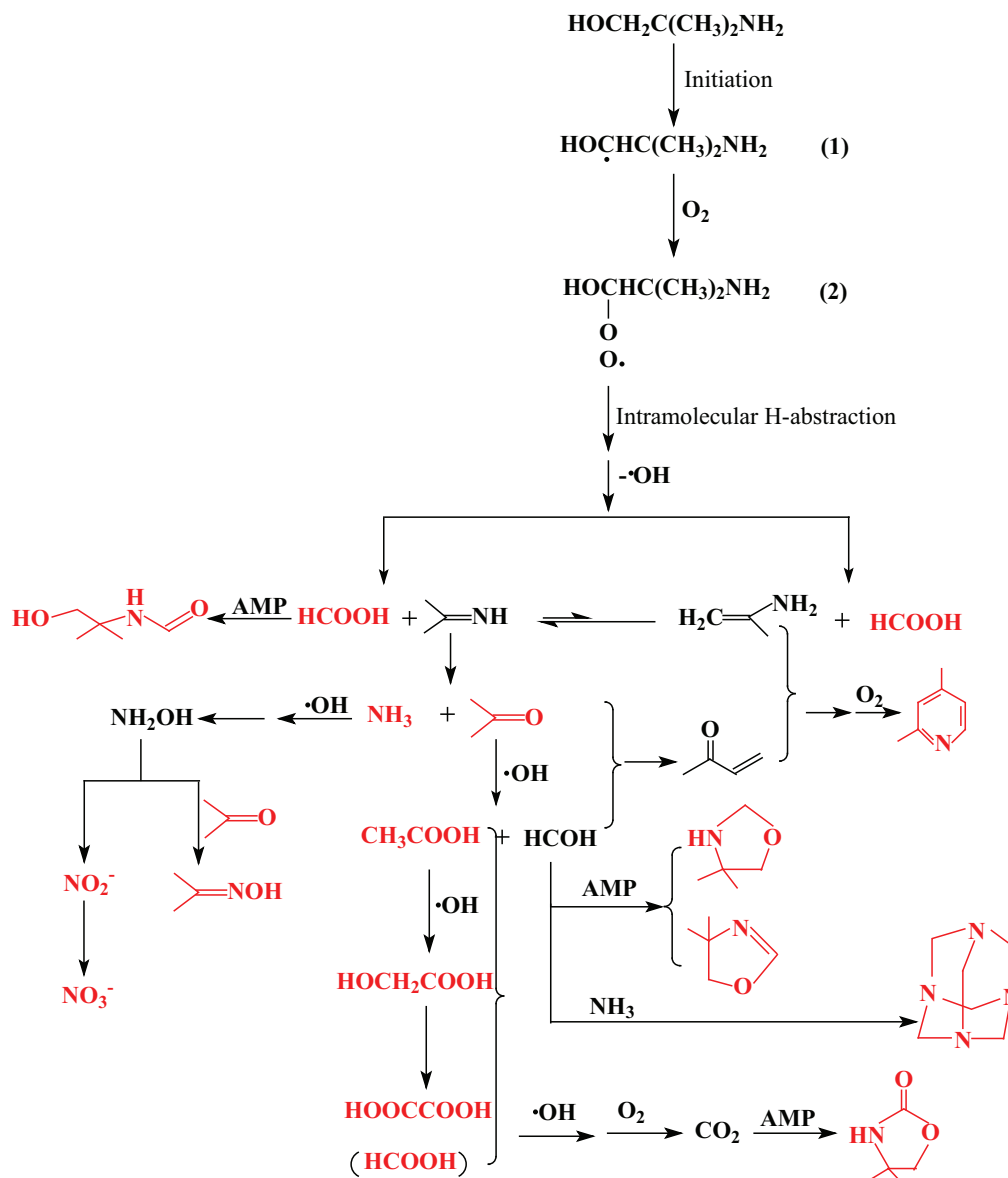


Figure 9.1 Summary of proposed pathways for formation of AMP oxidation products (the identified products are marked in red).

The oxidation rate of AMP solution with 0.3 mole CO_2 per mole AMP was faster than the rates of low CO_2 loading and unloaded solutions. No significant change of the overall

degradation rate and degradation products of AMP was observed when the initial AMP solutions were treated with addition of different amount of H₂SO₄. GC-MS analysis and anion IC analysis demonstrated that the dependence of AMP oxidation on CO₂ loading could be due to CO₂ induced reactions. As compared to degradation without CO₂ loading, the end concentrations of acetone, 2, 4-lutidine and carboxylate ions did not change, while the concentration of 4, 4-dimethyl-2-oxazolidinone increased 12 folds when the AMP solution was degraded with an initial loading of 0.3 mole CO₂ per mole AMP.

Oxidation of a structural analog of AMP, 2-amino-1-propanol was examined with 250 kPa O₂ at 120°C. The oxidation of the analog likely proceeds through a similar pathway as proposed for AMP. Since the 2-amino-1-propanol molecule contains an α -hydrogen atom, the initial hydrogen-atom abstraction might occur not only on the methylene group adjacent to OH group but also on the α C-H bond.

9.1.2 Degradation of AMP/PZ blends

9.1.2.1 Thermal degradation of an AMP/PZ blend

AMP/PZ blend (3.5 mol/kg AMP + 1.5 mol/kg PZ) was stable at least less than 135 °C under N₂ blanket gas. However, the blend thermally degrades in the presence of CO₂ at 135 °C. With an initial loading of 0.3 mol of CO₂/ mol total amine, the blend experienced 8.5% PZ loss and 6.4% AMP loss after 5 weeks reaction time. The pseudo first order reaction rate of AMP in the blend is close to that in a single AMP system, however, the estimated rate constant for PZ is 23 times greater than the reported rate for 8m PZ (Freeman, 2010).

The most abundant degradation products of thermally degraded AMP/PZ blend are N-methyl PZ (MPZ) and 4, 4-dimethyl-2-oxazolidinone (DMOZD). MPZ accounts for 34% of PZ loss and DMOZD accounts for 42% of AMP loss during the thermal degradation. The expected product 1-[2-(2, 2-dimethyl)-aminoethyl]piperazine was not detected with the available methods.

9.1.2.2 Oxidative degradation of PZ

Aqueous solution of 1.5 mol/kg PZ was degraded with 250 kPa O₂. The overall rate of PZ loss at 80 °C was 0.47 mmol/(kg·h) within 38 days. At 100°C, the overall degradation

rate was 1.2 mmol/(kg·h) within 19 days, which is approximate half of the rate observed for separately degraded 5 mol/kg AMP. These rates indicate that PZ is more resistant to oxidative degradation when tested in batch reactor and compared to AMP and MEA.

Except for the anionic products, the degradation products of PZ oxidation which were quantified at the greatest concentration were NH_4^+ , EDA, OPZ and FPZ. MNPZ, 2-(1H-imidazol-1-yl)ethanamine and 2, 5-dione were identified as minor products. A mass balance was performed on the end samples from a PZ oxidation experiment at 100°C, and ~46% of the lost nitrogen and ~21% of the lost carbon from PZ were recovered in the quantified degradation products.

A degradation pathway for PZ has been proposed based on identified products which were consistently detected in all the PZ degradation samples. Oxidation of PZ is believed to be initiated through H-abstraction followed by the formation of a peroxy radical in the presence of O_2 . As compared with AMP oxidation, the key difference in oxidation of PZ is the form of the peroxy radical decomposition.

9.1.2.3 Oxidative degradation of AMP/PZ blends

Blends of 3.5 mol/kg AMP + 1.5 mol/kg PZ were oxidized in the batch reactor at 80-120°C. The degradation products included the heat stable salts formate, acetate and oxalate, the AMP derived products including acetone, 2,4-lutidine and DMOZD, and the PZ derived products including EDA, OPZ and FPZ, etc. No new product was detected as compared to individually degraded AMP and PZ. The degradation rates of AMP and PZ were estimated. The degradation rate of AMP is close to that in the single AMP system, but PZ loss rate is higher than that in the single PZ system. The reactions of PZ with the AMP degradation products are likely reasons for the increased PZ loss rate in the AMP/PZ blends. The overall degradation rate of AMP decreased but not dramatically when the initial concentration of PZ was increased from 0 to 1.5 mol/kg.

9.1.3 Degradation of AMP/MEA blends

9.1.3.1 Thermal degradation of an AMP/MEA blend

One thermal degradation experiment was performed on AMP/MEA blend (3mol/kg AMP +2mol/kg MEA) with a CO_2 loading of 0.3 mol CO_2 /mol amine at 135°C. The rate

constant for the reaction of AMP with CO₂ was $1.9 \times 10^{-8} \text{ s}^{-1}$, which is one order of magnitude lower than that for MEA, $1.4 \times 10^{-7} \text{ s}^{-1}$. Since both MEA and AMP can attack the oxazolidinones derived from MEA and AMP, cross products were expected to be formed during the thermally degradation in the presence of CO₂. One of the expected products, 2-[(2-amino-2-methylpropyl) amino] ethanol (AMP/AE) has been identified. It is suspected that the other cross products, 2-ethylenediamine-2-methyl-1-propanol (EDAMP), 4,4-dimethyl-1-hydroxyethyl-2-imidazolidinone, and 1-hydroxytertbutyl-2-imidazolidinone (HTBI) are included in the unidentified products.

9.1.3.2 Oxidative degradation of AMP/MEA blends

Oxidation of AMP/MEA blends was studied in the autoclave reactors with O₂ pressures of 250 and 350 kPa at temperatures of 100-140°C. The same degradation products were detected under different composition, temperature and oxygen pressure, except that the relative amounts of the products varied. The oxidative degradation products in the AMP/MEA blends are similar to those observed in separately degraded AMP and MEA solutions. In the blends, the major MEA derived compounds included N-(2-hydroxyethyl)-formamide (HEF), N-(2-hydroxyethyl)-acetamide (HEA), N-(2-hydroxyethyl)imidazole (HEI). In comparison with degradation of single AMP and MEA samples, no new oxidative degradation product was detected in the AMP/MEA mixtures. This indicates that AMP and MEA can be oxidized in parallel in an AMP/MEA blend.

The calculated pseudo first order reaction constants for AMP and MEA show that the overall degradation rates of MEA and AMP increased with raising temperature and oxygen partial pressure, respectively. The rate of MEA degradation was higher than that of AMP in all the different blend composition at all experimental conditions. The inhibition effect of MEA on AMP degradation could be due to the fact that MEA degraded faster than AMP in the blends.

9.2 Recommendations

Aqueous AMP-based solutions are commercially attractive solvents for post-combustion CO₂ capture from coal-fired power plants. The main goal of this work was to gain a baseline understanding of degradation behaviour and pathways of AMP. Possible pathways for AMP

degradation have been proposed based on the identified products in this dissertation. However, the degradation mechanisms are still not well understood. There are some unanswered questions that should be investigated to understand the degradation of AMP more fully.

9.2.1 Identification of degradation products

The oxidative degradation experiments of aqueous amine solutions described in this project all suffer from a common failure to close the overall mass balance. This result indicates that there are still unidentified degradation products in the degraded systems. Therefore, one of the most important recommendations is the need for more sophisticated analytical methods to identify unknown degradation products. In this work, only liquid phase of the degraded amines was analyzed, but analysis of gas phase is important as well. Identifying the products is essential to understand the degradation mechanisms, and is important for studying the best way to reclaim them, understanding their environmental impact, and learning how to mitigate or prevent their production.

Although it is necessary, it is a hard work to identify the degradation products due to the complexity of the degradation products. Using of a single technique to characterize the oxidative degradation of alkanolamines is impossible (Supap et al., 2006). IC is limited to ionic products. Although GC-MS has been a powerful and heavily used tool in this work, its analysis can be limited to volatile products. Degradation products of high molecular weights might potentially be left undetected. LC might overcome this problem and could be used as a confirmation technique. In order to close the mass balance gap, the combination of different analytical techniques is required to allow the simultaneous identification and quantification of the various classes of the degradation products.

Additionally, oxidative degradation AMP is believed to be occurred via a radical mechanism. According to the proposed the schemes for AMP degradation, there are many intermediates formed during the degradation. In order to confirm the possible degradation pathway, the main intermediates, such as the peroxy radical, $\cdot\text{OH}$ radical, must be identified or confirmed.

9.2.2 Further investigation of oxidation

There are many effects related to AMP oxidation that were not fully explored in this work due to time or equipment constraints. First, the effect of O₂ mass transfer should be further explored. It is well known that mechanism studies for any reaction require knowledge of the kinetics of the reaction. The obtained data indicate that AMP oxidation could be O₂ mass transfer limited in the thermal accelerating conditions. The temperature control and agitation in the miniclave reactors were not good, more experiments are recommended to determine the kinetics of the degradation reaction. If the temperature control and agitation will be improved, the kinetics of AMP oxidation could be measured with better accuracy.

The effect of CO₂ concentration on AMP oxidation was not fully understood during the course of this work. Neither oxidative degradation of AMP with high CO₂ loading nor CO₂ loaded AMP degraded at typical absorber temperature was examined in this project. Additional experiments according to the conditions encountered in the absorber and absorber sump should be further investigated.

9.2.3 Effect of metal ion

The effect of metal ion is an important point since the use of stainless steel as a material of construction is the most likely choice of absorption-stripping systems for post-combustion CO₂ capture. The catalytic effects of metal ions, such as Fe (II), on the oxidation of AMP should be further investigated. As described in Chapter 2, the catalytic effects of metal ions on the oxidation of amines have been reported by many investigators, however in this work no significant effect on AMP oxidation was observed at thermal accelerating conditions with addition of 0.1 mM FeC₂O₄ or 0.1 mM CuSO₄, respectively. This result could be caused by O₂ mass transfer limitation. Additionally, the thermocouple well and liquid sampling tubing were made of stainless steel, which was contacted with AMP solution during the experiments in the present work. If experiments were developed to improve the O₂ mass transfer and prevent any steel parts of the reactor from contacting with amine solution, the effect of each catalyst could be determined with better accuracy.

Furthermore, though the effect of metal ion on amine loss has been widely studied, the catalytic mechanism has not been clarified and the effect of metal ion on the distribution of the final degradation products is not clear. For AMP degradation, the effect of metal ion with

different ligand on the loss of AMP and the distribution of the degradation products should be answered.

9.2.4 Environmental implications

Environmental implications of a CO₂ capture system based on AMP or AMP blends is a crucial issue but was not included in this project. One of the important issues is the unknown environmental impact of the oxidation products including volatility of the degradation products, reactions of volatile products in the atmosphere, and handling of wastes created in the reclaimer. These environmental concerns must be taken into account and thoroughly researched before full-scale implementation of AMP-based solvents.

Another important topic related to the environmental impact of AMP-based solvents is the generation and identification of nitrosamines produced during the solvent degradation. Nitrosamines are a class of compounds of the chemical structure R₁N(-R₂)-N=O, most of which are carcinogenic or potentially carcinogenic to humans, indicating the importance of identifying and handling any nitrosamine created during the amine solvent degradation. N-methylnitrosopiperazine (MNPZ) has been detected in the degraded AMP/PZ blends. How to prevent nitrosoamine formation or safely treat the formed nitrosoamine should be solved.

Flue gas contains NO_x which may be a source of nitrosamine formation in the amine-based absorption-desorption process. The nitrosation of amines may be initiated by NO_x in acidic, neutral or alkaline conditions. The effect of NO_x on the oxidation of AMP-based solvents and NO_x reaction products should be investigated under relevant CO₂ capture conditions.

References

Anslyn E.V. and Dougherty D.A. Modern Physical Organic Chemistry, University Science Books, Sausalito, CA, 2006.

Armstrong D.A., Asmus K.-D., Bonifačić M. Oxide radical anion reactivity with aliphatic amino compounds in aqueous solution: comparison of H-atom abstraction from C-H and N-H groups by O and OH. *J. Phys. Chem. A* 2004, 108: 2238-2246.

Aroonwilas A. and Veawab A. Characterization and comparison of the CO₂ absorption performance into single and blended alkanolamines in a packed column. *Ind. Eng. Chem. Res.*, 2004, 43: 2228–2237.

Aroonwilas A. and Veawab A. Integration of CO₂ capture unit using blended MEA-AMP solution into coal-fired power plants. *Energy Procedia*, 2009, 1: 4315-4321.

Bedell S.A. Amine autoxidation in flue gas CO₂ capture-Mechanistic lessons learned from other gas treating processes. *Int. J. Greenh. Gas Con.*, 2011, 5: 1-6.

Bello A. and Idem R.O. Comprehensive study of the kinetics of the oxidative degradation of CO₂ loaded and concentrated aqueous monoethanolamine (MEA) with and without sodium metavanadate during CO₂ absorption from flue gases. *Ind. Eng. Chem. Res.* 2006, 45: 2569-2579.

Blachly C.H. and Ravner H. Stabilization of monoethanolamine solutions in carbon dioxide scrubbers. *J. Chem. Eng. Data*, 1966, 11: 401-403.

Brúder P., Grimstvedt A., Mejdell T., et al. CO₂ capture into aqueous solutions of piperazine activated 2-amino-2-methyl-1-propanol. *Chem. Eng. Sci.*, 2011, 66: 6193-6198.

Chakma A., Meisen A. Identification of methyl diethanolamine degradation products by gas chromatography and gas chromatography-mass spectrometry. *J. Chromatogr.*, 1988, 457: 287-297.

Chakma A. and Meisen A. Methyl-diethanolamine degradation-Mechanism and kinetics. *Can. J. Chem. Eng.*, 1997, 75: 861-871.

Chakraborty A.K., Astarita G., Bischoff K.B. CO₂ absorption in aqueous solutions of hindered amines. *Chem. Eng. Sci.*, 1986, 41: 997-1003.

Chancheay A., Saiwan C., Supap T., et al. Off-gas emission in CO₂ capture process using aqueous monoethanolamine solution. *Energy Procedia*, 2011, 4: 504-511.

- Chi S. Oxidative Degradation of Monoethanolamine. The University of Texas at Austin. Master Thesis. 2000.
- Chi S. and Rochelle G. T. Oxidative degradation of monoethanolamine. *Ind. Eng. Chem. Res.*, 2002, 41: 4178-4186.
- Chin M. and Wine P.H. A temperature-dependent competitive kinetics study of the aqueous-phase reactions of OH radicals with formate, formic acid, acetate, acetic acid, and hydrated formaldehyde. In: Helz, G.R., Zepp, R.G., Crosby, D.G. (Eds.), *Aquatic and Surface Photochemistry*. Lewis Publishers, CRC Press, 85-96: 1994.
- Choi W-J., Cho K-C., lee S-S., et al. Removal of carbon dioxide by absorption into blended amines: kinetics of absorption into aqueous AMP/HMDA, AMP/MDEA, and AMP/piperazine solutions. *Green Chem.*, 2007, 9: 594-598.
- Choi W-J., Seo J-B., Jang S-Y., et al. Removal characteristic of CO₂ using aqueous MEA/AMP solutions in the absorption and regeneration process. *J. Environ. Sci.*, 2009, 21: 907-913.
- Closmann F.B. Oxidation and thermal degradation of methyldiethanolamine/piperazine in CO₂ capture. The University of Texas at Austin. Ph.D. Dissertation. 2011.
- Crea F., DeRobertis A., Sammartano S. Chromatographic behavior of open-chain polyamines NH₂-(CH₂)₂-[NH-(CH₂)₂]_n-NH₂ and their quantitative determination in sea water by high-performance ion-exchange chromatography. *J. Chrom. Sci.*, 2005, 43: 342-347.
- Cringle D.C., Pearce R.L., Dupart M.S. Method for maintain effective corrosion inhibition in gas scrubbing plant. US patent 4690740, 1987.
- Crooks J.E., Donnellan J.P. Kinetics of the reaction between carbon dioxide and tertiary amines. *J. Org. Chem.*, 1990, 55: 1372-1374.
- Dash S.K., Samanta A., Samanta A.N., et al. Absorption of carbon dioxide in piperazine activated concentrated aqueous 2-amino-2-methyl-1-propanol. *Chem. Eng. Sci.*, 2011, 66: 3223-3233.
- Davis J. D. Thermal Degradation of Aqueous Amines Used for Carbon Dioxide Capture. The University of Texas at Austin. Ph.D. Dissertation. 2009.
- Davison J. Performance and costs of power plants with capture and storage of CO₂. *Energy*, 2007, 32: 1163-1176.
- Dawodu O.F., Meisen A. Gas chromatographic analysis of alkanolamine solutions using capillary and packed columns. *J. Chromatogr.* 1993, 629: 297-307.
- Delfort B., Carrette P.-L., Bonnard L. MEA 40% with improved oxidative stability for CO₂ capture in post-combustion. *Energy Procedia*, 2011, 4: 9-14.

Denisov E.T. and Afanas'ev I. B. Oxidation and antioxidants in organic chemistry and biology. CRC press, Taylor & Francis Group, Boca Raton, 2005.

Dennis Jr.W.H., Hull L.A., Rosenblatt D.H. Oxidations of Amines. IV. Oxidative fragmentation. *J. Org. Chem.*, 1967, 32: 3783-3787.

Dionex Corporation, 2003. IonPac SCS 1 Silica Cation Separator, Sunnyvale, CA, USA.

Dionex Corporation, 2009. Product manual for ASRS[®] 300 and CSRS[®] 300. Document No. 031956.

Douglass M.L., Kabakoff B.L., Anderson G.A., Cheng M.C. The chemistry of nitrosamine formation, inhibition and destruction. *J. Soc. Cosmet. Chem.*, 1978, 29: 581-606.

Eide-Haugmo I., Lepaumier H., Da silva E.F., et al. A study of thermal degradation of different amines and their resulting degradation products. Presented in the 1st Post Combustion Capture Conference, Abu Dhabi, UAE, 17th-19th May, 2011.

Eller K., Henkes E., Roszbacher R., Höke H. "Amines, Aliphatic" in Ullmann's Encyclopedia of Industrial Chemistry, Wiley-VCH Verlag, Weinheim, 2005.

Franz G., Sheldon R.A. "Oxidation" in Ullmann's Encyclopedia of Industrial Chemistry, 5th ed.; VCH Verlagsgesellschaft mbH: Weinheim, Federal Republic of Germany, 1991.

Freeman S.A., Dugas R., Wagener D.H.V., et al. Carbon dioxide capture with concentrated, aqueous piperazine. *Int. J. Greenh. Gas Con.*, 2010a, 4: 119-124.

Freeman S.A., Davis J. Rochelle G. T. Degradation of aqueous piperazine in carbon dioxide capture. *Int. J. Greenh. Gas Con.*, 2010b, 4: 756-761.

Freeman S.A. Thermal Degradation and Oxidation of Aqueous Piperazine for Carbon Dioxide Capture. PhD dissertation, the University of Texas at Austin. 2011.

Furman O.S., Teel A.L., Watts R J. Mechanism of base activation of persulfate. *Environ. Sci. Technol.*, 2010, 44: 6423-6428.

Gabrielsen J., Svendsen H.F., Michelsen M. L., et al. Experimental validation of a rate-based model for CO₂ captures using an AMP solution. *Chem. Eng. Sci.*, 2007, 62: 2397-2413.

Gant T.G., Meyers, A.I. The chemistry of 2-oxazolines (1985–present). *Tetrahedron*, 1994, 50: 2297–2360.

Goff G.S., Rochelle G.T. Monoethanolamine degradation: O₂ mass transfer effects under CO₂ capture conditions. *Ind. Eng. Chem. Res.* 2004, 43: 6400-6408.

- Goff G.S. Oxidative Degradation of Aqueous Monoethanolamine in CO₂ Capture Processes: Iron and Copper Catalysts, Inhibition, and O₂ Mass Transfer. The University of Texas at Austin. Ph.D. Dissertation. 2005.
- Gouedarda C., Picq D., Launayc F., Carrette P-L. Amine degradation in CO₂ capture. I. A review. *Int. J. Greenh. Gas Cont.* 2012; 10: 244-270.
- Grayson J. I. and Dinkel R. An improved liquid-phase synthesis of simple alkyipyridines. *Helv. Chim. Acta.* 1984; 67: 2100-2110.
- Han L. Carbon dioxide capture with aqueous PZ/AMP. Presented at First Conference on Carbon Capture and Storage at the University of Texas at Austin (UTCCS1). Austin, TX, January 2012.
- Hilliard M. A Predictive Thermodynamic Model for an Aqueous Blend of Potassium Carbonate, Piperazine, and Monoethanolamine for Carbon Dioxide Capture from Flue Gas. The University of Texas at Austin. Ph.D. Dissertation 2008.
- Huang L., Li L., Dong W., Liu Y., Hou H. Removal of ammonia by OH radical in aqueous phase. *Environ. Sci. Technol.* 2008, 42: 8070-8075.
- Hull L.A., Davis G.T., Rosenblatt D.H. et al. Oxidations of Amines. III. Duality of mechanism in the reaction of amines with chlorine dioxide. *J. Am. Chem. Soc.*, 1967, 89: 1163-1170.
- Hull L.A., Giordiano W.P., Rosenblatt W.P., et al. Oxidations of amines. VIII. Role of the cation radical in the oxidation of triethylenediamine by chlorine dioxide and hypochlorous acid. *J. Phys. Chem.*, 1969, 73: 2147-2152.
- IEA. Global carbon-dioxide emissions increase by 1.0 Gt in 2011 to record high. 24, May, 2012.
- IPCC Fourth Assesment Report : Climate Change 2007 (AR4), 2007.
- Isaacs E.E., Otto F.D., Mather A.E. Solubility of mixtures of H₂S and CO₂ in a monoethanolamine solution at low partial pressure. *J. Chem. Eng. Data*, 1980, 25: 118-120.
- Ismael M., Sahnoun R., Suzuki A., et al. A study on the carbamates formation through the absorption of CO₂ by AMP. *Int. J. Greenh. Gas Con.*, 2009, 3: 612-616.
- Kadnar R. Determination of amines used in the oil and gas industry (upstream section) by ion chromatography. *J. Chrom. A*, 1999, 850: 289-295.
- Kaminski M., Jastrzebski D., Przyjazny A., et al. Determination of the amount of wash amines and ammonium ion in desulfurization products of process gases and results of related studies. *J. Chrom. A*, 2002, 947: 217-225.

- Karl M., Wright R.F., Berglen T.F., et al. Worst case scenario study to assess the environmental impact of amine emissions from a CO₂ capture plant. *Int. J. Greenh. Gas Con.* 2011, 5: 439-447.
- Keefer L.K., Roller P.P. N-nitrosation by nitrite ion in neutral and basic medium. *Science*, 1973, 181: 1245-1247.
- Kennard M.L. and Meisen A. Control DEA degradation. *Hydrocarbon processing, Int. Ed.*, 1980, 59, 103-106.
- Kennard M.L., Meisen A. Gas chromatographic technique for analyzing partially degraded diethanolamine solutions. *J. Chromatogr.* 1983, 267, 373-380.
- Kennard M.L. and Meisen A. Mechanisms and kinetics of diethanolamine degradation. *Ind. Eng. Chem. Fundam.*, 1985, 24, 129-140.
- Kohl A.L., Nielsen R.B. *Gas Purification*, 5th Ed., Gulf Publishing Company, Houston, TX, 1997.
- Krol J., Alden P.G., Morawski J. Ion chromatography of alkylamines and alkanolamines using conductivity detection. *J. Chrom. A*, 1992, 626: 165-170.
- Lalévée J., Allonas X., Fouassier J-P. N-H and α (C-H) bond dissociation enthalpies of aliphatic amines. *J. Am. Chem. Soc.*, 2002, 124: 9613-9621.
- Lawal O., Bello A., Idem R.O. The role of methyl diethanolamine (MDEA) in preventing the oxidative degradation of CO₂ loaded and concentrated aqueous monoethanolamine(MEA)-MDEA blends during CO₂ absorption from flue gases. *Ind. Eng. Chem. Res.*, 2005, 44:1874-1896.
- Layer R.W. The Chemistry of imines. *Chem. Rev.*, 1963, 63(5): 489-510.
- Lee D.B., Kim D.M., Cho J., et al. A comparative study on the carbon dioxide capture power between 30 wt% 2-amino-2-methyl-1-propanol and 30 wt% methyldiethanol amine aqueous solutions. *Korean J. Chem. Eng.*, 2009, 26: 818-823.
- Lepaumier H., Picq D., Carrette P.-L. New amines for CO₂ capture. II. Oxidative degradation mechanisms. *Ind. Eng. Chem. Res.*, 2009a, 48: 9068-9075.
- Lepaumier H., Picq D., Carrette P.-L. New amines for CO₂ capture. I. Mechanisms of amine degradation in the presence of CO₂. *Ind. Eng. Chem. Res.*, 2009b: 48, 9061-9067.
- Lepaumier H., da Silva E.F., Einbu A., et al. Comparison of MEA degradation in pilot-scale with lab-scale experiments. *Energy procedia*, 2011, 4: 1652-1659.

- Lijinsky W., Kovatch R.M. Carcinogenic effects in rats of nitrosopiperazines administered intravesically: possible implications for the use of piperazine. *Cancer letters*, 1993, 74:101-103.
- Ma'mun S., Jackobsen J.P., Svendsen H.F., Juliussen O. Experimental and modeling study of the solubility of carbon dioxide in aqueous 30 mass% 2-((2-aminoethyl)amino)ethanol solution. *Ind. Eng. Chem. Res.*, 2006, 45: 2505-2512.
- Mandal B.P., Biswas A.K., Bandyopadhyay S.S. Absorption of carbon dioxide into aqueous blends of 2-amino-2-methyl-1-propanol and diethanolamine. *Chem. Eng. Sci.*, 2003, 58: 4137-4144.
- Mandal B.P. and Bandyopadhyay S.S. Absorption of carbon dioxide into aqueous blends of 2-amino-2-methyl-1-propanol and monoethanolamine. *Chem. Eng. Sci.*, 2006, 61: 5440-5447.
- Messaoudi B. and Sada E. Kinetics of absorption of carbon dioxide into aqueous solutions of sterically hindered 2-amino-2-methyl-1-propanol. *J. Chem. Eng. JPN.*, 1996, 29: 193-197.
- Molnar I., Knauer H., Wilk D.J. High-performance liquid chromatography of ions. *J. Chromatogr.*, 1980, 201: 225-240.
- Mondal M.K., Balsora H.K., Varshney P. Progress and trends in CO₂ capture/separation technologies: A review. *Energy*, 2012, 46: 431-441.
- Mrklas O., Chu A., Lunn S. Determination of ethanolamine, ethylene glycol and triethylene glycol by ion chromatography for laboratory and field biodegradation studies. *J. Environ. Monit.*, 2003, 5: 336-340.
- Nguyen T., Hilliard M., Rochelle G.T. Amine volatility in CO₂ capture. *Int. J. Greenh. Gas Cont.*, 2010, 4: 707-715.
- Nielsen P.T. Piperazine degradation in pilot plants. Presented at First Conference on Carbon Capture and Storage at the University of Texas at Austin (UTCCS1), Austin, TX, January, 2012.
- Pearce R.L. Process for removal of carbon dioxide from industrial gases. US patent 4440731, 1984.
- Perkins M.J. Radical Chemistry. Ellis Horwood Limited, Hertfordshire, UK, 1994.
- Petryaev E.P., Pavlov A.V., Shadyro O.I. Homolytic deamination of amino alcohols. *Zh. Org. Khim.*, 1984, 20: 29-34.
- Pires J.C.M., Martins F.G., Alvim-Ferraz M.C.M., et al. Recent developments on carbon capture and storage: an overview. *Chem. Eng. Res. Des.*, 2011, 89: 1446-1460.

- Polderman L.D., Dillon C.P., Steele A.B. Why MEA solution breaks down in gas-treating service. *Oil & Gas Journal*, 1955, 54: 180-183.
- Poole C.F. *The Essence of Chromatography*. Elsevier, Amsterdam, Netherlands, 2003.
- Rao A.B. and Rubin E.S. A technical, economic, and environmental assessment of amine-based CO₂ capture technology for power plant greenhouse gas control. *Environ. Sci. Technol.*, 2002, 36: 4467-4475.
- Reza J. and Trejo A. Degradation of aqueous solutions of alkanolamine blends at high temperature, under the presence of CO₂ and H₂S. *Chem. Eng. Comm.*, 2006, 193: 129-138.
- Rochelle G.T., Bishnoi S., Chi S., et al. Research needs for CO₂ capture from flue gas by aqueous absorption/stripping. Final report for P.O: No. DE-AF26-99FT01029 U.S. Department of Energy. Federal Energy Technology Center, Pittsburgh, PA 15236, 2001.
- Rochelle G., Chen E., Freeman S., et al. Aqueous piperazine as the new standard for CO₂ capture technology. *Chem. Eng. J.*, 2011, 171: 725-733.
- Rooney P.C., Dupart M.S., Bacon T.R. Oxygen's role in alkanolamines degradation. *Hydrocarbon Process., Int. Ed.*, 1998, 77: 109-113.
- Rosenblatt D.H., Hull L.A., De Luca D.C., et al. Oxidations of amines. II. Substituent effects in chlorine dioxide oxidations. *J. Am. Chem. Soc.*, 1967, 89: 1158-1163.
- Saha A.K. and Bandyopadhyay S.S. Kinetics of absorption of CO₂ into aqueous solutions of 2-amino-2-methyl-1-propanol. *Chem. Eng. Sci.*, 1995, 50: 3587-3598.
- Sakwattanapong R., Aroonwilas A., Veawab A. Behavior of reboiler heat duty for CO₂ capture plants using regenerable single and blended alkanolamines. *Ind. Eng. Chem. Res.*, 2005, 44: 4465-4473.
- Sakwattanapong R., Aroonwilas A., Veawab A. Reaction rate of CO₂ in aqueous MEA-AMP solution: experiment and modelling. *Energy Procedia*, 2009, 1: 217-224.
- Samanta A. and Bandyopadhyay S. S. Absorption of carbon dioxide into aqueous solutions of piperazine activated 2-amino-2-methyl-1-propanol. *Chem. Eng. Sci.*, 2009, 64: 1185-1194.
- Sartori G., Savage D. W. Sterically hindered amines for CO₂ removal from gases. *Ind. Eng. Chem. Funda.*, 1983, 22: 239-249.
- Sawyer D.T. "Oxygen: Inorganic Chemistry" in *Encyclopedia of inorganic chemistry*. Ed. King B. R., Wiley, Chichester, 1994.
- Sexton A.J. *Amine Oxidation in CO₂ Capture Processes*. The University of Texas at Austin. Ph.D. Dissertation. 2008.

- Sexton A.J. and Rochelle G.T. Catalysts and inhibitors for oxidative degradation of monoethanolamine. *Int. J. Greenh. Gas Cont.*, 2009, 3: 704-711.
- Sexton A.J. and Rochelle G.T. Reaction products from the oxidative degradation of monoethanolamine. *Ind. Eng. Chem. Res.*, 2011, 50: 667-673.
- Sharma M.M. Kinetics of reactions of carbonyl sulphide and carbon dioxide with amines and catalysis by Brønsted bases of the hydrolysis of COS. *Trans. Faraday Soc.*, 1965, 61: 681-688.
- Sonntag V. and Schuchmann H.-P. "Peroxyl Radicals in Aqueous Solutions" in Peroxyl Radicals, Ed. Alfassi Z. B., Wiley, Chichester, 1997.
- Strazisar B.R., Anderson R., White C.M. Degradation pathways for monoethanolamine in a CO₂ capture facility. *Energy & Fuels*, 2003, 17: 1034-1039.
- Stenfan M.I., Hoy A.R., Bolton J.R. Kinetics and mechanism of degradation and mineralization of acetone in diluted aqueous solution sensitized by UV photolysis of hydrogen peroxide. *Environ. Sci. Technol.*, 1996, 30: 2382-2390.
- Stefan M.I., Bolton J.R. Reinvestigation of the acetone degradation mechanism in dilute aqueous solution by the UV/H₂O₂ process. *Environ. Sci. Technol.*, 1999, 33: 870-873.
- Stumm W. and Lee G. F. Oxygenation of Ferrous Iron. *Ind. Eng. Chem.*, 1961, 53:143-146.
- Sun W-C., Yong C-B., Li M-H. Kinetics of the absorption of carbon dioxide into mixed aqueous solutions of 2-amino-2-methyl-1-propanol and piperazine. *Chem. Eng. Sci.*, 2005, 60: 503-516.
- Supap T., Idem R., Veawab A. et al. Kinetics of the oxidative degradation of aqueous monoethanolamine in a flue gas treating unit. *Ind. Eng. Chem. Res.* 2001, 40: 3445-3450.
- Supap T., Idem R., Tontiwachwuthikul P., et al. Analysis of monoethanolamine and its oxidative degradation products during CO₂ absorption from flue gases: a comparative study of GC-MS, HPLC-RID, and CE-DAD analytical techniques and possible optimum combinations. *Ind. Eng. Chem. Res.*, 2006, 45: 2437-2451.
- Supap T., Idem R., Tontiwachwuthikul P., et al. Kinetics of sulfur dioxide- and oxygen-induced degradation of aqueous monoethanolamine solution during CO₂ absorption from power plant gas streams. *Int. J. Greenh. Gas Con.*, 2009, 3: 133-142.
- Takahashi S., Togo H. An Efficient Oxidative Conversion of Aldehydes into 2-Substituted 2-Oxazolines Using 1,3-Diiodo-5,5-dimethylhydantoin. *Synthesis*. 2009, 14: 2329-2332.
- Tanaka K., Ohta K., Fritz J.S. Ion-exclusion chromatography of ethanolamines on an anion-exchange resin by elution with polyols and sugars. *J. Chrom. A*, 1996, 739: 317-325.

- Tontiwachwuthikul P., Meisen A., Lim C. J. Solubility of carbon dioxide in 2-amino-2-methyl-1-propanol solutions. *J. Chem. Eng. Data*, 1991, 36: 130-133.
- Veawab A., Tontiwachwuthikul P., Chakma A. Corrosion behaviour in sterically-hindered amine for CO₂ separation. Proceedings of the 4th International Conference on Greenhouse Gas Control Technologies, 77-84, Interlaken, Switzerland, 1998.
- Voice A. Nitrosamine formation and mitigation in CO₂ capture. Presented at First Conference on Carbon Capture and Storage at the University of Texas at Austin (UTCCS1), Austin, TX, January, 2012.
- Wang M., Lawal A., Stephenson P., Sidders J., Ramshawa C. Post-combustion CO₂ capture with chemical absorption: A state-of-the-art review. *Chem. Eng. Res. Des.*, 2011, 89: 1609-1624.
- Weiss J. Handbook of Ion Chromatography. Wiley-VCH, Weinheim, Germany, 3rd Ed, 2004.
- Wolcott R.A., Pearce R.L., Pauley C.R. Process for the recovery of CO₂ from flue gases. US patent 4624839, 1986.
- Xiao J., Li C-W., Li M-H. Kinetics of absorption of carbon dioxide into aqueous solutions of 2-amino-2-methyl-1-propanol + monoethanolamine. *Chem. Eng. Sci.*, 2000, 55: 161-175.
- Xu S., Wang Y-W., Otto F. D., Mather A. E. Kinetics of the reaction of carbon dioxide with 2-amino-2-methyl-1-propanol solutions. *Chem. Eng. Sci.*, 1996, 51: 841-850.
- Yang H. Q., Xu Z. H., Fan M. H., et al. Progress in carbon dioxide separation and capture: A review. *J. Environ. Sci.*, 2008, 20:14-27.
- Ye Q., Zhang S. Methyl-diethanolamine degradation products in desulphurization process for acid waste gas. *Gaoxiao Huaxue Gongcheng Xuebao*, 2001, 15: 35-39.
- Yeh J.T., Pennline H.W., Resnik K. P. Study of CO₂ absorption and desorption in a packed column. *Energy & Fuels*, 2001, 15: 274-278.
- Yih S. M., Shen K. P. Kinetics of carbon dioxide reaction with sterically hindered 2-amino-2-methyl-1-propanol aqueous solutions. *Ind. Eng. Chem. Res.*, 1988, 27: 2237-2241.
- Zhang P., Shi Y., Wei J-W., et al. Regeneration of 2-amino-2-methyl-1-propanol used for carbon dioxide absorption. *J. Environ. Sci.*, 2008, 20: 39-44.

Appendix A Publications and Presentations

Journal articles

Paper I: Wang T. and Jens K.-J., 2012. Oxidative Degradation of Aqueous 2-Amino-2-methyl-1-propanol Solvent for Postcombustion CO₂ Capture. *Ind. Eng. Chem. Res.*, 51: 6529–6536.

Paper II: Wang T. and Jens K.-J., 2012. A study of Oxidative Degradation of AMP for Post-combustion CO₂ Capture. *Energy Procedia*, 23: 102-110.

Paper III: Wang T., López M., Hagen S.-T. Jens K.-J., 2012. Determination of Degraded Ethanolamines for Post-combustion CO₂ Capture Technology by Non-suppressed Ion Chromatography. *Fresen. Environ. Bull.*, 23: 2298-2303.

Paper IV: Wang T. and Jens K.-J., 2013. Oxidative Degradation of AMP/MEA Blends for Post-combustion CO₂ Capture. *Energy Procedia* (accepted by GHGT11).

Paper V: Wang T. and Jens K.-J. Comparison of Thermally and UV Radiation Accelerated Oxidation of Aqueous AMP Solvent (in preparation).

Paper VI: Wang T. and Jens K.-J. Oxidative Degradation of PZ and AMP/PZ Blends for CO₂ Capture (in preparation).

Conference presentations

Wang T. and Jens K.-J., 2011. Oxidative Degradation of 2-Amino-2-Methyl-1-Propanol, the 1st Post Combustion Capture Conference (PCCC1), Oral presentation, Abu Dhabi, United Arab Emirates, May 17-19.

Wang T., Chen C., Jens K.-J., 2011. A Study of Oxidative Degradation of AMP for Post-combustion CO₂ Capture, the 6th Trondheim Conference on CO₂ Capture, Transport and Storage (TCCS-6), Oral presentation, Trondheim, Norway, June 14-16.

Wang T., López M., Hagen S.-T. Jens K.-J., 2012. Determination of Degraded Ethanolamines for Post-combustion CO₂ Capture Technology by Non-suppressed Ion Chromatography, the 20th Norske Symposium i Kromatografi, Poster presentation, Sandefjord, Norway, January 8-10.

Wang T. and Jens K.-J., 2012. Degradation of AMP/MEA Blends, The First University of Texas Conference on Carbon Capture and Storage (UTCCS1), Oral presentation, Austin, the United States, January 25-27.

Wang T. and Jens K.-J., 2012. Oxidative Degradation of AMP/MEA Blends for Post-combustion CO₂ Capture, the 11th Greenhouse Gas Control Technology Conference (GHGT11), Poster presentation, Kyoto, Japan, November 19-22.

Appendix B List of Chemicals

All chemicals used for experimentation or analytical techniques were laboratory grade or purer. All chemical were used as received. Details of the materials used in this work are included in Table A1.

Table B1: Details of All Chemicals Used

*synonym

Reagent	Abbreviation	CAS#	Purity (%)	M.W. (g/mol)	Supplier
2-Amino-2-methyl-1-propanol	AMP	124-68-5	99	89.14	Acros Organics
Monoethanolamine *Ethanolamine *2-aminoethanol	MEA	141-43-5	99.5	61.08	Merck
Diethanolamine	DEA	111-42-2	98	105.14	Sigma-Aldrich
N-methyldiethanolamine	MDEA	105-59-9	99		Aldrich
Piperazine	PZ	110-85-0	99	86.14	Acros Organics
Ethylenediamine	EDA	107-15-3	99.8	60.1	Sigma-Aldrich
2-Amino-1-butanol	ABN	96-20-8	97	89.14	Aldrich
2-Amino-1-propanol *DL-alanine	APN	6168-72-5	98	75.11	Aldrich
Ammonia solution in water			25		Merck
Acetone		67-64-1	99.8	58.08	Aldrich
Acetone oxime		127-06-0	98	73.09	Fluka

Table B1: Details of All Chemicals Used (continued)

Reagent	Abbreviation	CAS#	Purity (%)	M.W. (g/mol)	Supplier
2,4-Lutidine		108-47-4	99	107.15	Aldrich
2-Oxazolidinone	OZD	497-25-6	98	87.08	Aldrich
Ammonium chloride		12125-02-9	99.8	53.49	Merck
Potassium formate		590-29-4	99	84.12	Aldrich
Potassium acetate		127-08-2	99	98.15	Sigma
Sodium glycolate		2836-32-0	97	98.03	Acros Organics
Potassium oxalate monohydrate		6487-48-5	99	184.23	Aldrich
Potassium nitrate		7757-79-1	99	101.1	Aldrich
Sodium nitrite		7632-00-0	99.999	69	Aldrich
Methylamine hydrochloride		593-51-1	99	67.52	Aldrich
Dimethylamine hydrochloride		506-59-2	99	81.54	Aldrich
Methanesulfonic acid	MSA	75-75-2	99	96.11	Merck
Acetonitrile	ACN	75-05-8	99.8	41.05	Sigma-Aldrich
Iron (II) oxalate dihydrate		6047-25-2	99	179.89	Aldrich
Chromium (III) sulfate hydrate		15244-38-9	99.999	392.18	Aldrich
Nickel (II) sulfate heptahydrate		10101-98-1	99	280.86	Aldrich

Table B1: Details of All Chemicals Used (continued)

Reagent	Abbreviation	CAS#	Purity (%)	M.W. (g/mol)	Supplier
Copper (II) sulfate pentahydrate		7758-99-8	99.995	249.68	Aldrich
Potassium persulfate		7727-21-1	99	270.32	Aldrich
Potassium hydroxide		1310-58-3	99	56.11	Aldrich
Sodium hydroxide		1310-73-2	99	40.0	Aldrich
Barium chloride dihydrate		1326-27-9	99	244.28	Merck
Hydro chloride acid (Titrisol)			1 mol/L		Merck
Hydro chloride acid		7647-01-0	37	36.46	Sigma-Aldrich
Sulfuric acid		7664-93-9	95-97	98.08	Merck
Hydrogen peroxide solution (in water)		7722-84-1	30	34.01	Fluka
Formaldehyde solution (in water)		50-00-0	37	30.03	Sigma-Aldrich
Formic acid		64-18-6	98	46.03	VWR
Propionic acid		79-09-4	99.5	74.08	Aldrich
Formamide		75-12-7	99.5	45.04	Aldrich
Acetamide		60-35-5	99	59.07	Fluka
1-Nitrosopiperazine	MNPZ			115.13	Sigma
1-Methylpiperzaine	MPZ	109-01-3	99	100.16	Aldrich

Table B1: Details of All Chemicals Used (continued)

Reagent	Abbreviation	CAS#	Purity (%)	M.W. (g/mol)	Supplier
Rose bengal		632-69-9	95	1017.64	Aldrich
N1-(1,1-dimethyl-2-hydroxyethyl)-2-methyl-1,2-propanediamine		72622-74-3		160.26	Aldrich
*2-[(2-Amino-2-methylpropyl)amino]-2-methyl-1-propanol					
N-Formylpiperazine	FPZ	7755-92-2	90	114.15	Aldrich
2-Aminoisobutyric acid		6257-7	98	103.12	Aldrich
4,4-Dimethyl-1,3-oxazolidine		51200-87-4		101.15	Aldrich
Hexamethylenetetramine		100-97-0	99	140.19	Sigma-Aldrich
*Methenamine					
N-(2-hydroxyethyl)-ethylenediamine		111-41-1	99	104.15	Aldrich
2-Piperizone		5625-67-2	97	100.12	Aldrich
Pyruvic acid		127-17-3	98	88.06	Aldrich
Isobutyric acid		79-31-2	99.5	88.11	Fluka
Glyoxylic acid monohydrate		563-96-2	98	92.05	Aldrich
Methacrylic acid		79-41-4	99	86.06	Aldrich
Carbon dioxide		124-38-9		44.01	AGA
Oxygen			99.999	32	AGA
Nitrogen			99.999	28	AGA

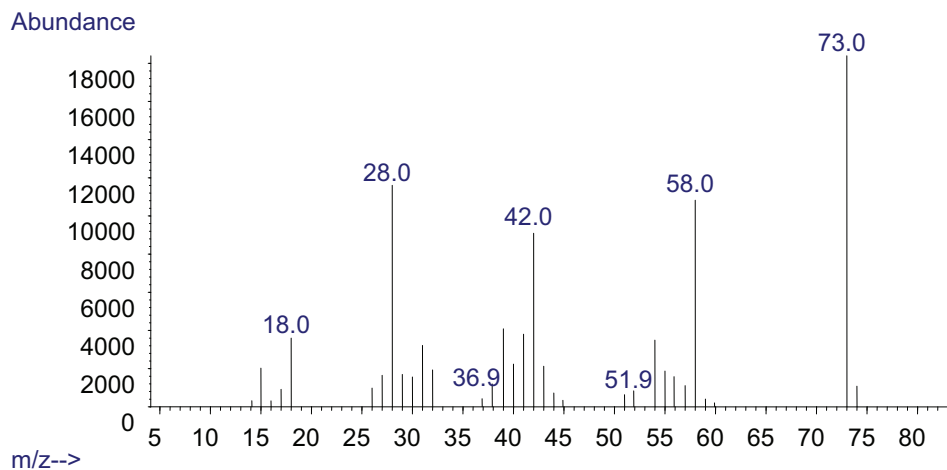
Table B1: Details of All Chemicals Used (continued)

Reagent	Abbreviation	CAS#	Purity (%)	M.W. (g/mol)	Supplier
Glycine		56-40-6	99	75.07	Sigma-Aldrich
Oxalic acid dihydrate		6153-56-6	99	126.07	Sigma-Aldrich
N-(2-hydroxyethyl)formamide	HEF	693-06-1	95	89.1	Aldrich
N-(2-hydroxyethyl)acetamide	HEA	142-26-7	Tech.	103.12	Aldrich
N-(2-hydroxyethyl)imidazole	HEI	1615-14-1	97	112.13	Aldrich
N-(2-hydroxyethyl)ethylenediamine	HEEDA	111-41-1	99	104.15	Aldrich
2-[(2-Amino-2-methylpropyl) amino] ethanol	AMPAE	68750-16-3		132.21	Aldrich
[(2-Aminoethyl)amino]acetic acid	AEAAC			118.14	Aldrich

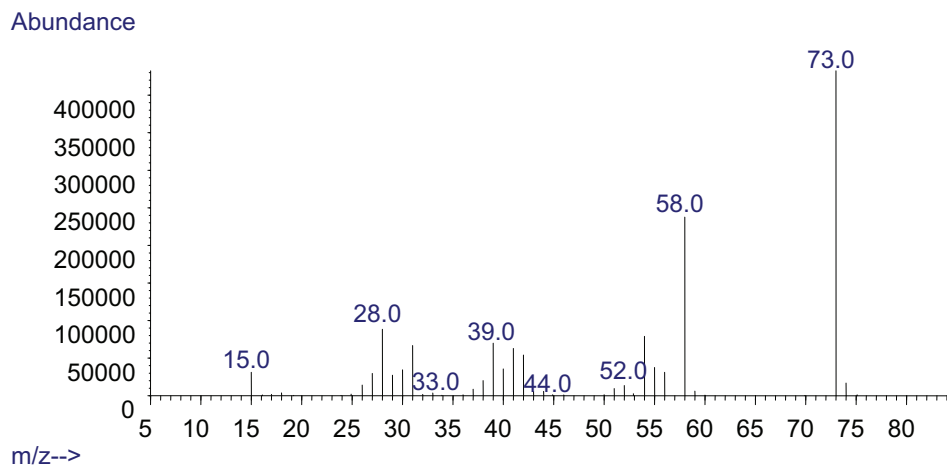
Appendix C Mass Spectra of Identified Products

This appendix will show mass spectra (Electron Ionization) for the identified products in oxidatively degraded AMP solutions, AMP/PZ blends and AMP/MEA blends, and mass spectra of the authentic standards. For each group of mass spectra, the former one is mass spectrum of the identified product in degraded amine samples, and the later one is the mass spectrum of the corresponding authentic standard chemical.

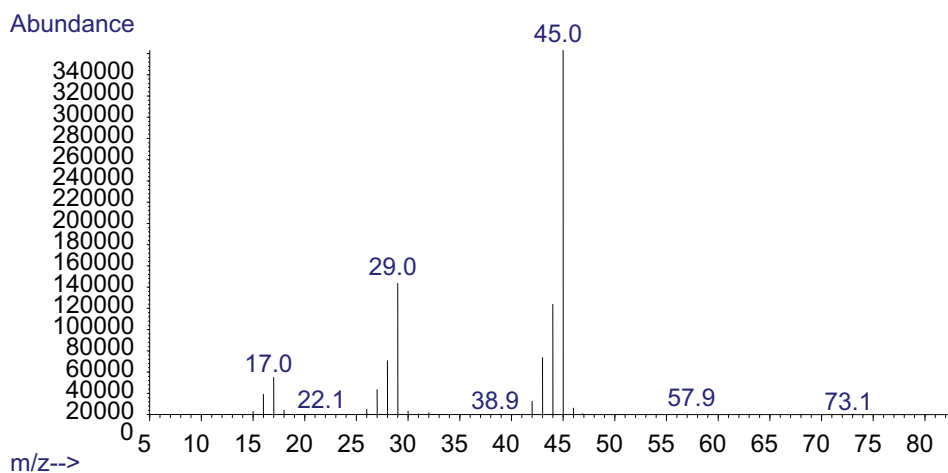
C1. Acetone oxime



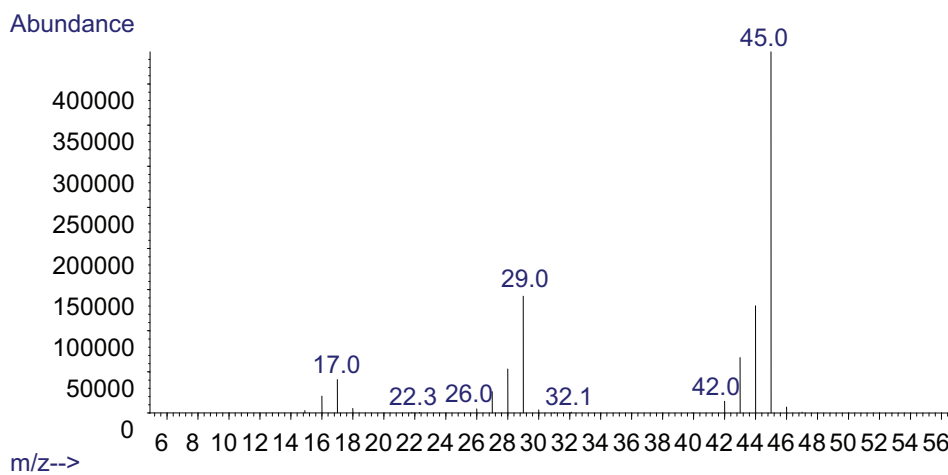
Mass spectrum of acetone oxime in a 5mol/kg AMP sample held at 80°C for 10 weeks.



Mass spectrum of an acetone oxime standard sample.

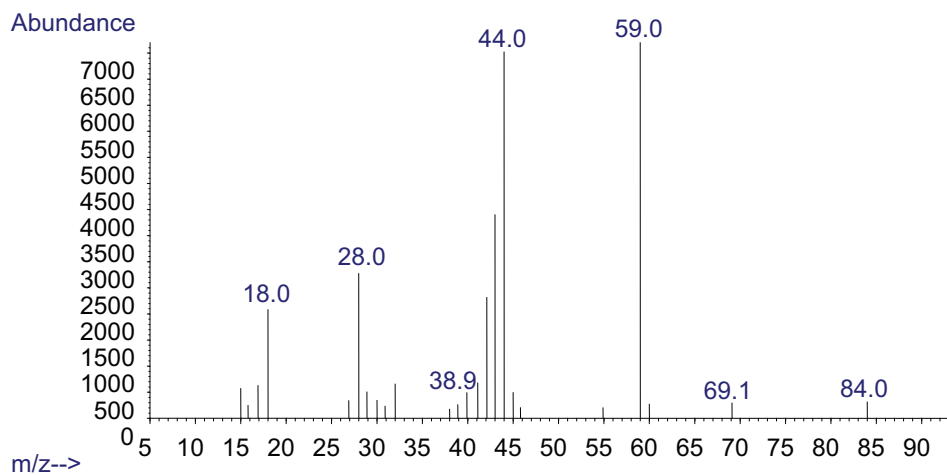
C2. Formamide

Mass spectrum of formamide in a 1mol/kg AMP sample held at 55°C for 30 hours in the presence of UV radiation.

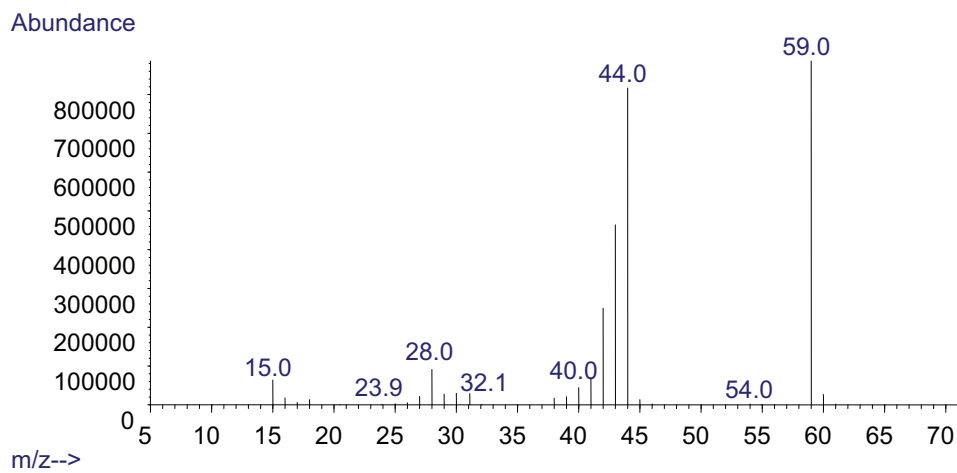


Mass spectrum of a formamide standard sample.

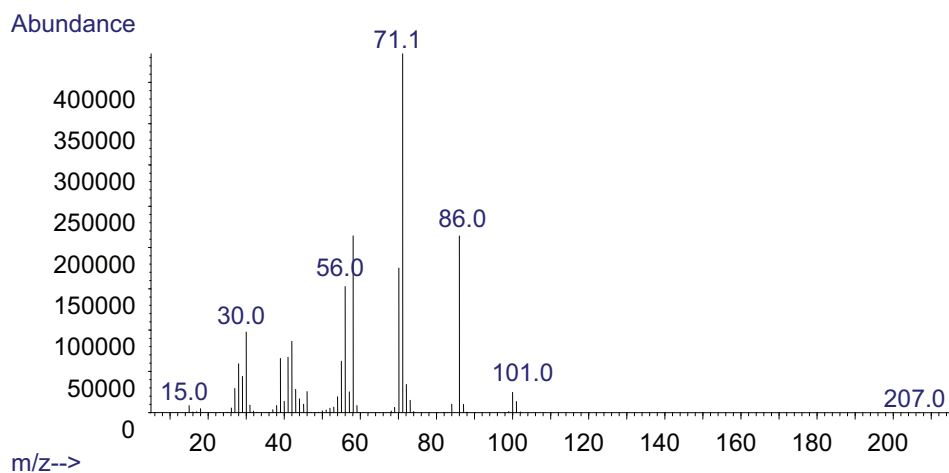
C3.Acetamide



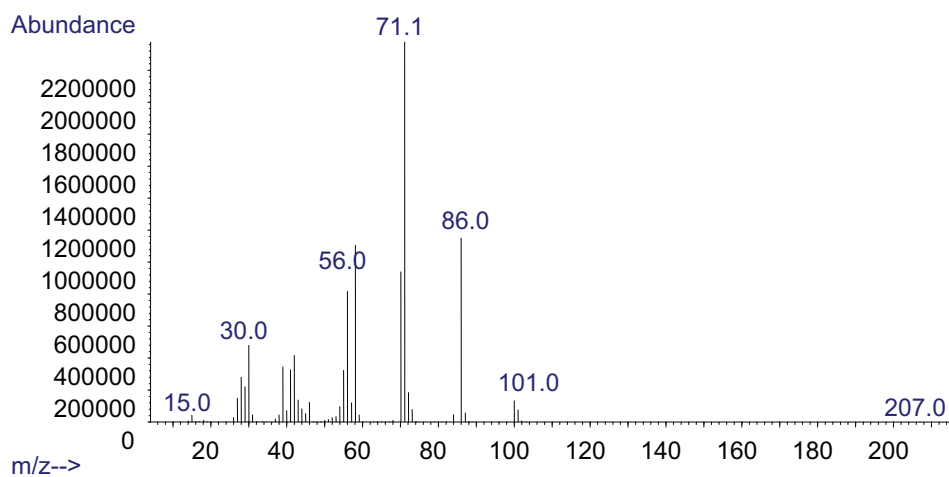
Mass spectrum of acetamide in a 1mol/kg AMP sample held at 55°C for 30 hours in the presence of UV radiation.



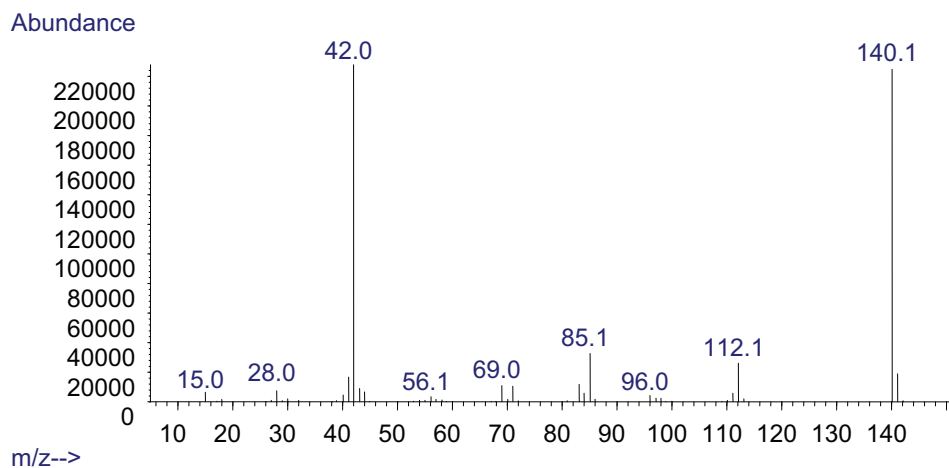
Mass spectrum of an acetamide standard sample.

C4. 4, 4-Dimethyl-1, 3-oxazolidine

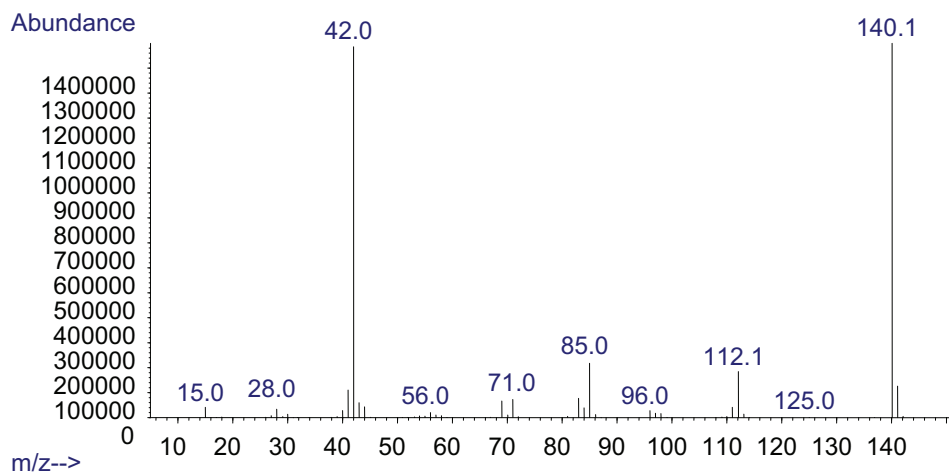
Mass spectrum of 4, 4-Dimethyl-1, 3-oxazolidine in a 1mol/kg AMP sample held at 55°C for 30 hours in the presence of UV radiation.



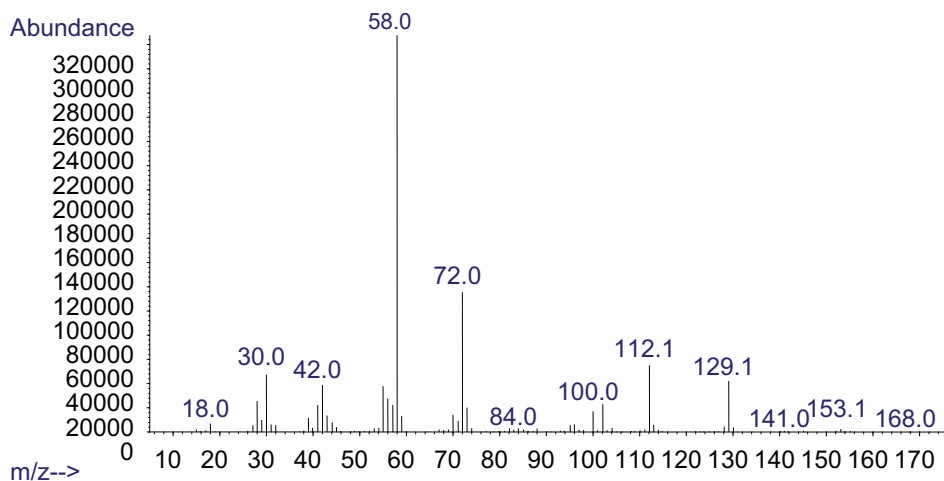
Mass spectrum of a 4, 4-Dimethyl-1, 3-oxazolidine standard sample.

C5. Methenamine

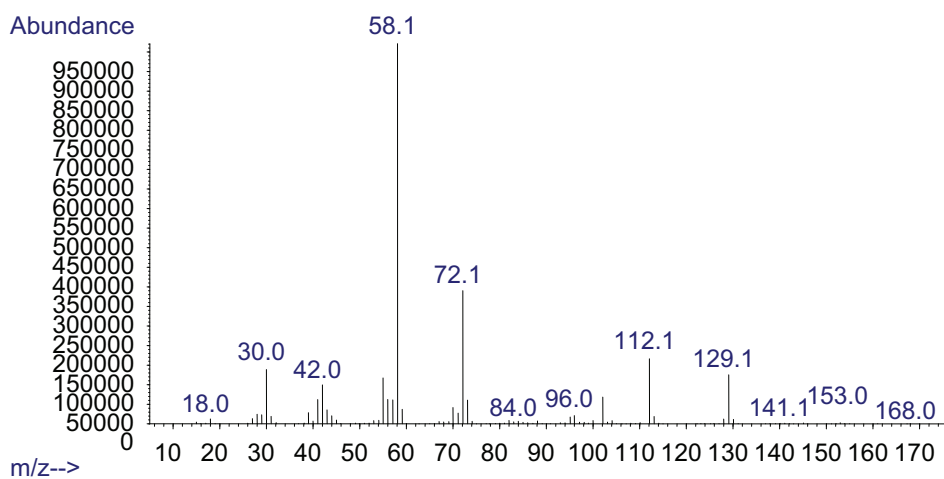
Mass spectrum of methenamine in a 1mol/kg AMP sample held at 55°C for 30 hours in the presence of UV radiation.



Mass spectrum of a methenamine standard sample.

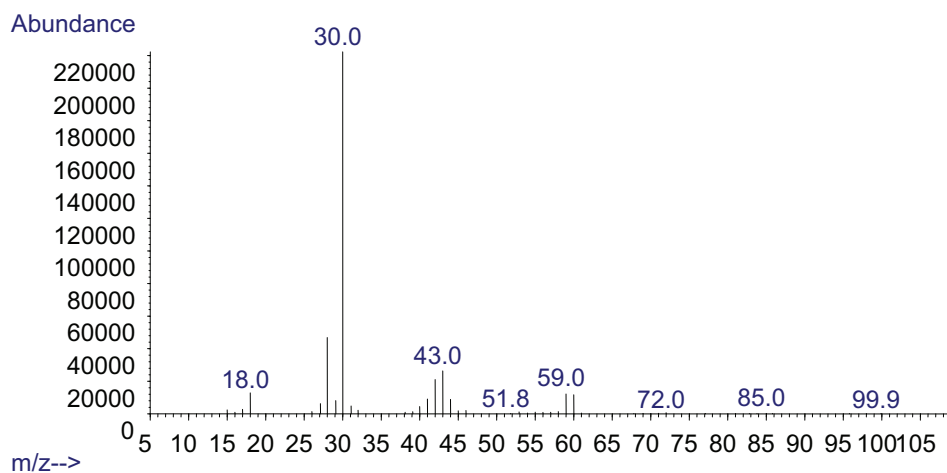
C6. N1-(1,1-dimethyl-2-hydroxyethyl)-2-methyl-1,2-propanediamine

Mass spectrum of N1-(1,1-dimethyl-2-hydroxyethyl)-2-methyl-1,2-propanediamine in a 4.75 mol/kg AMP sample with a loading of 0.3 mol CO₂/mol AMP held at 135°C for 5 weeks.

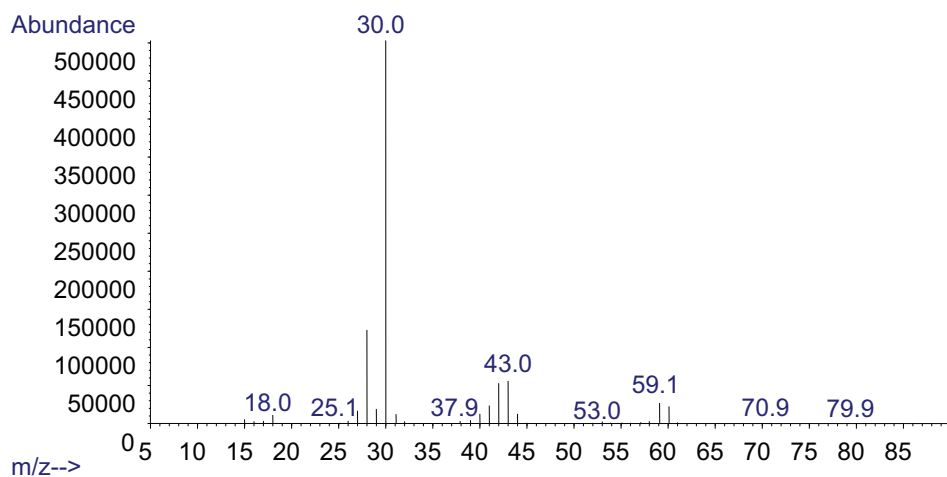


Mass spectrum of a N1-(1,1-dimethyl-2-hydroxyethyl)-2-methyl-1,2-propanediamine standard sample.

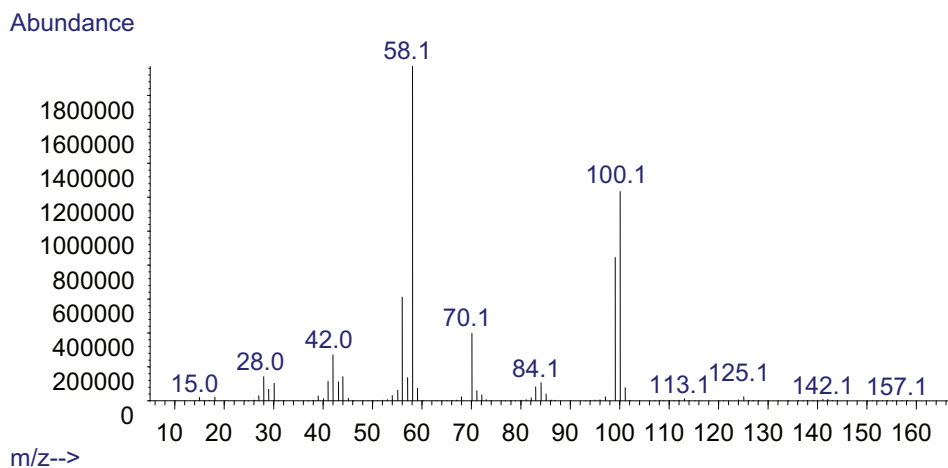
C7. Ethylenediamine



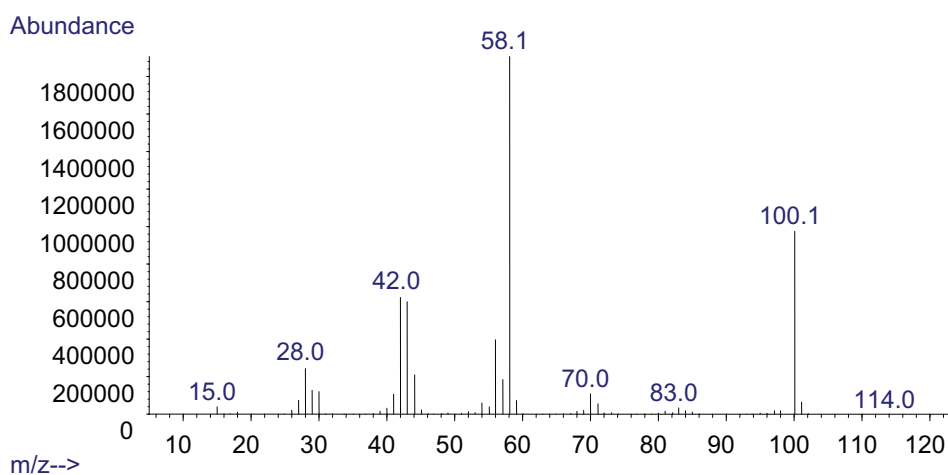
Mass spectrum of ethylenediamine in a 1.5 mol/kg PZ sample at 100°C for 19 days.



Mass spectrum of an ethylenediamine standard sample.

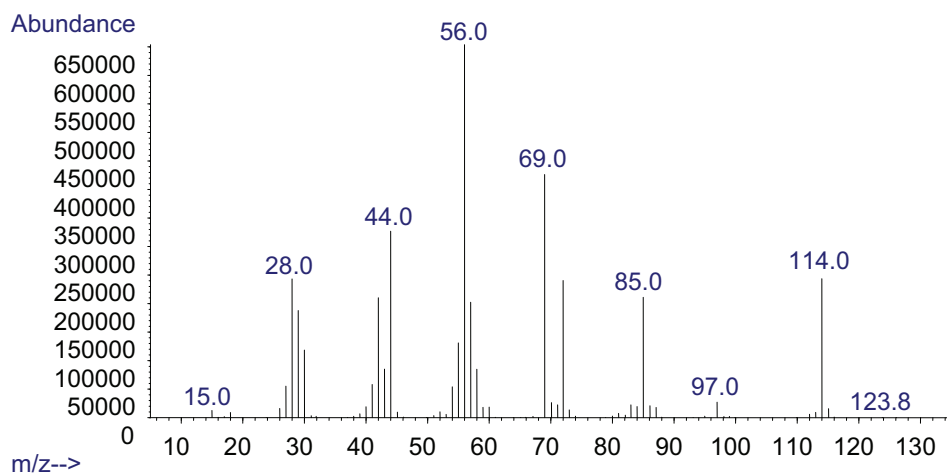
C8. 1-Methylpiperazine

Mass spectrum of 1-methylpiperazine in a (3.5 mol/kg AMP+1.5mol/kg PZ) sample with a loading of 0.3 mol CO₂/mol AMP held at 135°C for 5 weeks.

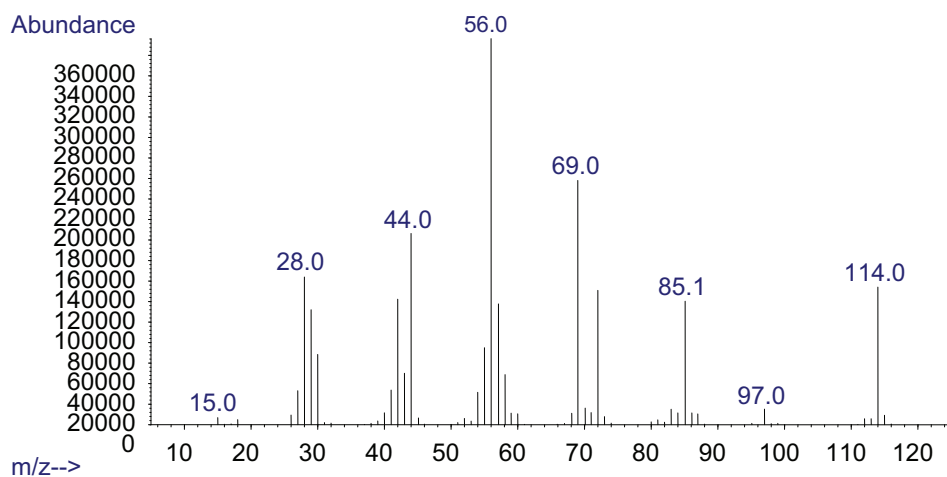


Mass spectrum of a 1-methylpiperazine standard sample.

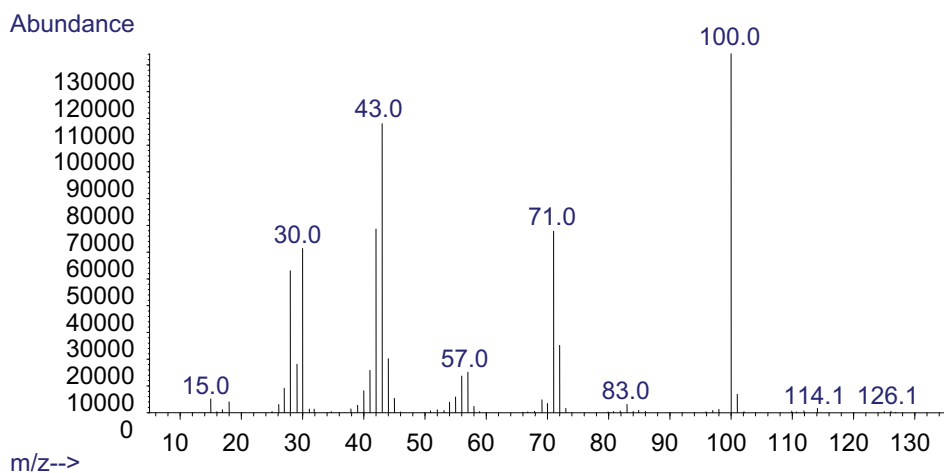
C9. 1-Formylpiperazine



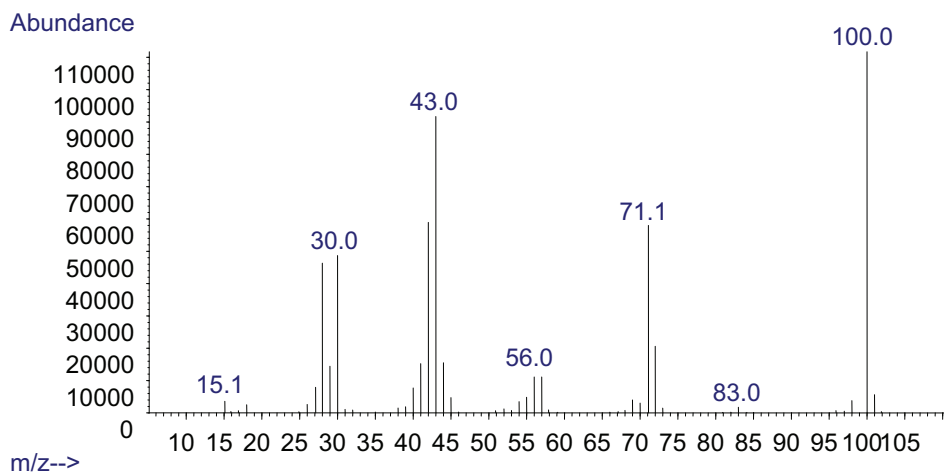
Mass spectrum of 1-formylpiperazine in a 1.5 mol/kg PZ sample held at 100°C for 19 days.



Mass spectrum of a 1-formylpiperazine sample.

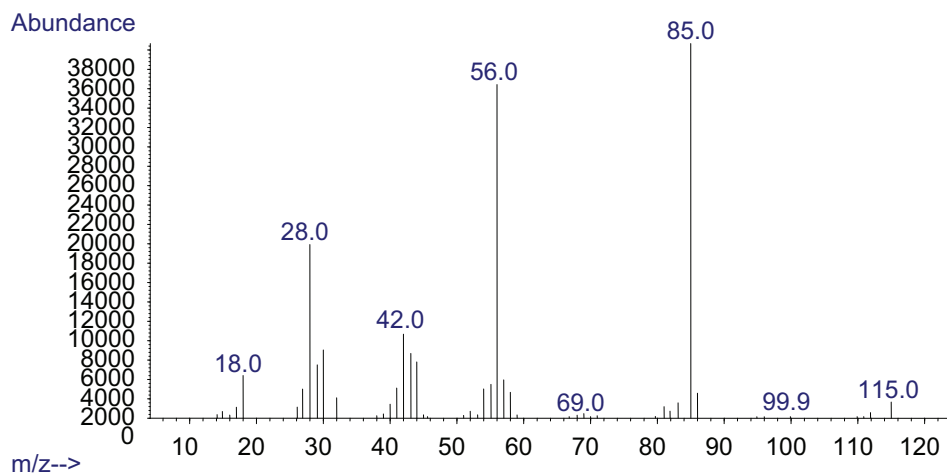
C10. 2-Oxopiperazine

Mass spectrum of 2-oxopiperazine in a 1.5 mol/kg PZ sample held at 100°C for 19 days.

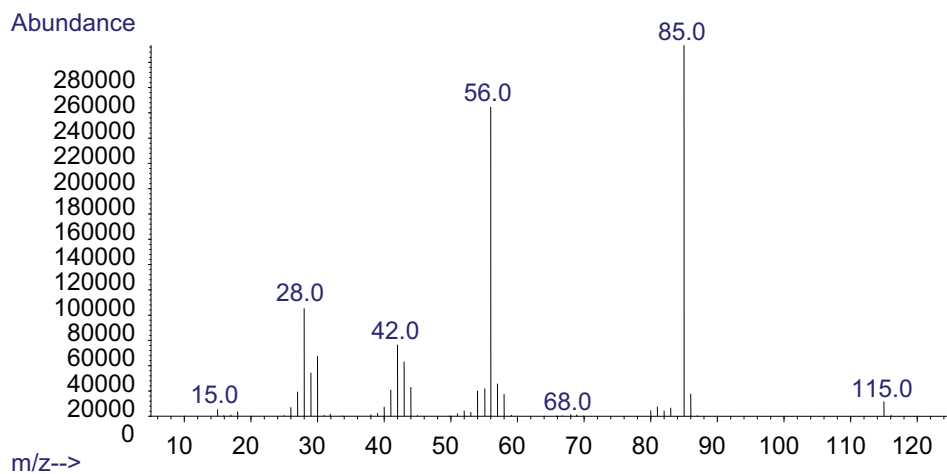


Mass spectrum of a 2-oxopiperazine standard sample.

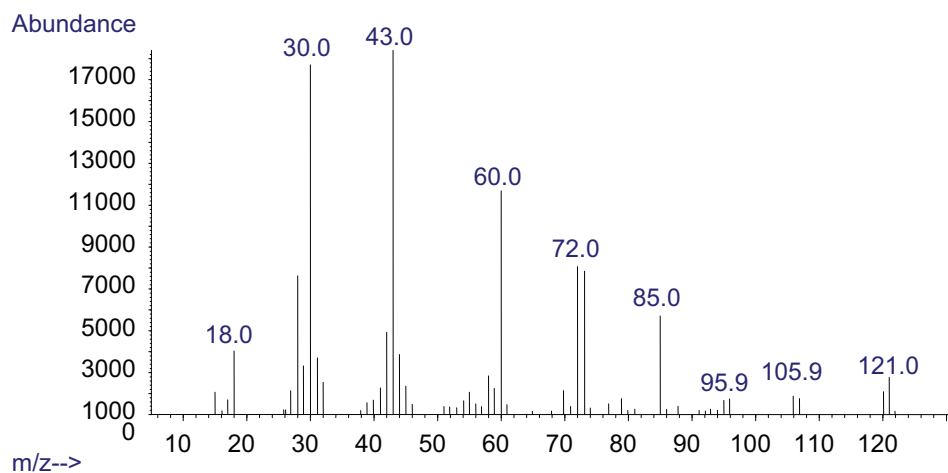
C11. 1-Nitrosopiperazine



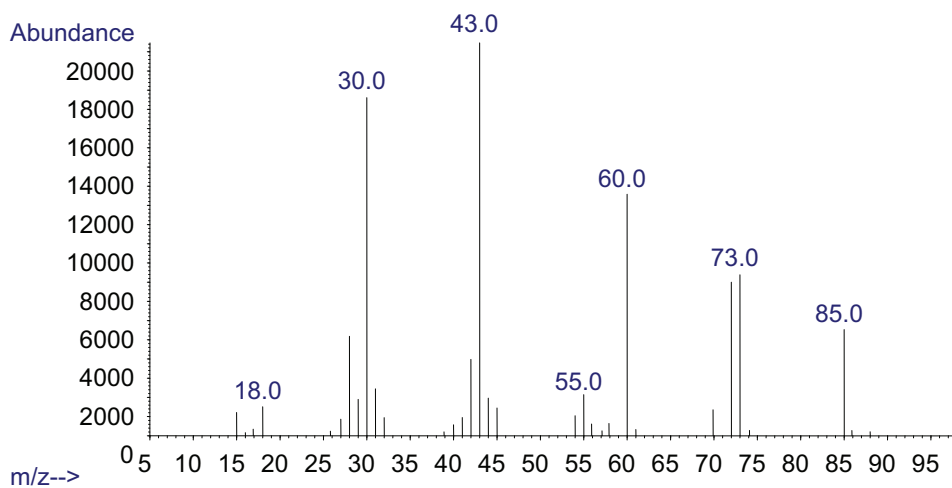
Mass spectrum of 1-nitrosopiperazine in a 1.5mol/kg PZ sample held at 100°C for 19 days.



Mass spectrum of a 2-oxopiperazine standard sample.

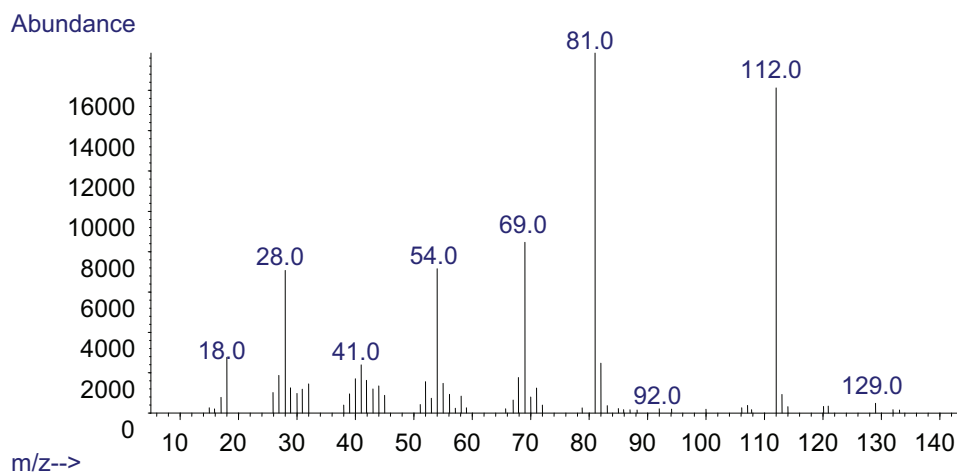
C12. N-(2-hydroxyethyl)acetamide

Mass spectrum of N-(2-hydroxyethyl)acetamide in a (3mol/kg AMP +2mol/kg MEA) sample held at 120°C for 1 week.

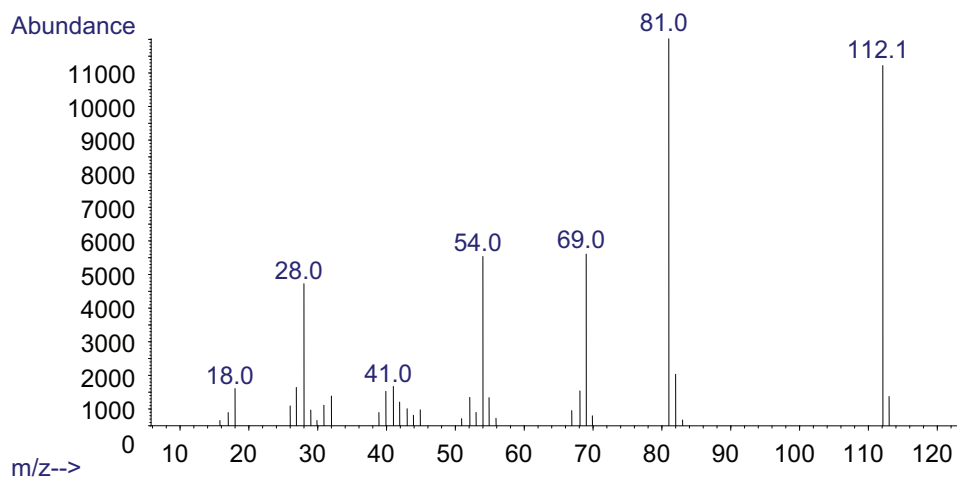


Mass spectrum of a N-(2-hydroxyethyl)acetamide standard sample.

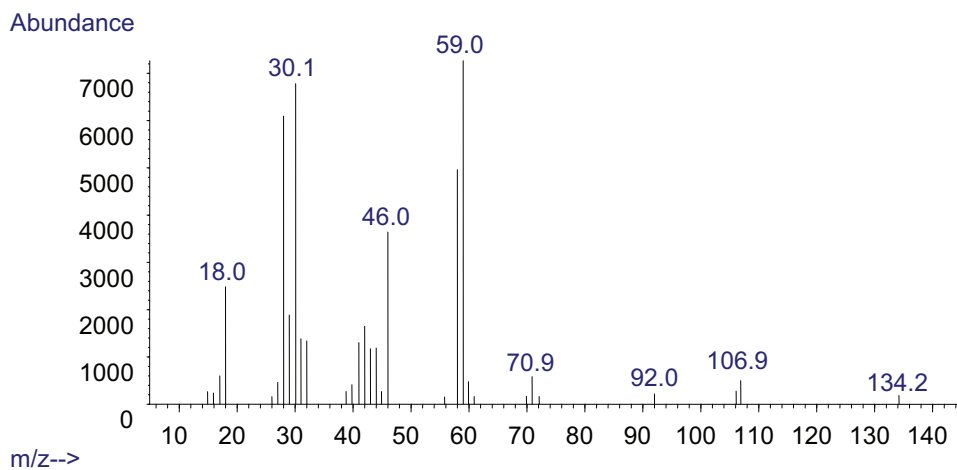
C13. N-(2-hydroxyethyl)imidazole



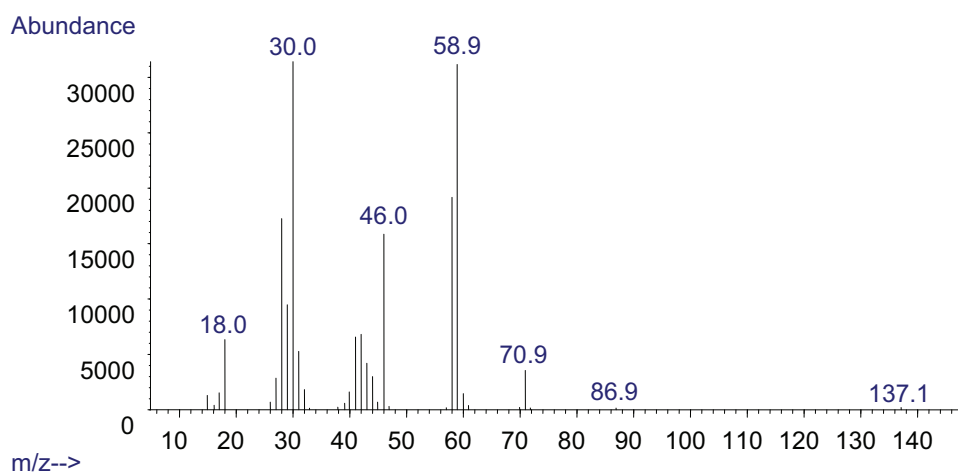
Mass spectrum of N-(2-hydroxyethyl)imidazole in a (3mol/kg AMP +2mol/kg MEA) sample held at 120°C for 1 week



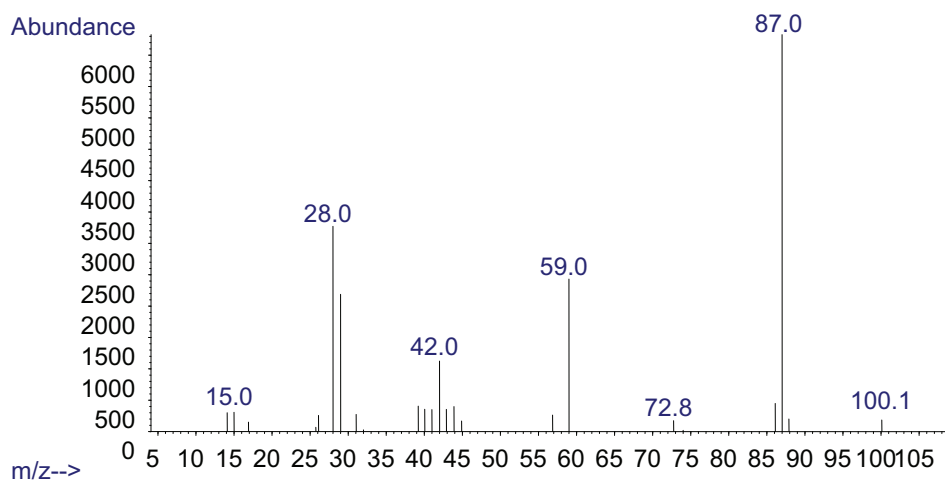
Mass spectrum of a N-(2-hydroxyethyl)imidazole standard sample.

C14. N-(2-hydroxyethyl)formamide

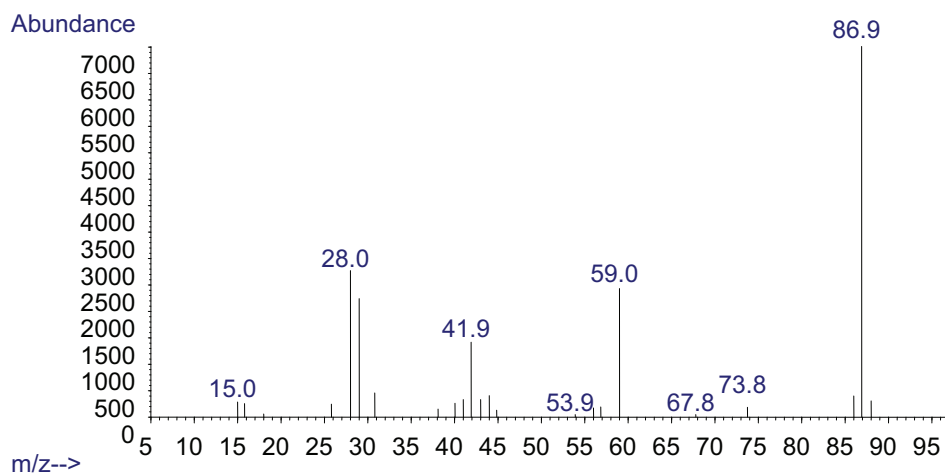
Mass spectrum of N-(2-hydroxyethyl)formamide in a (3mol/kg AMP +2mol/kg MEA) sample held at 120°C for 1 week.



Mass spectrum of a N-(2-hydroxyethyl)formamide standard sample.

C15. 2-Oxazolidinone

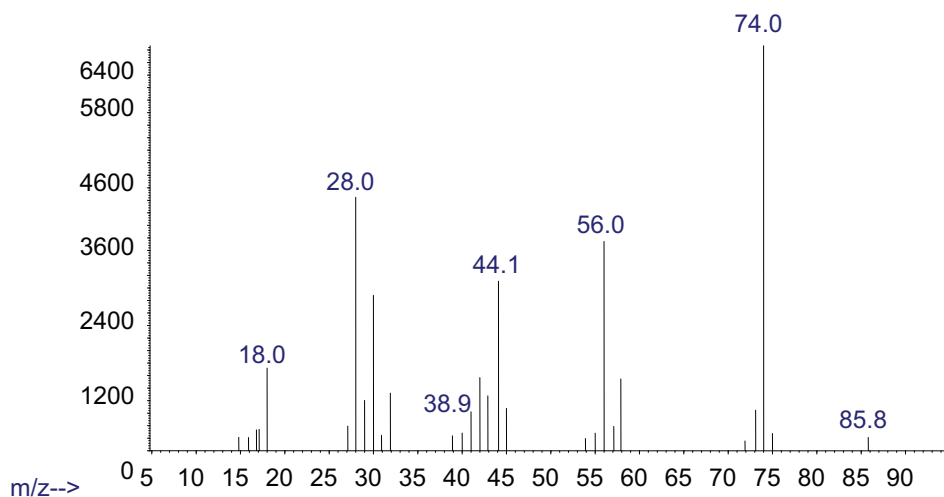
Mass spectrum of 2-oxazolidinone in a (3mol/kg AMP +2mol/kg MEA) sample with a CO₂ loading of 0.3 mol CO₂/mol total amine held at 135°C for 5 weeks.



Mass spectrum of a 2-oxazolidinone standard sample.

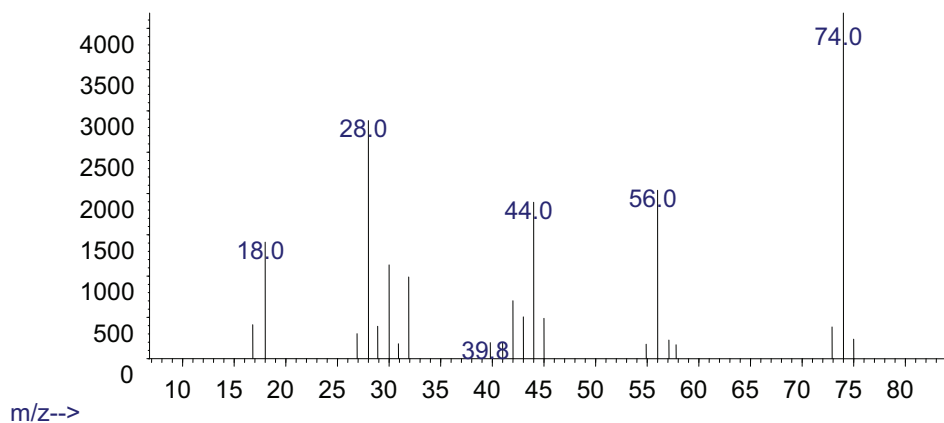
C16. N-(2-hydroxyethyl)ethylenediamine

Abundance

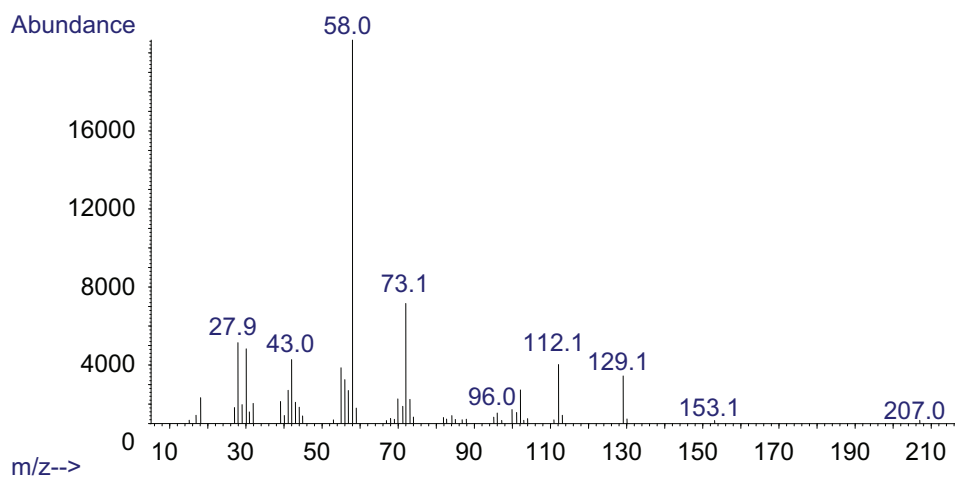


Mass spectrum of N-(2-hydroxyethyl)ethylenediamine in a (3mol/kg AMP +2mol/kg MEA) sample with a CO₂ loading of 0.3 mol CO₂/mol total amine held at 135°C for 5 weeks

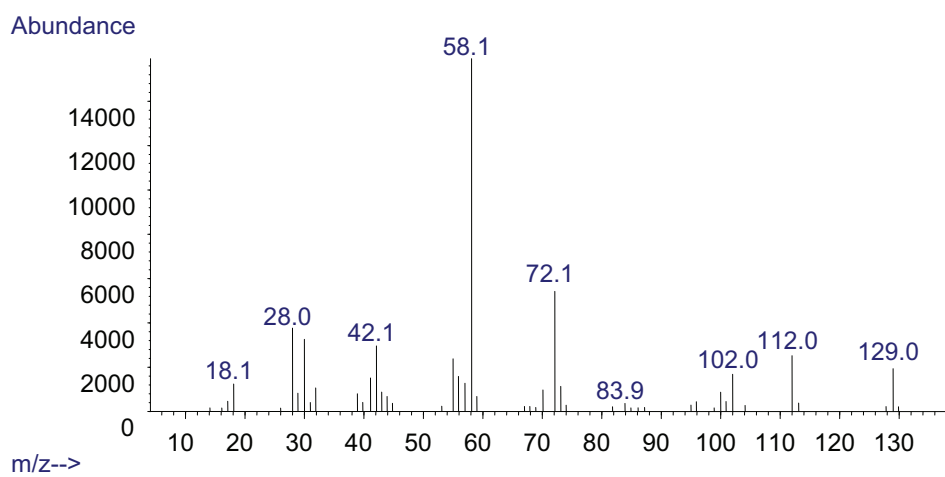
Abundance



Mass spectrum of a N-(2-hydroxyethyl)ethylenediamine standard sample.

C17. 2-[(2-Amino-2-methylpropyl) amino] ethanol

Mass spectrum of 2-[(2-Amino-2-methylpropyl) amino] ethanol in a (3mol/kg AMP +2mol/kg MEA) sample with a CO₂ loading of 0.3 mol CO₂/mol total amine held at 135°C for 5 weeks.



Mass spectrum of a 2-[(2-Amino-2-methylpropyl) amino] ethanol standard sample.

Appendix D Details of IC Methods

This appendix will document settings and programming for IC analytical methods covered in Chapter 3.

D1. Cation IC

Two different methods were used for cation IC analysis. The first method was used to quantify the concentration of ammonium, AMP, MEA, and other amines in experimental samples and was titled as 'DX_500 new pump.pgm'. The 20 minute method used 4 mM MSA as eluent and a 3 minute equilibration time at the start of the program. The second method was developed to separate ammonium, MEA, DEA and MDEA simultaneously. The program used, 'DX_500 new pump.pgm', was as follows:

DX_500 new pump.pgm

Pump_2.Pressure.LowerLimit =	10 [psi]
Pump_2.Pressure.UpperLimit =	3300 [psi]
Maximum Flow Ramp =	6.00 [ml/min ²]
Pump_2.%A. Equate =	"MSA 4mM"
Pump.Pressure.Lower Limit =	0 [psi]
Pump.Pressure.Upper Limit =	5000 [psi]
Pump.%A. Equate =	"%A"
%B.Equate =	"%B"
%C.Equate =	"%C"
%D.Equate =	"%D"
Pump_2_Pressure.Step =	Auto
Pump_2_Pressure.Average =	On
Data_Collection_Rate =	5.0 [Hz]
Temperature_Compensation =	1.7 [%/°C]
DS3_Temperature =	35 [°C]
SRS_Current =	Off
Pump.Flow =	0.00 [ml/min]
%B =	0.0 [%]
%C =	0.0 [%]
%D =	0.0 [%]
Pump.Curve =	5
Pump_2.Flow =	1.000 [ml/min]

```
Pump_2.Curve = 5
;----- inj-routine start -----
; sampler settings...
airgap=20
innerwash volume=900
outerwash volume=900
Work volume=800 ; volume= (loop x overfill[>5])+transporttubing
Wash speed=15;1ml syringe
-3.050 Wait sampler. ready
-3.000 Zone = samples
Tube = sample.Vialpos
-2.980 syringe speed=1
Suck air ;airgap
-2.750 z. nominal=33 ; depth in sample vial
-2.700 syringe speed=2 ;speed when asp sample
suck
-2.120 Pump_Inject Valve. State =Load Position ; injvalve to load - ready for load sample
-2.110 z=0
-2.100 zone=injport ; go to injport
tube=1
-2.050 z. nominal=56
-1.900 syringespeed=0.5 ;speed disp in injport
dispense
-0.500 Autozero
;-----inj-routine end-----
0.000 Autozero
Inject Position
Pump_2_Pressure.AcqOn
ECD_1.AcqOn
Pump_TTL_1.5v ;Trigger autosampler
0.500 Home Dilutor
1.000 wash
Innerwash volume=900
Outerwash volume=900
2.000 Home Dilutor
2.500 Home probe
20.000 Pump_2_Pressure.AcqOff
ECD_1.AcqOff
End
```

D2. Anion IC

The anion IC was used to quantify the concentration of expected anions in experimental samples, including formate, acetate, glycolate, oxalate, nitrite, nitrate, propionate, etc. The 30 minute method used a gradient ranging from 10 to 60 mM KOH and an 8 minute equilibration time at the start of the program. The program used, 'Anion Grad 60mM.pgm', was as follows:

Anion Grad 60mM.pgm

```

Pressure.LowerLimit =                200 [psi]
Pressure.UpperLimit =                3000 [psi]
%A.Equate =                          "%A"
%B.Equate =                          "%B"
%C.Equate =                          "%C"
%D.Equate =                          "%D"
Pump_InjectValve.State                LoadPosition
Data_Collection_Rate =               5.0 [Hz]
Temperature_Compensation =           1.7 [%/°C]
SRS_Current =                        300 [mA]

Flow =                                1.0 [ml/min]
%B =                                  0.0 [%]
%C =                                  0.0 [%]
%D =                                  0.0 [%]
Pump.Curve =                          5
Oven_Temperature =                   30 [°C]

;----- inj-routine start -----
; sampler settings...
airgap=20
innerwashvolume=900
outerwashvolume=900
Workvolume=800 ; volume=(loop x overflow[>5])+transporttubing
washspeed=15; 1ml syringe
-8.000 Concentration =                10.00 [mM]
EluentGenerator.Curve =              5
-3.050 Wait                          sampler. ready
-3.000 Zone =                         samples
Tube =                               sample.Vialpos

```

```
-2.980      syringespeed=1
            suckair ;airgap
-2.750      z.nominal=33 ; depth in sample vial
-2.700      syringespeed=2 ;speed when asp sample
            suck
-2.120      Pump_InjectValve.State =LoadPosition ; injvalve to load - ready for load sample
-2.110      z=0
-2.100      zone=injport ;goto injport
            tube=1
-2.050      z.nominal=56
-1.900      syringespeed=0.5 ;speed disp in injport
            dispense
-0.500      Autozero
;-----inj-routine end-----

0.000      Autozero
            Concentration =                10.00 [mM]
            EluentGenerator.Curve =        5
            Pump_InjectValve.State =injectposition; injecting sample
            ECD_1.AcqOn

0.500      Log                Pressure.Value
            Log                SRS_Current
            Log                ECD_1.Signal.Value
            Log                CartridgeRemainingLifeTime

2.000      wash; execute wash after inj sample. wash must be executed manually before first injection
3.500      sampler.home
4.000      Concentration =        10.00 [mM]
            EluentGenerator.Curve =        5
9.000      Concentration =        60.00 [mM]
            EluentGenerator.Curve =        5

20.000;----- injectionport wash 1/2 -----
            workvolume=900
            syringespeed=15
            sucksolvent
            wait sampler.ready

20.500      zone=injport
```

```

        tube=1
        z.nominal=56
        wait sampler.ready
;-----
28.000      ECD_1.AcqOff
28.100;----- injectionport wash 2/2 -----
        syringespeed=0.6
        dispense
        wait sampler.ready
;-----
30.000      Concentration =                60.00 [mM]
            EluentGenerator.Curve =        5
            Wait                            EluentGenerator.Ready
End
```